Dissertation

on

ELECTRON DENSITY VARIATIONS IN THE IONOSPHERE AT LOW LATITUDES (DUE TO LUNAR TIDES)

Presented

by

RAJENDRA PRASAD SHARMA

for

the degree of

DOCTOR OF PHILOSOPHY

of

THE GUJARAT UNIVERSITY

043

B4014

January 1971

PHYSICAL RESEARCH LABORATORY

AHMEDABAD

P R E F A C E

Ever since systematic ionospheric soundings began, it has been found that the ionizations in the lower E and F_1 layers behave in a fairly regular manner as expected from Chapman's theory; while the F_2 layer shows anomalous behaviour in its daily, seasonal and latitudinal variations. Martyn's (1947,1948) theory based on vertical electro-dynamical drifts showed reasonable agreement with the observed variations, provided suitable values were used for the amplitude and phase of the drift. Recent studies of the variations of the H-component of the geomagnetic field and the F_2 ionization at equatorial latitudes have indicated extremely close association between the equatorial electrojet and F_2 ionization.

From the observed data of solar daily variation of F_2 ionization, the heating, ionizing and gravitational effects of the sun cannot be easily separated as their periods are identical. Thus a proper estimate of the divergence term in the continuity equation has always been difficult.

The moon does not have either a heating or ionizing effect on the ionosphere but it has a gravitational tidal effect. Therefore, a study of lunar tidal effects in the F_2 region may be expected to be of help in analysing

the drift parameters of ionization. The lunar tide at different heights in the ionosphere would enable one to estimate the height variations of the divergence term and obtain a better understanding of the relationship between equatorial ionospheric currents and F_2 ionization.

Recent rocket studies have shown remarkable changes in the composition of the atmosphere in the F-region. A study of the dynamical behaviour of the F-region at different heights could locate this particular boundary in the ionosphere and its changes with season, if any. A systematic study was undertaken to correlate the lunar variations in the geomagnetic field and in F_2-ionization at different heights and at stations near the equator, near the S_q current focus, and, to some extent, near the crest region of the equatorial F_2 anomaly. Through the kind courtesy of the former CRPL Laboratories of USA, the electron density profile data of Huancayo (an equatorial station) were available to us. This has made such studies possible. The N(h) profile data for Puerto Rico published in CRPL Ionospheric Data Bulletins (part A) were also used to get similar informations for a middle latitude station. The thesis contains six chapters:

CHAPTER - I

The salient features of ionospheric and geomagnetic variations at low latitudes; and the theories of daily variations of F_2 ionization at low latitude stations are described.

CHAPTER - II

The various methods for computing lunar tidal effects are described. The computations of the probable errors and the significance of the results are also discussed.

A brief general review of lunar tides in the geomagnetic field and in various ionospheric layers is presented.

CHAPTER - III

The correlation between lunar tide in geomagnetism and in F_2 ionization is studied at the equatorial station, Huancayo. It is found that the height of the peak ionization $h_{max}\ F_2$ varies sympathetically with the changes in the H-component of the geomagnetic field, while the variations in maximum electron density N_{max} are opposite to that in h_{max} with a delay of about 1-2 hours. The amplitude of lunar oscillation in Y_m is smaller than that for h_{max} but the phases in both are same, suggesting that the oscillations in electron density have same phase but are of increasing amplitude with increasing height.

CHAPTER - IV

The lunar variations in H and various parameters of the F_2 region for San Juan, Puerto Rico, a station close to the focus of the dynamo current systems (Sq and L), are described and compared with those obtained at the equatorial station Huancayo. It is shown that the lunar oscillations of H at

San Juan are governed by the relative positions of the Sun and Moon, while those at equatorial stations are controlled by the absolute position of the moon.

CHAPTER - V

The lunar tidal effects in electron density N(h) at different heights at the equatorial station Huancayo, at Ahmedabad which is near the peak of the Appleton anomaly and at Puerto Rico which is near S_q focus are described. The amplitude and phase of the lunar tides in electron density at fixed heights of the ionosphere and for each individual solar hour are discussed. The amplitude of the tide is shown to increase with altitude within the F-region (above 180 km). The phase of the tide at various heights are different at different latitudes.

CHAPTER - VI

An attempt is made in this chapter to interpret the various observed results in the light of the existing theoretical knowledge. It is shown that most of the observed results can be explained on the basis of vertical electromagnetic drifts produced by the interaction of dynamo (lunar) electric fields and the earth's geomagnetic field.

All the figures, equations and tables are numbered in a serially increasing order, irrespective of the chapter

in which they occur. The tables are put together in the Appendix (pp.214-258).

All the computations using an IBM 1620 computer and other works in connection with preparation of the thesis were done by the author himself. The author has also been associated with the Beacon-satellite project, for the determination of the total electron content using faraday rotation of the signals from the satellite, at the Physical Research Laboratory, Ahmedabad. However, the results of these studies are not included in this thesis.

R G Rastogi
(R.G.Rastogi)
Professor-in-charge.

R P Sharma
(R.P.Sharma)
Author.

PUBLICATIONS

The following papers based on the work described in this thesis have been published in various international journals.

(1) 'Lunar tides in noon ionization at different heights of the ionosphere over Ahmedabad during IQSY' - R.G.Rastogi and R.P.Sharma, Proc.IQSY Symp. New Delhi, p.72 (1966).

(2) 'Lunar tides at fixed real heights in the ionosphere over Ahmedabad' - R.P.Sharma and R.G.Rastogi, J.Atmos. Terr.Phys.,29,1641 (1967).

(3) 'Lunar tides in noon electron density at fixed real heights in the ionosphere over Puerto Rico and Huancayo' - R.P.Sharma and R.G.Rastogi,J.Atmos.Terr. Phys.,30,453 (1968).

(4) 'Some studies of the phase reversal of lunar semi-monthly oscillations in midday foF2' - R.P.Sharma and R.G.Rastogi, J. Inst.Telecom. Engrs.,15,581 (1969).

(5) 'Ionospheric lunar tides over the magnetic equator' - R.G.Rastogi and R.P.Sharma, Proc.Third Inter.Symp. Equat.Aeor. (Ahmedabad) Vol.II,378 (1969).

(6) 'Lunar perturbations in geomagnetic field and in the characteristics of F-region over Huancayo' - R.P.Sharma and R.G.Rastogi, Pure App. Geophys. (formerly Geofis. Pura e Appl.) Italy, 19 80(III),288(1970).

(7) 'Lunar tides in the structure of F2-region and in H at Puerto Rico' - R.P.Sharma and R.G.Rastogi, Ann. de Geophys.,25,807 (1969).

(8) 'Lunar tidal effects in horizontal magnetic field at San Juan' - R.P.Sharma and R.G.Rastogi, Ann. de Geophys.,26, 337 (1970).

(9) 'Interrelations between geomagnetic and ionospheric lunar tides at equator' - R.P.Sharma and R.G.Rastogi, Ind.J.Pure. Appl. Phys.,8,853 (1970).

(10) 'Luni-solar tides in electron density at fixed heights of the ionosphere' - R.P.Sharma and R.G.Rastogi, Planet. Space Sci., (1971) (in press).

ACKNOWLEDGEMENTS

The author is extremely happy to express his deep indebtedness to his guide, Professor R.G.Rastogi, for introducing him to the subject, guiding and supervising his work with keen interest at all stages.

The author expresses his heartiest gratitude to Prof. K.R.Ramanathan for his continued interest and valuable discussions at various stages of his research work.

Thanks are due to other senior members of our group, especially to Dr.J.S.Shirke for help and frequent discussions. Thanks are also due to all other members of the ionospheric group for their continued co-operation; especially to Mrs. S.P.Jani and Miss.B.D.Bhatt for their help in the reduction of Ahmedabad ionograms for N(h) profiles, and to Mr.S.S. Deshikachar for his unstinting assistance in the computational work.

The entire computations presented in the thesis were carried out with the IBM 1620 computer facility at the Physical Research Laboratory. The author wishes to express his thanks to Mr.S.R.Thakore and the staff of the computing centre, in particular Mr.P.S.Shah, Mr.C.V.R.K.A.Rao, Mr.M.G. Rastogi and Mr.P.K.Shah for their kind co-operation.

The author is grateful to Mrs.G.Rajaram for reading the manuscript, and to Mr.P.Raghavan for the painstaking job of typing the thesis.

It is without hesitation that the author expresses his indebtedness to the former Central Radio Propagation Laboratories, Boulder, U.S.A. for providing the data which enabled such a study to be carried out.

The author was recepient of a scholarship from Ministry of Education, Government of India, which is acknowledged.

Finally, the author is indebted to his wife, Prem Balika, for the moral support and help at the most needed hours.

C O N T E N T S

	Page
Preface	i
Publications	vi
Acknowledgements	vii
CHAPTER I - INTRODUCTION	
1.1 Introduction	1
1.2 Daily variation of geomagnetic field	1
1.3 Daily variation of H at equator, equatorial electrojet	5
1.4 Electromagnetic drifts	12
1.5 Variations of F_2-ionization at low latitudes	12
1.6 Theories of equatorial F-region	17
1.7 Ionospheric lunar tide, and importance of its study	18
CHAPTER II - METHOD OF ANALYSIS AND GENERAL REVIEW	
2.1 Introduction	20
2.2 Lunar parameters	20
2.3 Various methods of analysis:	22
(a) Lunar daily variations at fixed age ν (L_ν)	24
(b) Whole lunation average lunar daily variation(L)	27
(c) Lunar monthly variations(M) at fixed solar hour	28

Page

2.4 Probable error and its significance 30

2.5 Lunar atmospheric tides 33

2.6 Geomagnetic lunar variations 35

2.7 Lunar tides in the D-region 41

2.8 Lunar variations in the E-region: 43

(a) Normal E-layer 43

(b) Sporadic E-layer (Es) 45

2.9 Lunar variations of the F1-layer 47

2.10 Lunar variations in the F2-region 48

(a) Magnetic control of the tide 49

(b) Luni-solar variations 52

(c) Seasonal effects 53

(d) Correlation with geomagnetic tides 54

CHAPTER III - INTERACTION OF GEOMAGNETIC AND IONOSPHERIC LUNAR TIDES AT MAGNETIC EQUATOR

3.1 Introduction 58

3.2 Perspective view of the annual average luni-solar variations 59

3.3 Annual average lunar monthly variations 65

3.4 Seasonal effects in lunar daily variations ($L_{\mathcal{Y}}$,L): 74

(a) H-component 74

(b) Ionospheric parameters 76

(c) Correlation between geomagnetic and ionospheric L variations 78

Page

3.5 Seasonal effects in lunar monthly variations(M): 80

(a) H-component 81

(b) Height of peak ionization (h_{max}) 84

(c) Maximum electron density (N_{max}) 86

(d) Semi-thickness of the layer(Y_m) 89

(e) Total electron content (N_t) 92

(f) Interrelations between M_2 tide in H and in ionospheric F_2 region. 95

3.6 Height variation of lunar tide 97

3.7 Conclusions: 100

(a) Lunar daily variations at fixed lunar ages ($L_{2\nu}$) 100

(b) Whole lunation lunar daily variation(L) 101

(c) Lunar monthly variations(M) 102

CHAPTER IV - INTERACTION OF GEOMAGNETIC AND IONOSPHERIC LUNAR TIDES AT A STATION CLOSE TO L-CURRENT FOCUS

4.1 Introduction 104

4.2 Luni-solar variation in H 105

4.3 Lunar daily variations of H at fixed lunar ages ($L_{2\nu}$) 107

4.4 Whole lunation average lunar daily variation (L) of H 108

4.5 Annual average lunar monthly(M) tide in H 109

4.6 Seasonal effects in lunar monthly oscillations of H 112

Page

4.7 Perspective view of annual average luni-solar tide in the characteristics of the F2 region at Puerto Rico 117

4.8 Annual average lunar monthly tides in the F2 region 123

4.9 Seasonal effects in the lunar daily variations (L_2, L) of ionospheric parameters 126

4.10 Seasonal effects in lunar monthly (M) tides in ionospheric parameters: 129

(a) Height of peak ionization (h_{max}) 129

(b) Maximum electron density (N_{max}) 133

(c) Total electron content (N_t) 137

4.11 Conclusions: 140

(a) Lunar variations of H at San Juan 140

(b) Lunar tides in the F_2 region at Puerto Rico 141

CHAPTER V - LUNAR TIDES IN ELECTRON DENSITY AT FIXED HEIGHTS OF THE IONOSPHERE AT EQUATORIAL, TROPICAL AND MIDLATITUDE STATIONS

5.1 Introduction 143

5.2 Lunar perturbations of noon electron density at fixed heights of the ionosphere at Ahmedabad 145

5.3 Height variation of lunar tide in the ionosphere at Huancayo and Puerto Rico (Preliminary results at noon only) 149

5.4 Annual average luni-solar variations of electron density in the ionosphere over Huancayo: 153

(a) Tide at fixed individual solar hours 153

Page

(b) Comparison with other similar results 157

(c) Average tide during day and night-time 158

(d) Detailed study of luni-solar effects 160

5.5 Height variation of lunar tide at Puerto Rico (Annual average oscillations of electron density): 163

(a) Tide at fixed solar hours 163

(b) Average day and night-time vertical profiles of lunar tide 166

(c) Luni-solar effects in electron density 168

5.6 Lunar perturbations in N(h) profiles at Puerto Rico during different seasons: 169

(a) D-months 169

(b) E-months 175

(c) J-months 179

5.7 Conclusions 183

CHAPTER VI - THEORY OF LUNAR TIDES

6.1 Introduction 187

6.2 Cause of lunar geomagnetic variations 187

6.3 Estimation of electric field for the semi-diurnal lunar current system 189

6.4 Cause of lunar tides in the E-region: 196

(a) Effect of lunar tidal wind (No magnetic field) 197

(b) Effect of vertical drifts on a Chapman layer 198

		Page
	(c) Interpretation of the observed results	201
6.5	Cause of lunar tides in the F-region at stations in middle latitudes	202
6.6	Interpretation of the results of the lunar tide in the F2 region at Puerto Rico	205
6.7	Cause of lunar tides in the F2 region in the magnetic equatorial zone:	207
	(a) Lunar variations in the day-time	208
	(b) Lunar variations in the night-time	209
6.8	Lunar variations of electron density at fixed heights	210
APPENDIX		214
Tables (1 - 29)		214 - 258
References		259

CHAPTER - I

INTRODUCTION

1.1 Introduction

The direction and magnitude of the earth's magnetic field are constantly fluctuating and these variations are recorded continuously at magnetic observatories distributed over the earth. The part of the geomagnetic field with the slowest variation is called the secular variation; it takes hundreds of years to produce a change of a few percent. The main field and its secular variations are known to be of internal origin. Besides this relatively slow variation, there are other and more rapid variations such as the daily variations and the geomagnetic storms which have their origin primarily outside the earth. The daily variations, on quiet days, are regular in nature and their periods are related to the solar and lunar day. The amplitude of these variations are different in the equatorial, tropical, auroral and polar zones. The geomagnetic field exercises a strong control on the motion of ionized particles throughout the earth's outer atmosphere and higher parts of the ionosphere and this geomagnetic domain is known as 'magnetosphere'.

1.2 Daily variations of Geomagnetic field

All components (H, D, Z) in geomagnetic records

occasionally show very smooth traces that indicate clear patterns of daily variation with respect to solar time. This occasion is called a 'geomagnetic quiet' period and the pattern is called a solar quiet daily variation denoted by S_q. The variation with respect to lunar time i.e. lunar daily variation, L, is not apparent on the magnetogram but can be derived by a long series of hourly values of geomagnetic field components using methods described in section 2.3.

From the data of large number of magnetic observatories all over the globe, it is now known that the solar daily variation of horizontal component (H) of earth's magnetic field, $S_q(H)$, is large during the day and attains maximum amplitude at about 11 hr local time. The H component, on the average, shows a flat daily variation at about 30° dip latitude. The direction of H variation changes near 30° dip latitude; H is minimum near noon for latitudes higher than 30°, while it is maximum for low latitude stations (MATSUSHITA and MAEDA, 1965). The amplitude of $S_q(H)$ decreases with increasing latitude from equator in either hemisphere and again becomes large in the auroral zone where auroral electrojet (FEJER, 1963) exists. At the equatorial stations in a narrow belt around the dip equator, a few degrees of latitude in width, $S_q(H)$ amplitudes are very large. This phenomenon known as equatorial electrojet is discussed separately in section 1.3.

In order to explain the geomagnetic quiet daily

variation (S_q) STEWART (1882) postulated an upper atmospheric current system fixed with respect to the sun. The earth moves, in course of its daily rotation, under this current field which causes the daily variation of the geomagnetic field. He suggested that these electric currents in the upper atmosphere are induced by dynamo action, i.e. the upper atmosphere behaves like an electric conductor, which moves across the earth's main geomagnetic field under the action of convective motion of air caused by solar heating, thus inducing electric currents in the conducting upper atmosphere. This explanation of the S_q(and L) variations is called the dynamo theory.

Early support came to this theory when SCHUSTER (1889) studied the geomagnetic variation field on a world-wide scope by the method of spherical harmonic analysis and estimated the equivalent current system responsible for geomagnetic daily variation. He concluded that greater part (67%) of the S_q variation field has its origin outside the earth and that remainder (33%) may be attributed to the earth currents induced by the varying external field. Since then similar studies of S_q using the geomagnetic data from different solar periods have been made by a number of workers: WALKER (1913), CHAPMAN (1919), BARTELS (1928), MCNISH (1937), BENKOVA (1940), HASEGAWA and OTA (1950), MAEDA (1953a) and MATSUSHITA and MAEDA (1965).

SCHUSTER (1908) developed the theory quantitatively and suggested that the required large conductivity of the upper atmosphere must be due to solar ultraviolet radiations. His formulation was re-examined and extended by CHAPMAN (1919) assuming anisotropic conductivity for the upper atmosphere. The historic trans-atlantic radio communication by MARCONI in 1901 and the discovery of ionosphere (APPLETON and BARNETT, 1925; BREIT and TUVE, 1925) proved the existence of conducting medium in the upper atmosphere and gave further impetus to this theory.

PEDERSEN (1927) emphasized the anisotropic nature of conductivities in the presence of geomagnetic field, resulting in the reduction of the conductivity. COWLING (1932, 1945), however, considered the effect of Hall currents and indicated that electric polarization of the medium might reduce the retarding influence of the geomagnetic field on electric conduction. These findings were later applied to the dynamo theory by HIRONO (1950a, b, 1952, 1953b), BAKER and MARTYN (1953) and FEJER (1953) who got better agreement between the theory and observations by using recent data of electron concentrations and winds in the ionosphere.

These currents flow in the region where the effective conductivity is large. MAEDA (1953b) showed that this conductivity strongly predominates in E-region over the F-region of the ionosphere. Also the conductivity in the F-region is much

reduced by the effect of induction drag (COWLING, 1945; HIRONO, 1953; BAKER and MARTYN, 1953). Distribution of the conductivities with height has been calculated by MAEDA (1952), FEJER (1953), BAKER and MARTYN (1953), MAEDA (1953b) CHAPMAN (1956) and MAEDA and MATSUMOTO (1962) which shows that the effective conductivity is largest in the E-region (100-130 km). From this, it is quite clear that the current responsible for the S_q field flows mainly in the E-region, although weaker currents may exist beyond this region. The geomagnetic daily variation is the effect of the total integrated current flowing overhead. The existence of a narrow current sheet in the E-region was also confirmed experimentally by rocket borne instruments which detected a discontinuity in magnetic field when the rocket crossed the region of current flow (SINGER ET AL, 1951; CAHILL, 1959; BURROWS and HALL, 1964; DAVIS ET AL, 1965).

1.3 Daily variation of H at Equator : Electrojet

When in 1922, a geomagnetic observatory at Huancayo near the dip equator was established, a new feature of the daily variation of earth's magnetic field came to light. Whereas the daily ranges of Declination, D, and vertical intensity, Z, at Huancayo are comparable to those of the stations in similar geographical latitudes, the diurnal range of H is abnormally large, being often more than double the value expected. This abnormal range in H was interpreted by MCNISH (1937) as being due to locally concentrated eastward

electric currents. EGEDAL (1947, 1948) reported that the diurnal range of H at six stations near the equator showed a sharply peaked curve, symmetrical about the dip equator and smoother than a plot against dipole latitude. Subsequent measurements at other places, i.e. in Uganda (CHAPMAN, 1948), Nigeria (ONWUMECHILLI and ALEXANDER, 1959a), Peru (FORBUSH and CASAVARDE, 1961) and in India (PRAMANIK and YEGNANARAYANAN, 1952; PRAMANIK and HARIHARAN, 1953; THIRUVENGADHAN, 1954), showed that this abnormal increase in $S_q(H)$ happens at all places near the dip equator. It, now, became clear that the enhancement was due to overhead current. This concentration of electric current flowing eastward in a narrow zone over the magnetic equator on the sunlit hemisphere was named 'equatorial electrojet' by CHAPMAN (1951a)

The cause of the equatorial electrojet lies in a special feature of the electrical conductivity and hence a brief description of conductivity is first presented.

Based on simple gas kinetic theory, conductivity of an ionized gas which is anisotropic in presence of a magnetic field may be represented by a tensor. Taking a cartesian coordinate system with its Z axis along magnetic field direction B, the conductivity σ is

$$\left[\sigma\right] = \begin{bmatrix} \sigma_1 & -\sigma_2 & 0 \\ \sigma_2 & \sigma_1 & 0 \\ 0 & 0 & \sigma_0 \end{bmatrix} \quad ---- \quad (1)$$

where σ_0, σ_1 and σ_2 are longitudinal, Pedersen and Hall conductivities respectively and are given by:

$$\left.\begin{aligned} \sigma_0 &= \frac{1}{B}\sum_i \left(\frac{n_i \omega_i}{\nu_i}\right) e_i \\ \sigma_1 &= \frac{1}{B}\sum_i \left(\frac{n_i \nu_i \omega_i}{\nu_i^2 + \omega_i^2}\right) e_i \\ \sigma_2 &= -\frac{1}{B}\sum_i \left(\frac{n_i \omega_i^2}{\nu_i^2 + \omega_i^2}\right) e_i \end{aligned}\right\} \quad - - - (2)$$

where subscript i denotes the i-th species of charged particles and e_i = charge ($e_i = -e$ for electrons) $\omega_i = e_i B/m_i$ the gyrofrequency, ν_i = collision frequency with neutral particles, n_i = density of charged particles and m_i = mass of the charged particles. The collisions between charged particles are excluded in (2). In a lightly ionized gas such as lower ionosphere, this exclusion is valid but becomes serious with increasing height and must be taken into consideration.

From (2) it is seen that σ_0, σ_1 and σ_2 are functions of n_i, m_i and ν_i which depends on neutral particle density. These parameters vary with time and space, horizontally and vertically; neutral particles change their composition and

their number density decreases with height. The height distributions of σ_0, σ_1 and σ_2 show that σ_1 or σ_2 are smaller than σ_0 and reach maximum at 110 to 140 Km (E-region); this result is independent of atmospheric model used for n_i and ν_i. The ratio of σ_2/σ_1 is about 10 around 100 Km during the day-time (MAEDA and MATSUMOTO, 1962).

When the medium is bound in Hall current direction, the flow of this current sets up a polarization field which opposes the flow of current. If the Hall polarization inhibits the Hall current, the effective conductivity of the medium (parallel to electric field) is greater than σ_1. In the ionosphere, Hall current leads to polarization which easily leaks away along the geomagnetic field lines except at the dip equator where the field lines are horizontal. The resulting increase in the conductivity is sufficient to account for the observed S_q field.

To derive the effective conductivity, the co-ordinates are changed with that x, y and z representing the magnetic southward, eastward and vertical upward directions respectively. The conductivity tensor in (1) then takes the general form

$$[\sigma] = \begin{bmatrix} \sigma_{xx} & \sigma_{xy} & \sigma_{xz} \\ \sigma_{yx} & \sigma_{yy} & \sigma_{yz} \\ \sigma_{zx} & \sigma_{zy} & \sigma_{zz} \end{bmatrix} \quad --- \quad (3)$$

If we consider ionosphere as a conducting spherical thin shell then currents cannot flow vertically as it is perpendicular to the shell and $J_z = 0$. The dynamo equation relating current density $\vec{J}$ and electric field $\vec{E}$:

$$\vec{J} = [\sigma]\,\vec{E} \qquad \text{(4)}$$

then becomes

$$\left.\begin{aligned} J_x &= \sigma_{xx} E_x + \sigma_{xy} E_y \\ J_y &= \sigma_{yx} E_x + \sigma_{yy} E_y \end{aligned}\right\} \qquad \text{(5)}$$

where

$$\left.\begin{aligned} \sigma_{xx} &= \sigma_0 \sigma_1 / (\sigma_0 \sin^2\phi + \sigma_1 \cos^2\phi) \\ \sigma_{xy} &= -\sigma_{yx} = \sigma_0 \sigma_2 \sin\phi / (\sigma_0 \sin^2\phi + \sigma_1 \cos^2\phi) \\ \sigma_{yy} &= (\sigma_0 \sigma_1 \sin^2\phi + \sigma_1 \sigma_3 \cos^2\phi) / (\sigma_0 \sin^2\phi + \sigma_1 \cos^2\phi) \end{aligned}\right\} \text{--(6)}$$

where ϕ = dip angle, and $\sigma_3 = \sigma_1 + \sigma_2^2/\sigma_1$ is the effective or Cowling conductivity to be used in the dynamo theory. Since $\sigma_2 \gg \sigma_1$ in the 100 Km region, σ_3 is very much enhanced over σ_1. σ_{xx}, σ_{xy} and σ_{yy} being functions of ϕ vary with latitude. Estimations show that height integrated effective conductivity over most of the earth is 5 to 10 times greater than Pedersen conductivity, even though the inhibition of Hall current is not complete at most places (HIRONO, 1950a, 1950b, 1952; MARTYN, 1948a; MAEDA, 1952; BAKER and MARTYN, 1953; CHAPMAN, 1956; and MAEDA and MATSUMOTO, 1962).

At the dip equator $\phi = 0$ and $\sigma_{xx} = \sigma_0$, $\sigma_{xy} = 0$ and $\sigma_{yy} = \sigma_3$. Thus the Cowling conductivity is enhanced by a further factor of 2 to 5 because the Hall current flow is vertical and hence is totally inhibited. This enhancement of σ_{yy} occurs in a narrow zone of half width of 3° lat.(BAKER and MARTYN, 1953) flanking the dip equator, but it decreases away from the equator and is the cause of equatorial electrojet.

Further studies of electrojet in different longitude zones have shown significant longitudinal differences. RASTOGI (1962a) showed that the electrojet is strongest in the American zone and weakest in Indian zone. Recent rocket measurements of electrojet current intensity in Peru (MAYNARD, 1967; DAVIS ET AL, 1967) and in India (SASTRY, 1968) also confirm this view. This longitudinal inequality may be due to longitudinal differences in the geomagnetic field, B, which gives rise to inequalities in the conductivity σ_{yy} (SUGIURA and CAIN, 1966). UNTIED (1967) has modified the σ_{yy} model of SUGIURA and CAIN (1966) to take into account the meridional currents also. This model yields stronger currents and a substantially larger width of the electrojet. UNTIED'S (1967) model has assumed a dipole magnetic field. SUGIURA and POROS (1969) have improved on this model by using a magnetic field configuration represented by a spherical harmonic expansion. They obtained significant longitudinal

differences and have constructed electrojet profiles for 0°, 40°, 80°, 180° and 280°E longitudes. The essential feature of the meridional current system is the existence of two current loops, one on each side of the dip equator and with an equator-ward current in the lower E-region, an upward current over the dip equator, and a return current flowing in the upper E-region. The intensities of the electrojet and the associated meridional current are significantly dependent on longitude, being strongest over Peru and weakest over India. The model also predicts a reversed (westward) current in a thin, narrow layer located at about 10° off the dip equator, which is due to a reversal of the vertical polarization field.

The S_q (H) under the electrojet undergoes a solar cycle variation, being greater during increased solar activity (RAO ET AL, 1967). The range of H close to electrojet is shown to change with season ; it is greater at equinoxes than at the solstices (CHAPMAN and RAJARAO, 1965). Also, there is evidence of a slow motion of the electrojet axis following the Sun (OGBUEHI and ONWUMECHILLI, 1964). In addition, day to day changes in all the parameters of the electrojet are known to occur. Recently, GUPTA (1970) has suggested the observed daily variability in the amplitude and the type of electrojet to be due to the irregularities in the influx of solar ultraviolet radiations.

1.4 Electromagnetic drifts

The earth's atmosphere is subject to tidal motions produced by the heating effect of the sun and the gravitational attraction of the sun and moon. As discussed in Sec.1.2, these tidal motions generate dynamo electric fields in the E-region. Current due to these fields flows in a complicated pattern and in general there is some separation of charge, which sets up an electrostatic polarization field. This electrostatic field in the dynamo region is transferred to the higher F-region along magnetic field lines which are, virtually, equipotentials due to high conductivity along them in the F-region. The electric field $\vec{E}$ is everywhere normal to the magnetic field $\vec{B}$ and causes the charged particles, both ions as well as electrons, to drift in the perpendicular direction with velocity:

$$\vec{v_d} = \frac{\vec{E} \times \vec{B}}{B^2} \qquad - - - \quad (7)$$

This effect is known as electromagnetic drifts. The drift velocity ($\vec{v_d}$) has components both vertical and horizontal. Among them, however, the vertical drift is known to have a serious effect on the ionospheric F_2 region (Section 1.6).

1.5 Variations of F2 - ionization at low latitudes

According to CHAPMAN (1931) theory of layer formation, the peak ionization of an ionospheric layer should vary with

solar zenith distance; it would be maximum at noon and greater in summer than in winter, and the ionization at a particular height would be more at equator than at high latitudes. The E and F_1 layers are found to obey the Chapman theory to some extent and exhibit strict solar control. The F_2-region, on the other hand, is anomalous in many respects. The observed characteristics show anomalies in the daily variations, seasonal variations, solar cycle variations and variations with latitude.

The first such anomalous behaviour of F_2 ionization was noticed in its seasonal variation by APPLETON and NAISMITH (1935) who showed that the noon value of critical frequency, f_oF_2, at Slough was less in summer than in winter. Further studies showed a geomagnetic control of the F_2 layer i.e. f_oF_2 values were similar at stations having same geomagnetic and not the same geographic latitude (RANZI, 1939; MAEDA ET AL, 1942). RASTOGI (1959a), further, demonstrated that the variations of F_2-ionization at low latitudes are governed by dip (magnetic) latitude instead of idealized geomagnetic latitude.

The abnormal behaviour of daily variation of f_oF_2 at low latitudes was first shown when BERKNER and WELLS (1934) noticed a noon bite out effect i.e. the peak of f_oF_2 is reached in morning and again in the late afternoon with a valley near noon. HIRONO and MAEDA (1954) compared the daily variation

of f_oF_2 at a few equatorial stations and found the curves to be very similar at all the stations. MAEDA (1955) showed that while this effect is typical of all low latitude stations; at middle latitude stations, f_oF_2 shows a single maximum in the afternoon. RASTOGI (1959b) studied the daily variation at few stations at low latitudes in the Asian zone. The curves (after RASTOGI, 1959b) are reproduced in figure 1. It is seen that the forenoon and evening times of occurrence of the two maxima at low latitude stations get closer with increasing latitude and finally converge to a strong single maximum around 25° dip (Bombay).

The above effect in the daily variation of f_oF_2 at low latitude stations manifests itself, in other form, in the latitudinal variation of noon value of f_oF_2. A plot of noon value of f_oF_2 as a function of dip latitude shows a pronounced trough (minimum) centred on the magnetic equator with two crests (maximum) on either side at about 30° dip (APPLETON, 1946; BAILEY, 1948). This phenomenon (shown in figure 2) is known as equatorial anomaly, geomagnetic anomaly or Appleton anomaly. The anomaly is also found in plots of electron density (N) at fixed heights below (CROOM ET AL, 1959) and above (KING ET AL, 1964) the F_2 peak. The main features of the equatorial anomaly are as follows:

(a) Diurnal development

During equinoxes of low sunspot years, f_oF_2 is

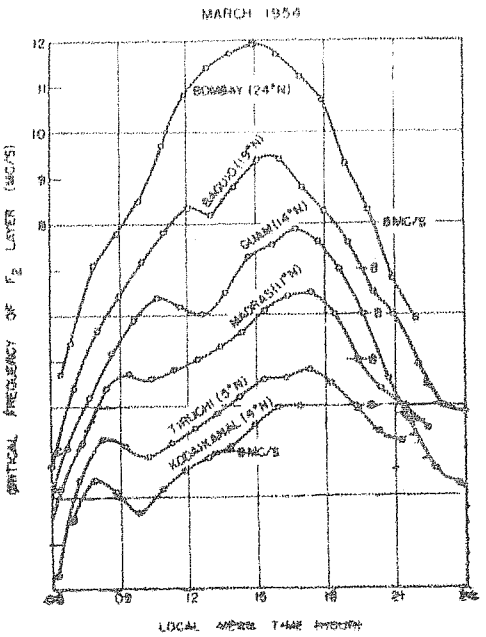


FIGURE - 1

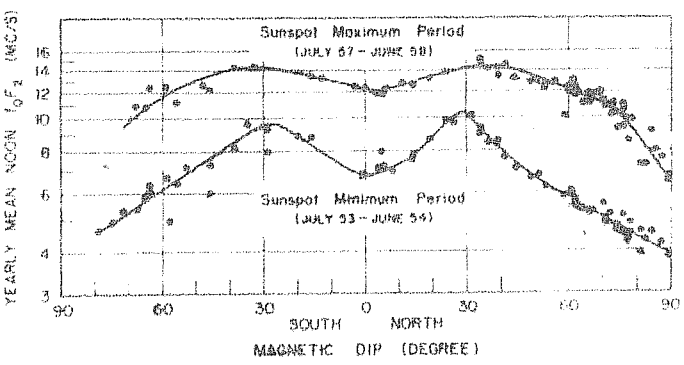


FIGURE - 2

maximum at sunrise at equator. At later hours, this maximum flattens and is followed by a weak maximum at low latitudes. With the progress of the day, the peak becomes more pronounced and simultaneously shifts to higher latitudes till about 14 hr, when the anomaly is most pronounced, after which the process reverses and at 20 - 21 hr, the anomaly disappears completely with a maximum of f_oF_2 at equator again (RASTOGI 1959b). During high sunspot years, however, the anomaly is known to persist until 02 hr and sometimes until sunrise (LYON and THOMAS, 1963).

(b) Seasonal effects

The anomaly is nearly symmetrical relative to the magnetic equator at equinox. During solstices, the crests in the summer hemisphere are broader and lower than those in winter hemisphere (LYON, 1963; THOMAS, 1968).

(c) Solar activity effects

The equatorial anomaly for the two periods of solar activity is shown in figure 2. It is seen that the peaks of f_oF_2 occur at $\pm$ 30° dip during low sunspot years, while at about $\pm$ 35° dip during high sunspot years. The proportionate depression of the equatorial trough decreases with increasing activity. Further, the southern peak is found to be slightly smaller than the northern peak.

Besides the above mentioned effects, the form of

anomaly is known to change with magnetic activity, with longitude and with lunar phase (RASTOGI, 1966). The changes of equatorial anomaly with lunar hour angle is shown to be the main cause of ionospheric lunar tidal variations at low latitudes (Section 6.7) .

1.6 Theories of equatorial F-region

The first suggestion for explaining equatorial anomaly was given by MITRA (1946) who proposed that electrons produced by solar ionization near the equator would diffuse along magnetic field lines causing an ionization minimum at equator, and an accumulation of ionization near the observed Appleton anomaly peaks. Considering horizontal diffusion with production and loss processes in the continuity equation, the behaviour of F_2-ionization was studied by many workers (KENDALL, 1963; RISHBETH ET AL, 1963; GOLDBERG ET AL, 1964; BAXTER, 1967). Their results produced a trough which is much shallower and narrower in latitude than the observed trough.

An alternative theory given by MARTYN (1955) and developed by DUNCAN (1960) is based on electromagnetic drift effects. According to this theory, an eastward electrostatic electric field is present during the day at equator and causes an upward drift of plasma (Sec.1.4). The ionization is lifted upwards due to this drift and then diffuses downward along the field lines to higher latitudes to form a peak there. This effect is known as fountain effect because of its

similarity with a water fountain. HIRONO and MAEDA (1955) showed that such electric fields may exist and the upward drift velocity is of the order of 10 m/sec. The equilibrium solutions of continuity equation, with diffusion and drift included, have been made by BRAMLEY and PEART (1965) and HANSON and MOFFETT (1966) who showed that a drift of this magnitude is sufficient to explain the main features of equatorial anomaly. This view was further confirmed by BAXTER and KENDALL (1968), who considered the time dependent effects of electrodynamic drifts. HANSON and MOFFETT (1966) further showed that the interhemisphere asymmetry of Appleton peaks can be produced by a neutral wind blowing from north to south; a wind of 60 m/sec causes 15 percent of asymmetry. The sunspot behaviour of the anomaly was explained by RASTOGI (1959a) as follows. During high sunspot period, the F_2-layer at equator is situated at higher heights and the transport of ionization is spread to wider latitudes, thereby producing broad maxima at slightly higher latitudes.

It is clear from above that diffusion in conjunction with upward plasma lift during day at equator is the main process controlling the F_2-ionization at low latitudes.

1.7 Lunar ionospheric tide and importance of its study

From the above discussions (sec 1.5 - 1.6), it is evident that electrodynamical drifts have profound effects in

the ionosphere. The periodic variations of electron density and height of ionospheric layers are known to exist with respect to both solar and lunar time and these are known as solar and lunar tides respectively. These ionospheric variations should, therefore, be closely related to the corresponding geomagnetic variations through the electromagnetic drift effects. While the lunar variations are due only to gravitational effect of the moon, the solar variations are due to heating effect, ionizing effect and the gravitational effect of the sun. The above mentioned correlation between ionospheric and geomagnetic variations can, therefore, be obtained directly from studies of lunar tides because of its simple nature. The results can then be applied to separate the gravitational and thermal or ionizing effects of the sun in solar daily variations of ionospheric parameters. An understanding of the effect of geomagnetic variations on ionospheric parameters through electromagnetic drifts would greatly help in increasing our knowledge of the dynamics of the ionosphere.

CHAPTER - II

METHOD OF ANALYSIS AND GENERAL REVIEW

2.1 Introduction

Besides producing oceanic tides, the moon's gravitational force affects many geophysical properties like atmospheric pressure and temperature, winds, geomagnetic field, and ionospheric heights and densities. The lunar tidal effects in these parameters are, in general, very small and are masked by large solar variations and other irregular variations. Their determination, therefore, requires a continuous series of geophysical data over many years and special methods of analysis. Some of the older methods are described in chapter 8 of 'Geomagnetism' by CHAPMAN and BARTELS (1940). Before describing the method of analysis in detail, a discussion of various parameters regarding the motion of the moon around the earth would be useful and hence is presented below.

2.2 Lunar parameters

In analogy to mean solar time t, a mean lunar local time τ is defined; it is determined by the motion of the mean moon which is considered to revolve uniformly round the earth. Just as t is counted in 24 solar hours from one midnight to the next, $\tau = 0$ for the lower transit of the mean moon, increasing by 24 lunar hr (or 360°) upto the next lower transit. The sidereal period of the moon's revolution.

around the earth is $27^d\ 7^h\ 43^m$, so that a mean lunar day equals $24^h\ 51^m$ or 1.03505 solar days.

The mean moon revolves, relative to the sun earth line, once in 29.5306 days, a period known as a synodic month, lunar month or a lunation. The moon's phases repeat after a lunation and depend upon the angle γ, between the meridian half planes containing the sun and the moon, which is reckoned positive when the moon is to the east of the sun. The angle γ is called lunar age, and can be expressed as 0 to 24 lunar hr or 0 to 360° from one new moon to the next in course of a lunation. From one solar day to the next the lunar age γ increases by 0.81272 hr.

The solar time t, lunar time τ, and lunar age γ, are related by the equation (see figure 3 which illustrates the relations between t, τ and γ for an observer at P):

$$t = \tau + \gamma \qquad \text{- - - -} \qquad (8)$$

where t, τ and γ may be expressed in hours or in degrees.

The geophysical lunar almanac by BARTELS and FANSELAU (1938) gives complete tables for the mean moon (referred to Greenwich mean noon) for the years 1850 - 1975. They have given values for $24 - \gamma = \mu$, instead of lunar age γ ; μ is known as lunar phase and was used in some of the earlier works. Recently SUGUIRA and FANSELAU (1966) have published tables for γ (for Greenwich noon) for the years 1850 to 2050.

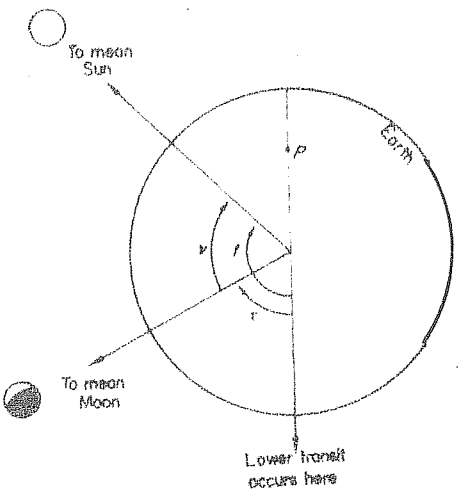


FIGURE - 3

2.3 Various methods of analysis

For computing lunar tides in a geophysical quantity three main methods are generally found in the literature. They are:

(a) Fixed age 'λ' method of computing lunar daily variations at fixed phases of the moon (L_λ).

(b) Method for computing whole lunation average lunar daily variation (L).

(c) Fixed solar hour 't' method of computing lunar monthly (M) variations at fixed solar hours.

The fixed age method, used earlier by BROUN (CHAPMAN and BARTELS, 1940), in its modern form, is due to CHAPMAN and

MILLER (1940). Its practical application to a series of geophysical data was described by TSCHU (1949) with a latter correction by CHAPMAN (1952). The method, in its simplest form, has recently been described by MALIN and CHAPMAN (1970). This method gives lunar daily variations of the parameter with periods related to one lunar day ($24^h\ 51^m$, $12^h\ 25^m$, $6^h\ 12^m$ etc) at fixed lunar ages. The advantage of the method is that dependence of lunar tides on lunar age i.e. Chapman's phase law (section 2.6), can be studied.

The second method determines lunar daily variations averaged over the whole lunation. This method is described by CHAPMAN and BARTELS (1940) and is the most widely used one, probably because it is the simplest of all the three methods. Because of purely lunar nature of variations obtained by using this method, it is very suitable for studying the correlation between lunar ionospheric and geomagnetic variations mentioned in section 1.7, while any study of luni-solar effects (i.e. dependence of lunar tide on solar time) is not possible with this method.

The third method is due to VAN' DER STOK (CHAPMAN and BARTELS, 1940). For a fixed solar hour, lunar monthly variations with respect to lunar age ($2\prime$), with periods related to a lunar month (29.53 days, 14.76 days etc) are computed. The main advantage of the method is that it enables detailed study of luni-solar effects of the tide.

In the present study lunar tidal variations in the ionospheric and geomagnetic parameters are computed by using all the three methods. The procedure of computing lunar tides according to different methods is described below.

(a) Lunar daily variations at fixed age) (L_2)

The ionospheric and geomagnetic parameters are generally available as a series of hourly values for each day of the month on monthly sheets. To compute (L_2), a method basically similar to CHAPMAN and MILLER (1940) is followed. Firstly, missing values are interpolated for, whenever possible. Secondly, the data on magnetically disturbed days ($Cp > 1.2$) are excluded to remove the irregular disturbance effects. The monthly mean value of the element at each hour is calculated and these are taken to represent average solar daily variation, S, during the month. In order to remove the S variation, the monthly mean value of the element for each hour is subtracted from all the values at that hour during the month. This is done for all the months for which data is utilized. This leaves a series of hourly deviations for each day which are free from solar variations but contain lunar variations. At this stage, the data are divided into three seasons viz:

(i) D-months - November, December, January & February.

(ii) E-months - March, April, September & October.

(iii) J-months - May, June, July & August.

Further analysis is done separately for each season as follows. For each day of a particular season, a series of hourly deviations are available; let us denote the deviations for day j by $a_i(j)$, where i is an integer ranging from 0 to 23 (i.e. i denotes solar hour).

Now, the days with same ν value are collected together and average hourly sequences for these days are obtained for each ν (ν ranges from 00 to 23 lunar hr). Mathematically, if total number of days with same ν value for the hour i be denoted by $N_i(\nu)$, then the following 24 sequences are obtained, one for each value of ν.

$$b_i(\nu) = \frac{1}{N_i(\nu)} \sum_{j=1}^{N_i(\nu)} a_i(j) \quad \text{---} \quad (9)$$

For further analysis, the sequences $b_i(\nu)$ for three consecutive ν values, centred at ν = 00, 03, 06, 09, 12, 15, 18 and 21 lunar hr, are grouped and average hourly deviations are calculated. This gives eight sequences of hourly values centred at the above mentioned ν values, i.e. we now obtain sequences $c_i(\nu)$ as follows:

$$\left.\begin{aligned} c_i(00) &= \frac{1}{3}\left[b_i(23) + b_i(00) + b_i(01)\right] \\ c_i(03) &= \frac{1}{3}\left[b_i(02) + b_i(03) + b_i(04)\right] \\ &\vdots \\ c_i(21) &= \frac{1}{3}\left[b_i(20) + b_i(21) + b_i(22)\right] \end{aligned}\right\} \quad - - - (10)$$

The above sequences represent lunar daily variation at fixed ages ($\mathcal{Y}$ = 00, 03, 06 .....18 and 21 lunar hr) in terms of solar hr. It is necessary to represent these variations in terms of lunar time rather than solar time. To do this, first the value corresponding to lunar time τ =00 is fixed using the relation $t = \tau + \mathcal{Y}$ (equation 8). For example, for c($\mathcal{Y}$ =00) sequence, the value at t = 0 hr corresponds to value at τ = 0 hr ; and for c ($\mathcal{Y}$ = 03) sequence, the value at t = 3 hr will give the value corresponding to τ = 0 hr. This value at τ = 0 hr is taken as the starting value of the sequence in terms of lunar time. The values at other lunar hours are obtained from the corresponding values in terms of solar hr by using the following arithmetical formula given by EGEDAL (1956).

$$L(h) = S(h) + (h-1) \times 0.035 \left\{ S(h+1) - S(h) \right\} \quad - - - (11)$$

Where h = the hour

L(h) = value at lunar hr h.

S(h) = corresponding value at hour h (using equation 8)

The resulting sequences in terms of lunar time τ, represent daily variations at fixed lunar ages (λ = 00, 03, 06.....18, 21 lunar hr), and are harmonically analysed for four harmonics. The amplitude and phase angle of first four harmonics of lunar daily variation at a fixed age λ (L_λ) is represented by the following equation known as the Chapman's phase law:

$$L_\lambda = \sum_{n=1}^{4} C_n \text{ Sin } \left\{ n\tau + (n-2)\lambda + \alpha_n \right\} \quad --- (12)$$

where C_n and α_n are the amplitude and the phase angle respectively, of n^{th} harmonic component of L_λ variation. When the initial data is in G.M.T. hrs, as is the case with geomagnetic data from most of the observatories, a proper longitude correction is applied to the phase angle α_n since the lunar tide depends on local lunar time at the station.

(b) Whole lunation average lunar daily variation (L)

To derive L variation, the above eight sequences of L_λ variations at λ = 00, 03, 06 .....18 and 21 hr are averaged. The resulting sequence represents a lunar daily variation averaged over a lunation and is analysed harmonically for four harmonics according to the equation:

$$L = \sum_{n=1}^{4} L_n \text{ Sin } (n\tau + \phi_n) \quad --- (13)$$

where L_n and ϕ_n denote the amplitude and the phase angle respectively, of the n^{th} component. In lunar tidal studies, the time of maximum positive variation is more meaningful than the phase angle and is given, for the n^{th} harmonic, by the relation

$$\beta_n = \frac{90 - \phi_n}{n} \qquad \text{---(14)}$$

The phases α_n, ϕ_n and β_n may be expressed in degrees or in lunar hr.

(c) Lunar monthly (M) variations at fixed solar hr

The procedure for obtaining M variation is the same as in the first method till the seasonal grouping is done. In each season a series of hourly deviations $a_i(j)$ for the j^{th} day is obtained. Now the analysis is done for a fixed solar hr (i.e. i = constant). For a particular solar hr (say i = 00) the deviations of all the days are grouped according to lunar age 00, 01, 02 .....21, 22 and 23 hr, and average value of all the deviations for a particular lunar age is obtained. Thus a sequence of deviations in terms of lunar age is obtained for a particular solar hour (i = 00 in this case). This process is repeated for each solar hour resulting in 24 sequences, one for each solar hr.

These sequences represent the lunar monthly (M) variations at different solar hours. Each sequence is then harmonically analysed for two harmonics according to the equation:

$$M_t = \sum_{n=1}^{2} r_n \sin (n\nu + \rho_n) \qquad \text{- - -} \quad (15)$$

where r_n and ρ_n are the amplitude and phase angle respectively, of the n^{th} component.

Since the value of 'ν' assigned to a day is referred to Greenwich noon, the following corrections in the phases ρ_n are necessary.

(i) Local time correction.

(ii) Longitude correction.

The lunar age ν_t at local solar time t at any station is related to the lunar age ν_0 at Greenwich noon through the following relation:

$$\nu_t = \nu_0 + 0.0339 \left\{ (t - 12) + \lambda \right\} \qquad \text{- - -} \quad (16)$$

Where λ = longitude of the station expressed in hours and is measured positive east of Greenwich.

The so corrected phase angles (ρ_n) can also be expressed in terms of lunar time using equation (8). In the

present study the phases of lunar monthly (M_1) or lunar semi-monthly (M_2) oscillations are denoted by θ_1 or θ_2 respectively, and represent the lunar time of maximum positive variation i.e. $\theta_n = \{ (90° - \rho_n)/n \}$.

2.4 Probable errors and their significance

Probable errors in the amplitude of the lunar variations are calculated following the method described by KASTOGI (1962b). The estimation of probable errors, in the present study, is done at an earlier stage of analysis rather than calculating them from the harmonic components of the L-variation. Here, the probable error calculations are made along with the calculation of average hourly sequences $b_i(\lambda)$ for each λ value (λ = 00 to 23 lunar hr) from the sequences $a_i(j)$. For a fixed age λ, the value $b_i(\lambda)$ corresponding to the i^{th} hour is the mean of $N_i(\lambda)$ values of deviations $a_i(j)$. The variance of this mean, denoted by $\sigma_i^2(\lambda)$, is calculated as:

$$\sigma_i^2(\lambda) = \frac{1}{N_i(\lambda)} \left\{ \sum_{j=1}^{N_i(\lambda)} a_i^2(j) \right\} - b_i^2(\lambda) \quad \text{---} \quad (17)$$

The weighted mean variance, $\sigma^2(\lambda)$, for all hours i=00 to 23, is then calculated for a fixed age λ as:

$$\sigma^2(\lambda) = \left\{ \sum_{i=0}^{23} N_i(\lambda) \cdot \sigma_i^2(\lambda) \right\} \Big/ \sum_{i=0}^{23} N_i(\lambda) \quad \text{---} \quad (18)$$

The probable error, P.E., in the amplitude of lunar daily variation at a fixed $\mathcal{V}$ value is then calculated as (RASTOGI, 1962b)

$$P.E.(\mathcal{V}) = 0.275 \times \bar{\sigma}(\mathcal{V}) \quad - - - \quad (19)$$

The probable error for the amplitude of whole lunation average lunar daily variation is obtained by first taking the weighted mean of $\bar{\sigma}^2(\mathcal{V})$ for $\mathcal{V}$ = 00 to 23 hr and then using equation (19).

By a similar procedure for a fixed solar hour t, probable errors in the amplitude of lunar monthly variations were also determined.

The magnitude of the probable error determines the significance of the harmonic coefficients of lunar variations of a geophysical quantity. According to CHAPMAN (1951b) the determination of a particular coefficient (i.e. amplitude and phase of lunar variation) is to be considered significant only if its value exceeds three times its probable error.

All the computations, in this thesis, for the lunar variations and their probable errors were done with an IBM 1620 computer with a manual check of intermediate stages.

The various symbols used in this thesis to describe various lunar tidal oscillations and their coefficients are listed below for the sake of clarity.

L — Lunar daily variation averaged over the whole lunation.

L_1 — Lunar diurnal variation averaged over the whole lunation, and also the amplitude of this variation.

L_2 — Lunar semi-diurnal variation averaged over the lunation, and also the amplitude of this variation.

In general

L_n, ϕ_n — Amplitude and phase angle of the n^{th} harmonic coefficient of the L variation (equation 13).

β_n — Time of maximum positive deviation of the n^{th} harmonic component of the L variation; it is related to ϕ_n by equation (14).

L_ν — Lunar daily variation at a fixed lunar age ν.

c_n, α_n — Amplitude and phase angle of the n^{th} harmonic component of the L_ν variation.

M_1, M_2 — Lunar monthly and semi-monthly variation at a fixed solar hour t.

r_1, r_2 — Amplitude of the M_1 and M_2 variations respectively.

Θ_1, Θ_2 — Time of maximum positive deviation of M_1 and M_2 oscillations respectively.

P.E. — Probable error in the amplitude of the lunar variation.

The term "phase" of a variation would mean the time of maximum positive variation unless otherwise specified.

2.5 Lunar atmospheric tides

The regular variations of meteorological parameters such as pressure, temperature and wind, whose periods are fractions of a solar or a lunar day are called " Atmospheric tides". The tide in barometric pressure is predominantly solar semi-diurnal, while solar variations with periods 24 hr, 8 hr, 6 hr and a lunar semi-diurnal variation are also known to exist. The amplitude of the lunar semi-diurnal tide in barometric pressure is maximum, about 90 microbars, at equatorial stations and it decreases to 10-15 microbars at 50°-60° latitude, and is about 1/20 of the amplitude of the solar semi-diurnal tide (CHAPMAN and WESTFOLD, 1956). The phase angle of lunar tide in pressure is 48° to 114° (i.e. maximum occurs at 11-1.5 lunar hr); and that of solar tide is 120° to 170°. (i.e. maximum occurs at 9.3 - 11 hr).

If atmospheric tides are produced because of gravitational forces of the sun and the moon then according to equilibrium theory of tides, the amplitude of lunar semi-diurnal tide (L_2) should be 2.4 times the amplitude of solar semi-diurnal (S_2) tide as actually is the case with oceanic tides. Thus the observed result that S_2 in atmospheric pressure is 20 times L_2 raised doubts regarding the validity of the equilibrium theory. To remove this difficulty Kelvin postulated that the atmosphere has a free period of oscillation very close to 12 hr, thereby enhancing the amplitude of S_2 through

resonance. PEKERIS (1937) and WEEKES and WILKES (1947) supported the resonance theory on the basis of a model atmosphere with an eigenvalue resonant depth of 7.9 km and concluded that the resonance theory accounts adequately for the observed solar semi-diurnal pressure variation. However, JACCHIA and KOPAL (1952), using temperature profiles obtained by rockets, showed that resonance corresponding to eigenvalue depth of 7.9 Km disappears and only very weak resonance may take place. They stressed that the thermal source should be given main importance in explaining the observed amplitude of S_2.

SIEBERT (1961) considered the absorption of solar radiations by water vapour in the troposphere and showed that substantial part of the solar semi-diurnal pressure oscillation may be attributed to the above cause. Further investigations by SMALL and BUTLER (1961) and BUTLER and SMALL (1963) proved the atmosphere to be decidedly non-resonant. They concluded that the main semi-diurnal and terdiurnal tides generated by the direct absorption of insolation by ozone in addition to that by water vapour can adequately account for the observed values at the ground level.

Thus the solar tide in barometric pressure is mainly due to thermal heating, while the lunar pressure oscillations are generated by the gravitational pull of the moon.

The surface temperature also, undergoes a lunar semi-diurnal variation of amplitude 0.0086°C, showing that tidal oscillations of atmosphere are adiabatic (CHAPMAN, 1951). The lunar tidal air-motion, like the tidal pressure oscillation, is very small with an amplitude of 1 cm/sec. However, because of the great variability of the wind, with much larger irregular variations than the lunar tidal amplitudes, no significant determination of lunar tidal wind have yet been made.

2.6 Geomagnetic lunar variations

The lunar influence on geomagnetic data was discovered in 1850 by Kreil. Later, Broun in 1874 studied the lunar tide in declination, D, of the geomagnetic field at Trivandrum for the period 1854 to 1864. He discovered that the lunar daily variation, when determined from a mean of number of lunations, is a semi-diurnal oscillation and that at any particular epoch in the lunation it departs from a pure semi-diurnal character. He determined L_ν variations centred at ν = 00, 03 ..... 18 and 21 lunar hr. At a fixed age ν, the lunar daily variation curve showed two waves of unequal amplitudes; the part of the curve which showed the greatest variation, occurred earlier and earlier in the lunar day as the lunation progressed, and happened during the daylight hours. Similar results in D and H components of the geomagnetic field at Bombay (1846-1872) were obtained by CHAMBERS (CHAPMAN and BARTELS, 1940). Moos (1910) suggested that these luni-solar variations at

fixed ages may be regarded as derived from the whole lunation average lunar daily variation (L) whose amplitude is enhanced for the daylight hours. He expressed the idea mathematically, taking the mean curve (L) as represented by the expression:

$$C \quad \cos (2\tau + \alpha) \qquad \text{---} \qquad (20)$$

The constant amplitude factor C was replaced by another factor A, which itself varies in course of a lunar day, such that A at a fixed ν is greatest during the day-time hours. This was done by writing.

$$A = C (1 - a \cos t) \qquad \text{---} \qquad (21)$$

So that

at midday $t = \pi$; $A = c (1+a)$

and

at midnight $t = 0$; $A = c (1-a)$

Thus the lunar daily variation at a fixed age ν, is given by

$$L_\nu = C (1 - a \cos t) \cos (2\tau+\alpha) \qquad \text{---} \qquad (22)$$

By taking a = 1, Moos compared the theoretical curves given by (22) with the observed curves and found them to be of similar form, which confirmed the idea that lunar daily variation is produced by the moon but that its amplitude is determined by the sun.

CHAPMAN (1913) extended the expression given by Moos (equation 22) by changing solar time t to lunar time τ , and emperically adding a term corresponding to the fourth harmonic component to the resulting identity. The expression thus obtained is

$$L_{\nu} = \sum_{n=1}^{4} C_n \sin \left\{ n\tau + (n-2)\nu + \alpha_n \right\} \quad - - - \quad (12)$$

which is known as Chapman's phase law.

It is seen from (12) that as ν changes from 0 to 2π during a course of a lunation, the phase of first harmonic component decreases by 2π, while that of third and fourth components increase by 2π and 4π respectively; the phase of second component remains unchanged. Owing to the steady change of phase by 2π and 4π during the lunation, all components save the second, whose phase is constant, average out in course of a lunation to give a pure lunar semi-diurnal variation.

Lunar geomagnetic variations are generally supposed to be produced by a lunar semi-diurnal motion of ionospheric layers. The electrical conductivity of these layers is a function of solar time; it is maximum near local noon and is very low during night-time hours. This dependence of the conductivity on solar time is the chief cause of the enhancement of lunar semi-diurnal variations during the day-time

hours, at any particular lunar age. The various harmonic components of L variation arise because of different harmonics in the expression for variation of the conductivity with solar time (CHAPMAN and BARTELS, 1940).

A detailed study of the solar and lunar variations of H and D components of the geomagnetic field at Huancayo and Batavia at different lunar ages, during different solar activity periods, has been made by SCHNEIDER (1936). Further, SCHNEIDER (1963) showed that the following terms, known as "geomagnetic partial tides", also exist, in addition to those described by Chapman's phase law, in the lunar variations of east component ( ) at Batavia during the D-months, and in the result of Chapman's analysis of Greenwich D published in 1925.

$$\left.\begin{aligned} \overline{\overline{=}}_1 &= \xi_1 \sin(\tau + 3\nu + \gamma_1) \\ \overline{\overline{=}}_2 &= \xi_2 \sin(\tau + 4\nu + \gamma_2) \end{aligned}\right\} \quad \text{---} \quad (23)$$

$$\left.\begin{aligned} L_1^* &= \ell_1^* \sin(\tau + \epsilon_1^*) \\ \overline{\overline{=}}_1^* &= \xi_1^* \sin(\tau + 2\nu + \alpha_1^*) \end{aligned}\right\} \quad \text{---} \quad (24)$$

The terms in (23) arise from the semi-diurnal (lunar) component of the air motion, while the terms in (24) are produced from the 24 hourly (lunar) component of the air movement. SCHNEIDER (1963) suggested to restate Chapman's phase law in a generalized form by converting all formulae (equation 12, 23 and 24) to solar time t by means of equation 8. The classical phase law, then, describes the terms $L_n(t)$, the phase of which decrease by 4π during the course of a lunation, regardless of n, whereas the partial tides $\overline{\overline{=}}_n$ have phases increasing by 4π during the lunar month. The partial tides L_n^* and $\overline{\overline{=}}_n^*$, in turn, have phases that decrease by 2π and increase by 2π respectively, in the course of a lunation.

BARTELS (1936) discovered that the lunar variations in the horizontal component of the magnetic field at Huancayo are abnormally large. Later results at other equatorial stations, e.g. at Ibadan (ONWUMECHILLI and ALEXANDER, 1959b), Kodaikanal (RAJARAO and SIVARAMAN, 1958), showed that this feature is typical of all the equatorial stations. From this MATSUSHITA (1962a) inferred that during solar daylight hours, a lunar equatorial electrojet seems to flow in a narrow zone centred on the magnetic equator. This is in analogy with the equatorial electrojet in the solar geomagnetic variation due to high Cowling conductivity during solar day-time (section 1.3). RASTOGI (1963a, b; 1964a, 1965) showed that the latitudinal as well as the longitudinal behaviour of the amplitude

of lunar variation in H-component, at the equatorial stations, is very similar to the corresponding variations of the electrojet current itself. He, therefore, suggested that lunar tides in magnetic field at equatorial stations are closely associated with the electrojet currents. The amplitude L_2 of lunar semi-diurnal variation, or the noon amplitude M_2 of lunar semi-monthly variation of H-component in equatorial zone, is found to be directly proportional to the solar daily range of H(KASTOGI and TRIVEDI, 1970) which confirms the above view.

Geomagnetic lunar variations have been studied by many workers and the results, in all the components of geomagnetic field, are now available at a number of stations all over the globe (MATSUSHITA and MAEDA, 1965a). These results show that the phase of the variation of H-component is reversed at a latitude 35°-40° dip (B_z = 0.2 - 0.3 gauss) which is the latitude of the focus of the lunar current system. By an spherical harmonic analysis of the various results of lunar variations from a total of 37 stations, MATSUSHITA and MAEDA (1965a) obtained external and internal lunar (L) current system, including the lunar equatorial electrojet, in each season for a mean lunation. The lunar current system which is responsible for the semi-diurnal (L_2) geomagnetic variations is shown in figure 4 (after MATSUSHITA, 1967) for E and J-months.

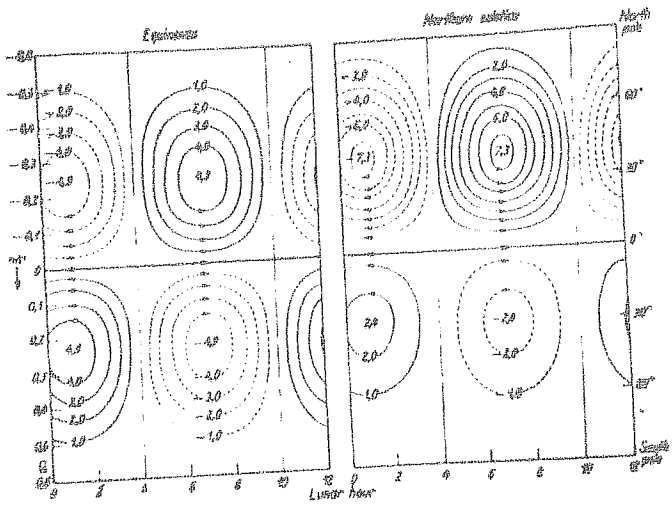


FIGURE - 4

In this thesis, lunar daily (L) as well as lunar monthly (M) variations of the H-component are computed at an equatorial station, Huancayo (Chapter 3) and at a mid-latitude station, San Juan (Chapter 4), and these are studied in relation to the corresponding variations of the ionospheric F_2-region parameters at the two places.

2.7 Lunar tides in the D-region

In the ionosphere, lunar tides are computed as variations of height or critical frequencies of the layers with lunar time. In case of D-region, regular measurements of height and critical frequency is not possible since it rarely

reflects radio waves in the frequency range employed in the routine ionosondes. Lunar tide in this region is, therefore, computed in the absorption of radio waves or in f_{min}, the minimum frequency for which reflection is recorded on the ionograms, which may be taken as an approximate parameter of absorption.

APPLETON and BEYNON (1949) analysed the noon values of absorption using 2 MHz radio wave for a period of six years at Slough, and found a lunar semi-monthly (M_2) variation of amplitude 0.03 nepers (~0.26 db) and its phase was 10.9 lunar hour. Later computations of lunar M_2 tide in absorption at other high latitude stations, e.g. at Pennysylvania (MITRA, 1955) and Freiburg (BOSSOLASCO and ELENA, 1960), gave a phase of about 10 lunar hr which is in confirmity with the result at Slough.

At low latitude stations, however, the phase is found to be 3 lunar hr (SKINNER and WRIGHT, 1964; RASTOGI, 1969c), indicating a possible phase reversal of tide between high and low latitudes. There are results (CHAKRAVARTY and RASTOGI, 1969) indicating that the phase reversal may be taking place at a latitude lower than dip 17° (mag. Lat 9°). The amplitude and phase of the tide are shown to depend on the season and sunspot activity (CHAKRAVARTY and RASTOGI, 1970); the phase in high sunspot years show a semi-annual variation

such that the phase during D-months and J-months is opposite to that during E-months.

BRADY and CROMBIE (1963) analysed routine relative phase observations made during 1962 at Boulder on VLF signals radiated from NPM, Hawaii, and NBA, Canal zone, for any evidence of a lunar variation. They found that the daytime observations of NBA show the presence of a significant semi-diurnal lunar height variation of 0.11 Km; the maximum height occurs 2 hours before lunar transit, which is in good agreement with the phase of M_2 tide in absorption at high latitude stations. The processes causing these variations are, however, not yet understood.

2.8 Lunar variations in the E-region

(a) Normal E-layer

Lunar tide in the ionosphere was first discovered in the virtual height (h') data of the E-layer at Slough by APPLETON and WEEKES (1939). They found a significant lunar semi-diurnal variation (L_2) of amplitude 0.93 km; the maximum height occurred at 11.2 lunar hr. Similar determinations in h'E data at Canberra were made by MARTYN (1948). The amplitude and phase of L_2 tide at Canberra were 0.19 km and 5.1 lunar hr respectively. A larger variation, but with a similar phase to that at Canberra, was found by MARTYN (1950) at Brisbane. These determinations of the tide in h'E were based on the

measurements of the layer height but did not distinguish between the normal E-layer and the sporadic E-layer, E_s, which is known to have large lunar variations (BROWN, 1967; MATSUSHITA, 1967). LITTLEWOOD and CHAPMAN (1955) tried to exclude $h'E_s$ values from h'E data at Ottawa, but used data for a very short period (Oct - Dec 1952). ZAGULYAYEVA ET AL (1967) computed lunar tide in h'E at Ibadan using the data for one year only. The most significant result of L_2 tide in the virtual height of the E-layer seems to be that of ROUGERIE (1961) who used 10 years data at Freiburg. The amplitude L_2 was found to be 0.1 Km with a maximum at 8.5 lunar hr.

The existence of a lunar variation in the critical frequency (f_o) of the E-layer was indicated by MARTYN'S (1948) results at Canberra. The tide was, however, not well determined since the scatter of points on the harmonic dial was so great, that the probable error ellipse enclosed the centre of the dial. ZAGULYAYEVA ET AL (1967) and BROWN (1967) using f_oE data at Ibadan for a period of one year and 14 years respectively, computed lunar tides in it. According to BROWN (1967), the amplitude L_2 (f_oE) is 1 KHz with time of maximum at 10.5 lunar hr. He showed that the phase varies considerably with season so that the amplitude of L_2 tide is very much reduced than that in any individual month which is about 6.5 KHz. He also studied lunar semi-monthly tide at fixed

solar hours and found that there is little variation in the amplitude of $M_2(f_oE)$ at individual hours from the mean for the whole day. This suggests that there is no significant luni-solar variation of tide in f_oE. A small lunar influence in the E-region electron density is also reported by HARNISCH-MACHER (1955). An interpretation of these results would require more determinations of tide at stations at different latitudes.

(b) Sporadic E-layer (Es)

MATSUSHITA (1953) first found that the occurrence frequencies of large values of f_oE_s and of weak or non-existant E_s depend on lunar time. He also computed lunar variations of f_oE_s at five widely spread stations viz. Slough, Washington, Kokubunji, Brisbane and Huancayo. The results show that the amplitude of L_2 tide, at these stations, lies in the range 0.2-0.4 MHz. The phase is similar between stations in middle latitudes and near the magnetic equator; the maximum f_oE_s occurs, at all stations, at 07-08 lunar hr. This was confirmed by WRIGHT and SKINNER (1959) for Ibadan, and by BROWN (1965) for Ibadan and Huancayo. Their results show a seasonal variation of tide; the amplitude being greater in D-months than in J-months. There is an appreciable luni-solar variation of the tide at Ibadan and at Huancayo; the amplitude during daytime being larger than that during night-time (BROWN, 1965).

Lunar tidal variations of $h'E_s$ were first studied by MATUSHITA (1953) using routine published data at a few stations.

THOMAS and SVENSON (1955) have examined the lunar tides in $h'E_s$ for Brisbane and used special night-time measurements only. WRIGHT and SKINNER (1959) computed tide in $h'E_s$ using day-time data at Ibadan. The results, of all the above mentioned authors, show that the phase of $L_2(h'E_s)$ variations is about 6-7 lunar hr at stations in middle latitudes as well as in the equatorial zone. The amplitude $L_2(h'E_s)$, however, is smaller in the equatorial zone than in middle latitudes. This is due to the fact that E_s in the middle latitudes is of a different type and origin to that in equatorial zone where its presence is known to be intimately connected with the equatorial electrojet current system (MATSUSHITA, 1962a).

The equatorial E_s often disappears around noon or early afternoon, if these times lie between 00 and 03 or 12 and 15 lunar hr (MATSUSHITA, 1957). This phenomenon of disappearance was explained by MATSUSHITA (1957) as the weakening of solar equatorial electrojet, which is known to be the cause of the day-time E_s in equatorial zone, by lunar electrojet which flows westward at lunar time 00-03 and 12-15 lunar hr. Dependence of the first appearance of E_s in the morning (KNECHT, 1959) and of the time of disappearance of E_s after sunset (BHARGAVA, 1963) on lunar time lend strong support to the above hypothesis. The various observed results of lunar tide in E_s in the equatorial zone has been explained on the basis of this hypothesis (MATSUSHITA, 1962a).

In the middle latitudes, E_s is supposed to be formed by vertical upward drift of charged particles which are due to the coupling effect between the earth's horizontal magnetic field and the electric fields caused by horizontal winds with a sharp height gradient. The lunar tide in E_s, in this zone, has been explained by MATSUSHITA (1967) as due to perturbations of the above mentioned upward charged particle drift by vertical lunar electromagnetic drifts which are produced by dynamo (lunar) electric fields.

2.9 Lunar variations of the F1 layer

A lunar variation in the height of the maximum electron density (h_p) of the F_1 layer was first determined by MARTYN (1947) at the equatorial station, Huancayo. The amplitude, $L_2(h_pF_1)$ was found to be 0.49 Km with time of maximum at 3.9 lunar hr. Later, MARTYN (1949), using smaller amounts of data for a number of stations throughout the world, determined lunar tides in the F_1-layer. He finds evidence of a semi-diurnal (L_2) variation of $h'F_1$, at all the places studied, but no statistically dependable evidence of a lunar variation in f_oF_1. According to MARTYN (1950), the results, except at Huancayo, of lunar tides in $h'F_1$ must be regarded as provisional in view of the small amount of data used. His results, however, show that the amplitude of $L_2(h'F_1)$ tide is 0.2 - 2 Km, for different stations, and its phase is approxi-

mately 6 lunar hr. The only determination of lunar tide in f_0F_1 is that at Canberra (MARTYN, 1948); the amplitude $L_2(f_0F_1)$ is about 0.13% with time of maximum at 7.5 lunar hr.

2.10 Lunar variations in the F2 region

The ionospheric parameters for which lunar variations have extensively been studied are f_0F_2, the critical frequency of the F_2-layer, $h'F_2$, the virtual height of the layer, and h_pF_2 the height of the maximum electron density N_{max} of the F_2-layer. h_pF_2 is estimated as the virtual height of the layer at a frequency 0.834 times f_0, assuming a parabolic electron density distribution with height. For each layer, N_{max} is related to its critical frequency (f_0) expressed in MHz by the following relation:

$$N_{max} = 1.24 \times 10^4 (f_0)^2 \qquad \text{- - - (25)}$$

Differentiating (25) for small values of Δf_0 and ΔN_{max}, which are deviations from their mean values, we obtain:

$$100 \Delta N_{max} / N_{max} = 200 \Delta f_0 / \text{mean } f_0 \qquad \text{- - - (26)}$$

Thus a small lunar variation in f_0, of an amount Δf_0, gives an approximate estimate of the percentage lunar variation in the maximum electron density of the layer, provided f_0 is known.

The first evidence of lunar tide in this region came when MARTYN (1947) found a large semi-diurnal (L_2) variation in h_pF_2, in $h'F_2$, and in f_oF_2 at Huancayo. The amplitude $L_2(f_oF_2)$ was 0.10 MHz ($\Delta N_{max}/N_{max} \sim 3.4\%$) with time of maximum at 4.3 lunar hr. The amplitude of L_2 tide in h_pF_2 was 5.2 Km which was twice as large as that in $h'F_2$. The phase of $L_2(h'F_2)$ variation (9.2 lunar hr) was retarded by almost an hour on that (8.4 lunar hr) of h_pF_2 variation. By studying the tide in $h'F_2$ and in h_pF_2 during individual seasons, MARTYN (1947) showed that tidal amplitudes in these parameters are greater in D-months than in J-months. From an analysis of lunar monthly (M) tide in f_oF_2 and in h_pF_2 at fixed solar hours, he further showed that the amplitude and phase of the semi-monthly (M_2) tide in these parameters vary markedly with solar time. The amplitude $M_2(h_pF_2)$ ranged from 0.34 km at 02 hour (solar) to as much as 16 Km at 16 hours. The $M_2(f_oF_2)$ variations were found to be larger during solar day-time and very small during night-time; the amplitude $\Delta N_{max}/N_{max}$ ranged from 14.6% at 05 hour to 2% at 07 hour.

(a) Magnetic control of the tide

Later studies of lunar variation in f_oF_2 at other stations showed that there were large changes in both the phase and the amplitude with position of the station (APPLETON and BEYNON, 1948; MARTYN, 1948, 1949; MCNISH and GAUTIER, 1949). From an analysis of noon f_oF_2 data at a number of stations,

MCNISH and GAUTIER (1949) concluded that the phase of $M_2(f_oF_2)$ tide at stations near the geomagnetic equator is about 04 lunar hr, while at stations at geomagnetic latitude greater than 20°, the phase is about 10 lunar hr. Further analysis of lunar variations, e.g. at Singapore (OSBORNE, 1952), Bombay (KOTADIA and RAMANATHAN, 1956), Ibadan (BROWN, 1956) and at Leopoldville (RASTOGI, 1961a), led RASTOGI (1961a) to conclude that the phase of the M_2 tide in noon f_oF_2 is governed by magnetic latitude rather than by geomagnetic latitude; and that the phase reversal between low latitude stations and middle latitude stations takes place around magnetic latitude 10° or magnetic dip 20°.

RASTOGI (1961b) computed M_2 tide in midday f_oF_2 for 18 stations within $\pm$ 40° magnetic latitude for a period of low solar activity. The latitudinal distribution of the amplitude and the phase of these determinations, together with the previous results, are shown in figure 5. The diagram for the phase clearly shows that the phase of $M_2(f_oF_2)$ variation is determined by the magnetic and not by the geomagnetic or geographic latitude. The reversal from the equatorial type of variation (phase equals 4 lunar hr) to the higher latitude type (phase equals 10 lunar hr) occurs at about $\pm$ 11° magnetic latitude.

The amplitude $M_2(f_oF_2)$, expressed either as absolute deviation or as percentage change, shows an enhancement (fig.5)

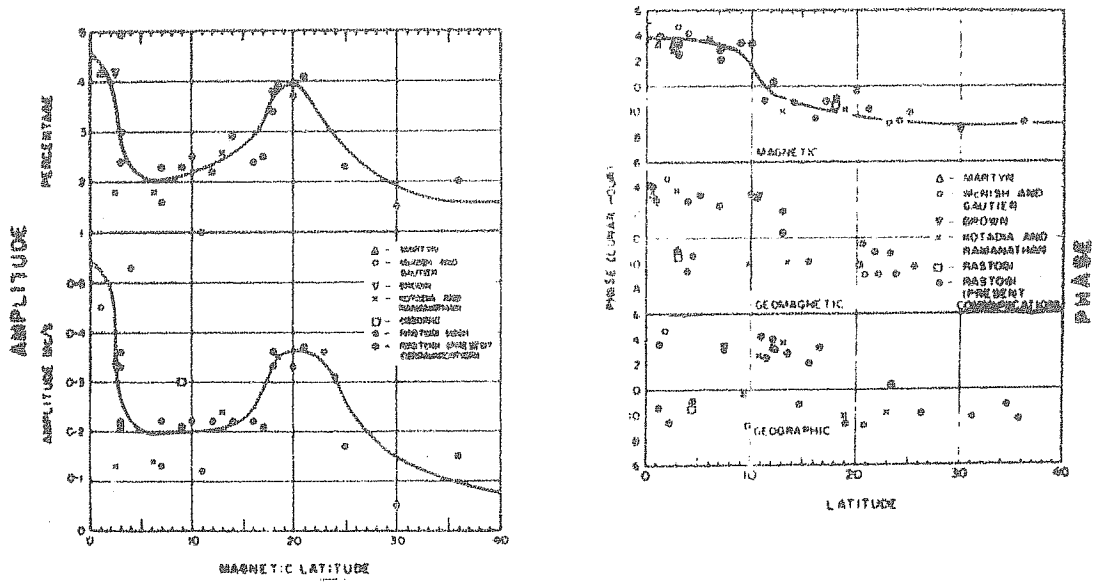


FIGURE - 5

in a narrow belt within ± 3° latitude of the magnetic equator, suggesting a possible association with electrojet. Somewhat broader maxima are also found centred at magnetic latitudes ± 20°; the amplitude at stations near the phase reversal zone (± 11° mag; Lat.) being quite small.

RASTOGI (1964b) further showed that the reversal of phase is most prominent during D-months and is almost absent during J-months. The enhancement of the amplitude at equator and at ± 20° magnetic latitude is also greater during D-months than during J-months.

The phase of $L_2(h'F_2)$ and $L_2(h_pF_2)$ also shows a small latitudinal variation. The maximum of lunar variation in either parameter occurs around 06-07 lunar hr in middle latitudes, and around 08-09 lunar hr in low latitudes. Thus, the phase of f_oF_2 variation (lunar) lags behind that of $h'F_2$ by about 3 lunar hr in middle latitudes, and by 6 lunar hr in the magnetic equatorial zone (MATSUSHITA, 1967). The amplitude of $L_2(h_pF_2)$ variation tends to increase with decreasing latitude (MARTYN, 1950).

(b) Luni-solar variations

MARTYN (1947, 1948) first showed that lunar tidal amplitudes in f_oF_2 and h_pF_2, both at Huancayo and Canberra, depend on solar time. This dependence was termed as luni-solar effect by him. The effect was confirmed when BURKARD (1951) found that the amplitude of tide calculated from day-time f_oF_2, at Huancayo, is almost four times larger than the amplitude calculated from all day f_oF_2; and that the night-time f_oF_2 does not show any lunar tidal variation. This effect in f_oF_2 is investigated for individual stations by a number of workers (e.g. BROWN, 1956; RASTOGI and ALURKAR, 1964, 1966; RASTOGI, 1968a, c, 1969b). Recently RUSH and VENKATESHARAN (1968) have studied luni-solar variations at a number of stations in low latitudes. The results of these studies show that the amplitude of lunar variation in f_oF_2 is larger for hours near the solar noon and is insignificantly small during

the night-time hours. The phase of $M_2(f_oF_2)$ tide also varies considerably with solar time at all the places. The Chapman's phase law is shown to be valid for lunar oscillations in f_oF_2 also (RASTOGI, 1968a, 1969a).

The luni-solar effects in $h'F_2$, h_pF_2 and Y_mF_2 which is the semi-thickness of the F_2-layer, at Ibadan were investigated by BROWN (1956). The M_2 oscillations in all the parameters are greater for hours near the solar midday. RASTOGI (1969a) showed that h'F ($h'F_1$ during daytime) at Huancayo shows a large luni-solar effect, and that the amplitude of tide was maximum at about 21 solar hr.

Recently, SHARMA and RASTOGI (1969, 1970a) have shown that all the parameters of the F_2-region viz. N_{max}, h_{max} (the true height of the N_{max}), Y_m and N_t (total electron content upto h_{max}) indicate a luni-solar variation.

(c) Seasonal effects

MARTYN'S (1947, 1948) analysis of lunar variation of $h'F_2$, h_pF_2 and f_oF_2 at Huancayo and at Canberra indicated that the amplitude of L_2 variation in the above parameters were greater in D-months than in J-months; and that the phase changed appreciably with season. This result was supported by BARTELS (1950) who showed that the amplitude of day-time f_oF_2 lunar tide at Huancayo in local summer (D-months) was about five times larger than in local winter (J-months). RASTOGI (1963c) analysed the midday value of f_oF_2 and h_pF_2 at all

the Indian stations to study the seasonal effects. The amplitude $M_2(f_oF_2)$ was found to be always greater in D or E-months than in J-months, while the phase varied by about 180° with seasons at all the stations. The tide in h_pF_2, however, did not change much with season.

By studying all the available results of $M_2(f_oF_2)$ tide for solar midday hours, RASTOGI (1964b) confirmed this seasonal dependence of the amplitude. The phase varied with season by about 2-3 lunar hr at subtropical latitudes and by less than 2 hours at equatorial latitudes. The available results of lunar variation in h_pF_2 indicate that these are stronger in D-months than in J-months (MATSUSHITA, 1967). Further, all the parameters of the F_2-region at Huancayo and at Puerto Rico show such a seasonal dependence in their tidal amplitudes (SHARMA and RASTOGI, 1969, 1970a). Thus the lunar tidal perturbations of F_2 region are, in general, stronger in December solstices and weakest in June solstices, independent of the location of the station.

(d) Correlation with geomagnetic tides

Even the earliest results of lunar tide in the F_2-region indicated the effect to be larger at the equatorial stations. The latitudinal behaviour of the amplitude and phase of the tide in now known to exhibit a distinct magnetic (dip) control. RASTOGI (1962b), computing M_2 tide in midday f_oF_2 for the two chains of stations near the magnetic equator

in South America and India, showed that the amplitude has a sharp maximum at the magnetic equator(see figure 6). Further, the amplitude showed a systematic variation with longitude along the magnetic equator; the maximum occurred in the American zone (about 0.63 MHz) and the minimum in the Indian zone (about 0.33 MHz). These features are similar to those exhibited by the solar daily range of H, $S_q(H)$ and the lunar tidal effects in H (section 1.3 and 2.6). Thus the lunar tidal variations of f_0F_2 and H, at equatorial stations, seem to be correlated with each other and are associated with the equatorial electrojet.

To study, in detail, the relations between the lunar tidal effect in f_0F_2 and the electrojet, the harmonic coefficients (r_2, θ_2) of M_2 tide in midday f_0F_2 at Huancayo for the period 1938-46 plus 1951-60 (RASTOGI, 1963d), and in range of H for the period 1922-39 (BARTELS and JOHNSTON, 1940) for each month are shown in the harmonic dial of lunar age in figure 7. It is seen that the amplitude r_2 in both the parameters is maximum in January and minimum in June-July. The phases θ_2 of M_2 (f_0F_2) and M_2 (range in H) tide, for any month, are opposite to each other and they vary from month to month maintaining this antiphase relationship. Thus a close interrelationship of lunar tide in f_0F_2 and in H may be established even in their seasonal behaviour.

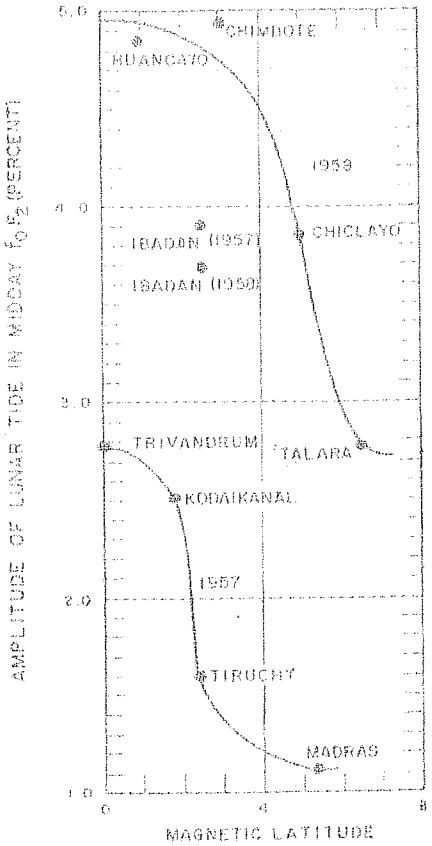


FIGURE - 6

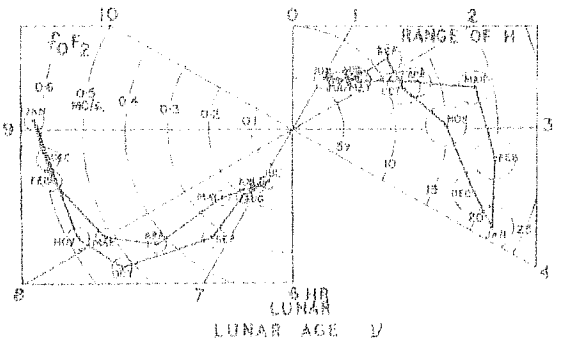


FIGURE - 7

RASTOGI (1965, 1968a, 1969a) and RASTOGI and ALURKAR (1966) compared the lunar daily variations, at fixed lunar age (L_ν), of f_0F_2 and of H at Huancayo. Their results show that, at any lunar age, the variations in both the parameters are larger for the solar daytime than night-time hours; and that the curves for f_0F_2 and H have almost opposite phases. The whole lunation average lunar daily variations (L) in these parameters also exhibit this antiphase relationship. Also, the solar daily variation of the amplitude $M_2(f_0F_2)$ and $M_2(H)$ show similar features. The amplitude in both f_0F_2 and H is very small during the night-time hours, starts increasing in the morning, and is maximum near or just after midday.

Further, the amplitude of L_2 variations of both f_0F_2 and H at Huancayo are shown to increase with solar activity, while their phases remain constant (RASTOGI, 1968a, 1968b, 1969a).

It thus appears, from the above discussions, that the lunar tidal variations in the F_2 region at equatorial stations are directly associated with the corresponding variations of the horizontal component of the magnetic field.

CHAPTER - III

INTERACTION OF GEOMAGNETIC AND IONOSPHERIC LUNAR TIDES AT MAGNETIC EQUATOR

3.1 Introduction

It is now well known that lunar tides in the F_2 region of the ionosphere exhibit a strong geomagnetic control; and that the lunar variations of f_oF_2 at equatorial stations are closely associated with the geomagnetic lunar variations (section 2.10). RASTOGI (1969a) computed lunar tides in f_oF_2 and h'F at Huancayo to explain the variations of peak ionisation density in the F_2 region. He concluded that simultaneous oscillations in f_oF_2 and height of F_2 region could not be established from the h'F data because h'F does not correspond to the height of peak F_2 ionisation density ($\simeq f_oF_2$) and is associated with F_1 rather than F_2 layer during the daytime. He suggested that lunar tidal oscillations in f_oF_2, $h_{max}F_2$ and H would clarify the interrelations between the lunar tidal oscillations in geomagnetism and ionosphere near the magnetic equator. With this view the computations of the lunar-daily and lunar-monthly tides (according to methods described in section 2.3) in magnetic field as well as in various parameters defining the structure of the F_2 layer at Huancayo (Geograph. Lat. 12°02'S, Lon. 75°20'W) were undertaken.

This chapter describes the lunar-daily (L) and lunar-monthly (M) variations in horizontal magnetic field (H), maximum electron density (N_{max}), height of the ionization peak (h_{max}), semi-thickness of the F_2 layer (Y_m) and the total electron content (N_t) in a vertical column upto the peak of the F_2 layer at Huancayo for the period January 1960 to December 1961.

The geomagnetic data used in the present analyses were kindly supplied by Mr.A.A. Giesecke and the F_2 parameters were taken from the electron density profiles computed and made available through the kind courtesy of Mr.J.W.Wright. A part of the work has already been published (SHARMA and RASTOGI, 1970a).

3.2 Perspective view of the annual average luni-solar variations

The annual average variations of the deviations in N_{max}, H and h_{max} on the co-ordinates of lunar time and lunar age are shown in figure 8. The shaded portions in the diagram indicate the solar night period. Referring to the diagram of H, one notices that within one lunar month there are two maxima and two minima of the deviations, the centres of which lie very close to local midday indicating the predominance of lunar semi-diurnal or semi-monthly tide. The largest density of contour lines happens during the midday hours and very few lines are present for the night-time hours. This indicates

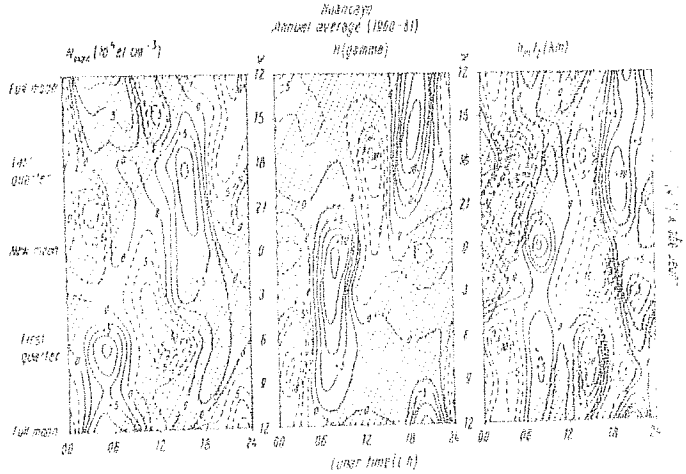


FIGURE - 8

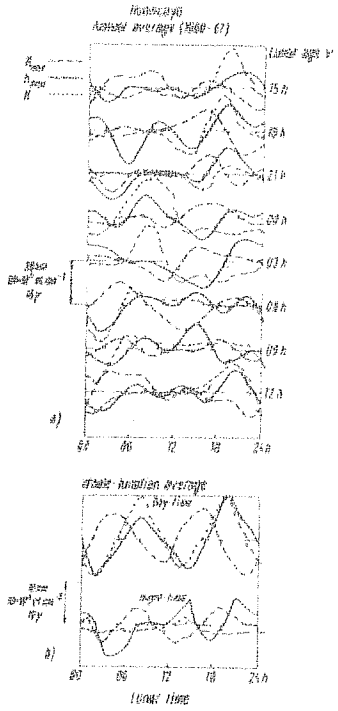


FIGURE - 9

that lunar tidal oscillations in H are strongest for the midday hours and are very small during nighttime. This is in confirmity with the computations done for other periods of solar activity (RASTOGI, 1968a, b). Referring to N_{max}, one again finds two maxima and two minima during one lunar month but the centres of these are shifted towards the evening hour. Further, there are sufficient number of contour lines for the nighttime hours. Thus though the lunar tide in N_{max} is semi-diurnal in character and is large mainly during the

daytime, these are not insignificant during the nighttime as in the case of H. Referring to the diagram for the height of the peak ionization h_{max}, one finds large number of loops, thus both the lunar diurnal and semi-diurnal character is evident. The density of contour lines is rather more in the night hours than for the day hours in contrast to that in H or N_{max}. It is seen that during the nighttime although the variations in peak electron density is low, the variations in the height of peak electron density are quite appreciable. The contour diagrams of N_t and Y_m are similar to those of N_{max} and h_{max} respectively, and hence are not shown.

The lunar daily variations in N_{max}, h_{max} and H averaged on three hourly groups of lunar ages for the whole period under study are drawn in figure 9 (a). It is seen that the curves for H and N_{max} show large deviations for the daytime hours and the curves are almost opposite in phase to each other. The curves for h_{max} show large deviations for the daytime as well as for night-time. The daytime curve is very similar to that of H.

To compare the lunar tides in daytime and in nighttime, whole lunation average deviations in N_{max}, h_{max} and H are computed separately for the daytime and nighttime and are shown in figure 9(b). It is seen that lunar tides are much stronger during daytime than in nighttime in any of these parameters. During daytime, the lunar variations in H and

h_{max} are almost identical; and in the nighttime the tides in h_{max} decrease to about half of their daytime values. No significant tides are seen in H during nighttime.

The lunar variation curves for individual lunar ages are harmonically analysed according to the equation (12). The harmonic coefficients C_n and α_n (upto n = 4) for each I_λ curve (at λ = 00, 03 .....18 and 21 lunar hour) for H, h_{max}, N_{max}, Y_m and N_t are collected in table 1, 2, 3, 4 and 5 respectively (see appendix for tables). The annual average coefficients C_n and α_n averaged over eight lunar ages are also given for each parameter in respective tables. The units for amplitudes C_n for each parameter are as under:

H	Gamma = 10^{-5} Guass
h_{max}	Km
N_{max}	10^4 Electrons/Cm^3
Y_m	Km
N_t	10^{11} Electrons/Cm^2

The amplitudes of lunar tidal variations in these parameters will always be expressed in these units unless otherwise specified. The phases α_n are given in degrees and so will be ϕ_n's. It is seen that the amplitudes of first

and second harmonics on individual days are almost of the same order, for any of the parameters (Tables 1 to 5); the second harmonic being only slightly larger than the first, and higher harmonics rapidly decrease with increasing order of harmonics. From the tables, it is noticed that the phases of $L_2(\mathcal{V})$ oscillations in H and h_{max} differ only by 01 lunar hr while between h_{max} and N_{max} it differs by 4 lunar hr. The oscillations of Y_m and N_t are almost in phase with that of h_{max} and H respectively.

To compare the interrelationships between the lunar tides in these parameters, the lunar variations averaged over whole lunation (L) are shown in figure 10. It is very clearly seen that the lunar daily variation in H is very similar to that in h_{max}, indicating that an increase or decrease in H causes almost simultaneous increase or decrease in the height of the F_2 peak. The variations in N_{max} are nearly opposite in nature to that of h_{max}. The minimum or maximum in N_{max} occurs about 1-2 hours after the maximum or minimum respectively of h_{max} indicating that a rise or fall in the height of F_2 peak causes, respectively, a diminution or enhancement in the electron density with some delay. The lunar variations in Y_m is similar to that of h_{max} though smaller in amplitude indicating that although the various levels of F_2 region are similarly affected, the amplitude of oscillation is larger at the top rather than at the bottom of

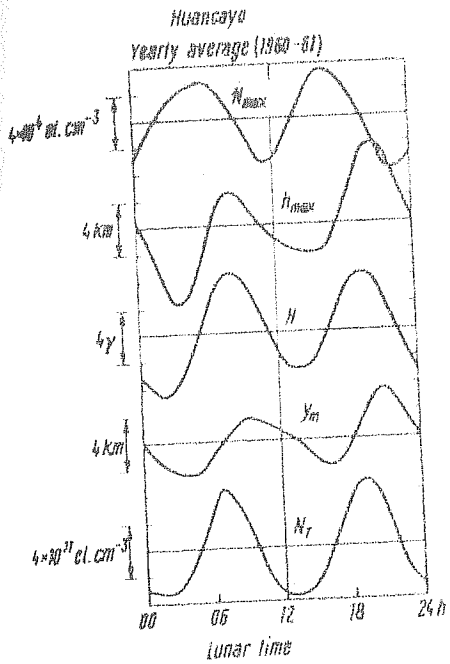


FIGURE - 10

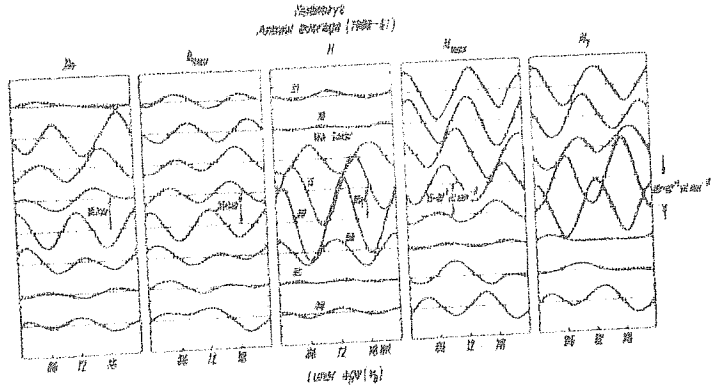


FIGURE - 11

the F_2 layer. The phase of total electron content curve is same as the phase of H or h_{max}.

These whole lunation average curves (L) are harmonically analysed according to equation (13) and the coefficients L_n and ϕ_n are given in table 6. The coefficients of lunar oscillations in H and F_2 parameters at Huancayo computed by earlier workers are also given in the table for comparison. It is seen that most prominent oscillation in any of the parameters is lunar semi-diurnal. The amplitude of lunar

diurnal oscillation (L_1) is much smaller as compared to the corresponding value for individual lunar days (mean C_1 in tables 1 to 5). This means that lunar diurnal component present on individual days appreciably, cancel out on averaging over the whole lunation. Similarly the third and fourth harmonics are reduced to insignificantly small magnitudes. It is noticed that the phase of $L_2(H)$ is 213° during 1951-55, 211° during 1957-59 and 223° during 1960-61. Thus the lunar tide does not seem to change its phase with solar cycle. This is analogous to earlier findings for the lunar tidal oscillations in the daily range of H by BARTELS and JOHNSTON (1940). The $L_2(N_{max})$ in the present study has a phase of 301°, while the phase of $L_2(f_oF_2)$ for the period 1951-55 is 331°, and for the period 1942-44 is 330°. L_2 oscillation in h_{max} according to MARTYN (1947) had a phase of 197° while the present analysis yields a phase of 182°. It is thus seen that the phases of lunar oscillations in H and the F_2 parameters in the present study are tallying reasonably well with similar determinations by previous workers.

3.3 Annual average lunar monthly variations

At fixed individual solar hours the lunar monthly oscillations are computed. The curves built up from the first two harmonics, at fixed solar hours, for all the parameters studied, are presented in figure 11. It is seen from the figure that the lunar monthly variations in all the parameters

at any hour of the day is predominantly semi-monthly in character. Referring to the diagram of H, one finds that $M_2(H)$ oscillations are very large in daytime (09-15) hours and are insignificantly small during nighttime. The M_2 component in h_{max} oscillations is evident for all the hours of of the day and night, but the amplitudes are large for the period 09-18 solar hr. In the case of N_{max}, the oscillations are largest during afternoon and evening (15-21) hours and is least in the early morning (06) hours. $M_2(N_t)$ exhibits largest variation around midday and is least during morning time. Y_m experiences similar monthly oscillations to those in h_{max}, but of lesser amplitude.

The amplitude (r_1) and phase (Θ_1) of lunar monthly variations at individual solar hours for each parameter are plotted on the harmonic dials of lunar age (λ) and lunar time (τ) in figure 12 and 13 respectively. The open and full circles in the diagrams represent the points for solar daytime and nighttime respectively. In case of H, the amplitude r_1 at any solar hour is found to be statistically insignificant. However, the phase Θ_1 shows some systematic variation with local solar time and hence is described here. It is seen from figure 12, for H, that on lunar age dial the daytime points cluster in a narrow sector between 19-21 lunar hr, while the nighttime points are grouped in the opposite sector between 5-9 lunar hr. Thus the maximum deviation due to M_1 tide occurs around the same lunar age i.e. around the same day.

HUANCAYO, ANNUAL, 1960-61.

LUNAR MONTHLY TIDE

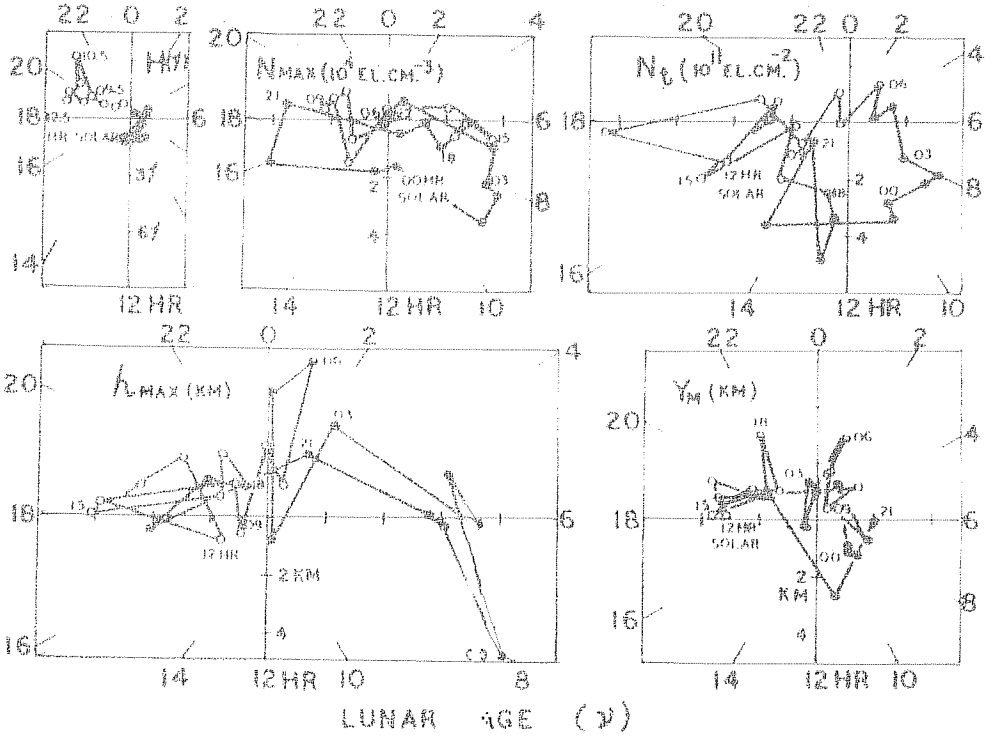


FIGURE - 12

HUANCAYO, ANNUAL, 1960-61.

LUNAR MONTHLY TIDE

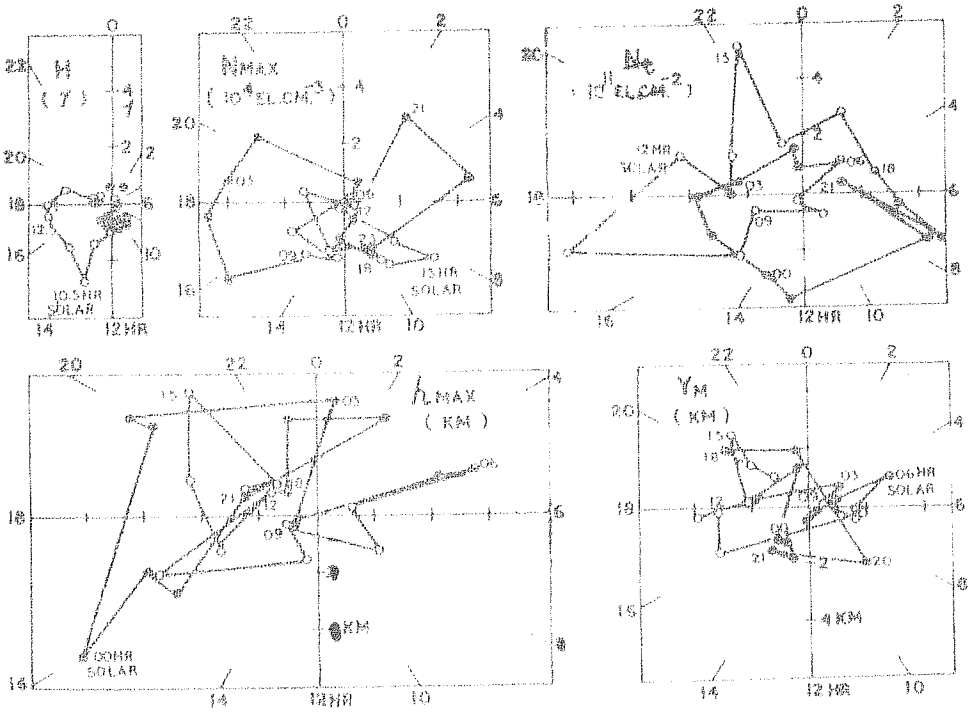


FIGURE - 13.

On the lunar time dial (fig.13), (r_1, θ_1) points move systematically round the origin such that the vector mean of all hours is reduced to a insignificant low value, which is anologous to the vanishing of $L_1(\nu)$ oscillation when averaging is done over the whole lunation. Thus it appears that $M_1(H)$ tide is controlled by some cause depending more on the lunar age rather than on lunar time. These findings are in confirmity with the earlier results of $M_1(H)$ at Huancayo (RASTOGI, 1968a, b) for other epochs of solar activity.

The amplitudes r_1 of $M_1(N_{max})$ tide, except of 01, 02 solar hr, are statistically insignificant. There is, also, no systematic variation of phase with solar time (fig.12, 13). However, the amplitude r_1 seems to be greatest near solar midnight hours.

The amplitudes $r_1(h_{max})$ are significant only for 00-01, 11, 15 and 23 solar hr; while $r_1(Y_m)$ is statistically insignificant at all hours except at 11, 13 and 15 solar hr. The (r_1, θ_1) points, both for $M_1(h_{max})$ and $M_1(Y_m)$ do not show any systematic variation with solar time either on lunar age or lunar time dial.

The r_1 amplitude of $M_1(N_t)$ tide is statistically insignificant for all hours except at 11 and 15 hr. On lunar age dial (fig.12), the daytime and nighttime points show opposite phases. On the lunar time dial, these points seem to move around the origin with progress of solar time.

The amplitude (r_2) and lunar time of maximum positive deviation Θ_2 (expressed in lunar hr) of lunar semi-monthly tide in H, h_{max}, N_{max}, Y_m and N_t, at individual solar hours, are presented in Table 7, 8, 9, 10 and 11 respectively. The mean probable error in the determination of r_2 for different parameters are also included in the respective tables. The amplitudes which are less than three times their probable error and hence are statistically insignificant are bracketed. It is noticed from the tables (7-11) that the tidal amplitudes in any parameter, are statistically significant during the daytime hours only. The average solar daily variation of the parameters along with their amplitudes (r_2) of semi-monthly (M_2) tide at different solar hours are plotted in figure 14.

Referring to the curves for H, one finds that the solar daily variation of $r_2(H)$ is identical to that of H itself. Both H and $r_2(H)$ are maximum slightly before midday and are very small during nighttime. This is in confirmity with the results of previous workers (RASTOGI, 1968a, b) for other periods of solar activity.

The amplitude $r_2(h_{max})$ has two peaks, one in the forenoon hours and another in the afternoon. It is seen that h_{max} itself is very high in the evening hours when $r_2(h_{max})$ is also maximum.

The amplitude $r_2(Y_m)$ has also two peaks which occur roughly at the same time when $r_2(h_{max})$ is high. The $r_2(Y_m)$

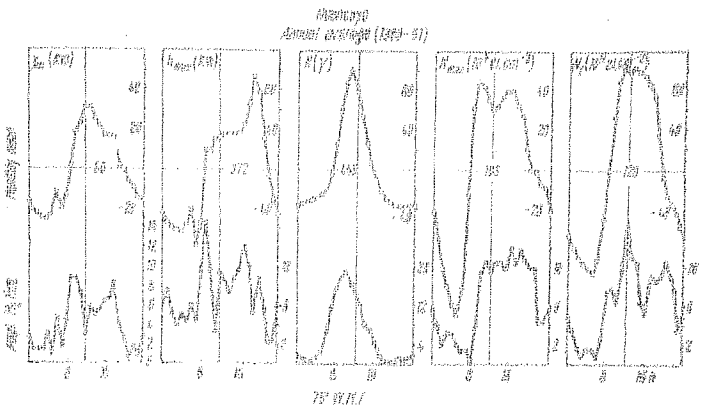


FIGURE - 14

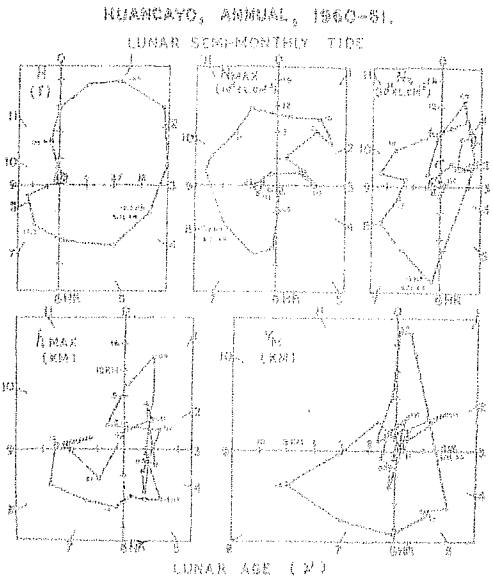


FIGURE - 15

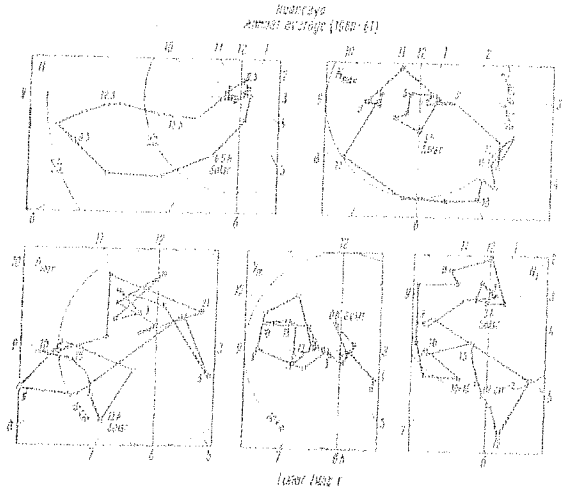


FIGURE - 16

shows a similar variation to that of $r_2(h_{max})$ but is smaller by a factor of two.

The $r_2(N_{max})$ amplitude varies with solar time in a similar manner to that of N_{max} variations but with a time lag of few hours. It is seen from the figure (14) that while N_{max} starts increasing at about 05 hr after reaching its minimum value in the early morning, the amplitude $r_2(N_{max})$ continues to diminish and starts increasing only after 04 hr. N_{max} is largest at 09 and 15 solar hours but $r_2(N_{max})$ is largest during the evening hours.

The amplitude $r_2(N_t)$ is maximum around midday when N_t itself shows a peak; but it rises again to a high value in the afternoon hours, while N_t values gradually decrease after midday.

Both the amplitude and phase of M_2 oscillations can be simultaneously described by the harmonic dial. The amplitude and phase (r_2, θ_2) of M_2 tide, in all the parameters, at each solar hr, is shown on the harmonic dial of lunar age (ν) and lunar time (τ) in figure 15 and 16 respectively. The diagrams for H show an increase of amplitude with sunrise with a maximum, a few hours before midday, and then a decrease till sunset. On the 'ν' dial (fig.15), the (r_2, θ_2) points for H move progressively around the origin with solar time; while the points for the night-time hours, though smaller in amplitude, group within a narrow sector between 09-10 lunar hr.

On lunar time (τ) dial (fig.16), the night-time points move round the origin and the day-time points are confined in a narrow sector between 08-09 lunar hr. Thus the phase of $M_2(H)$ at any solar hr is controlled by lunar time, i.e. by absolute position of the moon, rather than by lunar age, which is in confirmity with KASTOGI's (1968a, b) results at Huancayo for other periods of solar activity.

The lunar age dial for N_{max}(fig.15) shows a broad loop; the amplitude r_2 has a very broad maximum between 10-18 solar hr, while the phase Θ_2 within this period changes by about 180°. On the τ dial (fig.16), the points again show a broad loop, but the (r_2, Θ_2) points for 10-18 solar hr are all grouped together around 04 lunar hr. This behaviour of $M_2(N_{max})$ tide is similar to that in H. However, unlike H, the amplitude $r_2(N_{max})$ does not decrease after 18 solar hr but there is appreciable change of phase till about 21 solar hr after which the amplitude drops rapidly. It should be noted that the phase of $M_2(N_{max})$ tide during day-time hours lags behind that of $M_2(H)$ by about 05 lunar hr.

The (r_2, Θ_2) points for h_{max} seem to move round the origin on lunar age dial (fig.15); and the maximum value of r_2 occurs at 09 lunar hr. On the lunar time dial (fig.16), these points do not show any significant loop like those for H or N_{max}; but it is distinctly seen that all the points for the daytime hours are grouped within the sector 07-09 lunar hr,

while the points for the nighttime are grouped within the sector 11-01 lunar hr. Thus similarity in the phases of $M_2(H)$ and $M_2(h_{max})$ oscillations for individual solar hours is indicated for the daytime observations.

The harmonic dial on lunar age (fig.15) for $M_2(Y_m)$ tide shows that the amplitude r_2 is quite small during the night-time hours; and that the day-time points show larger amplitudes with phases changing continuously with the solar time such that they form a loop around the origin. The diagram for Y_m is quite similar to that of h_{max} indicating that the lunar oscillations in both are similar. The day-time (r_2, θ_2) points, on lunar time dial (fig.16), group themselves around 09-10 lunar hr indicating that the phase of Y_m tide lags behind that of h_{max} by about 01-02 lunar hr.

The harmonic dial on lunar age (fig.15) for N_t shows that the day-time points move around the origin; the maximum amplitude r_2 happens at 12 solar hr. The night-time points on 'ν' dial are grouped in the sector between 00-03 lunar hr. The daytime points, on τ dial (fig.16), have phases around 06 lunar hr, while the night-time points show changing phases with solar time. Thus the behaviour of M_2 oscillations in N_t is similar to $M_2(N_{max})$ variations. The phase of daytime $M_2(N_t)$ oscillations which is 06 lunar hr may be due to the fact that N_t is a product of N_{max} and Y_m which have phases 04 and 09 lunar hr respectively.

3.4 Seasonal effects in lunar daily variations (L_ν, L)

The lunar daily (L) as well as lunar monthly (M) variations of each parameter were computed separately for each season viz., D, E and J-months. The results of L_ν and L variations in all the parameters are described in this section, while the M variations will be discussed in the next section (3.5).

(a) H-component

The values of $\triangle H$ as a function of lunar time and lunar age are shown as contours of iso $-\triangle H$ values in figure 17 for all the three seasons. In any season, the contour lines are concentrated mostly in the day-time hours and very few lines are seen in the night-time hours (shaded portion), suggesting that L_ν(H) variations are larger during the day-time hours. Also in any season, one observes two high and two low loops indicating the predominance of lunar M_2 component. The loops are centred at about noon showing that maximum tide occurs near midday hours. The density of contour lines is seen to be more in D or E months than in J-months, which indicates that the tidal effects are larger in D or E months.

The lunar daily variations (L_ν) of H, centred at ν=00, 03 .....18 and 21 lunar hr, for each season, are shown in figure 18 and their coefficients C_n and α_n are given in table 1. It is seen from table 1 that the amplitudes

HUANCAYO, H, 1960-61.

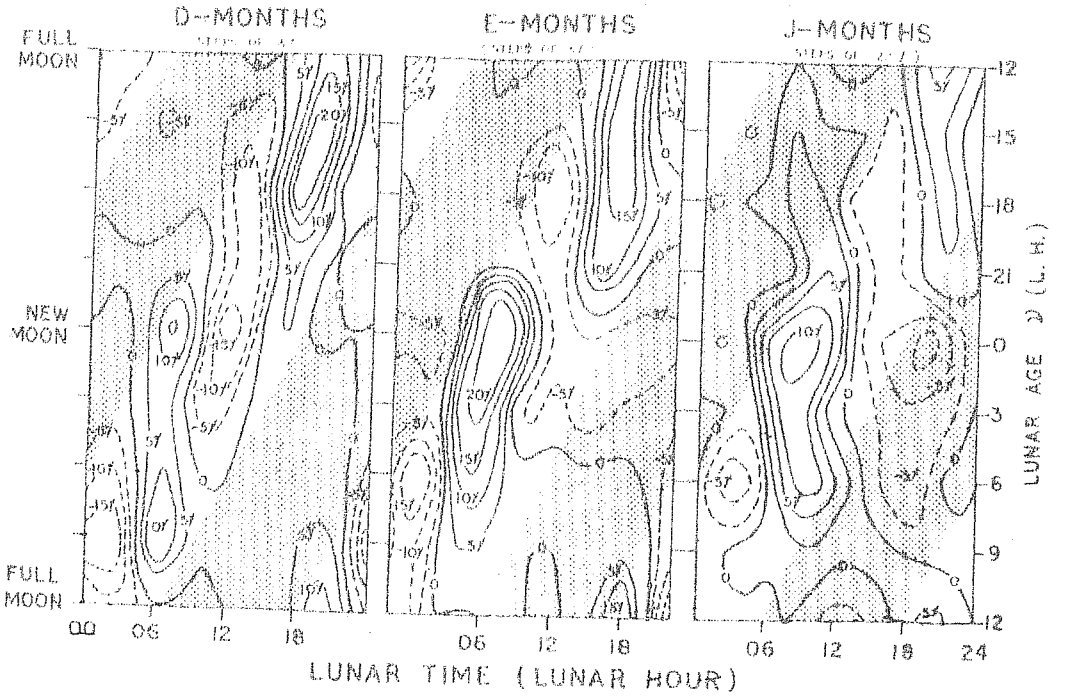


FIGURE - 17

HUANCAYO , H , 1960 - 61

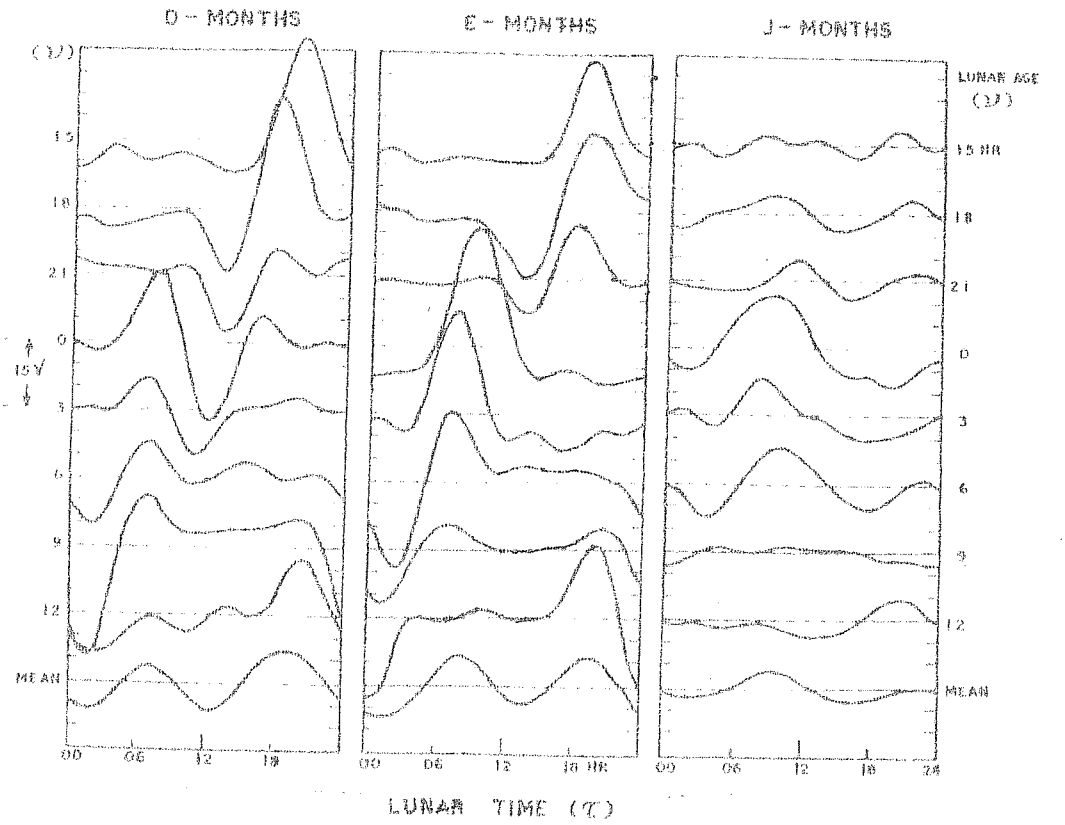


FIGURE - 18

C_1 and C_2, in any season, are of comparable magnitude and these are greater than the higher harmonics C_3 or C_4. At any particular age ν, the amplitudes C_2 in D and E-months are of the same order and are greater than C_2 during J-months. The same general conclusions are borne from figure 18.

The whole lunation average curve (L) is also shown in fig.18, for each season, and its coefficients L_n and ϕ_n, for only n upto 2 since higher harmonics are insignificantly small, are given in table 12. The L(H) variation in any season is found to be mainly semi-diurnal (fig.18). It is seen from table 12 that in D and E months the amplitude $L_2(H)$ is greater than $L_1(H)$; but during J-months, $L_2(H)$ is small and is of the same order as $L_1(H)$. Also $L_2(H)$ is maximum in E months, slightly less in D-months, and minimum in J-months.

(b) Ionospheric parameters

The lunar daily variation curves (L_ν) at eight lunar age groups during each season are shown for h_{max}, N_{max}, Y_m and N_t in figures 19, 20, 21 and 22 respectively; while the harmonic coefficients C_n and α_n of these curves are collected in tables 2, 3, 4 and 5 respectively. The whole lunation average curve (L) in each parameter during different seasons is also shown in the respective diagrams, and the coefficients L_n and ϕ_n are collected in table 12. It is seen from the diagrams 19-22 that L_ν curves for any parameter and season

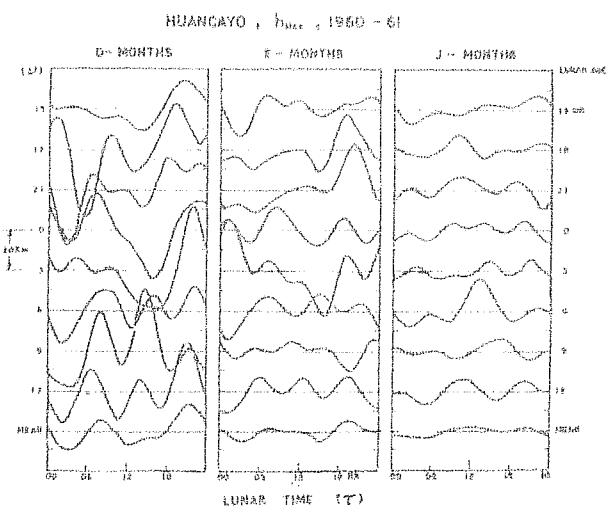


FIGURE - 19

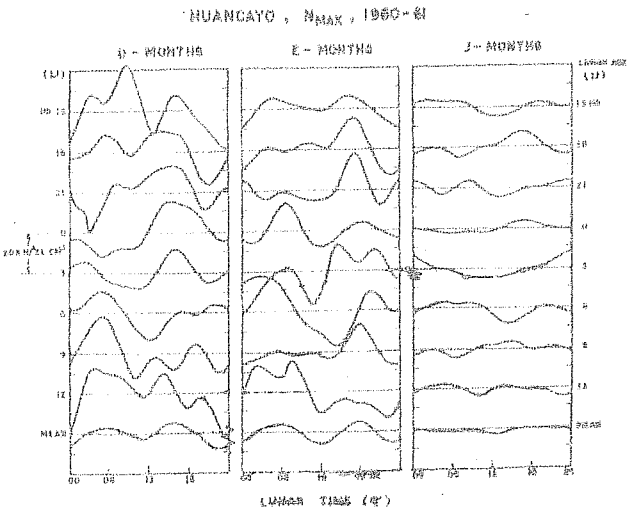


FIGURE - 20

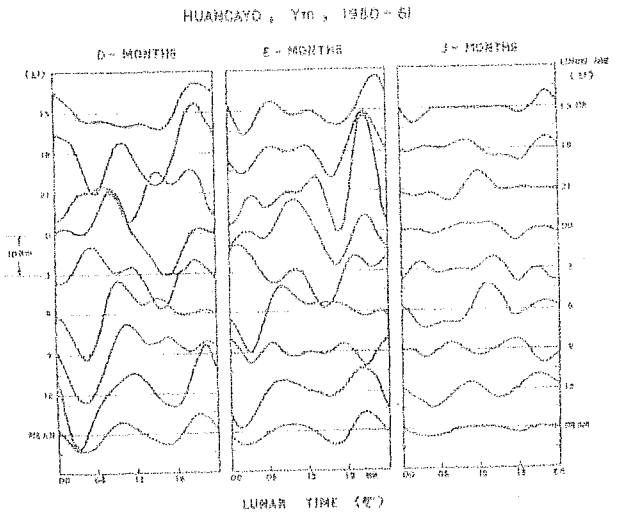


FIGURE - 21

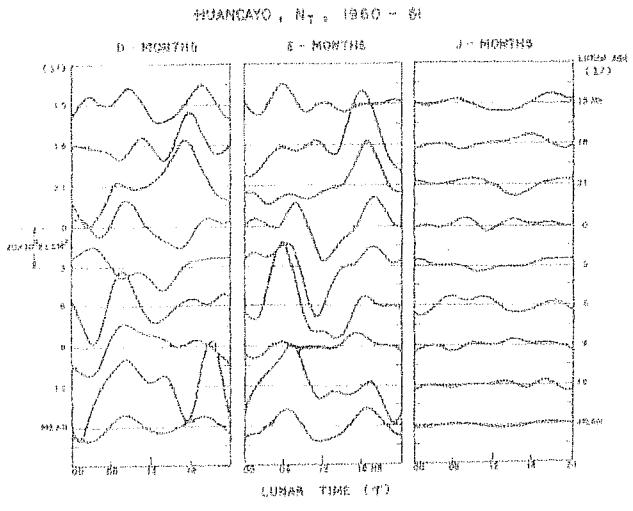


FIGURE - 22

indicate the presence of many harmonics. Tables 2-5 show that at a fixed age λ, the amplitudes C_1, C_2 and C_3 in any particular season and for a particular parameter are roughly of same magnitude and are slightly greater than C_4. The lunar tidal amplitudes, in any parameter, are seen to be greater in D and E months than in J-months.

The average L variation curve in any season shows a predominant semi-diurnal variation in case of N_{max}, Y_m and N_t (fig. 20-22), but an appreciable diurnal (L_1) component is seen to be present in the $L(h_{max})$ variations (fig.19). Table 12 shows that the amplitude L_2, in any parameter and season, is greater than L_1. Also, the lunar semi-diurnal (L_2) variation of N_{max} and N_t are greatest in E-months, slightly less in D-months, and are least during J-months. The $L_2(h_{max})$ and $L_2(Y_m)$ oscillations have maximum aplitudes during D-months, less in E-months, and minimum during J-months.

(c) Correlation between geomagnetic and ionospheric L variations

The whole lunation average lunar daily variations (L) of H and ionospheric parameters in each season are redrawn in figure 23. It is seen that during D and E months, the h_{max} variations follow the variations in H, while N_{max} varies in a opposite manner to that in h_{max} with a delay of about 1-2 hr; the $L(N_t)$ and $L(Y_m)$ variations are similar to L(H) and $L(h_{max})$ variations respectively. The L variations during J months are very small and the correlation is not evident.

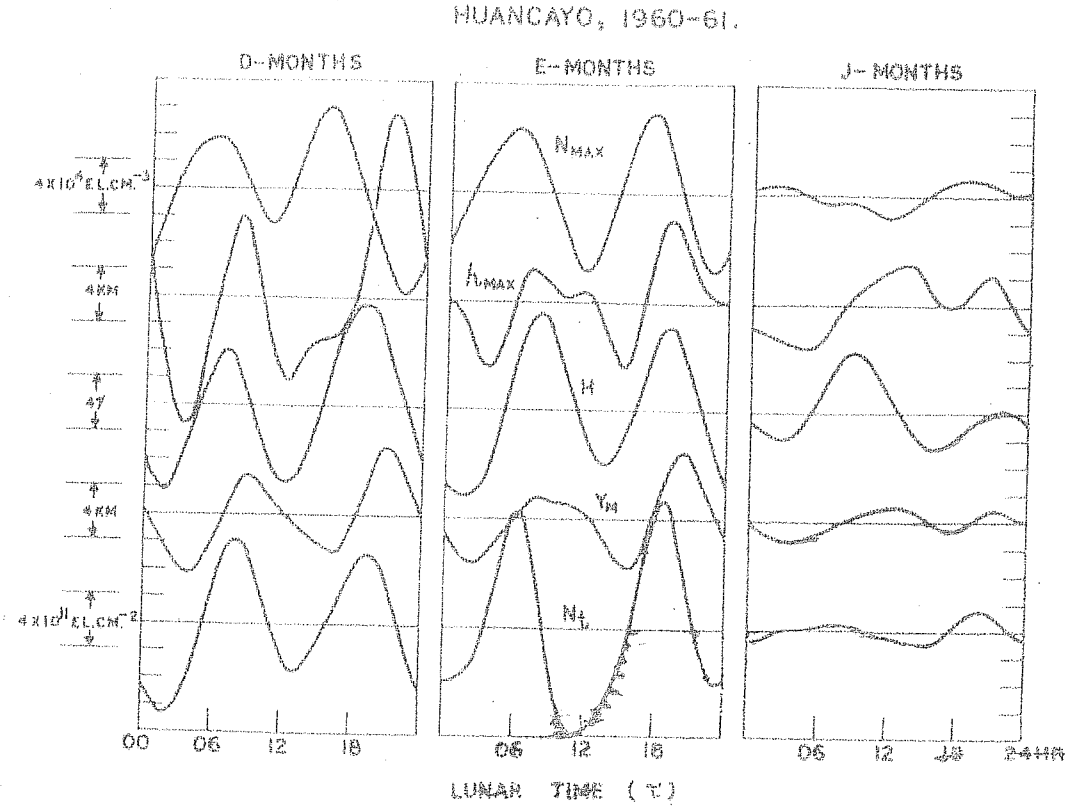


FIGURE - 23

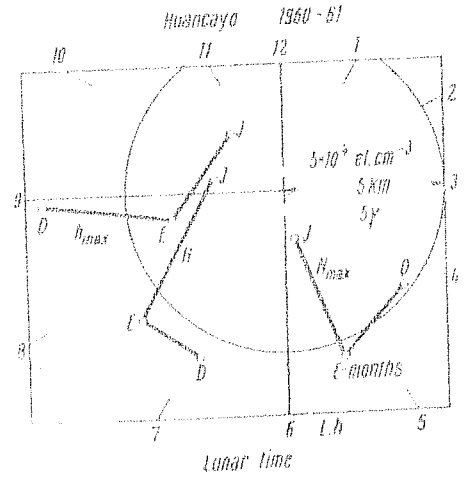


FIGURE - 24

To study the interrelations between these variations, the amplitude L_2 and lunar time of maximum variation (β_2) of L(H), L(h_{max}) and L(N_{max}) tide are shown on a harmonic dial in figure 24. It is seen that, during any season, the phase of $L_2(h_{max})$ variation lags behind the H-variation by about 1 hr; the variations in N_{max} have opposite phases to those of h_{max} with a delay of roughly 1 hr. Thus it seems that during any season, the lunar oscillations of H cause similar oscillations in h_{max} which, then, produce opposite variations of N_{max} with a delay of about an hour. Also the amplitude $L_2(h_{max})$ is greater than $L_2(Y_m)$ although the two variations are in the same phase, indicating that top of the F_2-layer is affected to a great extent than the bottom. These features are similar to those seen in the annual average L-variations.

It is also noticed from the diagram that β_2 for all the three parameters shows, in general, an increase from D to E to J-months. From D to J-months, β_2 is retarded by roughly 3 lunar hr in case of H and by about 1½ lunar hours for h_{max} and N_{max}. The amplitude L_2, in any parameter, considerably decreases from D to J-months.

3.5 Seasonal effects in lunar monthly (M) variations

The lunar M variations of each parameter were computed separately for individual solar hours in each season. The amplitude of the monthly component of these variations, r_1, was found to be always very small and statistically insigni-

ficant; and hence will not be discussed. The results of lunar semi-monthly (M_2) tide is described in this section, separately for each parameter.

(a) H-component

The lunar monthly (M) variations of H at different solar hours (00, 03, ...18 and 21 hr) in different seasons are shown in figure 25. The curves indicate a predominant semi-monthly component at all the hours. It is seen that the tide is significantly large for the day-time hours, and that the maximum tide in any season occurs near midday hours. The oscillations are smaller during night-time.

The amplitude and phase (r_2, θ_2) of M_2 tide at different solar hours, alongwith the mean values of H, are given in table 7 for each season separately. The mean values of probable errors are also given in the table. The statistically insignificant amplitudes are put into brackets. It is seen that only the day-time amplitudes are statistically well determined. The solar daily variation of H as well as the amplitude of M_2(H) tide in each season is shown in figure 26. The diagram shows that the M_2(H) amplitude and H vary in a similar fashion in course of a day; both are very small during night-time, start increasing with sunrise to attain a maximum at about 12 hr and then decrease to the night-time value by sunset. Thus it is very clear that M_2(H) oscillations at Huancayo are closely associated with the electrojet currents.

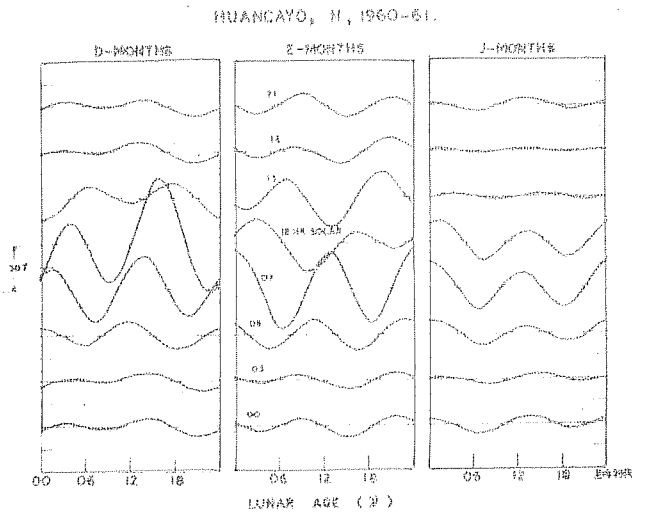


FIGURE - 25

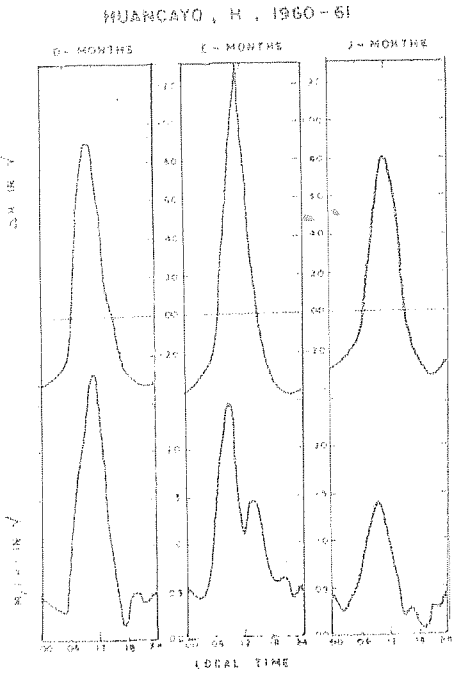


FIGURE - 26

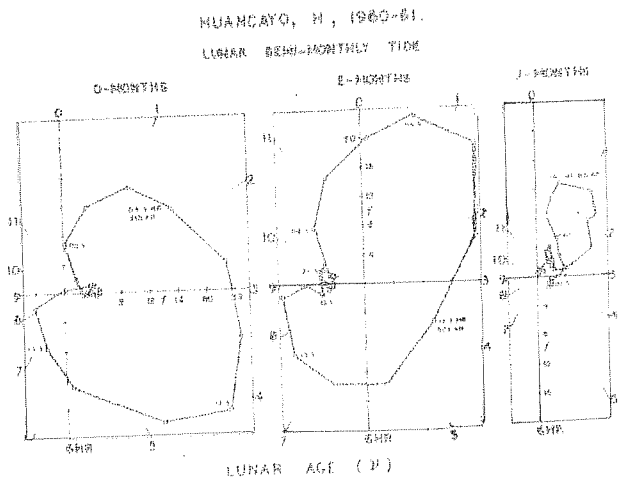


FIGURE - 27

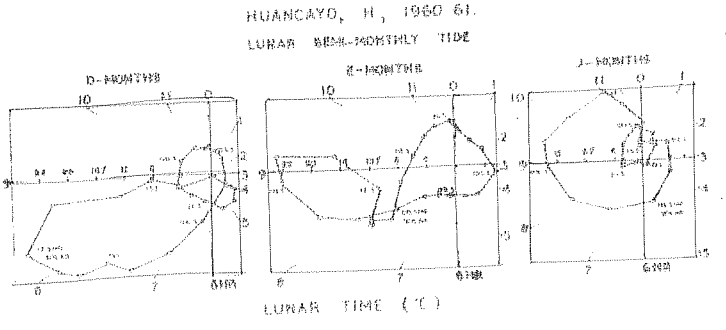


FIGURE - 28

Also, the range of H variation is greatest in E-months and is comparable in D and J-months, whereas the $M_2(H)$ oscillations are larger during D-months than E and J-months. The amplitude of $M_2(H)$ tide is least in J-months.

The amplitude and phase (r_2, θ_2) of $M_2(H)$ tide at different solar hours in each season are also shown on the harmonic dials of lunar age and lunar time in figure 27 and 28 respectively. It is seen from figure 27 that during D and E months, the night time (r_2, θ_2) points are clustered together, while the day-time points move around the origin forming a broad loop such that the vector average for all hours is reduced to a low value. On the lunar time dial (fig.28), the night-time points form a broad loop containing the origin, while the day-time points form a narrow elongated loop in a preferred direction; the vector average of all hours, in this case, is of the same order as individual amplitudes. During J-months, the day-time points show a narrow elongated loop on the '$\mathcal{J}$' dial (fig.27); while they move around the origin in a broad loop on '$\mathcal{T}$' dial (fig.28). The night-time points, during J months, are clustered together on '$\mathcal{J}$' dial and form a loop on '$\mathcal{T}$' dial.

Thus it is seen that daytime $M_2(H)$ tide at Huancayo is governed by absolute position of the moon (i.e. $\mathcal{T}$) in D and E months, while by relative positions of the sun and moon ($\mathcal{J}$) during J-months. During night-time, however, $M_2(H)$ tide in all the seasons is controlled by lunar age ($\mathcal{J}$).

(b) Height of peak ionization (h_{max})

The lunar M variations of h_{max} in each season are shown in figure 29 for three hourly groups of solar hour, while their coefficients r_2 and Θ_2 alongwith the mean values of h_{max} are given in table 8. Figure 29 shows that the variations are predominantly semi-monthly in character although lunar monthly component is also present at few hours; and that the variations are larger for late afternoon hours. During D and E-months, the amplitude r_2 is statistically significant only for forenoon and late evening hours. During J-months, all the r_2's, except at 06 and 19 hr, are statistically insignificant (table 8).

The solar daily variations of h_{max} and of the amplitude of $M_2(h_{max})$ tide are shown in figure 30. The solar daily variation of $r_2(h_{max})$ shows a number of peaks in each season. During E and J-months there is a small peak in h_{max} near sunrise hours corresponding to which one finds peaks in the r_2 amplitudes for the same hours. There is another sharp peak of $r_2(h_{max})$ at about 08 hr corresponding to the time when h_{max} is rising very rapidly following the sunrise. In all the seasons, a broad peak is also seen at 21 hr corresponding to the abnormal post sunset rise of the F_2 layer. Thus solar daily variations of the amplitude of lunar tide in h_{max} is closely associated with the daily variation of h_{max} itself. In other words the agencies which cause large solar daily variations in h_{max} have large lunar tidal effects.

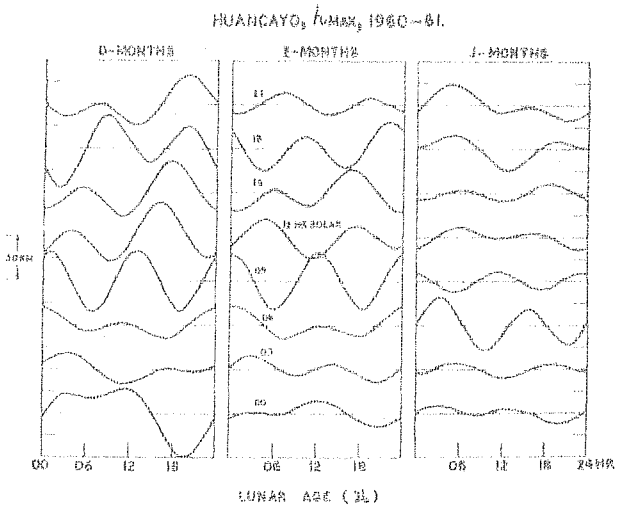


FIGURE - 29

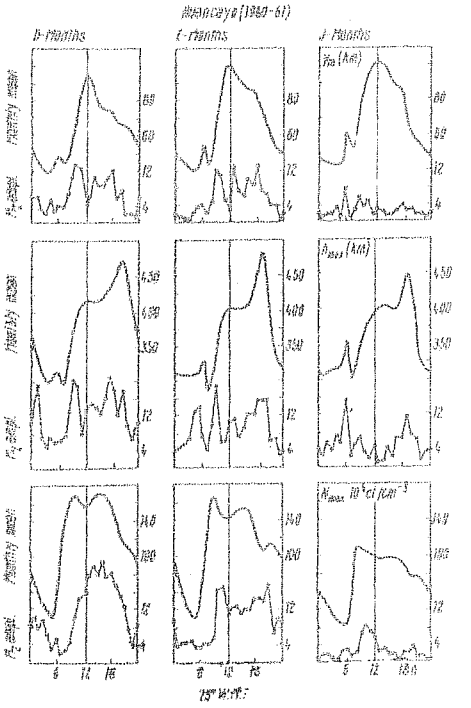


FIGURE - 30

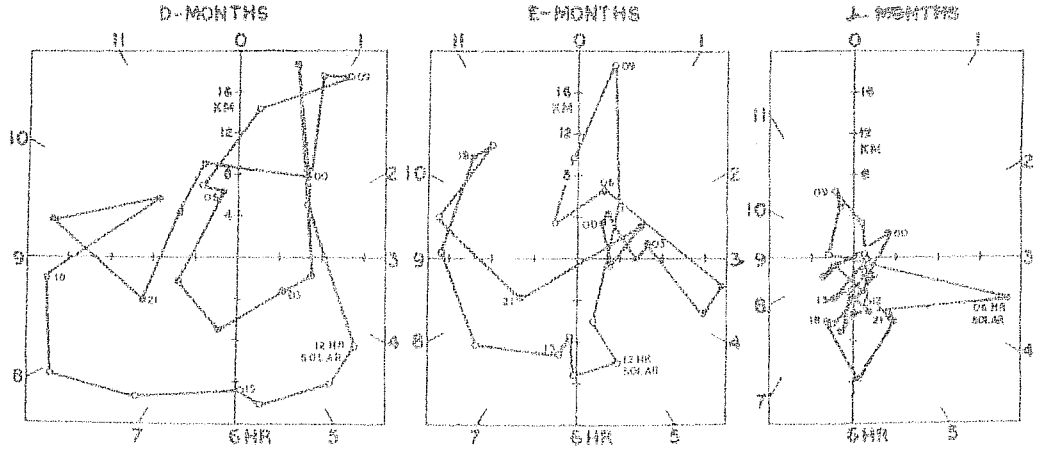


FIGURE - 31

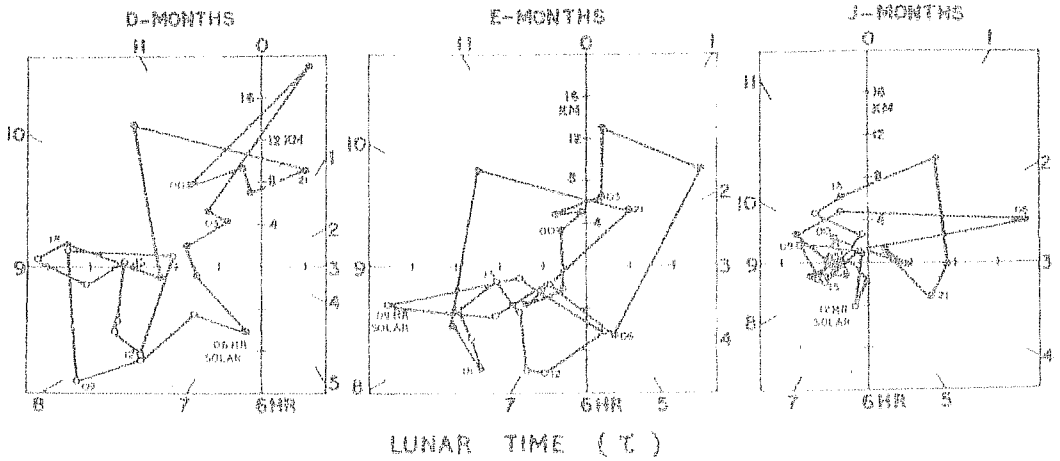


FIGURE - 32

The harmonic coefficients (r_2, θ_2) at individual solar hours are plotted on the harmonic dials of lunar age and lunar time in figure 31 and 32 respectively. Figure 31 shows that during D and E-months, the daytime points show a continuous retardation of phase with solar time; the night-time points do not show any systematic variation. During J-months, the amplitude r_2 at all hours is insignificantly small and hence no inference is drawn. On the lunar time dial (fig.32), the day-time points in D and E months are grouped in the sector 07-09 lunar hr, while the night-time points group themselves between 11-01 lunar hour; but there is no systematic variation of phase with solar time.

(c) Maximum electron density (Nmax)

The $M(N_{max})$ variations at three hourly group of solar hour (00,03.....18 and 21 hr) in each season are presented in figure 33. The harmonic coefficients (r_2, θ_2) of these variations and the mean N_{max} at each hour are given in table 9. It is seen from table (9) that the amplitudes are significant only for 09-21 hr during D and E months, and for 09-12 hr during J-months. The largest amplitudes occur during late afternoon hours. Also, the amplitude r_2 is maximum in D-months and minimum in J-months.

The solar daily variations of $r_2(N_{max})$ and N_{max} itself, are plotted in figure 30. The diagram for N_{max} shows that N_{max} values are greater in D-months, less in E-months,

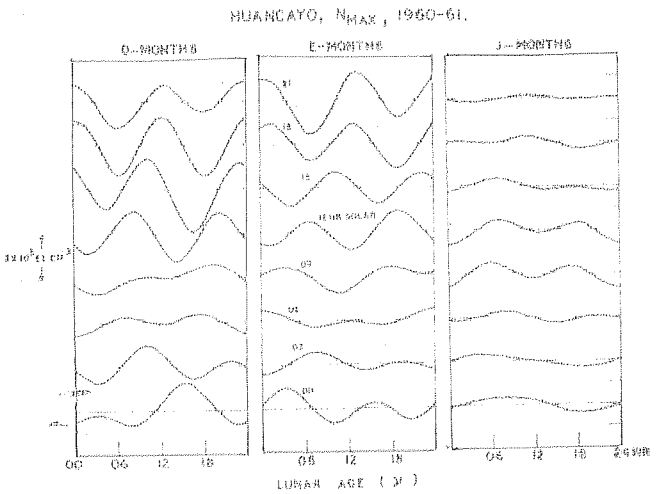


FIGURE - 33

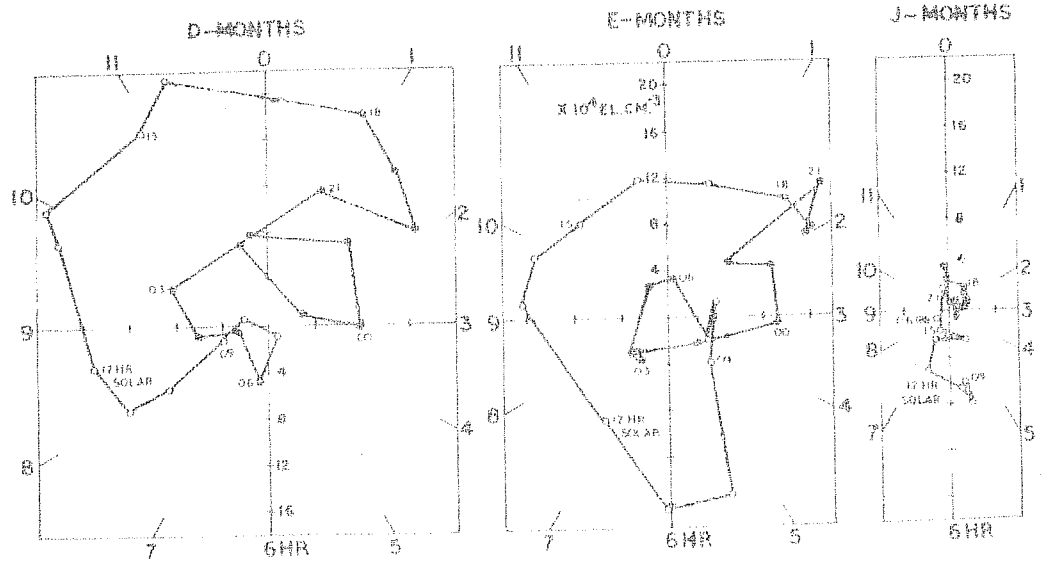


FIGURE-34

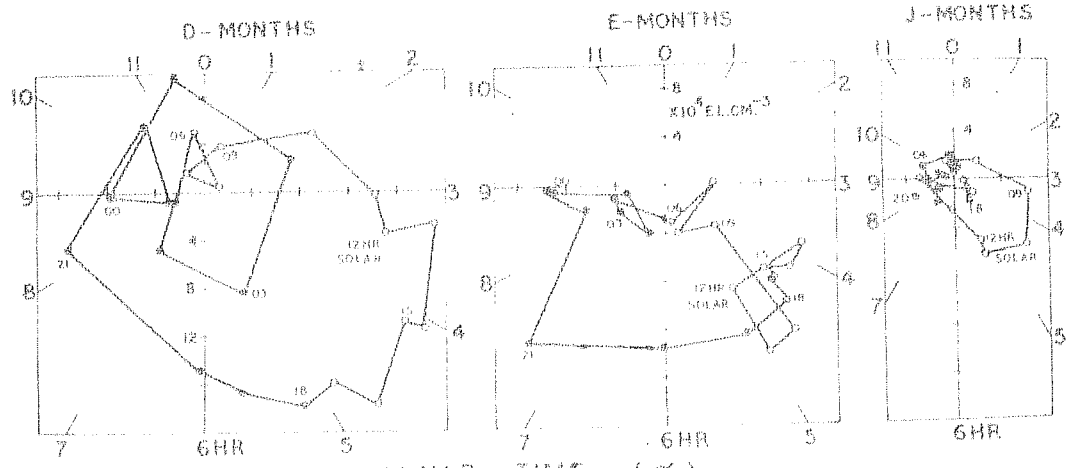


FIGURE-35

and least in J-months. The amplitude $r_2(N_{max})$ is also maximum in D-months and least in J-months. It is noticed that during D-months, $r_2(N_{max})$ shows a prominent peak in the afternoon hours which coincides with the afternoon peak of N_{max}. During E-months, it shows two peaks, first in the forenoon hours coinciding with forenoon peak of N_{max} itself, and another in the early hours of the night. In J-months, the amplitude of $M_2(N_{max})$ tide is very small but shows a peak in the forenoon hours when N_{max} is also largest. The time lag of solar daily variation of $r_2(N_{max})$ with respect to that of N_{max} variation is also very clearly seen in all the three seasons. N_{max} starts increasing in the morning from 06 hr, while $r_2(N_{max})$ starts increasing after about 08 hr.

To study the phase variation with solar time of $M_2(N_{max})$ oscillations, the coefficients r_2, θ_2 at individual solar hours are plotted on the harmonic dials of 'ν' and 'τ' in figure 34 and 35 respectively. During D and E months the (r_2, θ_2) points on the lunar age dial show a gradual retardation of phase with progress of solar time; the phase θ_2 from 06 to 18 solar hour changes by 180°. The vector average of (r_2, θ_2) points on 'ν' dial in D and E-months, is very small due to large change of phase with solar time. During J-months, the day-time points are clustered together around 06-08 lunar hr, while the night-time points show opposite phase of 00-02 hr.

In D-months, the points on the harmonic dial of τ (fig.35), show two broad loops, one for the day-time hours and another for the night-time. The day-time points, however, are in the sector 01-05 lunar hr. During E-months, the night-time points show a broad loop indicating a very large change of phase with time, but the day-time points are confined between 03-05 lunar hr sector. In J-months, the points, on 'τ' dial, are scattered in position. The day-time points, however, do form a loop in the 02-05 hr sector.

Thus during day-time, the lunar semi-monthly (M_2) oscillations in N_{max} in D and E months show a prefered phase on the 'τ' dial and hence seem to be controlled by lunar time. During J-months, the daytime $M_2(N_{max})$ oscillations show a better grouping on the 'λ' dial and hence seem to be governed by the lunar age(λ). This difference in control of $M_2(N_{max})$ variations during different seasons is similar to that observed for $M_2(H)$ (section 3.5a), and confirms the view that lunar oscillations in electron density in the F_2-layer at equator is directly associated with the oscillations in H.

(d) Semi-thickness of the layer (Ym)

Figure 36 shows the lunar monthly variations of Y_m at solar hours 00, 03,.....18 and 21, in different seasons. The amplitude (r_2) and phase (θ_2) of the second harmonic component of these variations are given in table 10

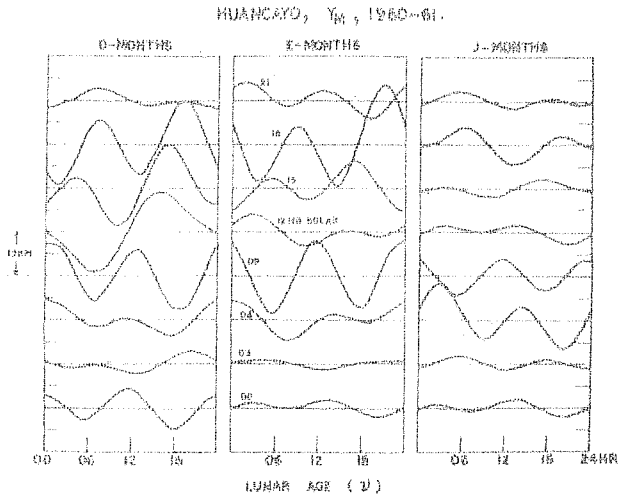


FIGURE - 36

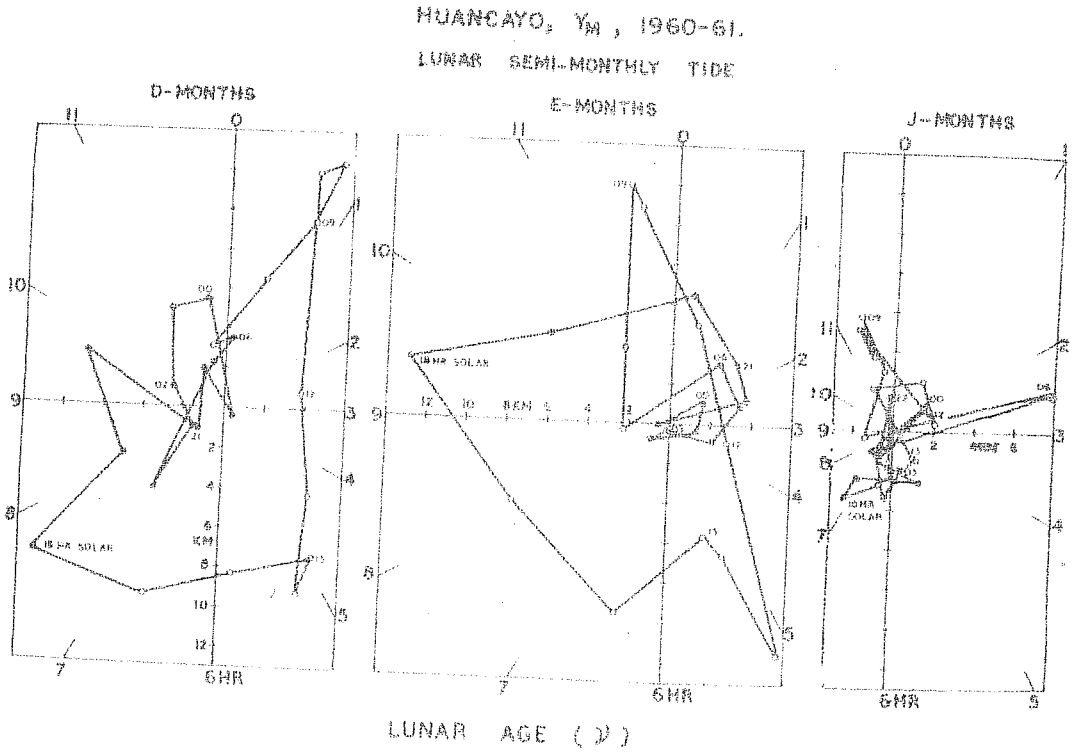


FIGURE -37

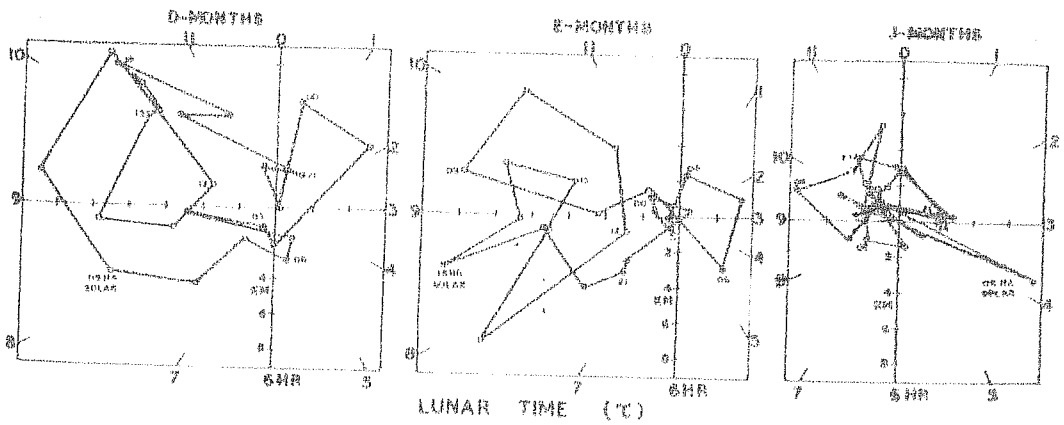


FIGURE - 38

alongwith the mean value of Y_m at each hour. It is seen from figure 36, that the $M(Y_m)$ oscillations are predominantly semi-monthly, and these are larger, in general, for 12-18 solar hours. It is seen from the table (10) that the amplitude of $M_2(Y_m)$ tide is, generally, significant only in the day-time and is insignificantly small in the night-time. In J-months, however, even in the day-time, the amplitude r_2 is significant only for 06, 09 and 18 hour. The $M_2(Y_m)$ oscillations at any solar hour is largest in D-months, less in E-months, and least in J-months.

The solar daily variations of Y_m and the amplitude of $M_2(Y_m)$ which are plotted, alongwith similar diagrams for h_{max} and N_{max}, in figure 30 shows that Y_m is largest at about midday in any of the seasons. Y_m also shows a small peak near sunrise time when h_{max} also has a peak. The $r_2(Y_m)$ amplitudes are seen to be greater in D-months, less in E-months and almost insignificant in J-months. The amplitude $r_2(Y_m)$ during D and E-months exhibit two peaks, one in the forenoon hours and another in the evening hours roughly coinciding with $r_2(h_{max})$ peaks. The tidal amplitudes in Y_m and h_{max} are of the same order which indicates that most of the variations in semi-thickness are caused by the rise and fall of the peak level, or in other words, lunar tidal oscillations in the base of F_2 layer should be very small. This is consistent with the results that lunar tidal variations in the F_2 region are greater at greater heights (SHARMA and RASTOGI, 1968).

The amplitude and phase of the $M_2(Y_m)$ variations at individual solar hours in each season are plotted on harmonic dials of lunar age and lunar time in figure 37 and 38 respectively. On the $\mathcal{V}$ dial, the night-time points in any season are clustered near the origin. The day-time points in D and E months show a gradual phase variation from pre-noon hours (08-11 hr) to evening hours (17-18 hr); the phase difference between the morning and evening hours being about 8 lunar hr. The r_2 amplitudes in J-months are very small and the points are scattered on the dial.

On the $\mathcal{T}$ dial (fig.38), the day-time points in D and E months do not indicate any systematic phase variation. However, they are all confined in the sector 08-10 lunar hr indicating that the F_2 layer during day-time is thickest at these lunar hours.

(e) Total electron content (Nt)

The lunar monthly variations of N_t at three hourly groups of solar hours in each season, which are plotted in figure 39, show that the variations are, in general, of semi-monthly character. Also, the oscillations are largest at 09 solar hr in D-months and at 12 hr in E and J-months. The mean value of N_t and the second harmonic component of $M(N_t)$ variations at individual solar hours are given in table 11, separately for each season. Table (11) shows that in general, only the day-time amplitudes are statistically reliable.

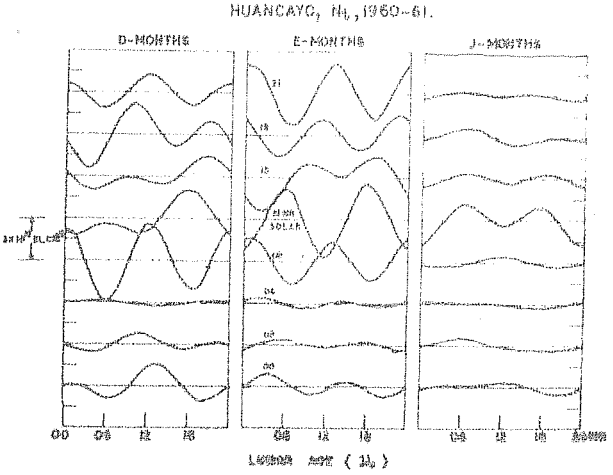


FIGURE -- 39

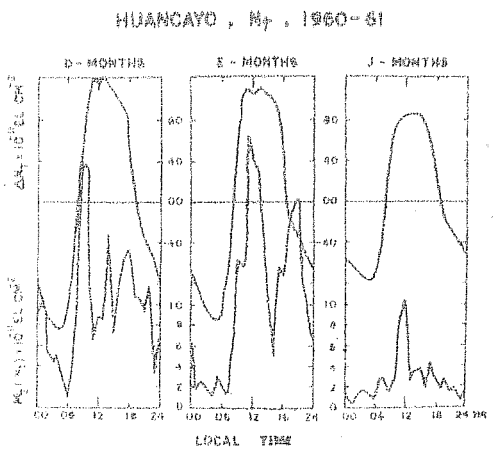


FIGURE - 40

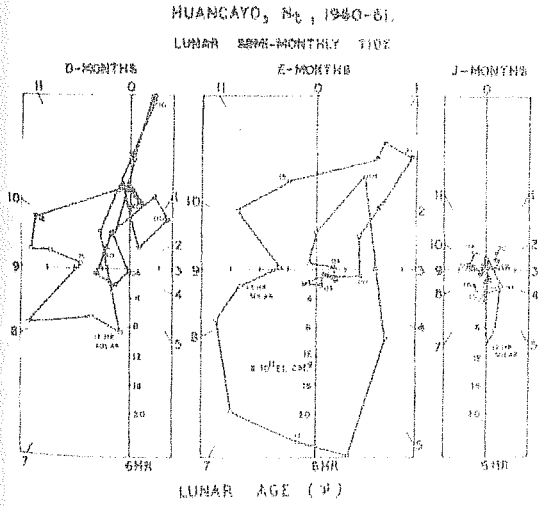


FIGURE - 41

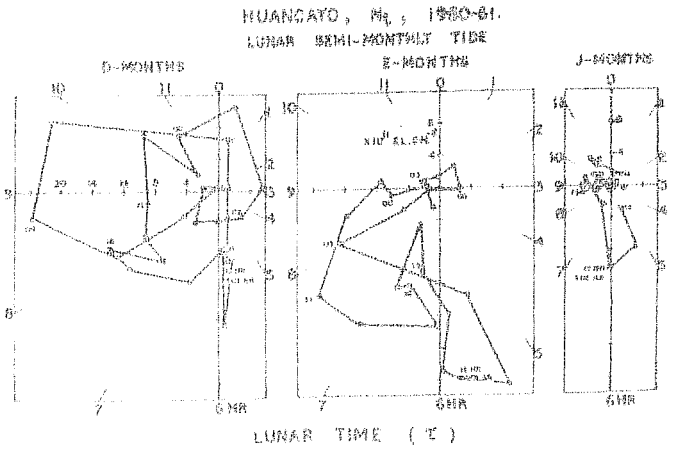


FIGURE - 42

During J-months, however, the amplitude of $M_2(N_t)$ tide is reliable only at 11 and 12 solar hr, and the rest are insignificantly small.

The amplitude of $M_2(N_t)$ tide, alongwith N_t value itself, is plotted as a function of solar time in figure 40. It is seen that N_t values are largest in D-months, less in E-months, and least in J-months; while the amplitude $r_2(N_t)$ is maximum in E-months and minimum in J-months. The solar daily variation of $r_2(N_t)$ in D-months exhibits a number of peaks, at 09, 14 and 18 hr, but the amplitude at 09 hr is the largest. During E-months, there are two peaks, one at 11 hr and another at 21 hr, but the peak at 11 hr is bigger. In J-months, $r_2(N_t)$ shows only one peak at 12 hr which coincides with peak of N_t.

The (r_2, θ_2) coefficients of lunar semi-monthly tide in N_t at individual solar hours are plotted on harmonic dials of lunar age and time in figure 41 and 42 respectively. During D-months, the night-time points on the 'ν' dial do not indicate any systematic phase variation, but there is a distinct change in phase θ_2 from morning (08-10 hr) to evening hours (17-18 hr). On the τ dial, however, two broad loops, one for the day-time and another for the night-time, are seen indicating a large and gradual phase change with solar time. In E-months, the points on the 'ν' dial show a continuous phase retardation starting from 07 hr in the morning till 00 hr midnight; the points between 01 to 06 hr

have smaller amplitudes and are clustered together on the dial. On the τ dial, the night-time points show a large phase variation, but the day-time points between 10 to 18 solar hr are in the same sector i.e. 05-07 lunar hr. In J-months, (r_2, θ_2) points on both 'ν' and 'τ' dial are scattered around the origin and do not show any systematic change in phase. However, the points for 10-13 hr form a small loop on the τ dial in the 05-07 lunar hr sector.

(f) Interrelations between M2 tide in H and in the ionospheric F2 region

To study the relationships between lunar semi-monthly tide in H and in the ionospheric F_2 parameters in different seasons, the (r_2, θ_2) harmonic dials, on lunar time, for H, N_{max}, h_{max} and Y_m are shown together for D and J-months in figure 43 and 44 respectively. It is seen from figure 43 that in D-months, the phases of $M_2(H)$ and $M_2(h_{max})$ oscillations for the day-time hours are similar and are between 08-09 lunar hr. The day-time $M_2(Y_m)$ tide shows a phase of approximately 08-10 lunar hr, while the phase of $M_2(N_{max})$ tide lies between 02-05 lunar hr.

It is thus seen that the lunar semi monthly variations in h_{max} are in the same phase with H-variations, which indicates that an increase or decrease in H component produces a uplifting or downward shift respectively, of the height of maximum electron density. This raising or lowering of the F_2

layer causes the layer to become more thick or thin respectively, after, probably, a delay of 1 hour as indicated by the phase of $M_2(Y_m)$ tide. The phase of $M_2(N_{max})$ tide (02-05 lunar hr) is opposite to that of $M_2(H)$ or $M_2(h_{max})$ tide (08-09 lunar hr). It appears that the rise or fall of the level of h_{max} produces, also, a diminution or enhancement respectively, of the maximum electron density (N_{max}) after a lag of about 1-2 lunar hr. These interrelations between M_2 tide in H and ionospheric parameters are similar to those found between the Lunar daily variations.

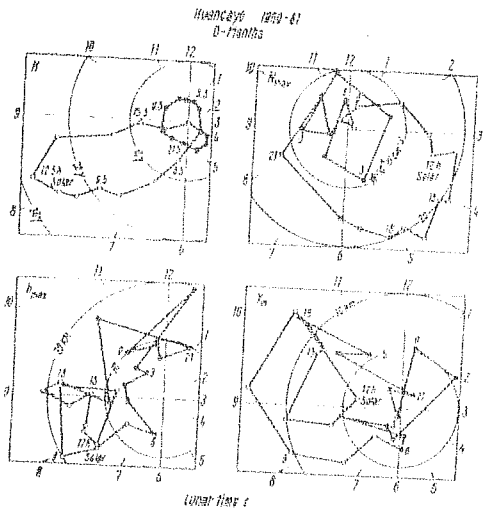


FIGURE - 43

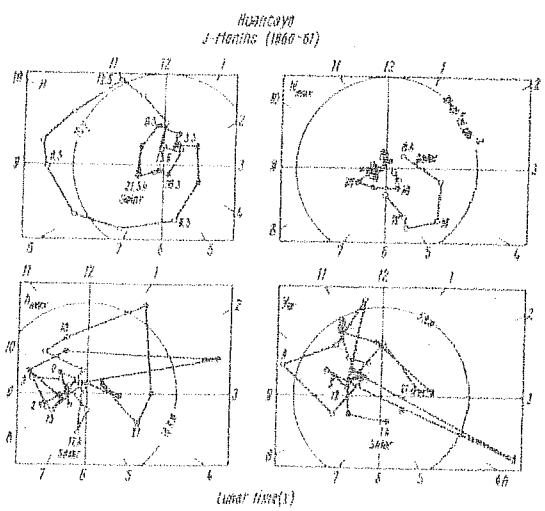


FIGURE - 44

During J-months (fig.44), the day-time points of $M_2(H)$ oscillations form a broad loop in the sector 06-00 lunar hr, while those for $M_2(h_{max})$ and $M_2(Y_m)$ tide are scattered in the sectors 06-10 lunar hr and 08-00 lunar hr respectively. The diagram for N_{max} shows that the day-time points form a small loop in the opposite sector of 01-05 lunar hr. Thus the $M_2(H)$ and $M_2(h_{max})$ oscillations are in the same phase; while $M_2(Y_m)$ variations are retarted by about 1 lunar hr, and the $M_2(N_{max})$ oscillations are in phase opposition with that of $M_2(h_{max})$.

Thus the interrelationship between the M_2 tide in H and ionospheric parameters is also clearly indicated even in J-months when the tidal amplitudes are generally very small.

3.6 Height variation of lunar tide

The present analyses have still one limitation that the amplitude and phase of M_2 tide in both N_{max} and h_{max} at different hours of the day are affected, beyond doubt, by the solar daily variation of the level of the F_2 peak. These luni-solar tides could also be affected by the solar daily variation in the rate of ion production and solar tidal drifts. Any definite evidence of possible height variation of lunar tidal effects in the F_2 region necessitates the availability of complete electron density profiles at each hour of the day. Notwithstanding this significant limitation, evidences of height variation of lunar tidal effects have been shown by

RUSH and VENKETESHWARAN (1968) and by BROWN (1968) by studying the variation of lunar tide in f_oF_2 or in h_{max} with mean value of h_{max}. RUSH and VENKETESHWARAN (1968) plotted, on a single diagram, the phase of $M_2(f_oF_2)$ tide versus average h_{max} at different hours of the solar day, for about a dozen stations and concluded that the height variation of the phase of lunar perturbation is same at all low latitude stations; and that the phase varies at the rate of 2-4 lunar hr/100 km during solar maximum and 5-6 lunar hr/100 km during solar minimum.

BROWN (1968) analysed f_oF_2 and h_{max} data of Ibadan covering the period 1954-66. He divided the data into 15 groups of mean h_{max} values irrespective of the solar time or season. He showed a sudden phase reversal in $M_2(f_oF_2)$ tide at 308 km above which the phase remains constant with height.

The present results of M_2 tide in h_{max} and N_{max} are studied for any evidence of a height variation of lunar tide. Out of the coefficients of annual average M_2 tides in h_{max} and N_{max} in Tables 8 and 9 respectively, notwithstanding the solar hour, the amplitude and phase θ_2 in both the parameters are plotted separately as a function of mean value of h_{max} in figure 45.

The amplitude of $M_2(N_{max})$ tide shows a increase in its magnitude with increasing h_{max} confirming the results of SHARMA and RASTOGI (1968) derived from the data for the midday hours only. The presence of any node as reported by BROWN(1968)

for Ibadan is not seen here, which may be due to the fact that the lowest value of h_{max} for present period happens to be about 300 Km.

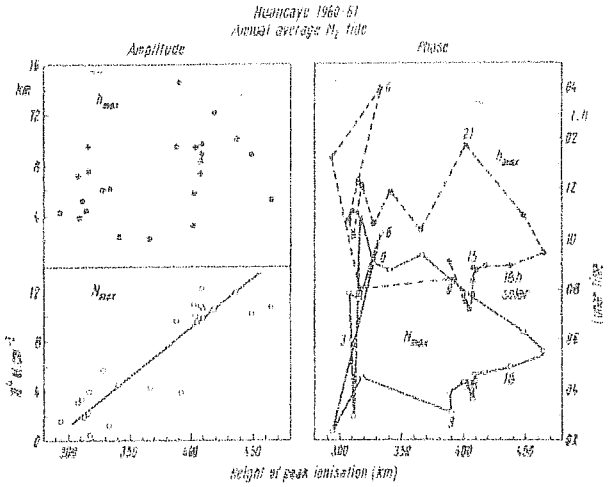


FIGURE - 45

The amplitudes $r_2(h_{max})$ show a wide scatter, such that no significant relation can be derived regarding its height variation. This is not in confirmity with the results of BROWN (1968) for Ibadan where an exponential increase of tidal amplitude $r_2(h_{max})$ is found with increasing h_{max}.

Referring to the variation of the phase Θ_2, of M_2 tide in N_{max} and h_{max} with mean value of h_{max}, one finds that the points form a loop during the course of a day. However, it is important to note that the phase of $M_2(N_{max})$ tide remains at 04$\pm$ 1 lunar hr for most of the daytime period (08–19 hours). Correspondingly, the phase of $M_2(h_{max})$ tide remains at 08 $\pm$ 1 lunar hr for the same period. In the nighttime, the phases in either of the parameters show a large and irregular variation with height. However, any definite conclusion about the height variation of the tidal oscillations can only be obtained by the analysis of lunar tides at fixed real heights based on the data of electron density profiles. Such an analysis has been done for a few stations and the results are described in chapter 5.

3.7 Conclusions

From the foregoing discussions of lunar daily (L) and lunar monthly (M) variations of H and various ionospheric parameters of the F_2 region at Huancayo, the following main conclusions are drawn:

(a) Lunar daily variations at fixed lunar ages (L_{2l})

H-component

(1) $L_{2l}(H)$ variations are maximum for the mid-day hours and are insignificantly small during night-time.

(2) In any season, the amplitudes C_1 and C_2 of first two harmonic components of $L_{\nu}(H)$ tide are of comparable magnitude and are greater than the higher harmonics C_3 or C_4 which are statistically insignificant.

(3) The amplitude C_2 of $L_{\nu}(H)$ oscillations in D and E months are of the same order and are greater than C_2 in J months.

Ionospheric parameters

(4) $L_{\nu}(N_{max})$ and $L_{\nu}(N_t)$ tide is maximum during evening hours and are very small during night-time, while $L_{\nu}(h_{max})$ and $L_{\nu}(Y_m)$ variations are larger for all the hours of the day.

(5) The amplitudes C_1, C_2 and C_3 of the L_{ν} variation in any ionospheric parameter during any season are, approximately, of the same magnitude, while C_4 is very small and insignificant.

(6) The semi-diurnal component C_2 of L_{ν} variation in any parameter is greater in D or E months than J-months.

(b) Whole lunation average lunar daily variation (L)

(7) The L variation in all the parameters is predominantly a semi-diurnal one i.e. $L_2 > L_1$.

(8) The lunar daily variations in h_{max} follow sympathetically the variations in H such that an increase or decrease of magnetic field causes the raising or lowering respectively, of the height of peak ionization. $L(N_{max})$ oscillations are opposite in phase to that of $L(h_{max})$

with a delay of about 1-2 hours, suggesting that an increase of height causes a decrease of maximum electron density.

(9) Lunar daily variations at all the levels of the F_2 region are similar but the peak of the F_2 layer is affected by greater amount than its base.

(10) The amplitudes $L_2(H)$, $L_2(N_{max})$ and $L_2(N_t)$ are maximum in E-months, slightly less in D-months, and least in J-months; but $L_2(h_{max})$ and $L_2(Y_m)$ are largest in D-months, less in E-months, and least in J-months.

(c) Lunar monthly variations (M)

(11) The amplitude (r_1) of lunar monthly variations of any parameter is, in general, statistically insignificant, for any solar hour; the principal component of the M variation being semi-monthly in character.

(12) Lunar monthly component of M(H) tide is found to be controlled by lunar age ν.

(13) $M_2(H)$ tide is governed by lunar time τ in D and E months, and by lunar age ν in J-months.

(14) The solar daily variation of $r_2(H)$ is very much similar to the daily variation of H itself.

(15) Both $r_2(h_{max})$ and $r_2(Y_m)$ vary with solar time in a similar fashion. Also $r_2(h_{max}) \simeq 2\, r_2(Y_m)$, which shows that the conclusion (9) holds good for lunar M_2 tide also.

(16) $r_2(N_{max})$ varies with solar time in a similar manner to N_{max} variation, but with a time lag of 2-3 hours.

(17) Solar daily variation of $r_2(N_t)$ and N_t are similar; both are maximum near midday.

(18) M_2 tide in any parameter is maximum during D-months and minimum during J-months.

(19) There is a close interrelationship between the lunar semi-monthly tide in H and in ionospheric parameters, in the day-time hours, which is similar to that observed in their L variations (conclusion 8).

(20) $M_2(N_{max})$ tide shows an increase of its amplitude with increasing height. The phase Θ_2 remains constant with height during the day-time. There does not seem to be any appreciable height variation of $r_2(h_{max})$.

A theoretical discussion of the correlation between geomagnetic and ionospheric tide is presented in chapter 6.

CHAPTER - IV

INTERACTION OF GEOMAGNETIC AND IONOSPHERIC LUNAR TIDES AT A STATION CLOSE TO L-CURRENT FOCUS

4.1 Introduction

The lunar oscillations of horizontal component (H) of earth's magnetic field are known to be quite small except at equatorial stations. It was shown in the preceding chapter that lunar geomagnetic variations at the equatorial station, Huancayo, are strongly affected by the equatorial electrojet; and that these cause perturbations in the F_2-region of the ionosphere. It was thought desirable to study the inter-relations between lunar tides in geomagnetism and ionosphere for a mid-latitude station where the oscillations are of smaller amplitude. RASTOGI (1969b) has studied lunar tides in f_oF_2 at the mid-latitude station Puerto Rico, which is close to the focus of the L current system, for the period of low solar activity. With the availability of electron density profiles at Puerto Rico (Geograph. 18°30'N, 67°06'W) and H values at San Juan (Geograph. 18°24'N, 66°06'W), it was decided to carry out the analyses for magnetic and ionospheric data at San Juan - Puerto Rico. The data used cover a period of 34 months from March 1959 to December 1961. The magnetic data for San Juan were kindly provided by the U.S. Coast and Geodedic Survey, Washington.

Both lunar daily (L_{ν}, L) and lunar monthly (M) variations of H-component at San Juan, and in N_{max}, h_{max} and N_t at Puerto Rico, have been computed following the methods described in section 2.3.

The results for H-component show some interesting basic differences between the lunar tidal effects at an equatorial and a non-equatorial station. Therefore, the lunar tides in H at San Juan and its comparison with the results at Huancayo are discussed first, in sections 4.2 to 4.6. The results of lunar tides in various parameters of the F_2-region, i.e. h_{max}, N_{max} and N_t, will then be described and compared with the lunar tides in H at San Juan to study their correlation. A part of the work has already been published (SHARMA and RASTOGI, 1969, 1970b).

4.2 Luni-solar variation in H

The annual average deviations ΔH, free from solar daily variation and geomagnetic disturbances, are arranged on the grids of lunar age(ν) and lunar time (τ). The contours of constant ΔH are then drawn on these co-ordinates. The contours drawn for San Juan (1959-61) and Huancayo (1960-61) are presented in figure 46. It is to be noted that contours for Huancayo are drawn in steps of 2.5 γ and those for San Juan in steps of 1.0 γ . The shaded portions indicate solar night period. It is seen that for Huancayo most of the contour lines are concentrated during solar day-time, while no such tendency

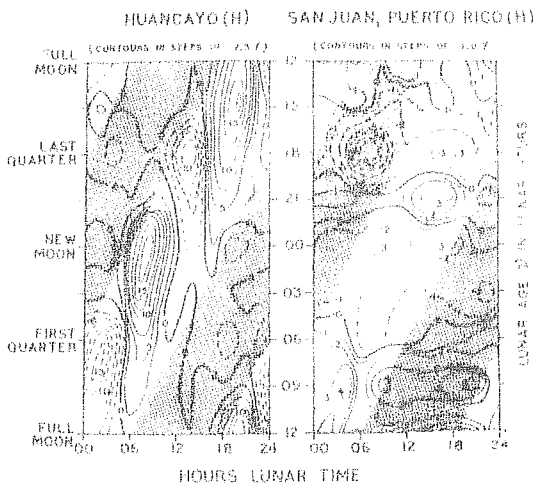


FIGURE - 46

PUERTO RICO, H , 1959-61.

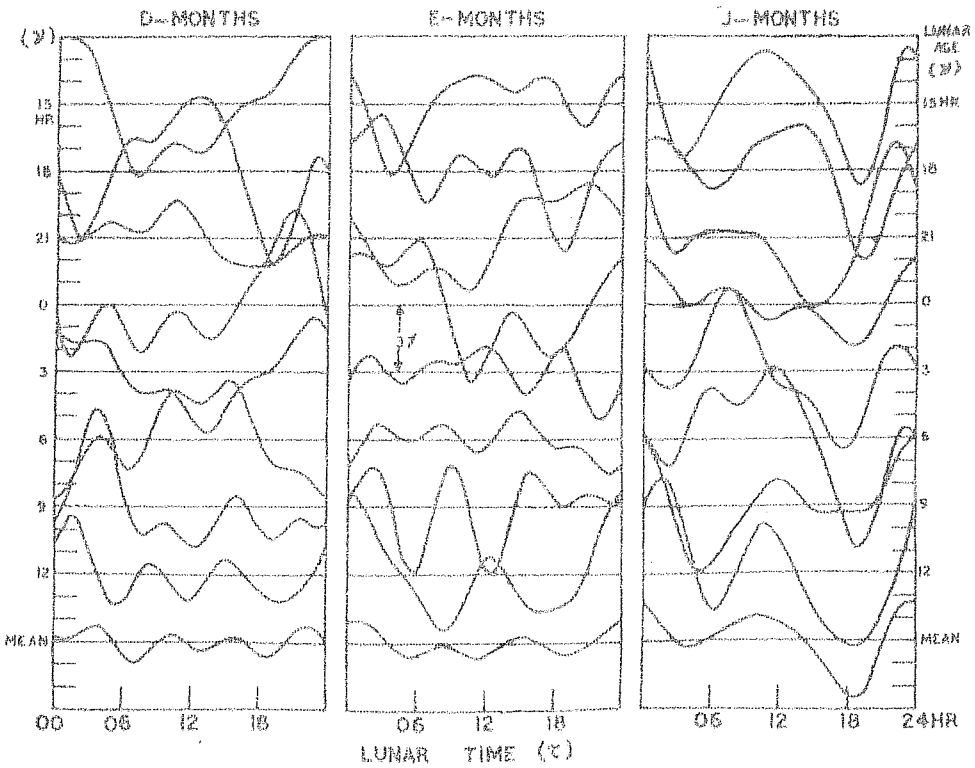


FIGURE - 47

is seen in the diagram for San Juan. Thus the lunar tide at San Juan is not appreciably affected by solar time, whereas for Huancayo it is enhanced around mid-day. Also the diagram for Huancayo exhibits a symmetry, i.e. it shows two high loops and two low loops during one lunar month, while no such symmetry is seen in the diagram for San Juan in which contour lines are distributed rather at random in one lunar month. Comparing the values of the contour lines it appears that the lunar effect at Huancayo is 4 to 5 times larger than at San Juan.

4.3 Lunar daily variations of H at fixed lunar ages (L_ν)

The data were divided into three seasonal groups viz. D, E and J months. The results of all three combined gave annual average results.

The lunar daily variations of H centred at three hourly groups of lunar age at 00, 03, 06, ...18 and 21 hr are plotted in figure 47 for each season separately. The first four harmonic coefficients (C_n, α_n) of these curves are collected together in table 13. The coefficients C_n, α_n of annual average L_ν curves, which are not shown in the figure, are also given in the table. It is seen from figure 47 that lunar variations at San Juan are equally large for solar day and night-time hours, which indicates that, unlike Huancayo, there is no luni-solar variation of H at San Juan. The curves, in any season, also indicate the presence of many harmonics.

In fact, it is seen from table 13 that in any season the diurnal and semi-diurnal components (C_1, C_2) of the L_ν variation at any lunar age are of approximately equal magnitude; while the higher harmonics C_3 and C_4 are small and decrease with increasing order.

4.4 Whole lunation average daily variation (L) of H

The individual daily variation curves of H at individual lunar ages for each season were averaged to give the mean daily variation of H averaged over a lunar month. These mean curves, L(H), are also shown in figure 47. The figure shows that the L(H) curves are not purely semi-diurnal, as is the case at Huancayo. These L(H) curves were harmonically analyzed for four harmonics according to equation (13). The amplitudes (L_n) and phases (time of maximum) β_n (equation 14) of first four harmonic components of L(H) variation in each season, together with annual results, are presented in table 14. The results of other workers have also been included in the table for comparison. Table 14 shows that in any season the first harmonic amplitude is slightly smaller than the second harmonic while higher harmonics are further reduced. The lunar semi-diurnal variation is maximum in J months, less in E months, and is least in D-months. According to the present analysis lunar time of maximum positive deviation β_2 of the semi-diurnal variation is 0.9 lunar hr in D-months, 1.2 lunar hr in E-months and 11.5 lunar hr in J-months. These results are in general

agreement with those of MATSUSHITA (1962b). However, RAJARAO (1962) found the phase to be about 10 lunar hr in any of the seasons, which is almost opposite to the present as well as MATSUSHITA's (1962b) results. It is to be noted that while the amplitude of the semi-diurnal oscillation is only 0.6 γ at San Juan, it is about 5 γ at Huancayo.

In table 15 are given the amplitude and time of maximum positive deviation of solar semi-diurnal (S_2) and lunar semi-diurnal (L_2) variations in H at San Juan and Huancayo. The S_2 component is about 25 γ at Huancayo and only 2 γ at San Juan. The annual average ratio (L_2/S_2) is 0.16 for Huancayo and 0.28 for San Juan. Thus the L_2 tide in H at San Juan, though small, is not insignificant in comparison to the corresponding S_2 component. This ratio for either of the stations is maximum in local summer and minimum in local winter months.

4.5 Annual average lunar monthly (M) tide in H

The lunar monthly variations of H were computed at different solar hours for each season separately. The annual average built up curves out of first two harmonic components at three hourly groups of solar hours (00, 03, 06.....18 and 21 hr) are shown in figure 48. Similar curves for Huancayo (1960-61) are also included in the diagram for comparison. It is seen that the lunar oscillations at San Juan are semi-monthly in nature at any hour of the day or night. The amplitude as well as phase of lunar oscillations in H at

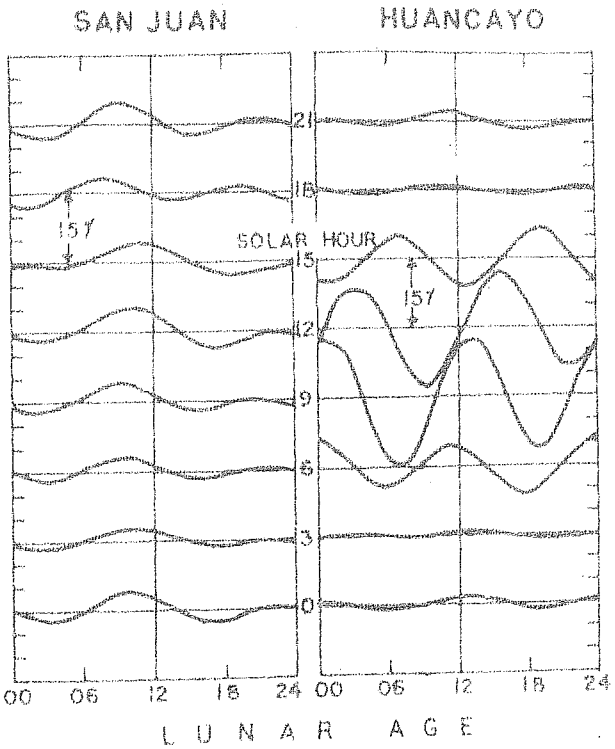


FIGURE - 48

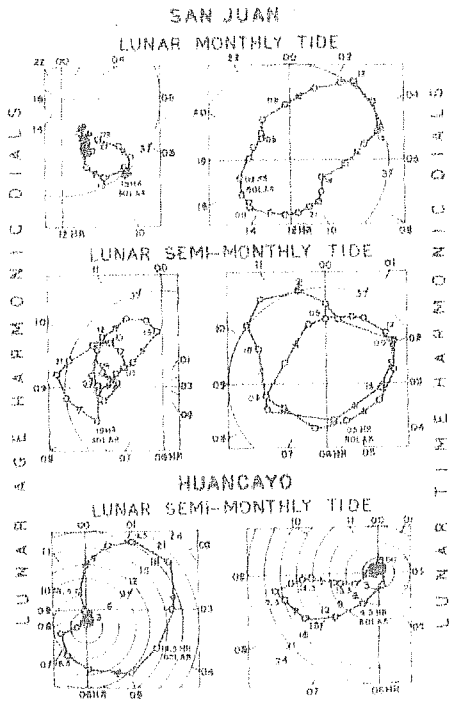


FIGURE - 49

San Juan is practically same at any solar hour. This is in contrast to the results at Huancayo where lunar variations in H are prominent only for the day-time hours and are very small during the night; further, the phase varies systematically with time of the day.

The amplitude and phase of lunar monthly and semi-monthly tide in H at San Juan are plotted on the harmonic dials of lunar age (ν) and lunar time (τ) in figure 49. Similar diagrams for semi-monthly tide in H at Huancayo are also included in the figure for comparison. It is seen that for San Juan the points showing amplitude and phase (r_1, θ_1) of lunar monthly tide on lunar time (τ) dial move uniformly around the origin such that when averaged for all the solar hours, the resultant amplitude is reduced to a insignificant value. The same coefficients (r_1, θ_1) on lunar age dial clustor in a narrow sector between 08 and 10 lunar hr such that 24 hourly average value is practically of the same order as that on individual hours. Thus the lunar monthly oscillations in H at San Juan are the same for any solar hour of a particular day, and are not affected by the position of the moon.

The coefficients (r_2, θ_2) of lunar semi-monthly tide in H at San Juan at different solar hours when plotted on lunar time (τ) dial form two loops around the origin (fig.49), one for 0 to 12 hours (solar) and another for 12 to 23 hours. The amplitude (r_2) for any hour is between 2 to 3 γ and is of

the same order as the amplitude of the monthly tide. The average amplitude of all the solar hours is reduced to a very small value (0.8 γ). The same coefficients (r_2, θ_2) on lunar age dial fall in the sector between 08 and 12 lunar hr. The average vector remains as significant ($\sim 2\gamma$) as the individual coefficients. Thus the lunar semi-monthly oscillations in H at San Juan, also, seem to be controlled by the lunar age (λ) and not by lunar time (τ). Comparing these dials with those for Huancayo, it is found that on the lunar age dial, all the points for the night-time are clustered close together; and that only the day-time points show larger amplitudes and move uniformly around the origin. On lunar time (τ) dial, the night-time points move around the origin and it is only day-time points which confine themselves in a narrow sector between 08-09 lunar hr. Thus it is seen that the lunar oscillations in H at both equatorial and non-equatorial stations are similar in the night-time. The lunar time (τ) control of lunar tide becomes evident only at the equatorial stations and for the day-time hours when the equatorial electrojet is existing.

4.6 Seasonal effects in lunar monthly oscillations of H

The variations of $\triangle$H versus the lunar age at fixed solar hours , 00, 03 .....21 hr, are shown in figure 50 for each season separately. The oscillations are predominantly semi-monthly in E-months, monthly in D-months, while in J-months both lunar monthly and lunar semi-monthly components

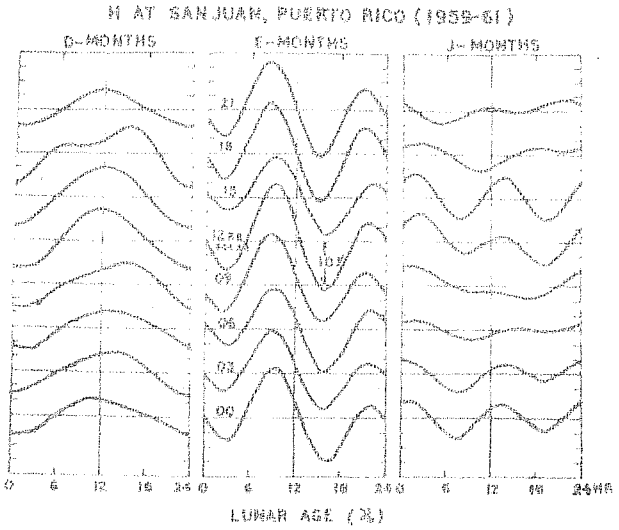


FIGURE - 50

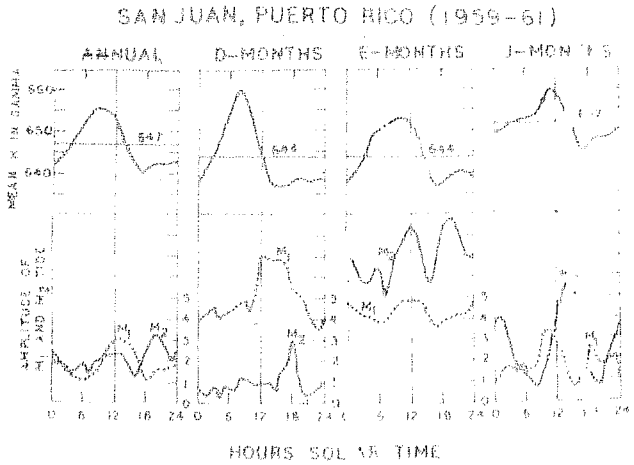


FIGURE - 51

are present. The amplitude r_2 and phase Θ_2 of lunar semi-monthly tide in H at individual solar hours, during each season, are given in table 16, which shows that $r_2(H)$ at any hour is maximum in E-months and minimum in J-months.

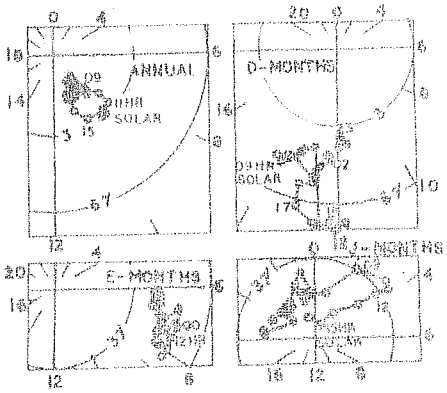
The solar daily variations of amplitudes $r_1(H)$ and $r_2(H)$, and of H itself, are presented in figure 51 for each season. It is seen that H at San Juan is maximum at 2-3 hr before mid-day in contrast to Huancayo where it is largest almost at noon. The amplitude $r_1(H)$ is greater than $r_2(H)$ in D-months, while it is less than $r_2(H)$ in E and J-months at any time of the day. The solar daily variation of $r_1(H)$ in any season shows a peak at midday hours. The maximum value of $r_1(H)$ is larger in D-months and smallest in J-months. The amplitude $r_2(H)$ shows a peak at 18 hr in D-months, at 12 and 20 hours in E-months; and exhibits two peaks, one just after midday (14 hr) and another at midnight, in J-months. Semi-monthly lunar oscillations are largest in E-months and are very small in D-months. It is to be noted that the solar daily variation of $r_2(H)$ at Huancayo shows a peak at about midday when H itself is maximum (fig.14). But, the shape of the solar daily variation of $r_2(H)$ at San Juan is different than the solar daily variation of H.

To study the variation of the phase Θ_1 with solar time, the coefficients (r_1, Θ_1) at each solar hour are plotted on the harmonic dials of lunar age (λ) and lunar time (τ)

in figure 52 and 53 respectively. The open and full circles indicate the day and night points respectively. In any season, the points (r_1, θ_1) on lunar time dial (fig.53) form a circle around the origin so that the mean amplitude of all the solar hours reduces to an insignificant low value. On the lunar age dial (fig.52), the corresponding points are grouped in a narrow sector in any of the seasons. The amplitude of the vector mean of the points on lunar age dial is of the same order as individual amplitudes. This is similar to the results at Huancayo where all the points (r_1, θ_1) cluster in a narrow sector on the lunar age dial (section 3.3; RASTOGI, 1968b). This indicates that the lunar monthly effects in H, both at equator and middle latitudes,are governed by the relative positions of the sun and moon (ν) and not by the absolute position of the moon (τ).

The amplitude and phase (r_2, θ_2) of lunar semi-monthly tide at different solar hours are plotted on lunar age (ν) and lunar time (τ) dial in figure 54 and 55 respectively. It is seen from fig.55 that (r_2, θ_2) points form two loops, centred at the origin in E-months, centred at a point outside the origin in J-months; while they cluster around a narrow sector in D-months. These points, in any season, group themselves in a narrow sector on the lunar age dial (fig.54). This feature is opposite to that at Huancayo where the olustering of points is seen more on the lunar time dial (section 3.5a). The relative importance of the two dials on ' ν ' and

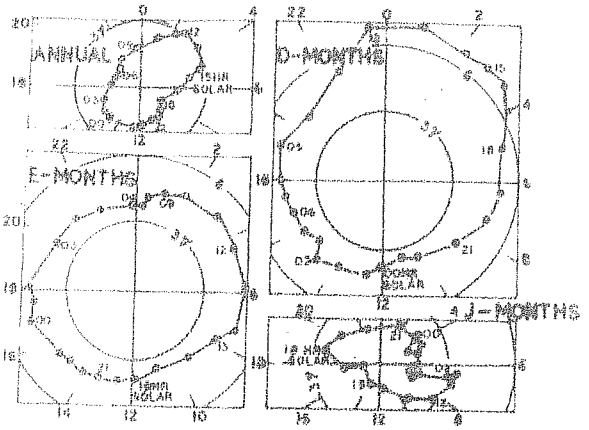
SAN JUAN, PUERTO RICO (1959-61)



HOURS LUNAR AGE (♈)

FIGURE - 52

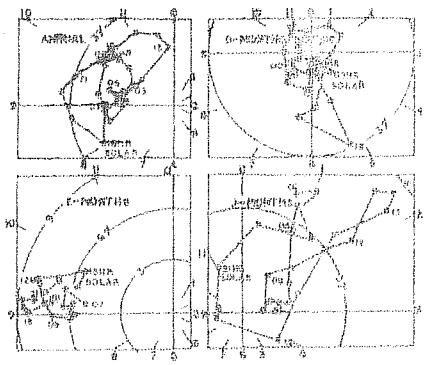
SAN JUAN, PUERTO RICO (1959-61)



HOURS LUNAR TIME (☌)

FIGURE - 53

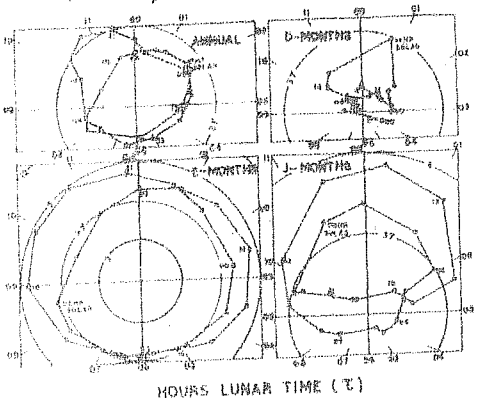
SAN JUAN, PUERTO RICO (1959-61)



HOURS LUNAR AGE (♈)

FIGURE - 54

SAN JUAN, PUERTO RICO (1959-61)



HOURS LUNAR TIME (☌)

FIGURE - 55

'τ' can be estimated from the vector mean of all the points on the two dials, and these are given in table 17 for both San Juan and Huancayo. The amplitude of the vector means on lunar age and lunar time dial are represented by $r_2(\nu)$ and $r_2(\tau)$ respectively. Table 17 shows that for annual average lunar semi-monthly oscillations, the ratio $r_2(\nu)/r_2(\tau)$ is 2.4 for San Juan and 0.3 for Huancayo. This clearly shows that lunar tide in H at San Juan is controlled by lunar age (ν) and it is controlled by lunar time (τ) at Huancayo. Further it is seen from the table that for San Juan, $r_2(\nu)/r_2(\tau)$ is 1.0 in D-months, 11.7 in E-months and 1.6 in J-months. The ratio for Huancayo is 0.4, 0.4 and 3.8 in D-months, E-months and J-months respectively. Thus, in any season, the lunar age control of lunar tide is evident at San Juan, which is in contrast to Huancayo where the tide is controlled by the lunar time except in J-months when lunar age control takes over (section 3.5a; RASTOGI, 1968b). Although the data utilised in the present analyses are of 34 months only, the results definitely show characteristic differences between geomagnetic lunar tides at equatorial and mid-latitude stations.

4.7 Perspective view of annual average luni-solar tide in the characteristics of the F2 region at Puerto Rico

The variations of the yearly average deviations ΔN_{max}, ΔH and Δh_{max} at Puerto Rico alongwith ΔN_{max} at Huancayo (reproduced from fig.8) on the grids of lunar time (τ)

and lunar age (ν) are shown in figure 56. The shaded portions in the diagram indicate night-time. Referring to the diagram for N_{max} at Puerto Rico, it is seen that in one lunar month, two high and two low major loops are present showing the predominance of lunar semi-monthly component in the lunar variations. The contour lines are dense in the daytime, but these are not significantly rare during the night. This suggests that lunar variations are present throughout the solar day and night, but these are stronger during the daytime hours only. A comparison with the diagram of N_{max} at Huancayo shows that the two diagrams are similar in nature except that high and low contour lines are interchanged in position. This indicates that lunar variation in N_{max} at Puerto Rico is opposite in phase to that at Huancayo, which is in confirmity with the earlier results of KASTOGI (1961b). The maxima and minima of contour lines for N_{max} at Puerto Rico are seen to be 2-3 times smaller than those at Huancayo. The diagram for H shows a number of high and low loops, randomly distributed, which indicates the presence of many harmonics in the lunar variation. These variations are seen to be slightly larger in the day than in the night-time. Lunar variations of h_{max} consist of many harmonics, and are larger during night than the daytime. The contour diagram for N_t at Puerto Rico, which is shown in figure 57, is similar to that of N_{max} (fig.56); indicating that N_{max} and N_t undergo similar lunar oscillations.

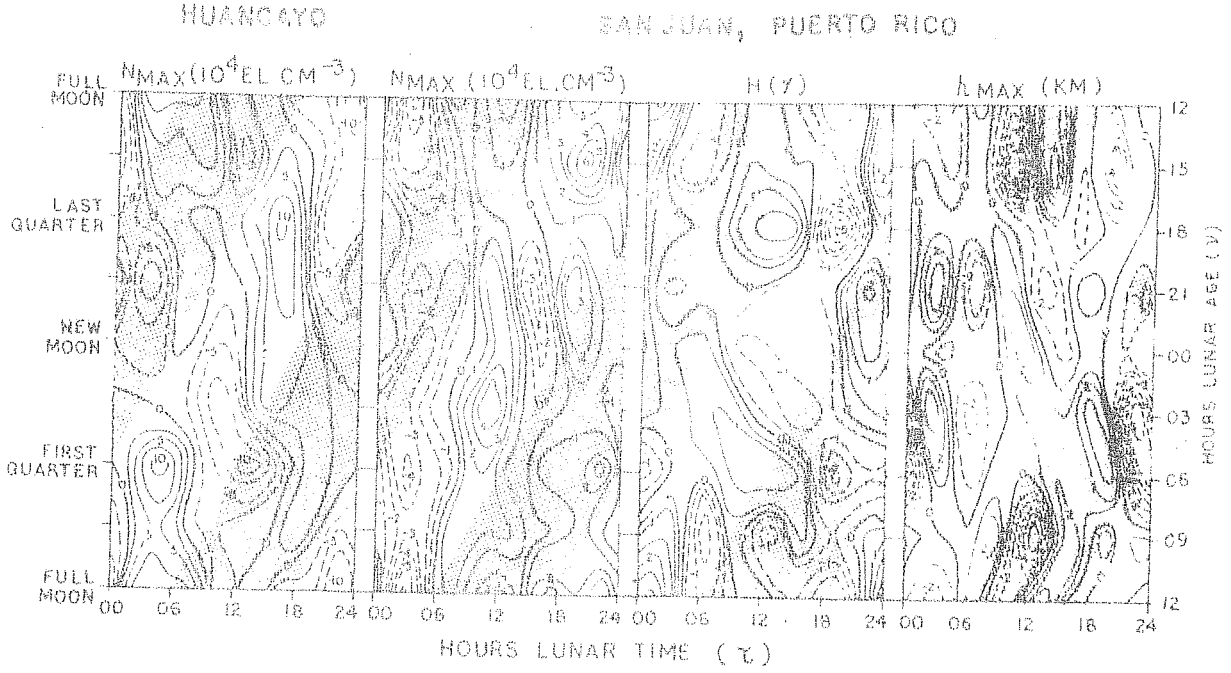


FIGURE - 56

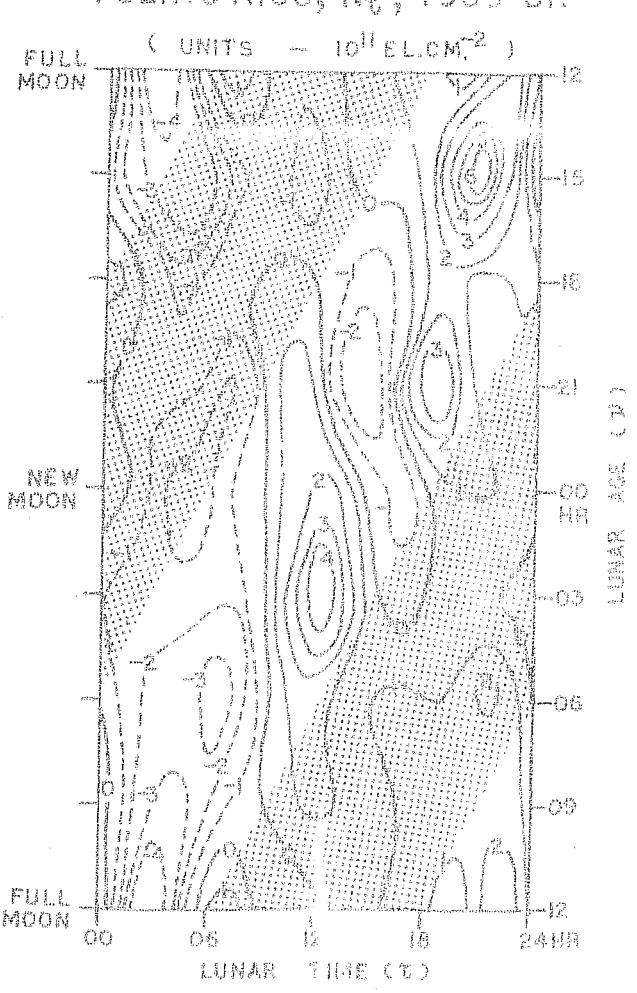


FIGURE - 57

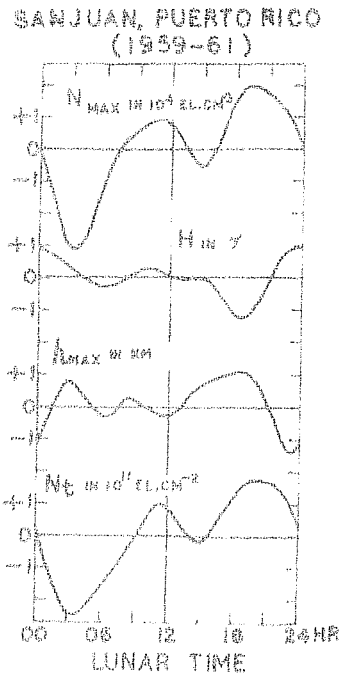
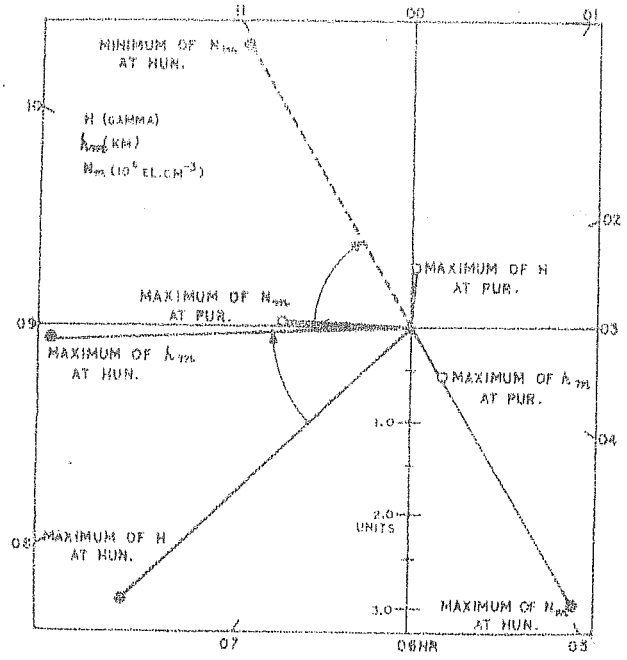


FIGURE - 58

The lunar daily variation averaged over a lunar month (L) is shown in figure 58 for all the parameters. The first four harmonic coefficients i.e. the amplitude and phase (L_n and ϕ_n) of these curves are presented in table 18. Figure 58 shows that the lunar variations of H and h_{max} are quite small and include many harmonics. The lunar daily variations of N_{max} and N_t, however, show mainly diurnal and semi-diurnal components, and are in the same phase. Referring to table 18, it is seen that the largest component in the lunar daily variation of H and h_{max} is L_2 while other harmonics are small. For lunar daily variation of N_{max}, firsttwo harmonic components (L_1, L_2) are larger than L_3 and L_4. The amplitude (L_2) and phase angle (ϕ_2) of lunar semi-diurnal component is $1.43 \times 10^4 EL.CM^{-3}$ and 178° respectively. RASTOGI (1969b) found the amplitude and phase of L_2 variation in f_oF_2 at Puerto Rico for the period 1951-55 to be 0.086 MHz ($\simeq 1.1 \times 10^4 EL.CM^{-3}$ for mean f_oF_2 of 5.2 MHz) and 184° respectively. Thus, both the results are fairly in agreement to each other. The slight increase of $L_2(N_{max})$ for period under study is due to sunspot number being higher during 1959-61 than 1951-55. It is, but, to be noted that while the present analysis gives the amplitude C_1 as $1.37 \times 10^4 EL.CM^{-3}$ which is only slightly smaller than C_2; RASTOGI's (1969b) results show that C_1 is considerably smaller than C_2. The phase of $L_2(N_t)$ is 160° which is nearly same as the phase of $L_2(N_{max})$, showing that the L_2 variations in N_t are closely controlled by that of N_{max}.

The interrelations between the phases of L_2 oscillations in H, h_{max}, and N_{max} are shown on the harmonic dial of lunar time (τ) in figure 59. Similar coefficients for Huancayo parameters (from table 6) are also included in the dial for comparison.

At Huancayo $L_2(h_{max})$ is in phase with $L_2(H)$ indicating that an increase of electrojet currents causes an increase of the height of the F_2-region with subsequent decrease of N_{max} with a certain delay time due to the definite recombination coefficient of the region. At Puerto Rico, the maximum $L_2(h_{max})$ occurs five hours after the maximum of $L_2(H)$ or an hour before the minimum of $L_2(H)$. Thus it does not appear logical that the oscillations in h_{max} at Puerto Rico are associated with the oscillations in H at the same place. However, it may be noted that the maximum of N_{max} at Puerto Rico occurs just after the maximum of h_{max} at Huancayo. It thus seems that the increase in the electric field at the equator causes the increase in H at the ground simultaneously, as well as the increase in the electrodynamic uplifting of the F_2-region at equator, resulting in a decrease of N_{max} at the equator and an increase of N_{max} at mid-latitudes. It is concluded that the lunar oscillations in whole of the equatorial anomaly region are associated with the variations of the electric field (or H) near the electrojet region.



LUNAR TIME (τ)

FIGURE — 59

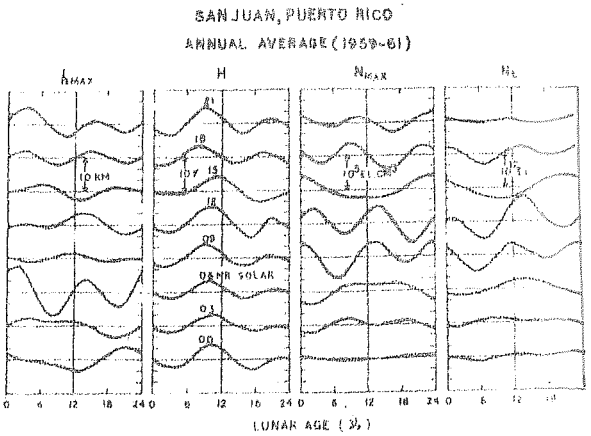


FIGURE — 60

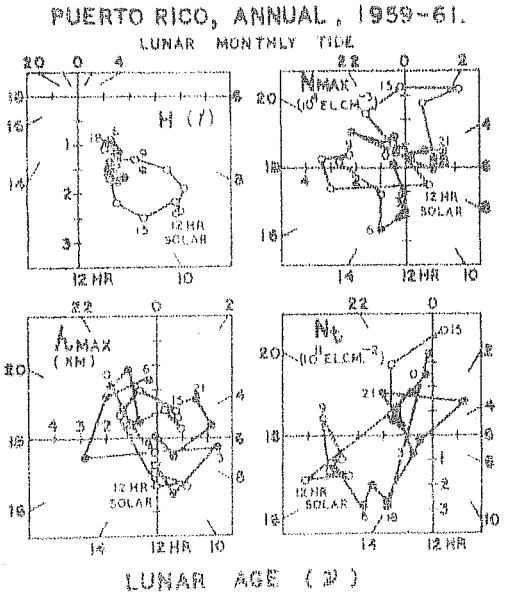


FIGURE — 61

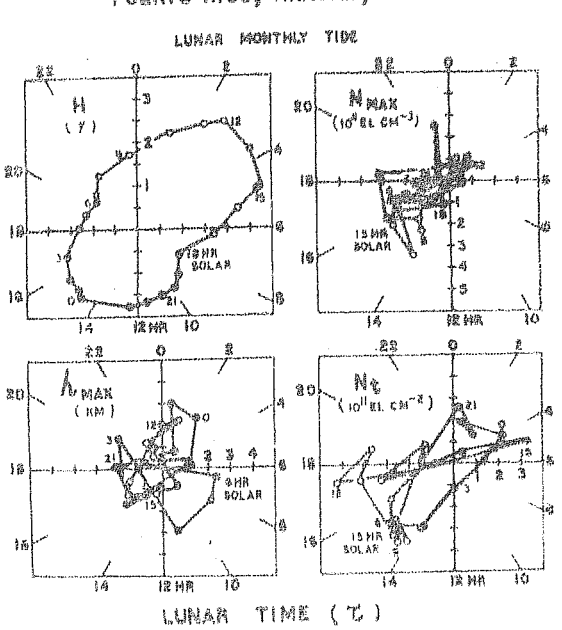


FIGURE — 62

4.8 Annual average lunar monthly tides in the F2 region

Lunar monthly variations (M) at different solar hours are computed for all the parameters. The built up curves out of the first two fourier components are drawn in figure 60. It is seen that the lunar monthly variations of H are of the same amplitude at all solar hours in contrast to Huancayo where these are stronger for the midday hours only (RASTOGI 1968a,b). The lunar monthly oscillations in h_{max} are seen to be present at all solar hours but these are largest at 06 hr. The variations of N_{max} and N_t are largest around 09-12 hrs and are least at midnight.

To study the solar time variation of the amplitude r_1 and phase Θ_1 of lunar monthly component of the M variation, these, for each parameter, are shown on the harmonic dials of lunar age ($\mathcal{U}$) and lunar time ($\mathcal{T}$) in figures 61 and 62 respectively. It is seen that only the M_1(H) tide shows a regular behaviour with solar time; which has already been described in section 4.5. The M_1 tide in the ionospheric parameters does not show any systematic variation either of amplitude or phase with solar time on both the dials.

The amplitude (r_2) and phase (Θ_2) of lunar semi-monthly tide in h_{max}, N_{max} and N_t are given in tables 19, 20 and 21 respectively, for each season separately. The probable errors in computing r_2 are also included in the tables. The amplitudes (r_2) which do not satisfy the

statistical significance test are bracketed. It is seen from the tables 19, 20 and 21 that the M_2 oscillations in N_{max} and h_{max} are statistically significant at most of the hours, while these in N_t are very small for 00-07 hours. To study the solar daily variations of the amplitudes r_2, these are plotted in figure 63, alongwith the average value of the parameter itself. It is seen from figure 63, that annual average H at San Juan is maximum at 09-10 hr and not at midday. The solar daily variation of h_{max} shows greater values at about 05 and 22 hours. The M_2 oscillations in h_{max} are stronger when h_{max} itself is greatest, i.e. at 05-06 hours and again at 23 hr; and these are minimum at about 08 hr. The $M_2(N_{max})$ and $M_2(N_t)$ tides are maximum at midday hours when N_{max} and N_t are also largest. There is a drop in $M_2(N_t)$ and $M_2(N_{max})$ curves at about 14 hr after which $M_2(N_{max})$ again attains a very high value at 17 hr, while $M_2(N_t)$ does not increase to great extent.

The solar daily variation of the amplitude and phase (r_2, θ_2) of the M_2 tide in all the parameters is also shown on the harmonic dials of lunar age (ν) and lunar time (τ) in figure 64 and 65 respectively. The diagram for H shows that all the (r_2, θ_2) points on 'ν' dial are contained between the sector 08-12 lunar hr, while they form two loops around the origin on the 'τ' dial resulting in a low value for the mean amplitude for all hours.

SAN JUAN, PUERTO RICO

ANNUAL AVERAGE (1959-61)

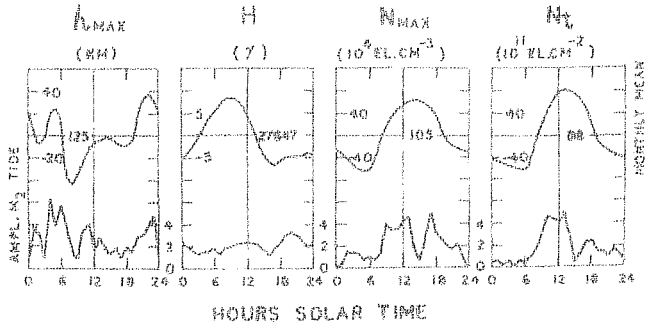


FIGURE - 63

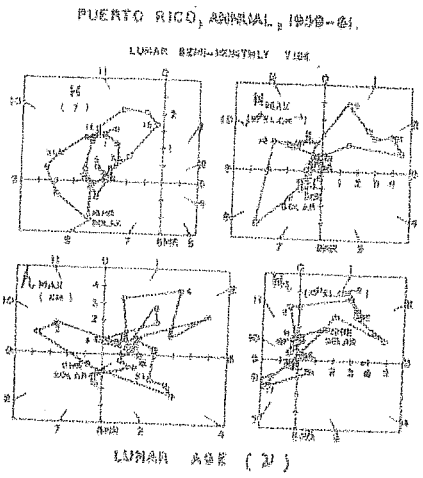


FIGURE - 64

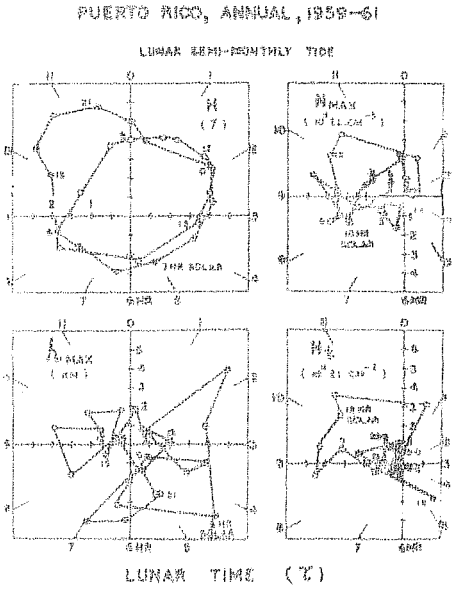


FIGURE - 65

The diagram for h_{max} on the ' $\mathcal{V}$ ' dial shows that $r_2(h_{max})$ amplitude is large at 06 and 23 solar hours; and that there is no systematic variation of either the amplitude or phase with solar time. On the ' τ ' dial, however, almost all the day-time points (09-16 hr) are confined in the sector 08-00 lunar hour, which indicates that $M_2(h_{max})$ tide during the solar day-time is governed by the absolute position of the moon (τ).

Referring to the diagram for N_{max} and N_t on the lunar age dial (fig.64), it is seen that the M_2 tide in both is greater for the hours near midday, and is small during the night-time hours. The (r_2, Θ_2) points for both N_{max} and N_t, between the hours 08-15 are confined in a narrow sector between 11-03 lunar hour. The lunar time harmonic dials for N_{max} and N_t(fig.65) are also quite similar. The day-time points (07-15 hr) for both the parameters from a broad loop between 08-03 lunar hr sector. These features show that the lunar semi-monthly oscillations of N_{max} and N_t are similar in nature. It is to be noted that M_2 tides in H, h_{max} and N_{max} or N_t do not indicate any correlation between them.

4.9 Seasonal effects in lunar daily variations ($L\mathcal{V}$, L) of ionospheric parameters

The lunar daily variations of h_{max}, N_{max} and N_t at three hourly groups of lunar ages centred at 00, 03, 06..... 18 and 21 hr, during different seasons are plotted in figure 66, 67 and 68 respectively. The first four harmonic components

PUERTO RICO, A_{HAR}, 1959-61.

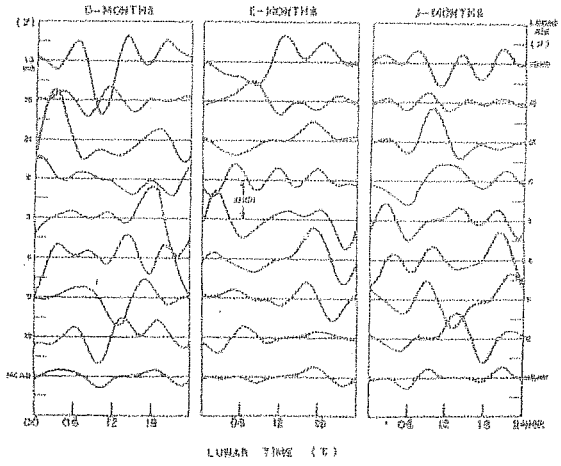


FIGURE - 66

PUERTO RICO, H_{HAR}, 1959-61.

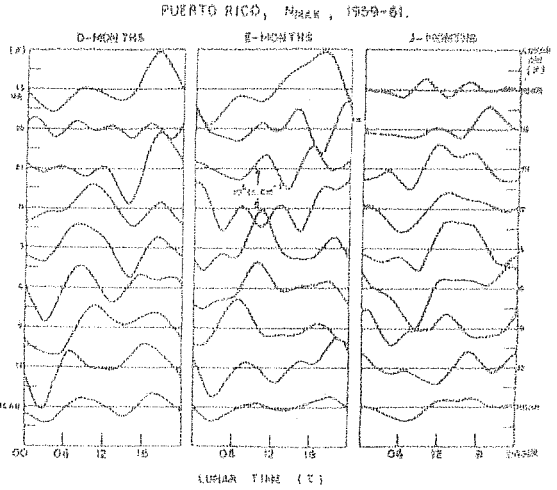


FIGURE - 67

PUERTO RICO, H_0, 1959-61.

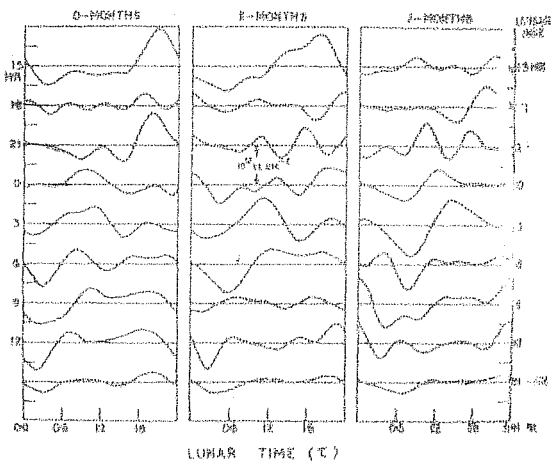


FIGURE - 68

SAN JUAN, PUERTO RICO, 1959-61.

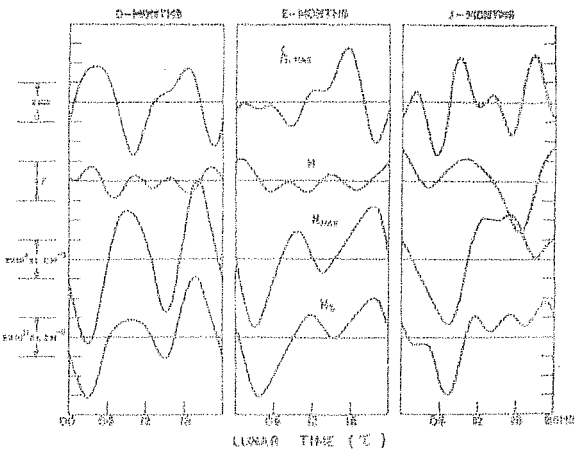


FIGURE - 69

(C_n, α_n) of these curves during different seasons are given for h_{max}, N_{max} and N_t in tables 22, 23 and 24 respectively.

It is apparent from figures 66, 67 and 68 that L_ν variations of all ionospheric parameters in any season contain many higher harmonics; and that these variations are appreciable during the day as well as in the night hours, i.e. the tides in h_{max}, N_{max} and N_t do not indicate any luni-solar effect. It is further seen from table 22 that the amplitudes C_1, C_2 and C_3 of first three harmonic components of $L_\nu(h_{max})$ variation at a fixed ν value are, approximately of equal magnitude; and that the amplitude of fourth harmonic component (C_4) is only slightly less than the first three. In case of L_ν (N_{max}) and L_ν (N_t) tides (tables 23 and 24), the amplitude of the first two harmonics C_1 and C_2 are nearly equal, while C_3 and C_4 are slightly less than these and are roughly of equal magnitude. Further, it is interesting to note that the lunar daily oscillations of N_{max} and N_t at any fixed age (ν) are very similar to each other (fig. 67 and 68) in any season.

The whole lunation average lunar daily variations(L) for all the parameters are also computed for three seasons separately; and these are plotted in figure 69 in order to study any interrelations between them. The first two harmonic coefficients (L_n, ϕ_n) of the L variation in all the parameters are given in table 25 for each season separately. It is seen

from figure 69 that the lunar daily variation of H is very small during D and E months, but is appreciable during J-months. There seems to be no correlation between L(H), and $L(h_{max})$, $L(N_{max})$ or $L(N_t)$ variations. However, the lunar daily variations of N_{max} and N_t during any season are very much similar to each other.

From table 25, it is seen that the L_2 oscillations in H are maximum in J-months and least in D-months. The lunar semi-diurnal tide in h_{max}, $L_2(h_{max})$, is maximum in D-months and least in E-months. $L_2(N_{max})$ or $L_2(N_t)$ oscillations are, however, stronger in D-months and least in J-months, which is in agreement with RASTOGI's (1969b) results.

4.10 Seasonal effects in lunar monthly (M) tides in ionospheric parameters

Lunar monthly variations (M) at individual fixed solar hours are computed in all the parameters (h_{max}, N_{max} and N_t) for each season separately. The lunar monthly component (M_1) was found to be generally less than the semi-monthly component (M_2), and does not show any regular behaviour with solar time (section 4.8). Therefore it will not be discussed. The results of the lunar semi-monthly tide in different seasons are described below, separately for each parameter.

(a) Height of peak ionisation (hmax)

Figure 70 shows the lunar monthly variations of h_{max} at 00, 03, 06 .....18 and 21 solar hr for each season

PUERTO RICO , h_{MAX} , 1959-61

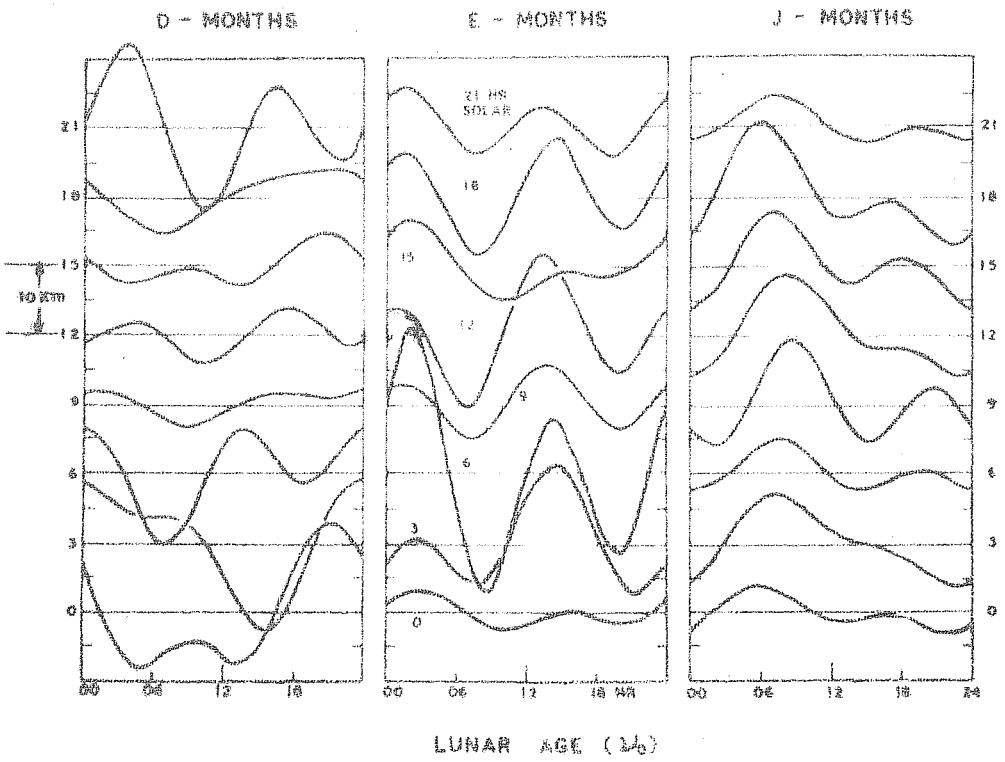


FIGURE - 70

SAN JUAN, PUERTO RICO (1959-61)

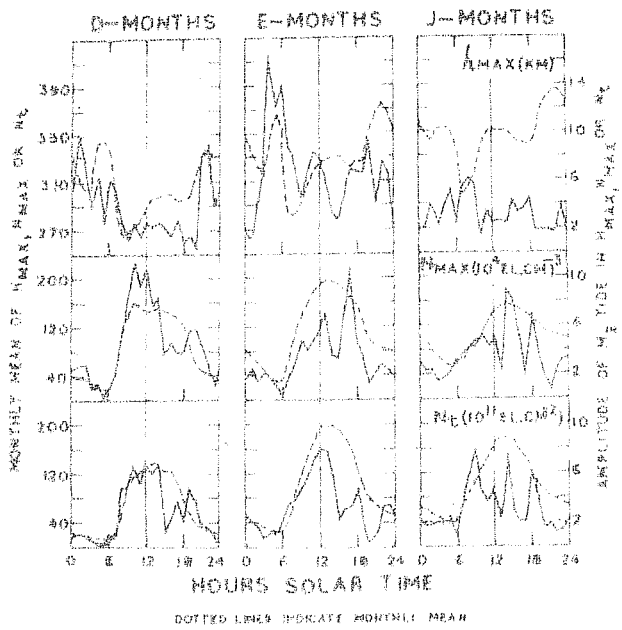


FIGURE - 71

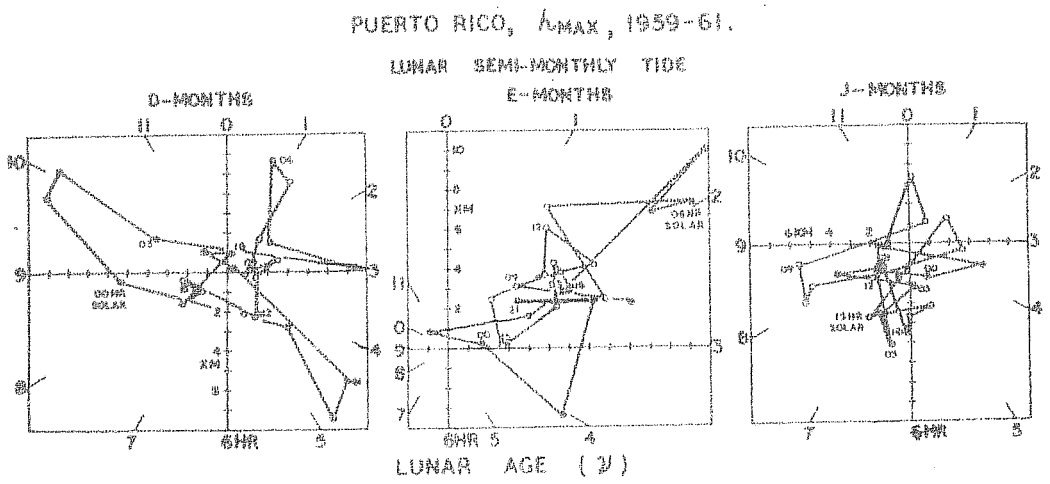


FIGURE - 72

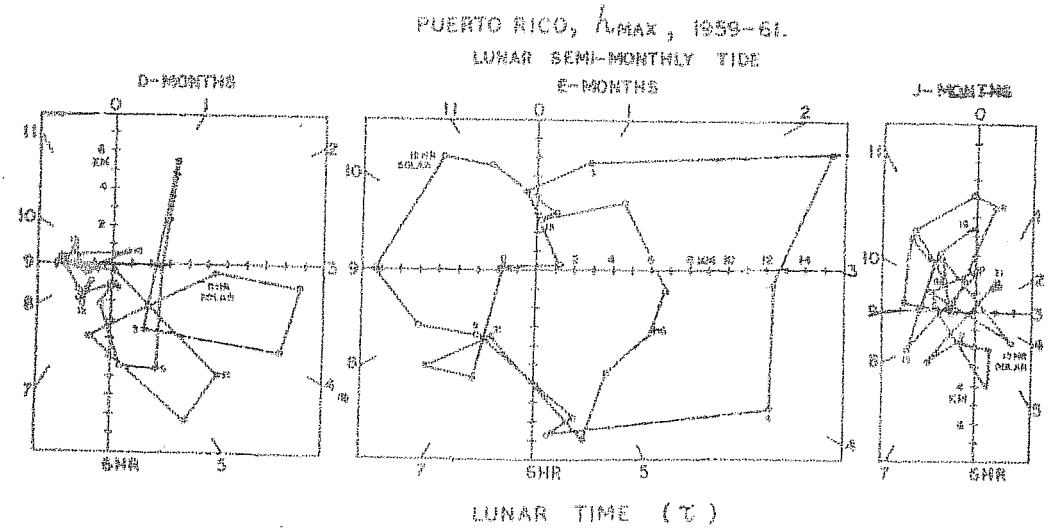


FIGURE - 73

separately. The coefficients (r_2, θ_2) of the $M_2(h_{max})$ tide at individual solar hours are given in table 19, for each season. It is seen from the table that the amplitude r_2 is, in general, significant at all the hours of the solar day. This is also apparent from figure 70, which shows appreciable variations at all the hours. The maximum oscillations of h_{max} is seen to occur around midnight hours (21, 00, 03 hr) in D-months, at 06 hr in E-months, and at 09 hr in J-months.

The solar daily variations of the amplitude $r_2(h_{max})$ and of h_{max} itself are shown in figure 71. The amplitude, $r_2(h_{max})$, in D and E-months is seen to be maximum at the time when h_{max} itself is very high; and shows an irregular variation in J-months.

The individual coefficients (r_2, θ_2) at each solar hour are also shown on the harmonic dials of lunar age (ν) and lunar time (τ) in figures 72 and 73 respectively. In D-months, the amplitude is seen to be maximum at 21-22 and 1-2 solar hours. Also the (r_2, θ_2) points on the ' ν ' dial show a large but irregular phase variation with solar time. The day-time points on the ' τ ' dial show a cluster near the origin, while the night-time points, except at 04 hr, are in the sector between 03-06 lunar hr.

Referring to the diagram for E-months on the ' ν ' dial (fig.72), it is seen that the amplitude is maximum at 04 solar hr; and that all the day-time points (r_2, θ_2), and most of the

night ones, are confined in a narrow sector between 01-03 lunar hour. On the 'τ' dial (fig.73), the points form two loops around the origin, one for the day-time and another for the night-time, such that 24 hourly mean amplitude reduces to an insignificant low value. This indicates that the lunar oscillations of h_{max} in E-months are controlled by the relative positions of the Sun and moon (γ), in similarity with the M_2(H) tides (section 4.5).

The coefficients (r_2, Θ_2) in J-months do not show any systematic solar time behaviour. The amplitude r_2 at any hour is quite small and is maximum at 09-10 solar hour.

(b) Maximum electron density (Nmax)

Lunar monthly (M) variations of N_{max} at different solar hours (00, 03, 06.....18 and 21) in each season are shown in figure 74. The harmonic coefficients (r_2, Θ_2) of semi-monthly variation at individual solar hours are given in table 20 for each season separately. The table shows that the amplitude is generally statistically significant at all the hours. It is seen from figure 74 that the lunar oscillations of N_{max} are maximum at 12-15 hours in D-months, and at 12-18 hours in E and J months.

The solar daily variations of $r_2(N_{max})$ and the mean N_{max} are plotted in figure 71. The amplitude r_2 (N_{max}) is seen to be maximum at midday in D-months, at 17 hr in E-months, and at 14-15 hours in J-months. Further, the amplitude is

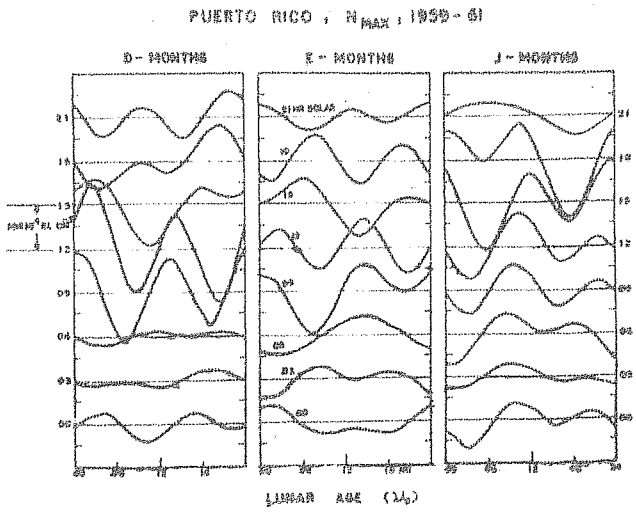


FIGURE - 74

PUERTO RICO, N_{MAX}, 1959-61.

LUNAR SEMI-MONTHLY TIDE

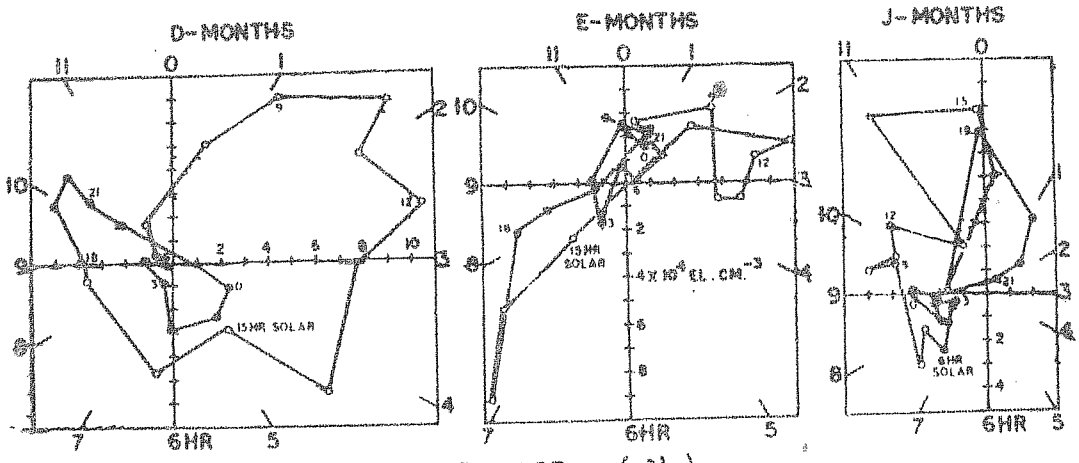


FIGURE - 75

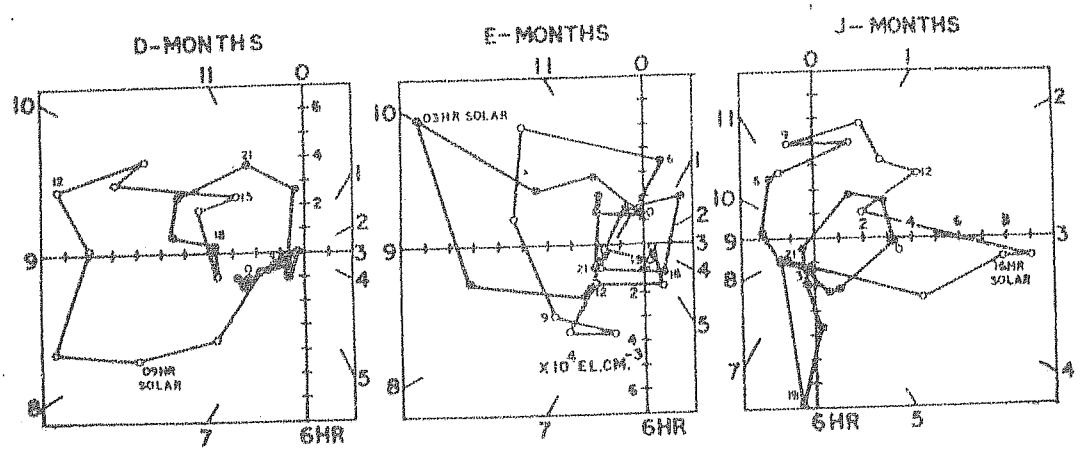


FIGURE - X
76

maximum in D-months, less in E-months, and least during J-months. This seasonal behaviour of the $M_2(N_{max})$ tide is similar to that observed for the equatorial station Huancayo (section 3.5 c).

The coefficients (r_2, θ_2) at individual solar hours are shown on the harmonic dials of lunar age (ν) and lunar time (τ) in figures 75 and 76 respectively. During D-months, the (r_2, θ_2) points on the ' ν ' dial show a gradual phase retardation of the $M_2(N_{max})$ tide with solar hour. They form two loops, one broad for the hours 07-22 and another a small one for the hours 23-06, around the origin such that the 24 hourly mean amplitude reduces to a low value. On the ' τ ' dial (fig.76), the points corresponding to hours between 23-08 which have smaller amplitudes are clustered together in the 08-09 lunar hr sector. The points between 08-22 solar hour form a broad loop contained in the 07-11 lunar hour sector so that 24 hourly mean amplitude is of the same order as the individual amplitudes. This indicates that the $M_2(N_{max})$ tide in D-months is controlled by lunar time τ .

During E-months, the night-time points on the ' ν ' dial (fig.75) are grouped together near the origin, while the day-time points show a very large phase change with solar time; the phase varies by about 180° (6 lunar hr) from 1-3 lunar hr at 08-13 solar hr to 7-8 lunar hr at 15-19 solar hours. Thus the mean amplitude of all the hours is reduced to a very low value. On the ' τ ' dial (fig.76), the night-time points show a large irregular variation with solar hour. On

the other hand, most of the day-time points are confined in the sector of lunar time 05-09 hr. It thus appears that the phase of $M_2(N_{max})$ tide in E-months is governed by lunar time τ; maximum value of N_{max} at any hour occurs at lunar time 05-09 hr.

During J-months and on the ' ν ' dial, the points between 22-05 solar hr are grouped together near origin, while the day-time points (06-17 hr) move uniformly on the dial showing a large phase change with time. However, the loop formed by the day-time points do not enclose the origin. On the ' τ ' dial (fig.76), the night-time points show a large and irregular phase change with solar hr; and the day-time points form a broad loop enclosing the origin so that the 24 hourly mean amplitude is very low. Thus a lunar age control of the $M_2(N_{max})$ tide is indicated in J-months.

It is clear from the above discussions that the lunar tide in N_{max} is controlled by the absolute position of the moon (τ) in D and E-months, and probably by lunar age in J-months. It should be noted that $M_2(H)$ tide at San Juan in any season is controlled by lunar age (ν) and not by lunar time (τ) (section 4.6). Thus the lunar age or time control of lunar tides in N_{max} and H at the same place is different. However, it is recalled that the lunar oscillations of H at the equatorial station, Huancayo, shows a lunar time (τ) control in D and E months and a lunar age (ν) control in J-months (section 3.5a). This behaviour of $M_2(H)$

tide at Huancayo is similar to the $M_2(N_{max})$ tide at Puerto Rico, which suggests that the lunar perturbations of the peak electron density at Puerto Rico may be associated with the corresponding oscillations of H at the equator.

(c) Total electron content (Nt)

Lunar monthly oscillations of N_t at solar hours 00, 03, 06.....18 and 21, are presented in figure 77 for each season separately. The coefficients (r_2, θ_2) of the semi-monthly component of these variations are given in table 21 for individual solar hours. It is seen from the table that the tidal amplitudes are, in general, statistically well determined. Figure 77 shows that larger oscillations occur near midday hours (09-12) and these are semi-monthly in nature at these hours.

The solar daily variations of $r_2(N_t)$ and of N_t itself, are shown in figure 71 which also shows the solar daily variation of N_{max} and $r_2(N_{max})$. It is seen that in any season, the solar daily variation of N_t is similar to that of N_{max}; both show maximum values a few hours after solar noon. The $r_2(N_t)$ generally varies in a similar manner to N_t itself, being maximum when N_t is also very high. The amplitude r_2 is greater at 12-13 hr in D and E months and at 09, 14 and 18 hrs in J-months.

To study the solar daily variation of the phase of $M_2(N_t)$ tide in each season, the coefficients (r_2, θ_2) at

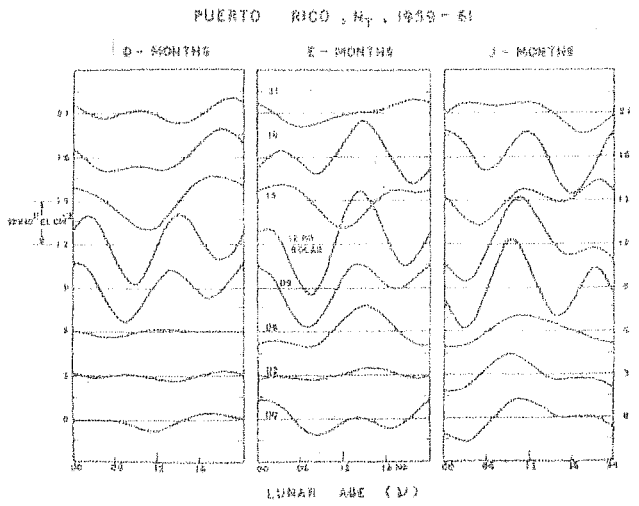


FIGURE - 77

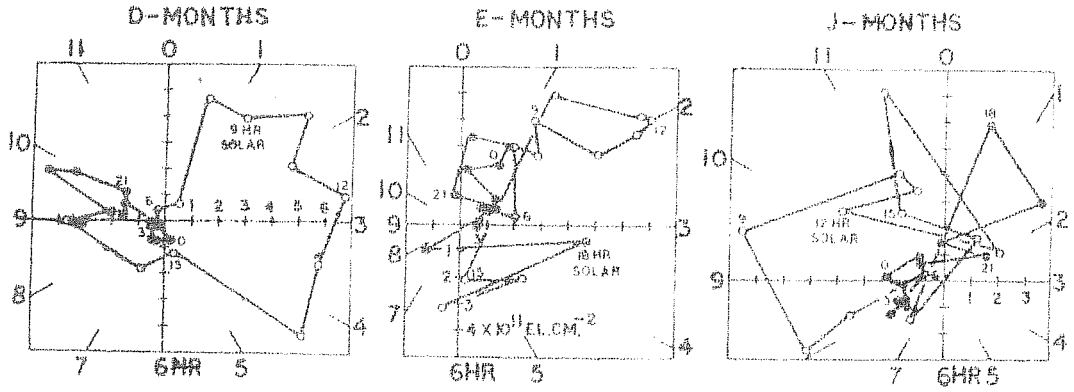


FIGURE - 78

PUERTO RICO, N_L , 1959-61.

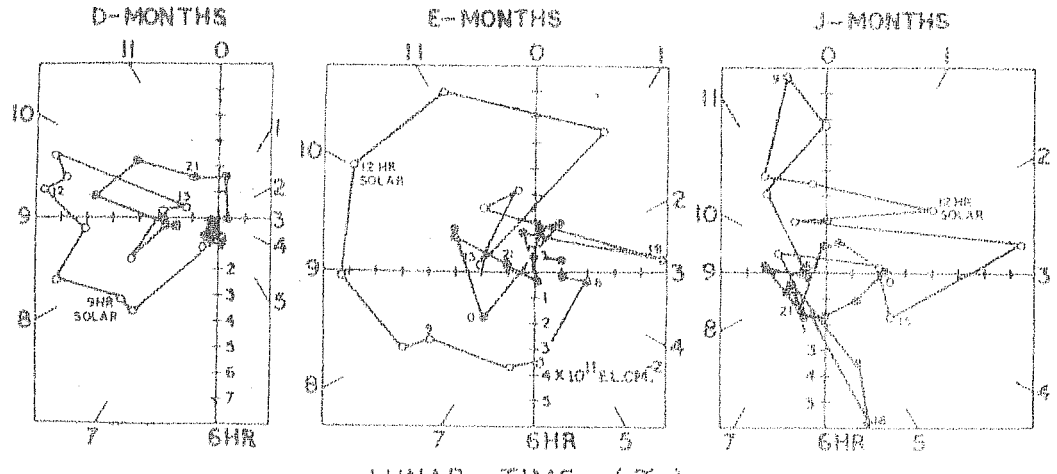


FIGURE - 79

individual solar hours are plotted on the harmonic dials of lunar age and lunar time in figures 78 and 79 respectively. A comparison with similar diagrams for N_{max} (fig.75 and 76) shows that there is quite a similarity between the corresponding diagrams for any season.

During D-months, the night-time points on the ' ν ' dial are clustered near the origin; while the day-time points form a broad loop giving a low value for the mean amplitude. The day-time points on the ' τ ' dial form a narrow loop in the sector 08-10 lunar hr indicating a lunar time control of the tide.

In E-months, the night-time points on the ' ν ' dial do not show any regular variation and are grouped together. The day time points undergo a large phase change, as much as by 180° between prenoon (06-14 hr) and the evening hours (15-18 hr). On the ' τ ' dial, the night-time points are scattered around the origin, and the day-time points form a broad loop which is confined in the sector between 06 and 00 lunar hr.

In J-months, the night-time points on both the dials show irregular variation with solar hour. However, they show a grouping on the ' ν ' dial, and form a small loop around the origin on the ' τ ' dial. The day-time points on the ' ν ' dial (fig.78) form a broad loop outside the origin in the 08-11 lunar hr sector. On the ' τ ' dial, these form a

loop in the opposite sector of 11-04 lunar hr.

These features of $M_2(N_t)$ variations are similar to those shown by the $M_2(N_{max})$ tide (section 4.10b).

4.11 Conclusions

From the discussions in the main body of this chapter, the following important conclusions are drawn:

(a) Lunar variations of H at San Juan

(1) There is no luni-solar effect in the tide in H.

(2) The whole lunation average lunar daily variation (L) of H is not a pure semi-diurnal curve as is the case at Huancayo, but contains appreciable diurnal component as well.

(3) The amplitude of the semi-diurnal lunar oscillations of H at San Juan is approximately 8 times less than at Huancayo.

(4) The amplitude $L_2(H)$ is maximum in J-months, less in E-months, and minimum in D-months.

(5) Lunar monthly component (M_1) of the tide in any season is governed by the lunar age (ν) at equatorial as well as non-equatorial stations.

(6) Lunar $M_2(H)$ tide during night-time is controlled by the relative positions of the Sun and Moon (ν) for equatorial as well as mid-latitude stations; but for equatorial stations and in the day-time when electrojet exists, the

tide is controlled by the lunar time (τ).

(7) The amplitude $r_2(H)$ of semi-monthly tide is maximum in E-months, less in J-months, and least in D-months.

(b) Lunar tides in the F2 region at Puerto Rico

(8) The phase of lunar variations of $N_{max}\ F_2$ is opposite to that at Huancayo.

(9) Lunar perturbations of N_{max} and N_t are very similar to each other.

(10) Lunar variations of electron density at Puerto Rico is not associated with the corresponding oscillations of H at the same place. The results indicate that lunar oscillations of the electron density in whole of equatorial anomaly region are controlled by the variations of H at the equator.

(11) The lunar daily variations, averaged over a lunation, of h_{max}, N_{max} and N_t are not purely semi-diurnal but contain apreciable diurnal and ter-diurnal components.

(12) The amplitude L_2 of semi-diurnal component of the tide in h_{max} is maximum in D-months and minimum in E-months.

(13) $L_2(N_{max})$ and $L_2(N_t)$ tide is maximum in D-months, less in E-months, and minimum in J-months. This is similar to the seasonal behaviour of $L_2(H)$ at Huancayo.

(14) The lunar semi-monthly (M_2) oscillations in h_{max} are appreciable for all the hours of the day, but are maximum at about 06 hour when h_{max} itself is very high.

(15) $M_2(N_{max})$ and $M_2(N_t)$ tide is maximum near the midday hours (09-12) when N_t itself is maximum.

(16) The lunar semi-monthly variations of N_{max} seem to be governed by lunar time (τ) in D and E months and by lunar age (ν) in J-months. This feature is similar to that of $M_2(H)$ tide at Huancayo.

(17) The amplitude $r_2(h_{max})$ is maximum in E-months and minimum in J-months, while $r_2(N_{max})$ is largest in D-months and least in J-months.

CHAPTER - V

LUNAR TIDES IN ELECTRON DENSITY AT FIXED HEIGHTS OF THE IONOSPHERE AT EQUATORIAL, TROPICAL AND MIDLATITUDE STATIONS

5.1 Introduction

Lunar tidal phenomena in the ionosphere have been extensively studied for many stations using, generally, the critical frequency and virtual height data of the layers since the original works of APPLETON and WELKES (1939) and MARTYN (1947, 1948). A study of the variation of lunar tidal effects with height is rather important because this would give the ionospheric movements through whole of the ionosphere. There are two methods of approaches, found in literature, to study this problem.

In the first method, the lunar variations of f_oF_2 are computed at different solar hours of the day. Using the fact that the f_oF_2 values during the course of a day happen to be at different heights, a curve between the amplitude $r_2(f_oF_2)$ and the height of peak ionisation, h_{max}, is plotted giving the height variation of lunar tidal effects in electron density. This procedure has been followed by BROWN (1968) and RUSH and VENKATESWARAN (1968). The height variation of lunar tide in $N_{max}F_2$ at Huancayo, computed according to this method, shows that the tidal amplitude increases with altitude (section 3.6). However, this method is not accurate for the fact that data of

all solar hours are used without any discrimination. Further, the physical and electrodynamical properties of the ionosphere at a particular level has large daily variations, which are again height dependent.

In the second method, which is more laborious, the true height electron density profiles, N(h), are used and lunar tidal effects are derived at fixed heights of the ionosphere. This is the most accurate method because of obvious reasons; but necessitates availability of a long series of N(h) profile data, which have been computed, so far, for a few stations only. Recently, BURKARD (1965, 1966), SHARMA and RASTOGI (1967, 1968) and ZAGULYAEVA and FATKULLIN (1966, 1969) have computed height variation of lunar tide using this method. The lunar tidal effects in f_0F_2 are now known to depend on solar time (section 2.10b). The various workers, so far, have not taken into account these luni-solar variations in computing the lunar tides in N(h) profile. SHARMA and RASTOGI (1967, 1968) have used only the noon data; BURKARD (1965, 1966) has used data collectively for 08 through 17 solar hours, while ZAGULYAEVA and FATKULLIN (1966, 1969) have used data for all the solar hours taken together.

To study the luni-solar effects, it is desirable to compute the height variation of lunar tide, individually at fixed solar hours. As a first step, noon hour was chosen, since the tidal variations are known to be large at about

noon, and the tides in electron density at fixed levels of the noon ionosphere over Ahmedabad (1963-65), Huancayo (1960-61) and Puerto Rico (1959-61) were computed. Later, the lunar tides in N(h) profiles at Huancayo (1961) and Puerto Rico (1959-61) were computed at individual solar hours. The results of these computations are described in the following sections.

5.2 Lunar perturbations of noon electron density at fixed heights of the ionosphere over Ahmedabad

Firstly, all ionograms at Ahmedabad (Geog. Long. 72°36'E, Lat.23°01'N) for 1200 solar hour in the period January 1963 to December 1965, i.e. the data of 36 months, were analysed to compute electron density profiles N(h) of the ionosphere. The computations were done upto the height of h_{max}. Secondly, the data were divided into three seasonal groups viz. D-months, E-months and J-months. For a particular season, lunar semi-monthly (M_2) tides in N(h) were calculated for fixed heights (h) at height intervals of 20 km, following the method described in section 2.3c).

For comparison, the data of critical frequency, f_oF_2 in MHz, maximum electron density (N_{max}) and the height of maximum electron density (h_{max}) were analysed for lunar semi-monthly component.

The mean values of these F_2 parameters, the amplitude r_2 of M_2 tide expressed in absolute units as well as fraction of the mean value, and the phase Θ_2 are collected in table 26.

The value of h_{max} is maximum (315 Km) in J-months and minimum (263 km) in D-months. The corresponding M_2 tide has an amplitude of 8 Km with a maximum at 11.3 lunar hr during J-months and 5.2 km with a maximum at 7.2 lunar hr during D-months. The mean f_oF_2 is maximum in E-months and minimum in J-months, while the amplitude $r_2(f_oF_2)$ is maximum (0.7 MHz) in E-months and minimum in D-months (0.4 MHz).

In table 27 are given, for each season, the values of the mean electron density (N_h) at fixed heights h, the amplitude r_2 in units of electrons per c.c., the ratio r_2/N in percent, and the phase (θ_2) of M_2 oscillations in terms of lunar time. The height variations of the mean electron density and of the amplitude of M_2 tide for each season are shown in figure 80; while the phases of M_2 oscillations at different heights during each season are plotted in figure 81.

Referring to figure 80, one finds that the mean electron density below about 150 Km is maximum in J-months and minimum in D-months; while above 180 Km, reverse is the case. This suggests that below 150 Km, the noon ionosphere over Ahmedabad obeys the Chapman laws of ionisation. It is interesting to note that although N_{max} is maximum in E-months, the electron density at any fixed level above 160 Km is maximum in D-months, less in E-months, and least in J-months.

Referring to the upper diagram in figure 80, which shows the tidal amplitudes at different heights, one notices that

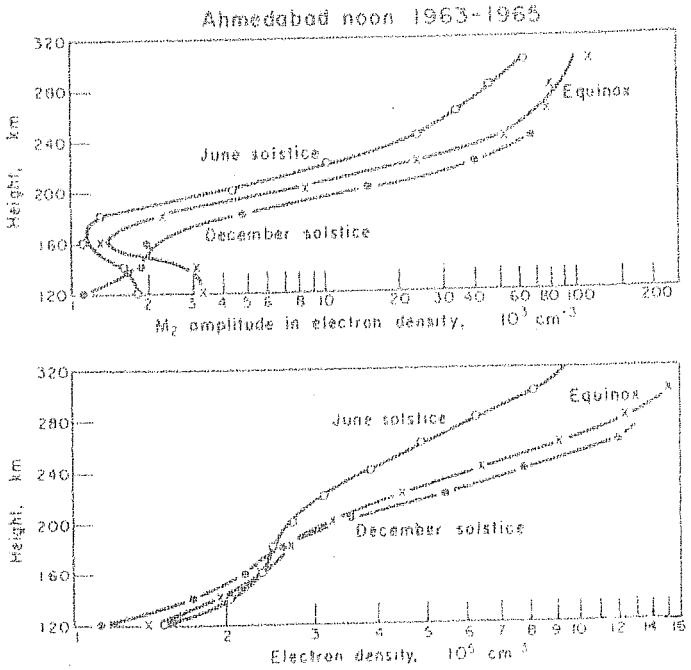


FIGURE - 80

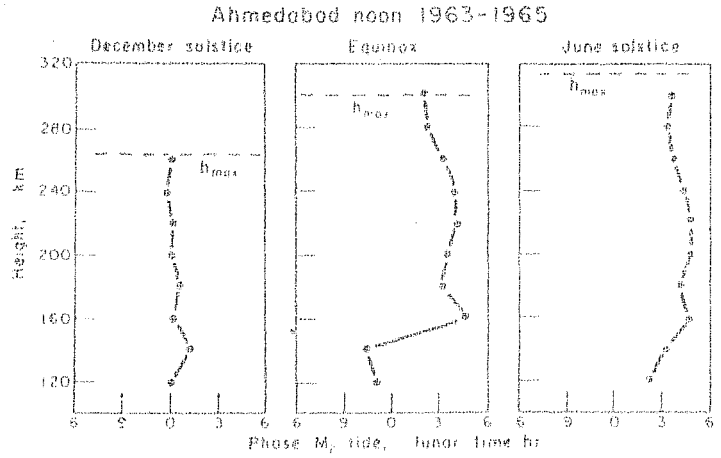


FIGURE - 81

between 120 and 160 Km the amplitude decreases with height in E and J-months, while it apparently increases with height in D-months. However, the amplitudes in this height range are very small of the order of 10^3 electrons/cm^3 or about 1% of the mean electron density. Above 160 Km, the tidal amplitudes steadily increase with height. At 180 Km, the amplitudes are of the order of 10^3 electrons/cm^3 or about 1% of the mean electron density at that level; while at 280 Km, the tidal amplitudes are of the order of 10^5 electrons/cm^3 or about 10% of the mean electron density. The amplitudes could not be calculated upto the level of h_{max} because of decreasing number of values of N(h) available near those levels. Thus within 100 Km of the F_2 region, the mean electron density increases by a factor of 10 but the tidal amplitude increases by a factor of about 100. BURKARD (1966) found that the amplitude of tide in N(h) at Puerto Rico during January 1960 is 2.6% at 150 Km, 4.3% at 290 Km, and 5.9% at N_{max}. This smaller increase of the tidal amplitude with height in Burkard's calculations may be due to the fact that he used data for all hours of the day, whereas the present analysis refers only to the noon, when the tides are strong.

Regarding the seasonal variation of the tide, it is seen that at any fixed level below h_{max}, the amplitudes are largest in D-months, less in E-months, and least in J-months.

Referring to figure 81, the phase of the lunar tide in N(h) is found to be independent of height (h) in any of the seasons. This again is different from BURKARD's (1966) results where the phase of M_2 tide at Puerto Rico progressively changed with height.

It is concluded that the amplitude of lunar semi-monthly tide in electron density within the F_2 region of the ionosphere over Ahmedabad increase with height during each season; and that it is maximum in D-months and minimum in J-months for any height. Also, above 160 Km, the phase does not seem to depend on height in any of the seasons.

5.3 Height variation of lunar tide in the ionosphere at Huancayo and Puerto Rico (Preliminary results at noon only)

A similar analysis, to that done at Ahmedabad, was extended for Huancayo and Puerto Rico for the periods January 1960 to December 1961 (2 years) and March 1959 to December 1961 (34 months) respectively, using the noon data only; and the results were published (SHARMA and RASTOGI, 1968). The curves of mean electron density versus height, for Huancayo and Puerto Rico, are reproduced in figure 82; while the height variations of the amplitude (r_2) and phase (θ_2) of M_2 tide in N(h) is shown in figures 83 and 84 respectively, for each season separately.

It is seen from figure 82 that at Puerto Rico, the mean electron density below 160 Km is largest in J-months (summer)

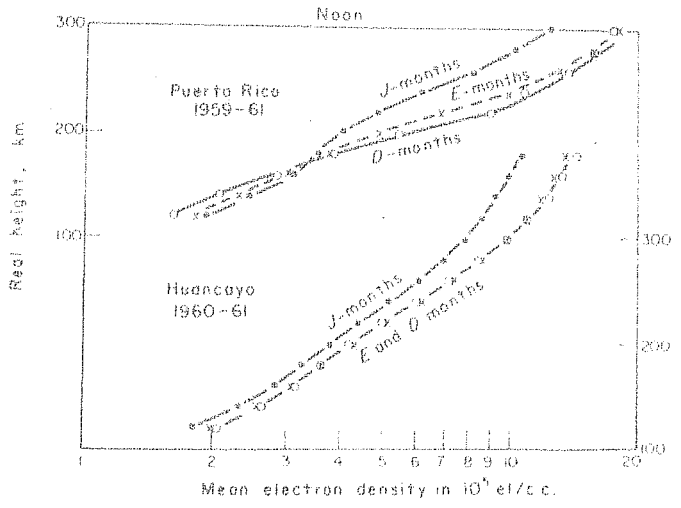


FIGURE - 82

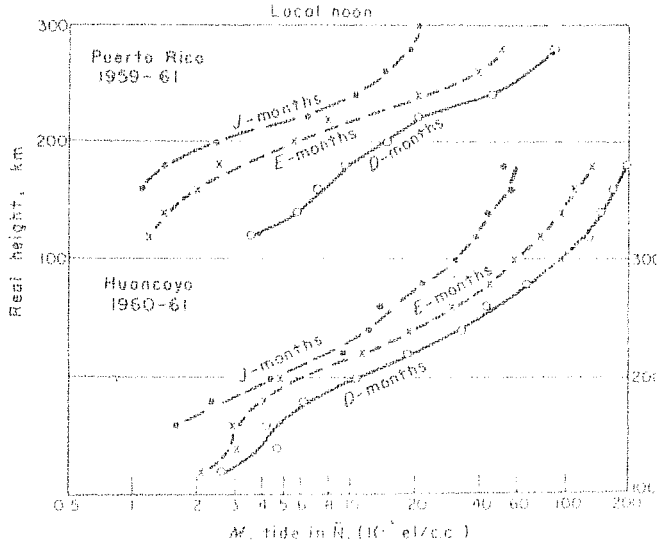


FIGURE - 83

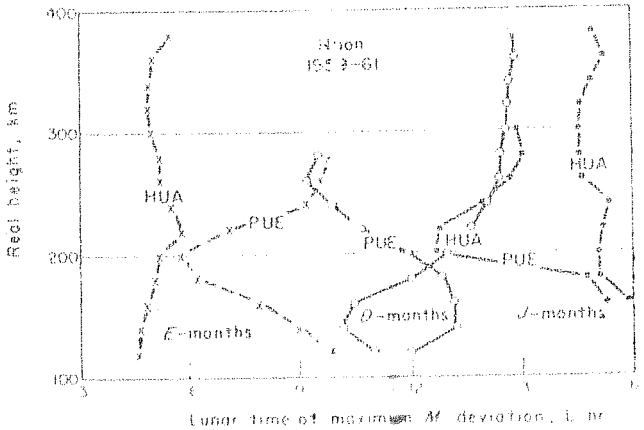


FIGURE - 84

and least in D-months. This indicates that the seasonal variation of the electron density at a fixed height below 160 Km follows the suns zenithal distance. But above 160 Km, the electron densities in E and D months are higher than those in J-months. The electron density at any height above Huancayo is maximum in D-months (summer), slightly less in E-months, and least in J-months (winter).

Figure 83 shows that at both the stations the tidal amplitudes in any season, increase with height; even the percentage change of the electron density continuously increases with height. This is rather different from the conclusion of BURKARD (1966) that the amplitude at Puerto Rico grows almost linearly with mean electron density. This discripency may be due to thefact that BURKARD's (1966) analysis refers to the tide averaged over all hours of the day (07-17 hr) while the present analysis refers to noon time only.

At Puerto Rico, the amplitude at 160 Km. in any season is of the order of 10^3 electrons/cm^3 or about 0.5 to 1.0% of the mean electron density. At 280 Km, the relative amplitude (r_2/N) amounts to about 6% during D-months, 3% during E-months and 2% during J-months. BURKARD (1966) obtained a slightly lower values of 4.3% at 290 Km during the D-months, which is due to the averaging over all hours of the day-time. The M_2 amplitude at Huancayo is about 1% of the mean electron density at 160 Km in any of the seasons. The relative amplitude (r_2/N)

at 380 Km increases to 14% in D-months, 10% in E-months and 5% in J-months. Thus the enhancement of tide with height is most significant in D-months, just as the electron density itself.

The diagram for height variation of the phase (figure 84) shows that at Huancayo, the phase does not vary with height during J-months and E-months, while during D-months it varies from 10 lunar hr at 150 Km to 3 lunar hr at heights above 250 Km. For Puerto Rico, the phase varies appreciably with height during all the seasons. In D-months it varies from a value of 1 lunar hr at lower heights to about 9.5 lunar hr at 280 Km. In J-months the phase changes from about 6 lunar hr at lower heights to 3 lunar hr at higher heights. In E-months it decreases from about 9 lunar hr at low levels to 6 lunar hr at about 200 Kms and again increases to 10 lunar hr at 280 Km. It is interesting to note that in any season, the phases of the tide in electron density at 180 to 200 Km are very similar at Huancayo and Puerto Rico.

It is thus concluded that the amplitude of the M_2 tide at both the stations increases monotonically with height during any season, there being about 50 times enhancement of tidal amplitude from the base to the peak of the F_2 region. At any fixed height, the amplitude is largest in D-months and least in J-months. The phase of the tide seems to remain constant with height at Huancayo, but it varies considerably

with height at Puerto Rico.

5.4 Annual average luni-solar variations of electron density in the ionosphere over Huancayo

To study the solar effects in the vertical profiles of lunar variations of electron densities, these were computed at Huancayo and Puerto Rico at each individual solar hour separately. As the N(h) data used for Huancayo is only for one year i.e. January to December 1961, no seasonal grouping of the data is done and only the annual average lunar semi-monthly tides in N at fixed heights h, at intervals of 10 Km, are calculated. For Puerto Rico, however, data for 34 months (March 1959 - December 1961) is utilized and the height variation of tide is computed for annual as well as three seasons separately. The results of these computations for Huancayo is discussed in this section; while those for Puerto Rico is presented in the following sections (5.5 and 5.6).

(a) Tide at fixed individual solar hours

In table 28 are given the amplitudes (r_2) alongwith their probable error (P.E) and phases (Θ_2) of the lunar semi-monthly oscillations of electron density at fixed real heights (at intervals of 10 Km) of the ionosphere over Huancayo for each individual solar hour. The statistically insignificant amplitudes are put into brackets. Almost all the amplitude determinations are seen to be reliable. Table 28

also gives the average electron density (N) at different heights and hours. The amplitude r_2, N and P.E. are all expressed in units of 10^{-4} electrons cm^3. r_2 is also expressed as percentage of mean electron density at the corresponding height i.e. as $r_2/N\%$.

The height variations of the amplitude r_2 at individual solar hours (00, 01, 02 .....22 and 23) are shown in figure 85. The amplitude r_2 is plotted on a logarithmic scale so as to show its relative changes with height. The following main features are noticed from the diagram.

(1) The amplitude r_2 for the night-time hours (19-05 hr) shows either no change or a slight increase with height. The amplitudes during night-hours are generally around 2 to $4x10^4$ electron/cm^3(7-15%). The amplitudes, at any height, are lowest ($\sim 2 \times 10^4$ electrons/cm^3) at 03 to 05 and 22 solar hour.

(2) The amplitude r_2 during day-time hours (06-18 hr) at first shows a decrease with height starting from 110 Km, reaching a minimum at 130 to 180 Km depending on solar time; it then starts increasing monotonically with height. However, this increase saturates at a height very close but slightly lower than h_{max}, afterwhich the amplitude seems to decrease. The rate of increase of tidal amplitude with height is maximum in the height range 180-240 Km and minimum for heights near h_{max}.

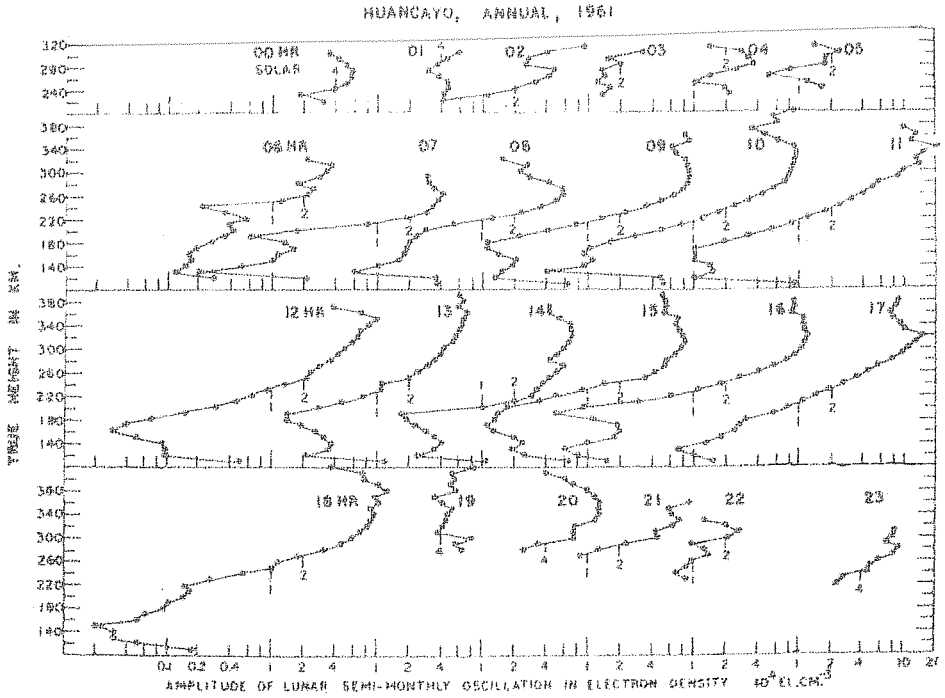


FIGURE - 85

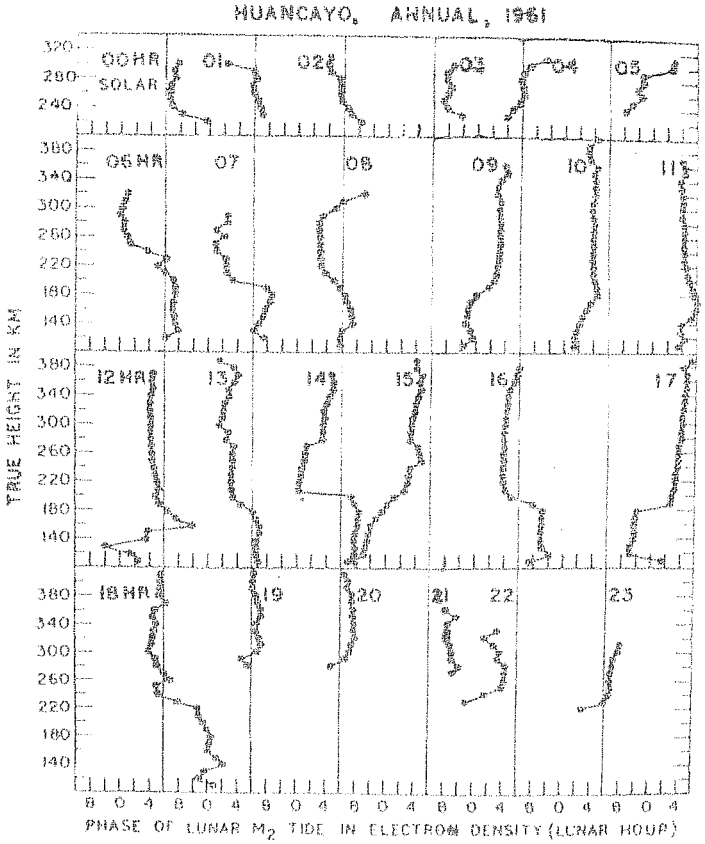


FIGURE - 86

(3) The amplitude of the tide at the E-region heights is about 10^3 electrons/cm^3, while it is about 10^5 electrons/cm^3 at heights near h_{max}. Thus there is a 100 times amplification of tidal perturbations from E-region to the top of the F-region. Even the percentage amplitude, r_2/N, in the day-time increases from approximately 1% in the E-region to about 5-8% in the higher F-region.

(4) The amplitude at any height is seen to be greater in the day-time than in the night-time hours, which confirms the luni-solar behaviour of the tide in electron density. However, it should be noted that percentagewise the amplitude ($r_2/N\%$) does not show this luni-solar behaviour. This shows that the electron density in the night-time is reduced from its day-time value by a greater factor than its tidal amplitudes.

(5) The maximum tidal amplitudes at the higher heights happen to be at 17 hr In general, the amplitudes at these heights are greater for the afternoon hours, which confirms our earlier results of $M_2(N_{max})$ tide at Huancayo (section 3.3).

The height variations of phase (Θ_2) at different individual solar hours plotted in figure 86 shows that the phase in the night-time remains practically constant at all heights. The phase is also constant at the F-region heights (> 220 km) during the day-time and is roughly 04 lunar hr. However,

the $M_2(N)$ tide at E-region heights (100-190 Km) in the day-time, shows a different phase than for the F-region; the change of phase from lower heights to higher heights occurring at about 160-190 Km. It should be noted that the amplitude profiles also showed a cusp of low values around this region (150-180 Km). It is concluded that above about 180-190 Km, the tidal amplitudes increase with height while the phase remains constant. This is consistent with the observations that the lunar oscillations at the top and the bottom of the F_2 layer at Huancayo are in the same phase (section 3.2).

(b) Comparison with other similar results

In order to compare our results at Huancayo with previous results by ZAGULYAEVA and FATKULLIN (1969) who used data collectively for all solar hours, the vectors (r_2, θ_2) at individual solar hours are averaged for all the hours, at each fixed height. The height variations of so averaged amplitude $(\overline{r_2})$ and phase $(\overline{\theta_2})$ are presented in figure 87 alongwith the corresponding results of ZAGULYAEVA and FATKULLIN (1969). It is seen that both the curves of amplitude variation are quite similar and show an increase in tidal amplitude with increasing height. It should be noted here that the height variation of the amplitude r_2 does not show any node around 300 Km as reported by BROWN (1968). The nature of the curves showing phase variation with height is also similar. The phase is about 8 lunar hr at E-region (120-180Km)

heights and around 4-5 lunar hr at F-region (230-400 km) heights. The transition from a phase corresponding to lower altitudes to that at higher altitudes takes place around 200 Km. The slight difference between the values of phases between the two curves may be due to the fact that the data used by the two authors are for different periods of solar activity. However, allowing for the above mentioned fact, the results are in good agreement with each other which shows the consistency of the lunar tidal computations, inspite of the smallness of the effect, noticing the fact that the methods of analyses in the two cases are also different.

(c) Average tide during day and night time

To estudy the differences in lunar tidal effects during day and night-time, the coefficients r_2 and Θ_2 are averaged for solar daytime hours (06-18 hr) and night-time hours (19-05 hr) separately, for each height. The variations with height of the amplitude and phase during the daytime as well as the nighttime hours are shown in figure 88. It should be noted that in the night-time, the N(h) profiles are available only above a height of 200-250 Km. It is seen that the amplitude (r_2) during daytime for heights 100-170 Km is very small; it increases with height rather rapidly between 190-220 Km and then rather slowly for higher heights, reaching a maximum value at around

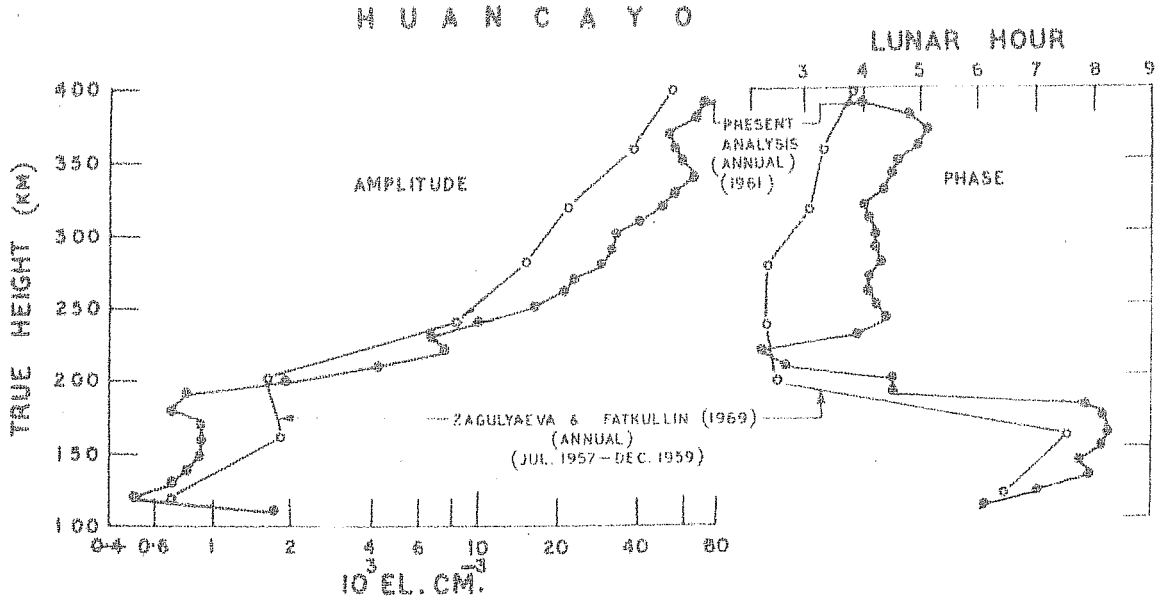


FIGURE – 87

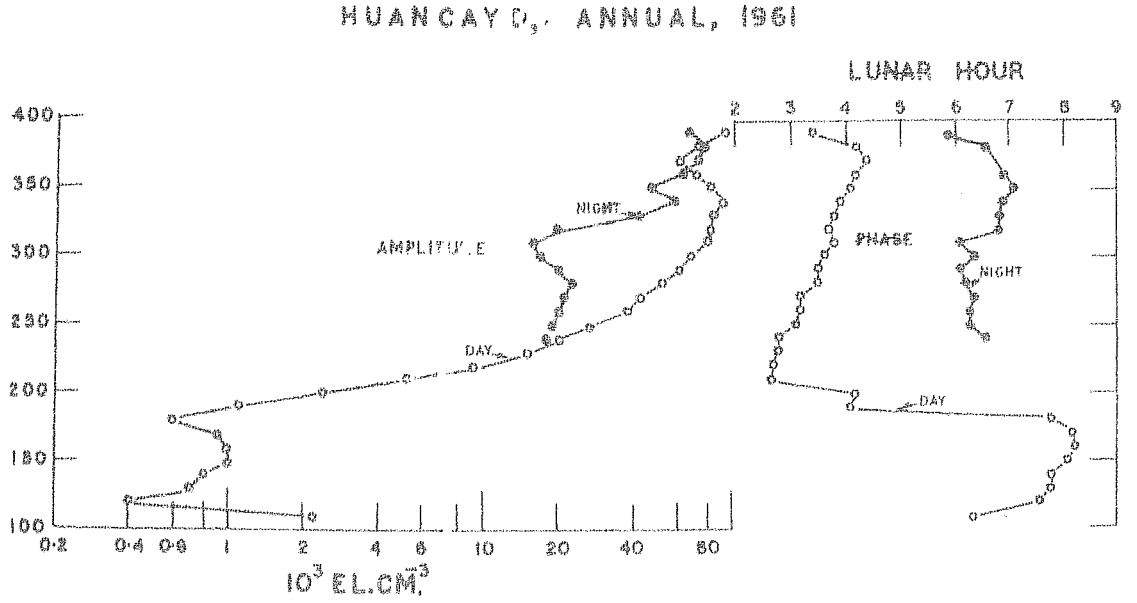


FIGURE – 88

340 Km. The amplitude (r_2) during night time is roughly constant for heights 240-300 Km and increases afterwards attaining the maximum value at 380 Km. The day-time phase is about 7-8 lunar hr for heights between 120-190 Km and about 3-4 lunar hr for heights between 220-400 Km. Thus the phases in these two height ranges are opposite to each other and the phase reversal occurs around 200-210 Km region. The phase during night time shows very little variation with height and is about 6-7 lunar hr for heights between 240-400 Km. It should be noted that the phases during day-time and night-time are in phase quadrature with each other for F-region heights.

It thus appears that during day-time, the processes causing the lunar tidal variations are different below and above 180 Km, which is thought to be the region separating the lower photochemical regime and the upper electrodynamical regime. Thus the lunar tidal phenomenon is electrodynamical in nature in the F-region where the motion of electrons is constrained by earth's geomagnetic field and they cannot move across the field lines. While below the transition level, collisions are the dominant factor and hence electrons move with the neutral wind which would be more effective in causing the lunar variations.

(d) Detailed study of luni-solar effects

To study these effects in detail, the average electron

density profiles and the amplitude of lunar tide in them at three hourly groups of solar hours centred at 00, 03..... 18 and 21 hr are plotted in figures 89 and 90 respectively; while the corresponding diagram for the phase (θ_2) is shown in figure 91.

It is seen from figure 89 that the mean electron density at any height is greater in the day than in the night-time. A slight kink in the profiles at 06 and 18 hours appears due to the fact that for some days, at these hours, only either the lower or the top half portion of the profile is obtained; and averaging over a year produces this kink. The minimum electron density at any height, happens to be at 03 hr, while the maximum is at 09 or 12 hr.

Figure 90 shows that the amplitude (r_2) at any solar hour is minimum generally around 120-160 Km, after which it starts to increase, at first rapidly (170-220 km) and then either very slowly or is constant for heights above 300 Kms. It is very interesting to note that at about 200 Km, the tidal amplitude is identical for any solar hour; while around 150 and 250 Kms, there is a large variation with time of the day. For greater heights, around 350 Km, there is no change of amplitude either with time or height. This fact also confirms that so far as lunar tides in N(h) at Huancayo are concerned, the ionosphere can be divided into two regions; one below and another above a height of 200 Km which is the transition zone.

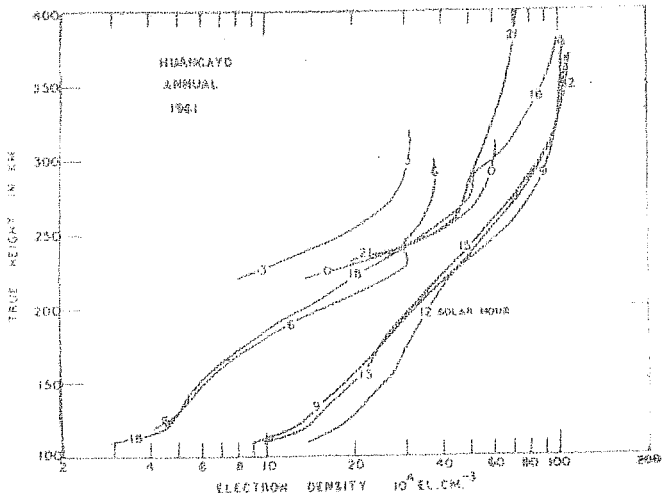


FIGURE -89

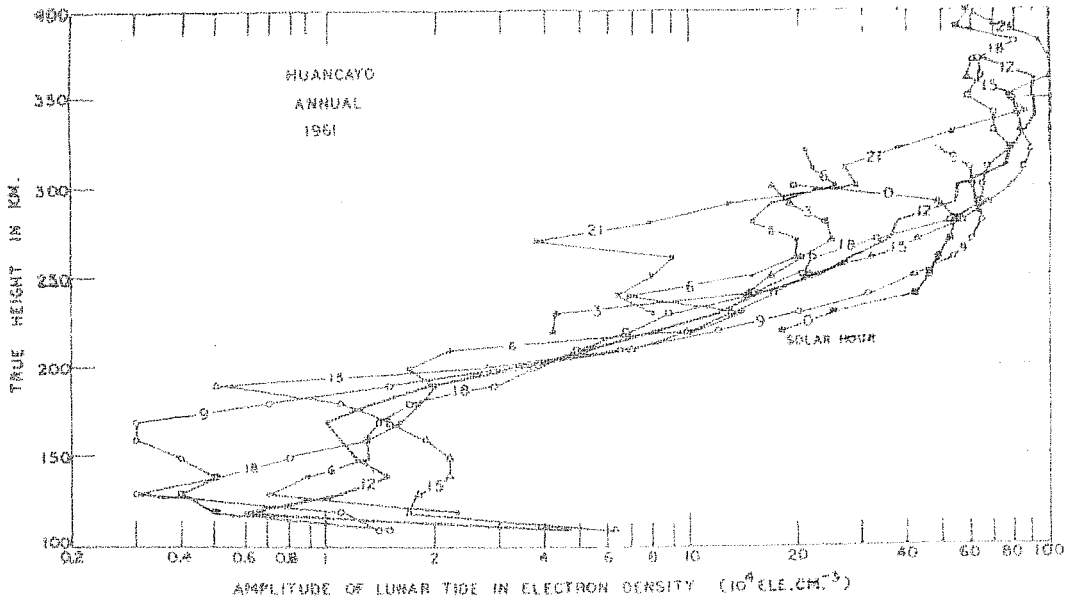


FIGURE-90

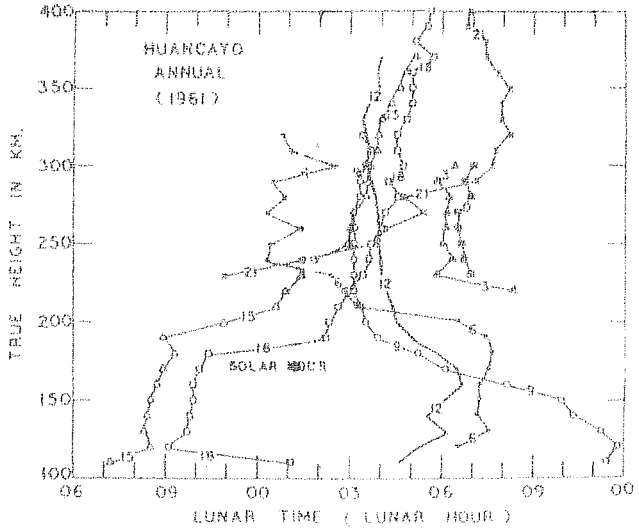


FIGURE - 91

Also a comparison of figures 89 and 90 shows that while the electron density at any particular level is quite small in the night than the day-time, the amplitude r_2 at that level does not reduce to such a large extent with the result that r_2/N is quite large in the night-time as seen from the table 28.

Referring to figure 91, for the phase, it is seen that the phase at any solar hour shows a sharp change at heights about 190 Km. The phase below this height is in the range 6 to 10 lunar hr, for any solar hour; while above this height, it lies in the range 01 to 08 lunar hour. The variation of phase with solar time for heights at about 200 Km is seen to be very small. At heights greater than 200 Km, the phase is roughly 04 lunar hr in the daytime and about 07 lunar hr in the night time. It should be noted that for day-time hours and for heights below 200 Km, lunar variations in electron density are in phase with the similar variations in the magnetic field which is maximum at about 08 lunar hr at Huancayo (section 3.2), while for heights above 200 Km the phase is opposite to that in magnetic field.

5.5 Height variation of lunar tide at Puerto Rico (Annual average oscillations of electron density)

(a) Tide at fixed solar hours

The amplitude (r_2) and phase (Θ_2) of the annual average lunar semi-monthly oscillations in electron density

at fixed real heights of the ionosphere at Puerto Rico are given in table 29, separately for each individual solar hour. Statistically, almost all the determinations are found to be significant.

The height variations of the annual average amplitude r_2 at individual solar hours are plotted in figure 92. It is seen that the tidal amplitude generally shows an increase with height at any solar hour; this increase being smaller in the night than in the day-time. The amplitude of the tide during the day-time hours is approximately 10^3 electrons/cm^3 at the E-region heights (110-140 Km) and it is about 10^5 electrons/cm^3 at heights near h_{max}. Thus there is a 100 times amplification of the tide from E to the top of the F_2 region as is the case at Huancayo. In the night-time, the amplitude at heights near h_{max} is about 4×10^4 electrons/cm^3 to 10^5 electrons/cm^3 depending on solar hour. The amplitude of the tide is minimum at 19 hr and maximum at 17 hr. Thus a luni-solar effect of the tide is seen, but it is less than at the equatorial station, Huancayo.

Figure 93 shows the height variation of phase Θ_2 at individual solar hours. The behaviour of phase with height is seen to be different at different hours. The phase during night-time hours either remains constant with height (e.g. 21, 22 hr) or shows a little variation (e.g. 23, 00-05, 19-20 hr). At all the day-time hours, however, the phase shows a

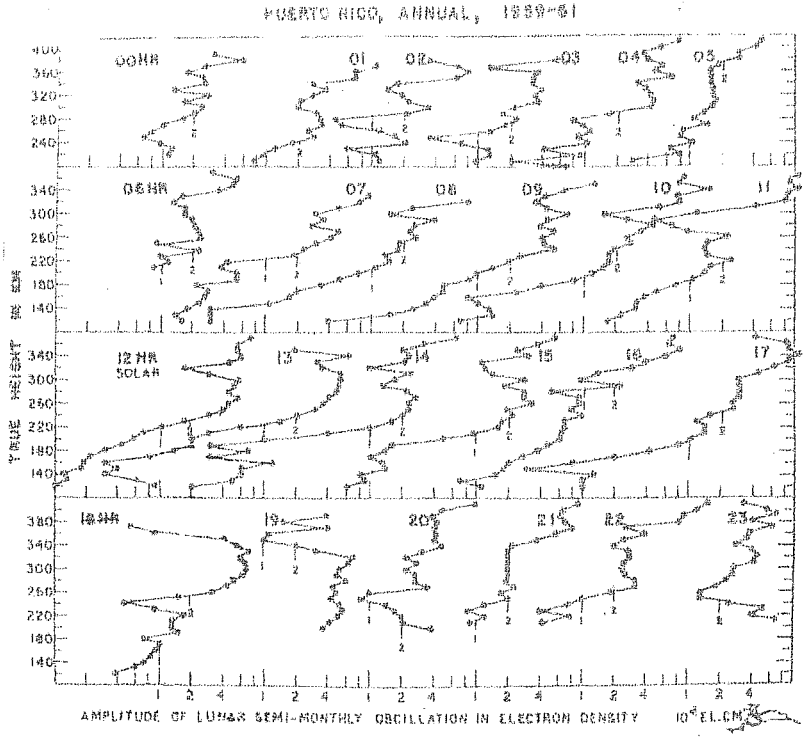


FIGURE -92

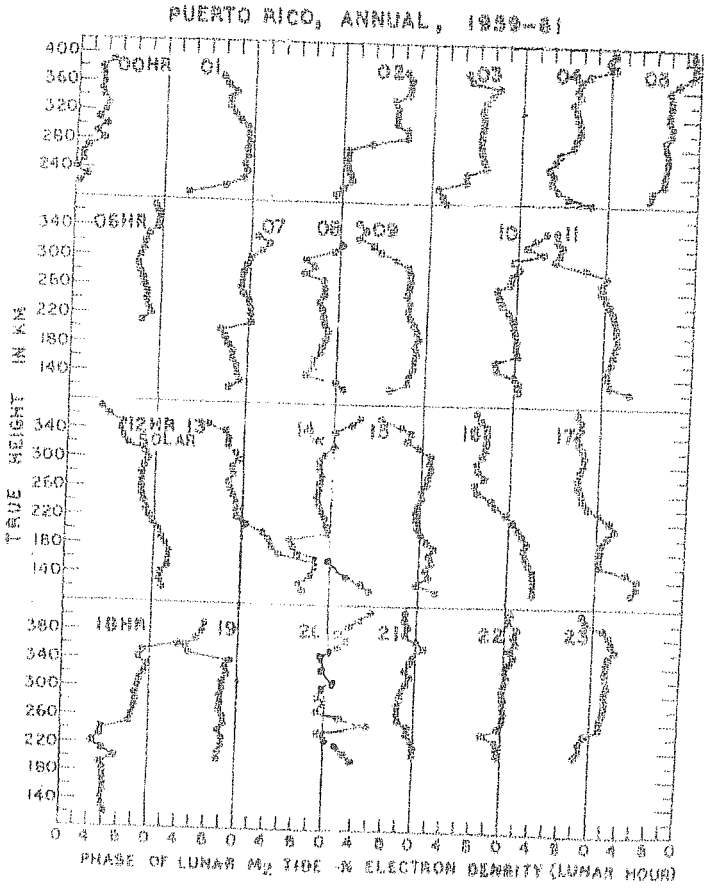


FIGURE-93

systematic height variation which is different at different hours. Thus, while at Huancayo, the tidal phase is constant at all solar hours, it shows a change with height during the day-time at Puerto Rico.

(b) Average day and night-time vertical profiles of lunar tide

As done for Huancayo, the coefficients (r_2, Θ_2) of lunar semi-monthly tide at a particular height were averaged for the day (07-17 hr) and night-time hours (18-06 hr) separately. The height variations of so averaged coefficients are shown in figure 94. It is seen that the day-time amplitude starts increasing from a low value of 0.5×10^3 electrons/cm^3 at 130 Km, and reaches the maximum value of 35×10^3 electrons/cm^3 at about 270 Km above which it tends to decrease. The night-time amplitude $(\overline{r_2})$ also shows, for the available height range (210-400 km), a maximum around 300 Km. The phase of the tide during the day shows a gradual retardation with increasing height. It is about 1 lunar hr at about 120 Km and becomes 10.5 lunar hour at 280 Km. The night time phase also shows a similar retardation with height and varies from 11 lunar hr at 220 Km to 10 lunar hr at 380 Km. There is no difference between the values of the phase during day and night-time, which is in contrast with Huancayo. Thus it appears that the processes responsible for lunar tidal variations at Puerto Rico are similar during the day and night and are different than at the equator. Also, it should be noted that the phase

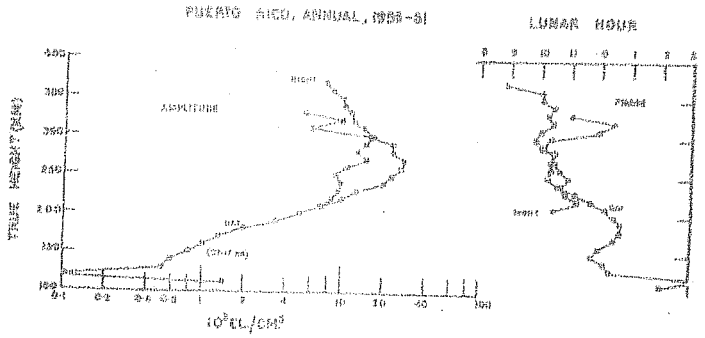


FIGURE-94

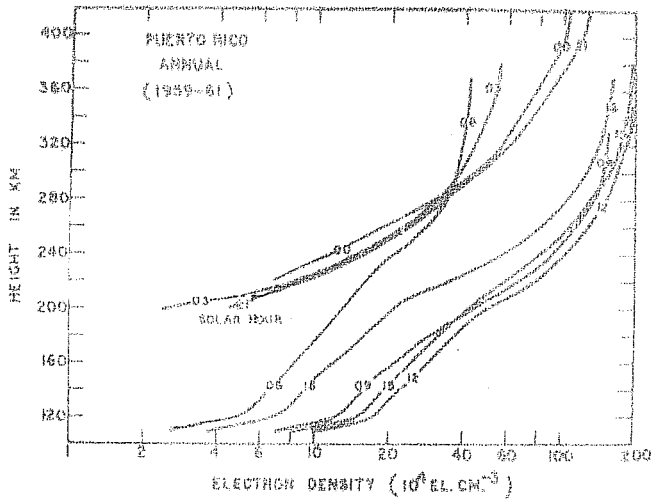


FIGURE-95

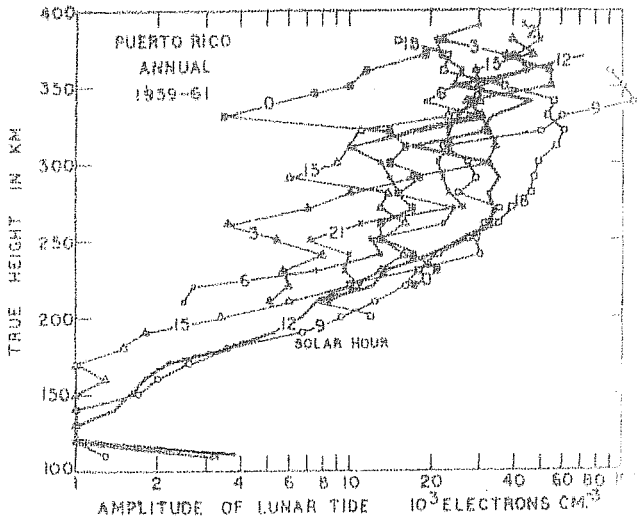


FIGURE-96

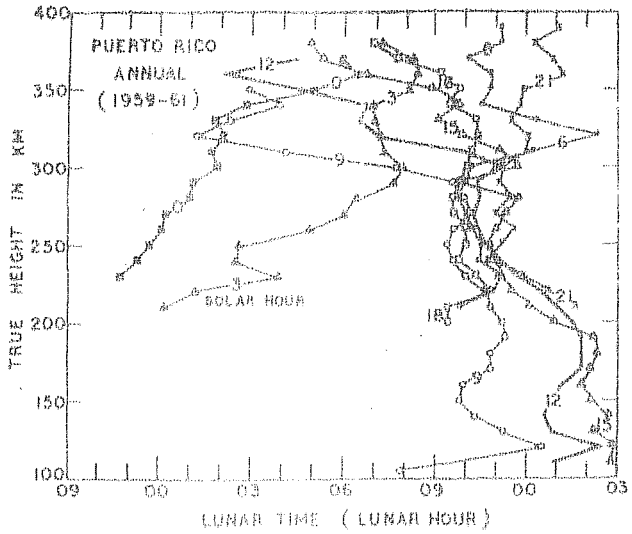


FIGURE-97

of the electron density variations in the E-region is approximately the same as the lunar oscillations of H at San Juan, Puerto Rico (section 4.2).

(c) Luni-solar effects in electron density

The annual average mean electron density profiles at three hourly groups of solar hours, centred at 00, 03, 06 .....18 and 21 hr, are plotted in figure 95. The amplitude (r_2) and phase (Θ_2) of lunar semi-monthly tide in these profiles are shown in figure 96 and 97 respectively. It is seen from figure 95 that the profiles at 09-15 hr fall in one group and those at 00, 03 and 21 hr fall in another group; the sunrise (06 hr) and sunset (18 hr) time profiles falling in between the two. The electron density N(h) at any height (h) is maximum at 12 hr, while it is very low in the night-time.

From figure 96, the tidal amplitudes are seen to be minimum at about 120-150 Km, and then increase with height during the daytime hours (09, 12 and 15 hr) only, till a height of about 220 Km after which there is no consistent increase with height. The night time amplitudes, however, do not show any consistent height variation. The luni-solar effects are not clear for any height, although these seem to be present for all the heights. The behaviour of the tidal amplitude with height and time of the day are quite different at Huancayo (section 5.4d) and Puerto Rico indicating that different mechanisms are responsible for lunar variations at

the two places.

Figure 97, for the phase shows that for the daytime hours i.e. (09-12-15 hr), the phase shows a gradual retardation with height till about 300 Km, where it changes suddenly. The phase at heights near the peak of the F_2 layer is about 4-7 lunar hr, while an analysis of lunar oscillations in N_{max} gave a phase of about 10 lunar hr (section 4.8). It should be noted that this discrepancy between the phase of the oscillations in N_{max} is seen at Ahmedabad also (section 5.2). This discrepancy may be due to the changes in the height of the maximum electron density during the course of a day. The phases(θ_2) for 18 and 21 solar hr are almost constant with height (210-360 Km). At 00 and 03 hr, the phase of the tide gradually advances with increasing height.

5.6 Lunar perturbations in N(h) profiles at Puerto Rico during different seasons

The lunar tides in N(h) profiles at fixed solar hours were also computed for three seasons separately, and the results are described below.

(a) D-months

Figure 98 shows the vertical profiles of lunar tidal amplitude at individual solar hours. The amplitude of the lunar oscillations of electron density at any solar hour shows, generally, an increase with height. This increase,

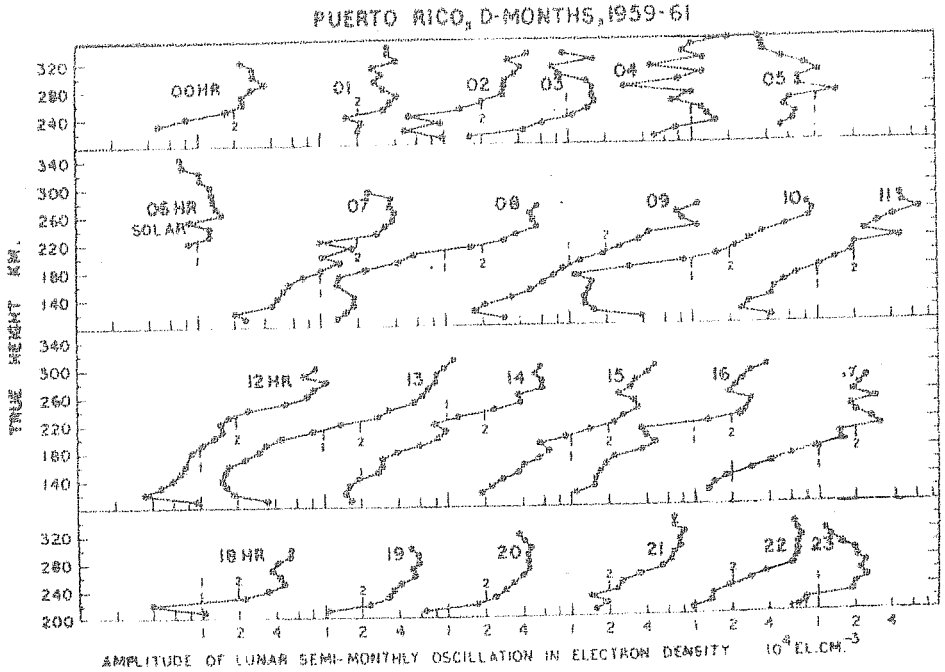


FIGURE - 98

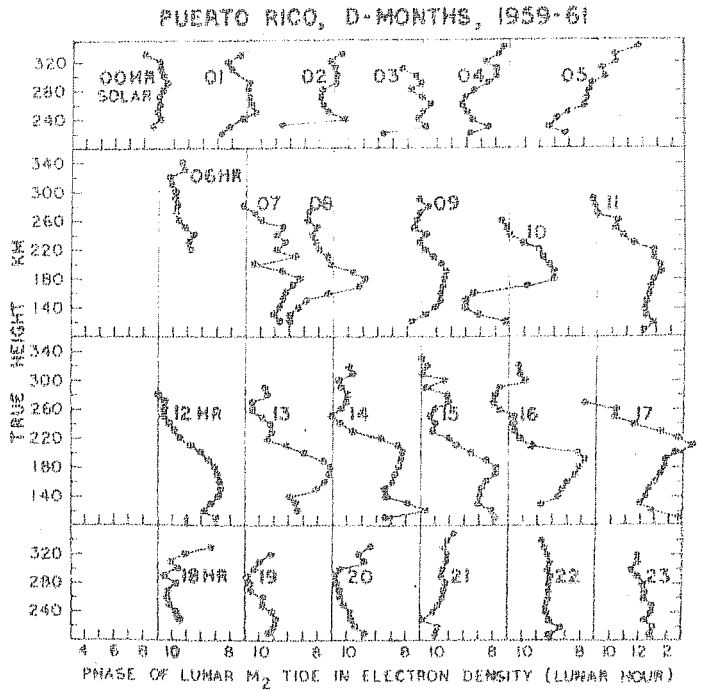


FIGURE - 99

however, saturates at a height slightly lower than h_{max} to give a maximum aplitude there. A further decrease, above this level, of the amplitude is seen, especially during the night-time hours. The amplitude at E and F region heights is 10^3 and 10^5 electrons/cm^3 respectively, showing a 100 times enhancement from the former to the later region; which is true for all the stations studied so far. Also, the maximum amplitude at a particular height happens at 13 hr and minimum at 05 hr. In general, the amplitude is greater in day than night-time hours.

From the height variations of phase (Θ_2) at individual solar hours (figure 99), it is seen that the phase of the tide is constant with height for the hours near mid-night (21-03 hr). There is a systematic change of phase with height at all the other hours; this change being greater for the day-time hours.

In order to compare the present results with those of BURKARD (1966), the vectors r_2, Θ_2 for 07 through 17 solar hours for heights 120 to 280 Kms have been averaged. The height variation of the so averaged phase, $\overline{\Theta}_2$ is shown in figure 100 alongwith the curve given by BURKARD (1966). The similarity of the two curves is very evident, although the method of analysis employed by the two authors are quite different. This shows the consistency of these results inspite of the smallness of lunar tidal amplitudes in electron density.

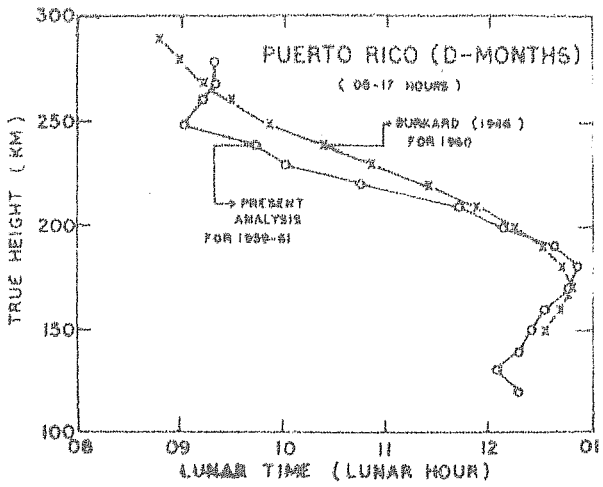


FIGURE-100

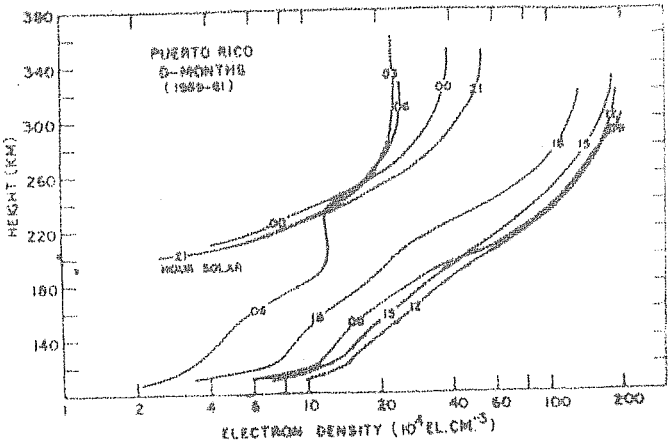


FIGURE-101

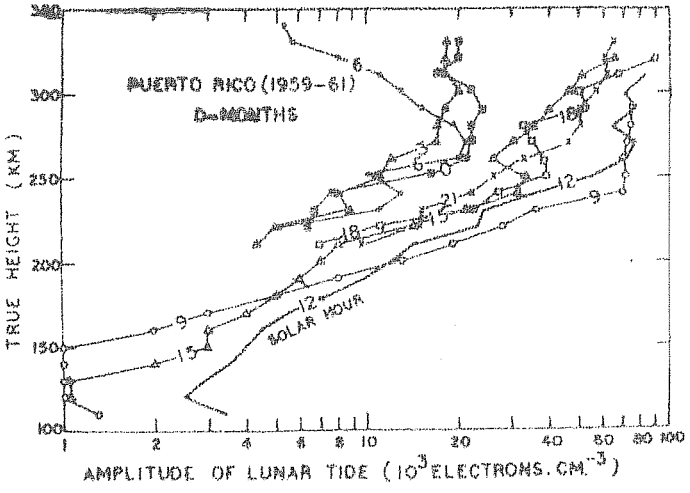


FIGURE-102

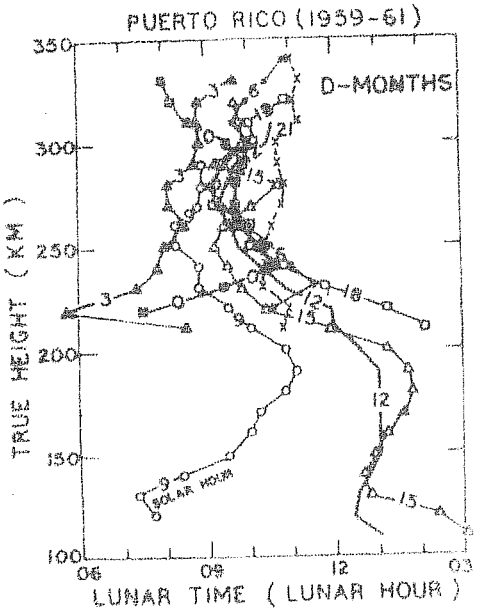


FIGURE-103

The phase $\overline{\Theta}_2$ remains between 12 and 01 lunar hr for heights 110-190 Km, it then decreases systematically from 12 lunar hr to about 09 lunar hr between 190 to 250 Km. A slight deviation between the two curves for higher heights may be due to decreased and unequal number of data points for heights near h_{max}.

To illustrate the luni-solar effects in the tide in electron density, mean electron density profiles and the amplitude of M_2 tide in them are shown in figure 101 and 102 respectively, for three hourly groups centred at 00, 03, 06 .....18 and 21 solar hour. It is seen from figure 101 that the day-time and night-time profiles are quite separated showing a large difference between the electron density during the day and night-time. The electron density at any height is reduced by a factor of 4-5 during the night-time from its corresponding value during the day. Figure 102 shows that the amplitude of the semi-monthly tide at any solar hour increases with height. The maximum lunar tidal variation happens to be at about 280 Km at any solar hour. This level of maximum tidal amplitudes does not coincide with the height of the peak ionisation (h_{max}) which varies with the time of the day. Also this level is lower than h_{max} for any solar hour. Another important fact is that the rate of increase of the tidal amplitude is larger at lower heights than for heights near h_{max}; the only exception being that of 06 hr at which the amplitude decreases after reaching a maximum at 270 Kms.

It is also seen from the figure that at a particular height, the amplitude is maximum near solar mid-day and minimum near solar mid-night confirming the luni-solar nature of the tide in electron density at any particular height.

The variation of phase of the lunar tide with height at 00,03,06.....18 and 21 solar hrs is shown in figure 103. It is seen that at any solar hour the phase is almost constant with height for the height range of 250-340 Kms. Also there is no appreciable variation of phase with solar time for this height range where the maximum deviation in electron density occurs between 09-11 lunar hours. Below about 220 Km height, there is a large variation of phase in the solar day-time hours. Thus, there exists two regions, one in which phase remains constant with height and solar time; the other where the phase varies with height as well as with time. It is interesting to note that the transition level coincides roughly with the height of formation of the F_1 layer.

It appears, therefore, that the processes causing lunar tidal perturbations below 200 Km have large luni-solar effects and are different than the corresponding processes above this height which do not show any such effects. This feature is similar to that observed at Huancayo (see figure 91, section 5.4d), but is different than the annual average behaviour at Puerto Rico; which indicates that lunar tidal effects

in electron density have large seasonal variations.

(b) E-Months

The amplitude r_2 of the lunar semi-monthly tide in electron density at different heights is shown in figure 104 for each solar hour of the day. The amplitude of the tide at any solar hour increases with altitude. The maximum tidal oscillations occur generally at a height lower than h_{max}. A clear decrease of tidal amplitude above this level of maximum amplitude is also seen for most of the hours. This decrease is most pronounced at 15 hr and is almost absent at 16 and 17 hr. The tidal amplification from E to the top of F-region is about 100 in this season also. Further the maximum and minimum amplitudes, at any height, occur at 17 and 02 hours respectively. In general the nature of the height variation of amplitude (r_2) is similar to that observed at other stations (Huancayo, Ahmedabad) and seasons.

Figure 105 shows the height variation of the phase (Θ_2) at different solar hours. It is seen that unlike in D-months, the phase at most of the hours remains constant with height. At some particular hours e.g. 00, 02, 12, 16 and 17 hr, the phase does show a systematic change with height; but this is quite small as compared to D-months.

To study the luni-solar effects, in detail, the mean electron density profiles, N(h), computed at three hourly

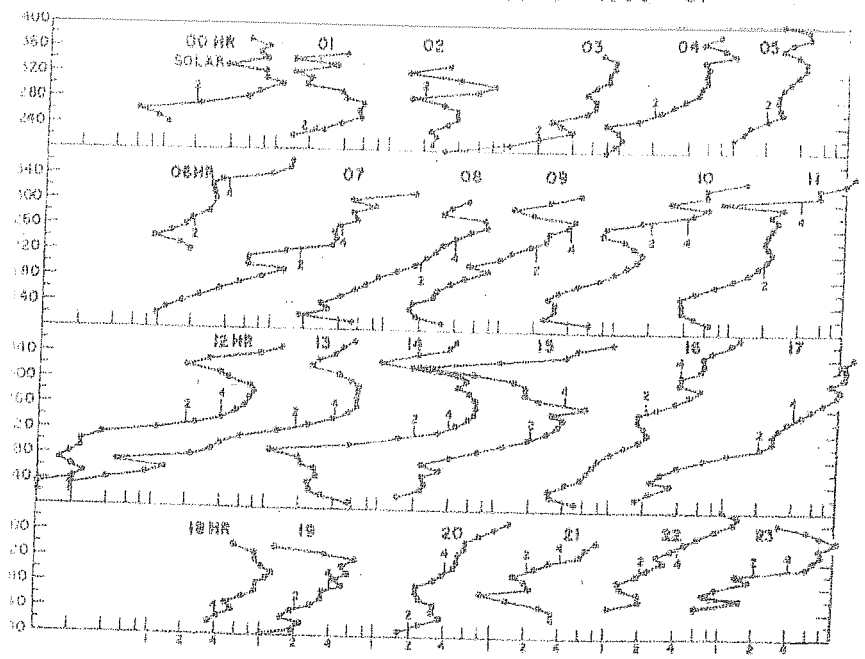


FIGURE-104

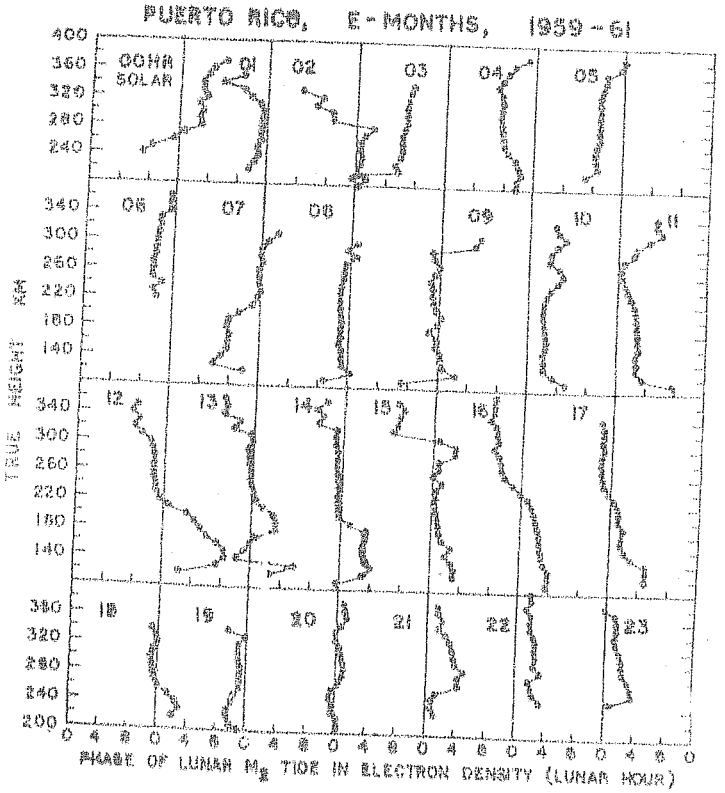


FIGURE-105

groups of solar hr, 00, 03, 06.....18 and 21, are shown in figure 106. The diagram shows that the electron density at any height in the day-time is approximately 5 times greater as compared to the corresponding value during the night-time. The vertical profiles of the amplitude r_2, which are shown in figure 107, however, do not show such large differences between the day and night-time values. In consequence, the percentage amplitude (r_2/N) is higher in the night than the day-time hours, andis maximum at 18 hr. Further, it is seen from figure 107 that the amplitude (r_2) at first decreases with height and is minimum around 130-150 Km; it then increases monotonically with increasing height. It is of interest to note that the amplitude around 180-200 Km is the same for any solar hour. Below and above this region, there is a large luni-solar variation of the tidal amplitude. This feature is very similar to that observed at Huancayo (see fig.90, section 5.4d) and lends strong support to the idea that the physical processes causing lunar tidal phenomena in the E and F_2 regions are different.

The variation of phase (Θ_2) with height at three hourly groups of solar hours is shown in figure 108. The phase at any hour varies slowly and systematically with height. Between the height range 200-250 Km, the luni-solar effects in the phase of the tide is seen to be minimum; while above 250 Km, there is large change of phase with solar

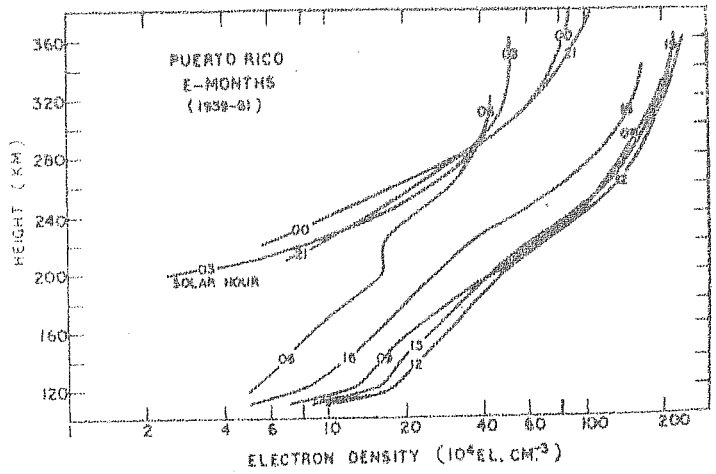


FIGURE - 106

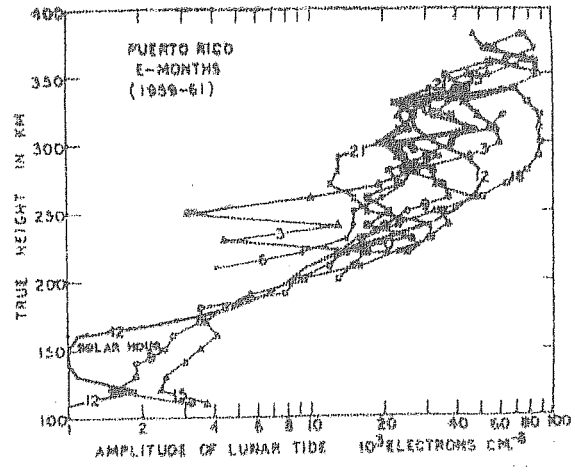


FIGURE-107

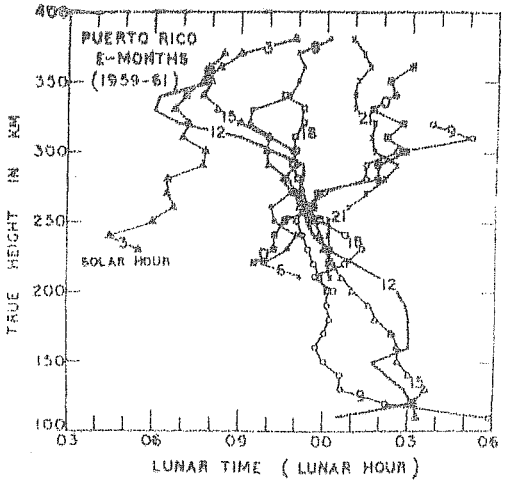


FIGURE-108

time. The luni-solar effect is also present below about 200 Km, but this is quite small. This feature is very different than in D-months, where the phase at higher heights ($>$ 250 Km) does not show much variation with solar time.

(c) J-Months

The height variation of the lunar tidal amplitudes in electron density at different solar hours is shown in figure 109. The main features which are seen in other seasons can be noticed here also. The amplitude, at any hour, shows generally a increase with height. This increase is greater during the day than night time hours. The maximum amplitude, at any height, occurs around the afternoon hours; and the amplitude during the night-time hours is smaller than the day-time, showing the luni-solar effect of the tide. The amplitudes around E and F region (near h_{max}) heights are approximately 10^3 and 10^5 electrons/cm^3, which indicates a 100 times amplification of lunar oscillations. An interesting feature, in this season, is that at some of the hours e.g. 06 and 19 hr, the amplitude is maximum at the lowest heights and decrease with increasing height .

The height variation of phase Θ_2 at each solar hour, which is plotted in figure 110, shows that at 09, 10, 17, 19 and 21 hr, the phase at all heights is practically the same. The phase at other hours shows a variation with height. The nature of this variation, however, is different at different

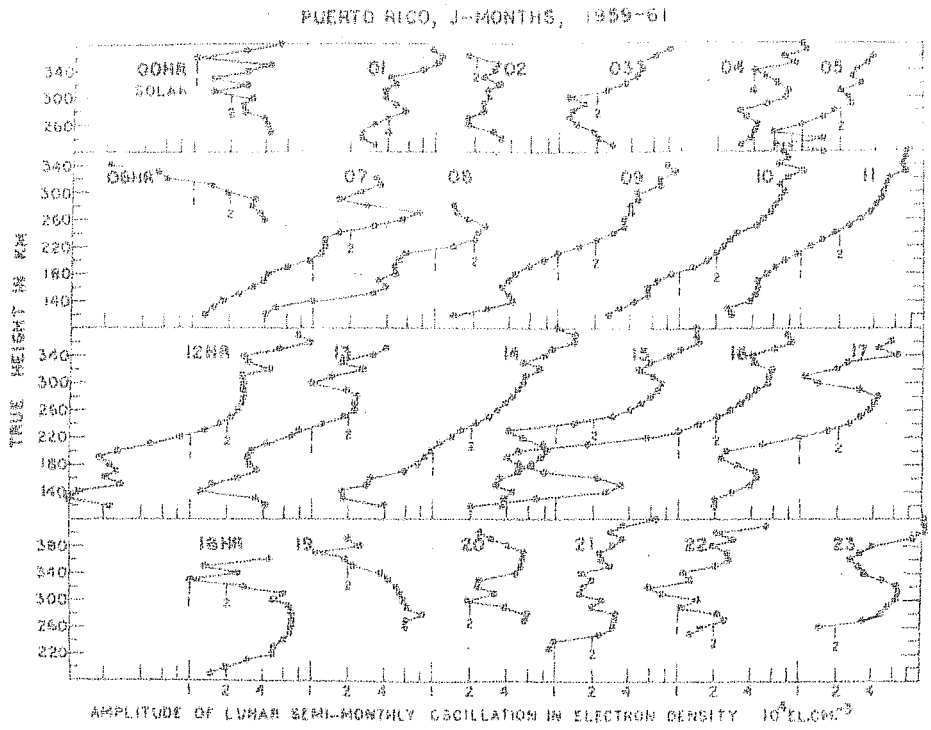


FIGURE-109

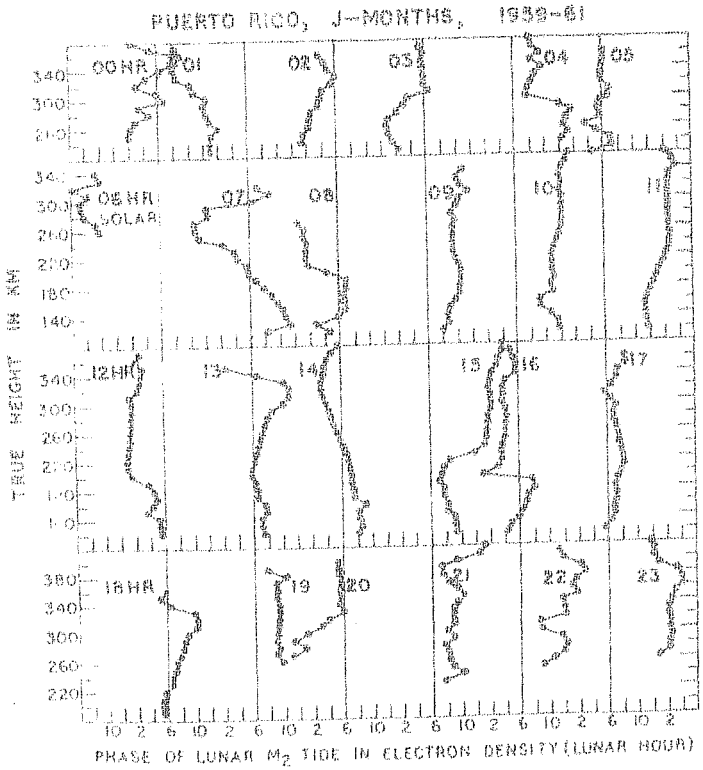


FIGURE-110

hours.

To study the luni-solar variations in the electron density at various heights in detail, the mean profiles at solar hours 00, 03, 06 .....18 and 21 hr are shown in figure 111. The height variations of the amplitude (r_2) and phase (θ_2) of lunar oscillations in these profiles are plotted in figure 112 and 113 respectively. The electron density at a particular level is again greater during the day than night-time hours; but the ratio of the average electron density in the day to the corresponding value in the night is only about 3 (see figure 111). The amplitude of the lunar variations of N at first decreases with height and is minimum around 130-150 Km (figure 112). Above this height the amplitude increases with attitude; the rate of increase being quite large at first, but becomes small as h_{max} is approached. Also, at any particular height, the amplitude shows an appreciable variation with solar time. Thus in J-months, the luni-solar effects in the electron density are present through whole of the ionosphere.

The diagram for phase θ_2 (figure 113) shows that the phase at any solar hour changes slowly but systematically with altitude. At any particular level in the ionosphere, the phase of the M_2 tide in electron density is quite different at different solar hours, indicating the luni-solar effects to be present at all the heights.

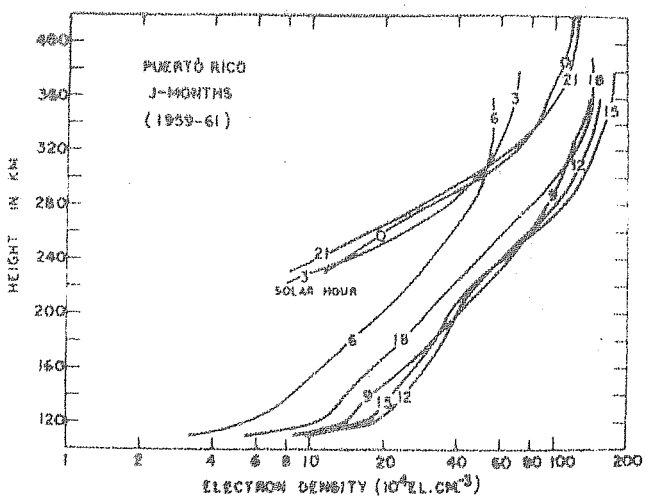


FIGURE-111

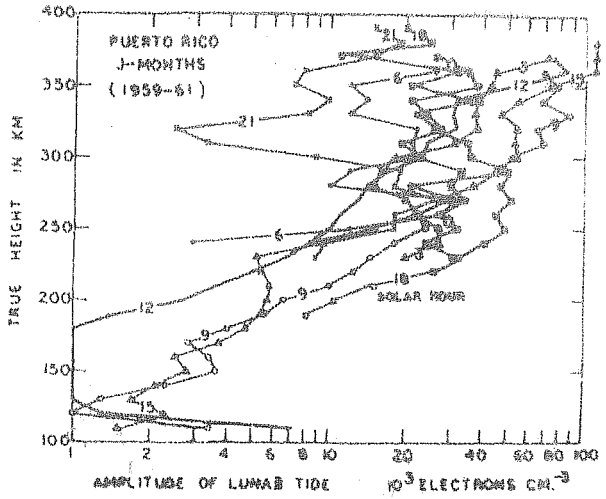


FIGURE-112

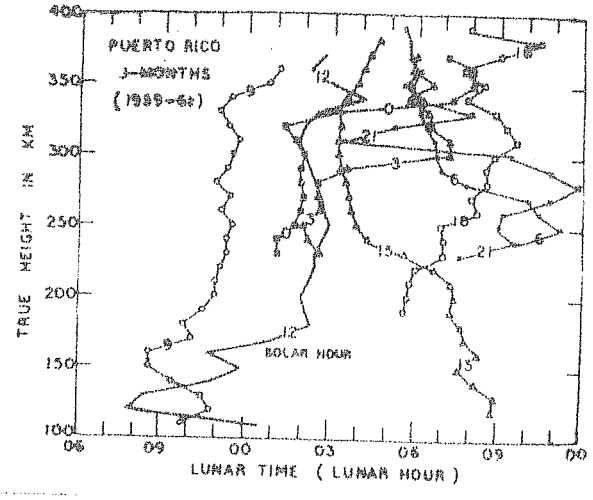


FIGURE-113

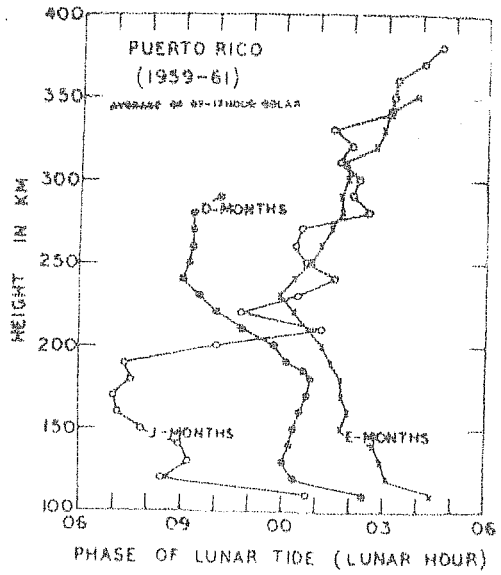


FIGURE-114

From the foregoing discussions, it is seen that the amplitude of the tide at different hours shows a similar type of height variation in all the seasons. But the height variation of the phase at any hour shows different behaviour in different seasons. To illustrate the point further, the day-time (07-17 hr) vector average phase ($\overline{\Theta}_2$) was computed at each height in each season. The so averaged phase $\overline{\Theta}_2$ in each season is plotted versus height in figure 114. Below about 200 Km, the phase shows a large seasonal change. At about 200 Km, the phase in any season is approximately 1-2 lunar hr. Above this height, the phases in E and J-months are the same and are different than that in D-months. It is recalled that above about 200 Km, there is little luni-solar effects in phase during D-months, whil[illegible] it is quite large in E or J-months. Further, it is noticed from the diagram that the change of phase with height is least in E-months and greatest in J-months.

5.7 Conclusions

The following main conclusions are drawn from the study of lunar tides in N(h) profiles at Ahmedabad, Huancayo and Puerto Rico.

Ahmedabad (1200 hr only)

(1) The amplitude of the lunar semi-monthly tide in noon electron density during any season increases uniformly with height in the F-region (above about 160 Km) of the ionosphere.

(2) At any fixed height above 160 Km, the amplitude of the lunar variations is maximum during winter and minimum during summer.

(3) The phase of the tide during any season remains constant with height.

Huancayo

(4) The amplitude of the tide at any solar hour shows generally an increase with altitude in the F-region.

(5) At any fixed height, the amplitude is maximum in D-months and minimum in J-months.

(6) The amplitude of the lunar variations in the electron density at about 200 Km remains the same at any solar hour. Above and below 200 Km, there is, however, an appreciable luni-solar variation.

(7) The lunar electron density variations in the E-region are approximately in the same phase (07-08 lunar hr) with corresponding variations of the horizontal component of earth's magnetic field.

(8) There is a sharp change in the phase around 190-200 Km during the day-time. The phase at heights greater than 200 Km is about 03-04 lunar hr. Thus the electron density variation at these heights are in phase opposition, with a further delay of 01-02 hr, with the H variations.

(9) The phase of the lunar variations of electron density in the night-time is roughly the same as that of H variations (07 lunar hr).

Puerto Rico

(10) The amplitude of the tide in electron density in the F-region of the ionosphere increases with altitude during any season.

(11) At solar noon, the amplitude of the lunar electron density variations at any fixed height is greatest in D-months and least in J-months.

(12) The phase of the tide at individual solar hours shows generally a small but systematic variation with height.

(13) The luni-solar effects in the electron density at different heights is found to be very different in different seasons.

(14) The lunar oscillations of electron density in the E-region is in phase conjuction with the lunar variations of the H-component at Puerto Rico.

(15) The phase in the day or night-time shows a gradual advancement with height, i.e., it has a negative height gradient. Also the phase during the day or night is not different, which is in contrast with theresults at Huancayo.

In general, it is concluded that the lunar variations of electron density, at any station, increase with height. At all the stations for which analyses were done, the tidal amplitudes in the E and the top of the F-region were found to be 10^3 and 10^5 electrons/cm^3 respectively; which shows a 100 times amplification from the former to the later region.

These results are discussed in the light of our existing theoretical knowledge of the lunar geomagnetic and ionospheric variations in the next chapter.

CHAPTER - VI

THEORY OF LUNAR TIDES

6.1 Introduction

In the preceding chapters the results of the lunar variations in geomagnetic field and in ionosphere have been described. The aim of this chapter is to discuss the theoretical interpretations of these observed results.

6.2 Cause of lunar geomagnetic variations

Electric currents flowing in the ionosphere are mainly responsible for the geomagnetic daily variations. The dynamo theory of geomagnetic variations (section 1.2) states that motion of ionized air across the vertical component (B_Z) of the earth's magnetic field produces a horizontal electric field (dynamo field). This effect is clearly strong at higher latitudes and may disappear at the magnetic equator because of lack of vertical component of the geomagnetic field. However, in order to make the steady current system possible, a certain distribution of electrostatic charge must develop in the upper atmosphere. This charge distribution will make a polarization field having an electrostatic potential which, together with the above mentioned dynamo field, makes a closed current system. Thus the current system which is produced by a coupling effect of the vertical component (B_Z) and a horizontal lunar tidal wind system at

about 100 Km altitude is the chief cause of the lunar daily variations of the geomagnetic field.

Using recently obtained results of lunar geomagnetic analysis and recently developed theories and values of the conductivities in the ionosphere, MATSUSHITA (1967) obtained the current system which is responsible for the semi-diurnal lunar geomagnetic variation. This current system is shown in figure 4 (page 41). The following points must be emphasized in regards to this current system.

(1) The centre or focus of the current system is located at a higher latitude in summer than in Winter. The reason being that the magnitude of the electrical conductivity varies with the position of the sub-solar point in different seasons.

(2) In order to eliminate longitudinal inequalities, the best ordinate of the current system will be B_z.

(3) The intensity of the lunar current in summer will be about three times larger than that in winter.

(4) The boundary between current systems in the summer and winter hemispheres seems to be the magnetic equator, in the same manner as in equinoxes.

(5) During solar day-time hours, a lunar equatorial electrojet seems to flow in a narrow zone centred on the magnetic equator. This is analogous to the equatorial electrojet in the solar geomagnetic variation due to high Cowling electrical conductivity during solar day-time.

Recently, TARPLEY (1970) investigated the current generating properties of individual tidal modes and of wind fields which contain height variations. He derived the equation describing the response of the ionosphere to a horizontal wind-induced e.m.f. This equation was solved to obtain the electric current distribution produced by different models of the lunar semi-diurnal tide. Tidal wind systems with large vertical wavelength are found to be much more efficient producers of current than wind systems of short wave length. He found that the current patterns produced by the lunar (2,2) mode with a maximum amplitude of 7.5 m/sec and a vertical wavelength of 85 Km are very similar to the L current patterns deduced from geomagnetic observations.

6.3 Estimation of electric field for the semi-diurnal lunar current system

Most of the mathematical studies of the dynamo theory have been based on the assumption that the ionospheric currents are flowing horizontally in what is effectively an infinitesimally thin shell in the E-region - the so called

dynamo layer. There is indeed evidence from rocket measurements that the horizontal currents are confined to quite a thin layer. The dynamo layer is generally taken as that portion of the ionosphere where the transverse conductivities are high. It extends from about 80 to 150 Km. Thus the thickness of the dynamo layer is less than 1% of its radius. Further, in dealing with the problem of global atmospheric dynamo it is the practice to assume coincidence of the earth's magnetic axis and the rotating axis, and the wind and conductivity fields to be symmetric with respect to the equator. Under these assumptions conjugate points are equipotentials and vertical currents in the dynamo layer are completely inhibited. Then the relation between the horizontal components of resultant electric field $\vec{E}$ and horizontal components of the current density $\vec{J}$ is given approximately by the layer equations:

$$\left.\begin{aligned} J_x &= \bar{\sigma}_{xx} E_x + \bar{\sigma}_{xy} E_y \\ J_y &= \bar{\sigma}_{yx} E_x + \bar{\sigma}_{yy} E_y \end{aligned}\right\} \qquad - - - (5)$$

where x, y and z represent southward, eastward and vertical upward directions respectively, and $\bar{\sigma}_{xx}$, $\bar{\sigma}_{xy}$ and $\bar{\sigma}_{yy}$ are the layer conductivities given by equation (6) (chapter 1).

The measured geomagnetic variations are due to the spacial integration of the electric current. Until we know

enough about the ionospheric wind varying with height, we can only adopt such an approximation that $\overrightarrow{E}$ represents the mean total field. The total conductivity tensor $[\Sigma]$ and the total electric current intensity, $\overrightarrow{I}$, integrated with height from z_1 to z_2 are

$$[\Sigma] = \int_{z_1}^{z_2} [\sigma]\, dz \qquad \text{---} \quad (27)$$

and

$$\overrightarrow{I} = \int_{z_1}^{z_2} \overrightarrow{J}\, dz \qquad \text{---} \quad (28)$$

where z_1 and z_2 are the heights of the bottom and top of the dynamo layer respectively. Using equations (27) and (28), we get from equation (5) the following equations of the total horizontal electric current.

$$\left.\begin{aligned} I_x &= \Sigma_{xx} E_x + \Sigma_{xy} E_y \\ I_y &= \Sigma_{yx} E_x + \Sigma_{yy} E_y \end{aligned}\right\} \qquad \text{---} \quad (29)$$

The total electric field $\overrightarrow{E}$ is the sum of dynamo electric field and the polarization field. Let V_x and V_y denote the

southward and eastward components respectively, of the horizontal tidal wind V. Hence, $V_y B_z$ and $- V_x B_z$ are the x and y components of the dynamo electric field respectively. When the electrostatic potential S is introduced, then $- \partial S/a \partial\theta$ and $- \partial S/a \sin\theta \partial\lambda$ would be the x and y components of the electrostatic polarization field respectively; where "a" is the distance between the earth's centre and the dynamo layer in which the lunar current flows, θ is the co-latitude and λ is the east longitude. Therefore

$$\left.\begin{aligned} E_x &= V_y B_z - \partial S/a \partial\theta \\ \text{and} \\ E_y &= -V_x B_z - \partial S/a \sin\theta \partial\lambda \end{aligned}\right\} \quad \text{- - - (30)}$$

At latitudes higher than the focus of the current system, the dynamo electric field predominates over the electrostatic field and the current system is therefore regulated by B_z. At lower latitudes the electrostatic field is considerably greater than the dynamo electric fields. In this case the electrical conductivity is very effective for the current and is dependent on the dip angle (see equ.(6), chapter 1) which has a similar distribution to B_z in low latitudes. Thus the electric current system everywhere is regulated by B_z (section 6.2). The lunar tidal effects in the F_2 region which are caused mainly due to the electromagnetic

drifts which in turn depend on the electro-static fields in the dynamo region (section 6.5 - 6.8) will also be regulated by B_z or the dip angle. Thus the magnetic control of the lunar tide in f_oF_2 (section 2.10a) can be explained on this basis.

To obtain the total electric field distribution, MATSUSHITA (1967) proceeded as follows. Except near the magnetic equator, Sin ϕ and $\text{Sin}^2\phi$ (ϕ = dip angle) can be approximated as 1. Then using equation (6) (chapter 1) for the conductivities, equation (29) reduces to:

$$\left.\begin{aligned} I_x &= \Sigma_1 E_x + \Sigma_2 E_y \\ I_y &= -\Sigma_2 E_x + \Sigma_1 E_y \end{aligned}\right\} \quad \text{- - - (31)}$$

If the current function R is known, I_x and I_y can be obtained from

$$\left.\begin{aligned} I_x &= \partial R/a \, \text{Sin}\,\theta \, \partial\lambda \\ \text{and} \\ I_y &= -\partial R/a \, \partial\theta \end{aligned}\right\} \quad \text{- - - (32)}$$

As an approximation of the current system shown in figure 4, except the magnetic equatorial zone, the current function R is indicated by

$$R = a \times 10^{-6} \cos (2\lambda + 150^{\circ}) P_3^2 \text{ e.m.u.} \quad - - - (33)$$

where P_3^2 is the Schmidt's normalized spherical function.

An estimation of the distribution of gas dehsity and of other physical behaviour with height based on rocket observations leads to:

$$\left.\begin{aligned} \Sigma_1 &= 6.9 \times 10^{-9} \text{ e.m.u.} \\ \text{and } \Sigma_2 &= 1.5 \times 10^{-8} \text{ e.m.u.} \end{aligned}\right\} \quad - - - (34)$$

Except in the magnetic equatorial zone, the electric field $\vec{E}$ at different locations may be calculated using equations (31) to (34) and is shown in figure 115(after MATSUSHITA, 1967).

Near the magnetic equator, $\phi = 0$ and $B_z = 0$. Also $\Sigma_{xx} \sim \Sigma_0$, $\Sigma_{xy} = -\Sigma_{yx} \sim 0$ and $\Sigma_{yy} \sim \Sigma_3$. Therefore $I_x = 0$ and hence $E_x \sim 0$. Then the only electric field is E_y and is given by (from equation 29).

$$E_y \sim I_y / \Sigma_3 \sim \Delta X / 2\pi\Sigma_3 \quad - - - (35)$$

where ΔX is the northward component of the lunar geomagnetic variation and Σ_3 is the total Cowling conductivity. Based on

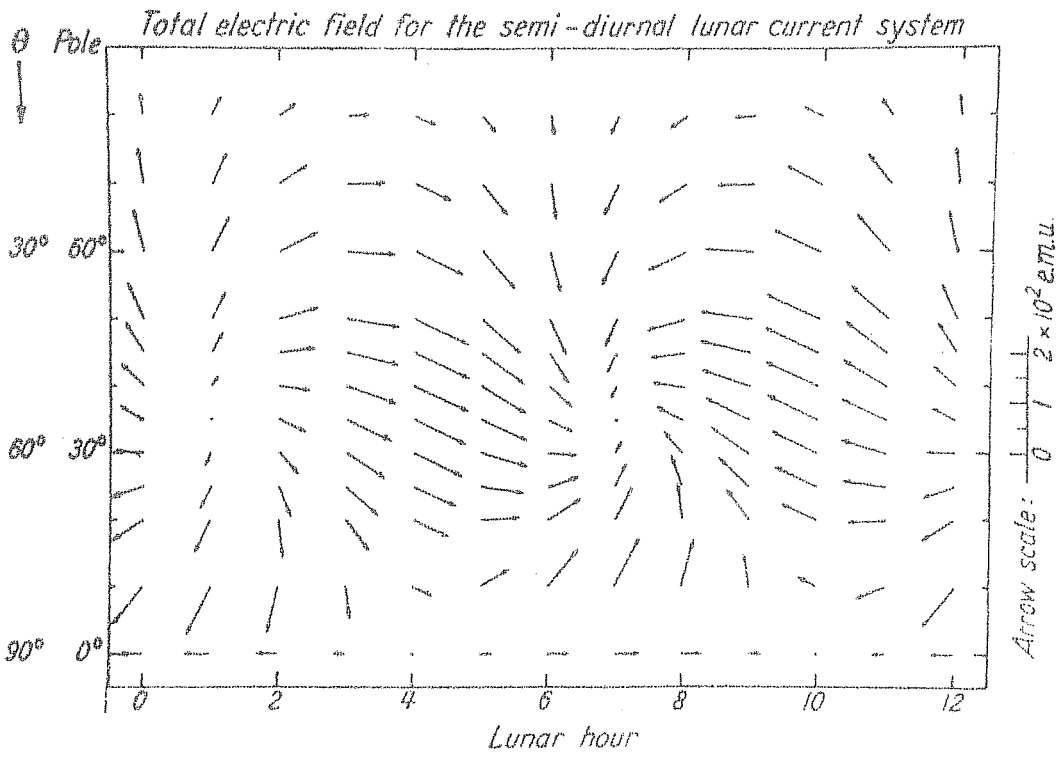

Total electric field for the semi-diurnal lunar current system
θ Pole
30° 60°
60° 30°
90° 0°
0
2
4
6
8
10
12
Lunar hour
Arrow scale: 0 1 2 × 10² e.m.u.

FIGURE - 115

the observations of ΔX at Huancayo and Ibadan, E_y at equator was calculated by MATSUSHITA (1967) and is shown in the figure 115.

These horizontal electric fields in conjunction with horizontal component of the earth's magnetic field give rise to vertical electromagnetic drift of charged particles (section 1.4) which cause lunar variations in the ionosphere.

6.4 Cause of lunar tides in the E-region

CHAPMAN (1931) developed a theory of formation of ionospheric layers based on production of ionization by absorption of solar radiations in an isothermal atmosphere of uniform composition. According to this theory, the rate of ion (pair) production $Q(\chi, h)$, has a maximum value $Q(\chi)$ at the height $h(\chi)$ where

$$h(\chi) = H \log_e (A \rho_o H \operatorname{Sec} \chi) \quad \text{---} (36)$$

and $$Q(\chi) = D S_\infty \operatorname{Cos} \chi / H \exp 1 \quad \text{---} (37)$$

where H is the scale height of the atmosphere, S_∞ the intensity of the ionizing radiation above the earth's atmosphere, A its absorption coefficient, ρ_o the atmospheric density at the ground, χ the zenith distance of the sun at the given time and place, and D the number of ion-pairs produced by the

absorption of unit quantity of radiation.

(a) Effect of lunar tidal wind (No magnetic field)

The influence of tidal air motion on ion production can directly be seen from equations (36) and (37). If the small changes in H resulting from the adiabatic heating and cooling of the atmosphere under compression and dilation are ignored, then the only influence of tidal motions is to superpose a small sinusoidal variation on ρ_o. Thus the height at which maximum ion production occurs, $h(\chi)$, will oscillate up and down by a small amount, but the rate of ion-production at this level will remain unchanged.

The variation in the height of the E-layer can, therefore, be inferred from variations of ρ_o. Differentiation of (36) give

$$dh = H\, d\rho_o/\rho_o$$

In England, for the lunar barometric variation $d\rho_o/\rho_o$ at the ground is about 10^{-5}. If this oscillation could be magnified some 3000 times in the E-region, then taking H as 10 Km gives $dh \sim 0.3$ Km which is comparable to the value 0.93 Km found experimentally by APPLETON and WEEKES (1939).

Thus on these grounds, and with extreme assumptions concerning the tidal amplification, it might be possible to account for the observed lunar height variations of the

E-region. According to this simple theory based on tidal rise and fall of isobaric surfaces, the phase of the lunar variations should be almost the same all over the globe (section 2.5). However, the phases of lunar variations of h'E at Canberra and Brisbane are opposite to that observed at Slough, England (section 2.8a). This important result is, therefore, not explainable on the basis of above theory.

On the other hand, the dynamo electric fields and currents reverse their directions in the vicinity of latitude 35° (figure 115). Thus the electromagnetic vertical drifts associated with these electric fields will have opposite directions at latitudes lower and higher than 35° latitude. It seems reasonable, then, to think that lunar variations in the E-region may be caused due to these vertical drifts. However, it must be emphasized that life time of ionization in the E-region is of the order of only a few minutes. Hence, the ionization is lost quickly by recombination before it is moved to any appreciable distances under the influence of vertical drifts. Under these conditions vertical drifts can cause only a small perturbation in the ionized layer.

(b) Effect of vertical drifts on a Chapman layer

APPLETON and LYON (1955) discussed the effect of a small vertical velocity W on an ionospheric layer obeying Chapman's laws, and showed that the change in maximum electron

density (ΔN_m) and in height of peak ionization (ΔZ_m) is given by

$$\frac{\Delta N_m}{N_m} = -\frac{1}{2\alpha N_m}\frac{\partial W}{\partial Z} - \frac{1}{4H^2}\left(\frac{W}{2\alpha N_m}\right)^2 \quad \text{---} \quad (38)$$

and $$\Delta Z_m = \frac{W}{2\alpha N_m} \quad \text{---} \quad (39)$$

where H is the scale height of the layer, α the recombination co-efficient and W is measured positive upwards.

It is seen from equation (39) that height of the peak varies in phase with W; i.e. vertically upward and downward drift raises or lowers the layer respectively. The change in N_{max} is not so explicit and depends both on W as well as its height gradient. If the drift velocity is uniform at all heights, $\partial W/\partial Z = 0$, then according to (38) the electron density would decrease irrespective of sign of W.

MARTYN (1947, 1948) suggested that the solar and lunar variations of ionospheric parameters are caused by the corresponding variations of the vertical drift velocity which itself is generated by the interaction of horizontal electric and

magnetic fields at those levels. The lunar tidal variations of W are associated mainly with the variations of the electric field, $\overrightarrow{E}$, which itself is generated by the interaction of horizontal lunar tidal winds with the vertical component (B_z) of the geomagnetic field. Thus we have a mechanism connecting horizontal lunar tidal winds with ionospheric tides through the vertical drift velocity.

The kinematic viscosity which is inversely proportional to gas density (ρ) would increase with increasing altitude due to the decrease of ρ with height. Thus with increasing height, the damping will increase, thereby decreasing the amplitude of lunar tidal winds. Consequently the vertical drift velocity would have a negative height gradient. Also, above the lunar current system the direction of W and $\partial W/\partial Z$ must be opposite; vertical upward W decreasing upwards will give a negative $\partial W/\partial Z$, while downward W decreasing with height would result in a positive $\partial W/\partial Z$. Since the vertical drift velocity W due to lunar dynamo electric fields is very small, while its height gradient may be considerable, the contribution of second term in (38) to N_{max} variations is much smaller than the first term. $\triangle N_m$ thus depends directly on $\partial W/\partial Z$ which is negative and positive for upward and downward drift velocities respectively. Therefore, for a Chapman layer, N_{max} increases or decreases with a upward or downward velocity respectively.

(c) Interpretation of the observed results

At Huancayo

The direction of $\vec{E}$ and hence of $\vec{W}$ is reversed at latitudes around the focus of lunar current system. At the magnetic equator, an upward W would be obtained by a eastward electric field (E_y) since H-component of geomagnetic field there is north-ward. The E_y varies in phase with the eastward current (I_y) which is approximately given by $\Delta X/2\pi$ (equation 35). The lunar variation of the horizontal component H(or X) at Huancayo has its maximum value at 07-08 lunar hr (section 3.2). The maximum upward drift velocity W will therefore occur at 07-08 lunar hr. Thus the lunar variations of electron density in E and F_1 layers, which are known to be fairly Chapman-like, would be maximum positive at 07-08 lunar hr at Huancayo. It is seen from figures 87 and 88 (page 159, section 5.4) that the lunar tide in N for any height from 120 to 180 Km has its maximum at 08 lunar hr which is the time of maximum positive change of the H-component or maximum eastward electric field (E_y). Thus lunar tidal variations in the E and F_1 regions of the ionosphere at equator are explainable by this theory.

At Puerto Rico

As discussed above, the electron density variations in the E and F_1 regions should be in phase with the variations of the

H-component. At Puerto Rico (52° dip) which is on the polar side of the L-current system focus, the variations in the H-component would be in phase opposition with the corresponding variations at the equatorial stations. Hence the maximum upward drift would occur at 01-02 lunar hr at Puerto Rico (section 4.4). The electron density would then be maximum at 01-02 lunar hour. It is seen from fig.94 (page 167, section 5.5) that the lunar variations in N at these heights are maximum at about 01 lunar hr, which is in confirmity with the above theory.

6.5 Cause of lunar tides in the F-region at stations in middle latitudes

In the F-region the electric fields existing are mainly the ones which are communicated from the dynamo region along the geomagnetic field lines and these cause vertical drifts. Thus the changes in vertical drift velocity in the F-region would be in phase with the changes in electric field in the dynamo region connected to it.

In the F-region, the life time of ionization is generally of the order of a few hours, so that the production and loss terms in the continuity equation are small compared to the tidal divergence terms. Under these conditions the continuity equation becomes

$$\partial N/\partial t = -\partial (NW)/\partial Z \qquad \text{---(40)}$$

where N is the electron density and W is the vertical drift velocity.

If we assume a uniform vertical drift velocity at all heights, equation (40) reduces to

$$\partial N/\partial t = -W \partial N/\partial Z \qquad ---(41)$$

If the drift is simusoidal in time, of form $W_o \cos \Omega t$, then Z_m has the variation $W_o/\Omega \sin \Omega t$, thus lagging the drift velocity by $\pi/2$ in phase. If the distribution of the electric field in the F_2 layer is the same as in the E-layer, the maximum eastward electric field occurs at around 4-6 lunar hr in middle latitudes (figure 115). Then the maximum of Z_m occurs at 7-9 lunar hr which is in fairly good agreement with the observed results (section 2.10a). In order to explain the observed amplitude of Z_m of about 3 Km, the amplitude of W should be about 42 cms/sec (MATSUSHITA, 1967). However, as this situation is a simple rise and fall of height without any change of distribution of ionization, the N_{max} variations are not explainable by this theory.

MARTYN (1950) showed that the variations in N_{max} can be caused by the height gradients in the recombination coefficient α. Supposing that the drift produces an oscillation in Z_m of amount $Z_o \cos \Omega t$, and that α varies with height as $\alpha = \alpha_0(1-bZ)$, the differential equation for N_m for night-time

conditions is

$$dN_m/dt = -\alpha_0(1-b\ Z_0\ \cos\Omega t)N_m^2$$

where d/dt is taken to mean differentiation "with the motion" of the level of maximum ionization. The solution of this equation for small variations ΔN_m is:

$$\Delta N_m/N_m = -\alpha_0\ N_m\ t + \left(\alpha_0\ N_m\ b\ Z_0/\Omega\right)\cos\ (-\Omega t - \pi/2)$$

The first term on the right-hand side of this equation simply expresses the normal decay of ionization; the second is an oscillatory variation in N_{max} which lags behind that in Z_m by a phase angle $\pi/2$.

A similar treatment assuming $\alpha = \alpha_0\ e^{-Z/H}$ was given by DUNCAN (1956). However this expression is approximately equal to $\alpha_0(1-Z/H) \simeq \alpha_0(1-bZ)$ and hence the two cases are not basically different.

Taking $\alpha_0 = 3\times10^{-10}$ cm^3/sec; $N_{max} = 2.5\times10^5$/cm^3; $Z_0 =$ 2.5 Km; $\Omega = 1.4\times10^{-4}$; and $b = 1/H = 1.4\times10^{-7}$/cm as representative of the F_2 region at night; MARTYN (1950) obtained $\Delta N_m/N_m = 1.9\%$ for the amplitude of semi-diurnal lunar variation in N_{max}. This value is in fairly good agreement with the observations. The observed phase lag of N_{max} variations on

that of h_{max} variations by about 3 lunar hr (section 2.10a) at middle latitude stations is thus explained on the basis of this theory.

GLIDDON and KENDALL (1964) studied the effect of a small, uniform vertical electrodynamical drift of sinusoidal type with a varying phase on a model F_2-region. They obtained the height profiles of the perturbation for various phases at noon, and the time variation of perturbation at the height of maximum electron density. They compared their results with the RASTOGI's (1961a) observations of the lunar variation of f_oF_2 at Leopoldville. This comparison indicated that the magnitude of the vertical lunar tidal electromagnetic drift in the F_2 region is about 40 cms/sec, yielding a three percent variation of f_oF_2. This value of W is consistent with that obtained by MATSUSHITA (1967).

6.6 Interpretation of the results of the lunar tide in the F2 region at Puerto Rico

The figure 94 (page 167, section 5.5) for height variation of phase of the lunar oscillations in N during the day as well as night shows that there is an appreciable retardation of phase with height. MARTYN (1947) has discussed the effect of a drift velocity varying in phase with height in the F_2 region considering only the transport term of the equation. He showed that taking $W = -W_o \sin(-\Omega t + \sigma Z)$, the changes in peak electron density and height of the peak

ionization are given by:

$$N_m = 1 - (\sigma W_o / \Omega) \sin (\Omega t + \sigma Z_m)$$

$$Z_m = - (W_o / \Omega) \cos (\Omega t + \sigma Z_m)$$

provided $\sigma W_o / \Omega << 1$

where Ω = angular frequency

σ = height gradient of phase

Z = height above some arbitrary level Z_o

When σ is positive, then the maximum in electron density happens when vertical drift velocity is maximum downward. The variations in the height of peak density (Z_m), then, leads the N_{max} variations by 3 hour. Thus the variations in N_{max} are in phase opposition to those in W. Since at Puerto Rico, W is maximum upwards at 1-2 lunar hr, we should expect a maximum in N_{max} at 7-8 lunar hr. The height of the peak density should be maximum at 4-5 lunar hr. The computations of lunar tidal oscillations in Z_m and N_{max} at Puerto Rico gave a phase (time of max) of 5 lunar hr and 9.1 lunar hr respectively (table 18). This is in good agreement with the above theory. Also the lunar tidal variations at the highest heights ($\sim N_m$) in fig.94 (page 167, section 5.5) give a phase of 10 lunar hr which is in good

agreement with above, if due allowance is made for the sluggishness of the ionization to respond to electric fields. Fig.94 shows that the phase in F_2-region retards with height and hence σ is positive. Also σ is seen to be very small and hence the condition $\sigma W_0/\Omega \ll 1$ is applicable. Thus the above theory explains fairly well the lunar tidal variations in N at Puerto Rico.

6.7 Cause of lunar tides in the F2 region in the magnetic equatorial zone

The effect of the vertical drifts in the equatorial ionosphere was discussed first by MARTYN (1947) by taking $W = -W_0 \text{ Sin } (\Omega t + \sigma Z)$ and solving the continuity equation (40). However, the phase of the lunar variation of N which is 6 hr later than the phase of the height variation (section 2.10a) could not be explained. This phase relationship was successfully explained by DUNCAN (1956) by assuming the ionization rate Q to be decreasing exponentially with height, and Z_m varying as $Z_0 \text{ Cos } 2\Omega t$. However, he did not explain why the maximum of Z_m happens at 8-9 lunar hr. The lunar variationsof N_{max} at stations near the magnetic equator are notably larger during the day-time and are very small in the night-time. This luni-solar effect was interpreted by MARTYN (1947) as an effect due to superposition of two vertical drift velocities; one is due to the solar quiet dynamo current system, S_q, and the other is due to the lunar current system, L.

(a) Lunar variations in the day-time

The eastward S_q electric field and consequently the upward drift velocity is maximum during the day-time. This solar component of drift velocity W_s is known to lift the ionization in the equatorial F_2 region causing the well known equatorial anomaly (section 1.6). The lunar effect on this velocity is to cause a small perturbation W_L. At 07-08 lunar hr (when W_L is maximum upward), $\overrightarrow{W_s} + \overrightarrow{W_L}$ will be maximum and the anomaly will be more pronounced; while at 01-02 lunar hr (W_L is maximum downward), $\overrightarrow{W_s} + \overrightarrow{W_L}$ would be minimum and anomaly will be reduced. Therefore the lunar effects in electron density (N) at F_2-region heights would cause a maximum decrease (minimum N) at 07-08 lunar hr and a maximum increase (maximum N) at 01-02 lunar hr. Thus the lunar tidal oscillations of N in the lower E and F_1 regions would be opposite to that in the F_2 region (section 6.4c). Due to sluggishness of the ionosphere, the changes in electron density of a layer lag behind the forces causing the change by a time approximately equal to $1/2\alpha N$ which is of the order of few minutes in the E-region and about 1-2 hours in the F_2-region. Thus even-though the maximum upward drift $(\overrightarrow{W_s} + \overrightarrow{W_L})$ occurs at 07-08 lunar hr, the maximum decrease in electron density is felt around 09-10 lunar hr(or maximum N at 03-04 lunar hr). Thus the correlation between the geomagnetic and ionospheric tides at the magnetic equator (section 3.2) is explainable on the basis of the above theory. The increase in the H-component (and E_y) would

increase the upward velocity W_L; the layer rises and after a delay of 1-2 lunar hours a minimum value of N_{max} is obtained.

Also, the variations of N_{max} at stations near the Appleton anomaly peaks would be opposite to the variations at the equatorial stations. Hence, the maximum N_{max} due to lunar tidal drifts in middle latitudes, within the anomaly region, will occur at 09-10 lunar hr, which agrees fairly well with the observed results (section 2.10a).

By a quantitative analysis based on the above theory, MAEDA(1955a) obtained 7.1 Km and 7.6% for the amplitude of lunar semi-diurnal variations of the F_2 height and density variations, and 10 lunar hr and 05 lunar hr for their phase respectively. This agrees well with the observations.

Thus it is seen that the lunar variations in the F_2 region at equatorial stations are caused by the perturbations of the equatorial anomaly by lunar electromagnetic drifts.

(b) Lunar variations in the night-time

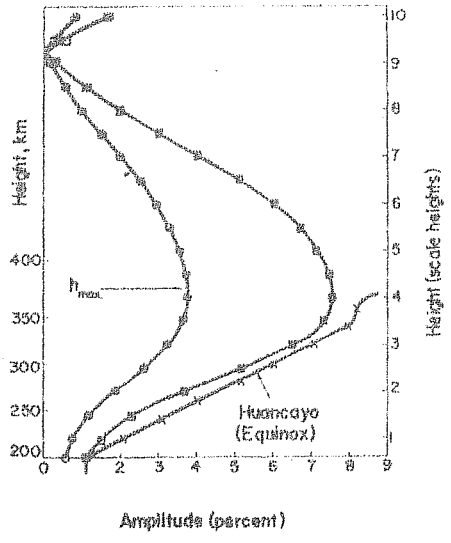
During the night-time, the situation is different as W_S is downward and the equatorial anomaly is absent. The layer after sunset decays without any change in its shape under the influence of attachment and horizontal diffusion. A small upward (or downward) velocity will bring the decaying

layer in a region of low (or high) loss coefficient β and hence electron density increases (or decreases). Thus the lunar tidal oscillations in N are expected to be in phase with W_L(and $\triangle H$). It is seen from fig.88 (page 159, section 5.4) that the variations of N during the night-time are roughly in phase agreement with the variations in the H-component ($\sim$ 7 lunar hr).

6.8 Lunar variations of electron density at fixed heights

Considering the lunar variations of electron density as due to the changes in the equatorial anomaly by a small lunar tidal drift, DUNFORD (1969) has computed the height variations of the lunar tide at magnetic latitudes 0° and 18.5°. He compared the computed profiles at latitudes 0° and 18.5° with the observed results at Huancayo and Ahmedabad respectively, which were published by SHARMA and RASTOGI (1967, 1968).

Both the calculated as well as the observed vertical profile of the tide is shown (after DUNFORD, 1969) in figure 116 and 117 for Huancayo and Ahmedabad respectively. The curve represented by crosses (x) in figure 116 is that due to SHARMA and RASTOGI (1968). The drift velocities were taken in units of Hd_o where H is the scale height which is assumed to be 50 Km and d_o = diffusion rate. He took W_s=3 as the normalized vertical drift velocity due to the solar



X SHARMA and RASTOGI(EXP'L).; ● THEORETICAL

FIGURE-116

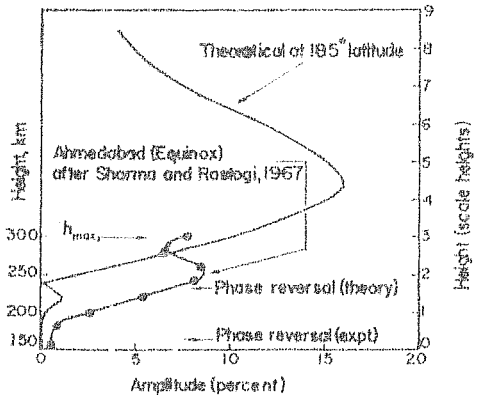


FIGURE-117

dynamo action, which corresponds to an absolute value of 7.5 m/sec and gives rise to the anomaly crests at 15° magnetic latitude. Now taking W_L = 0.6 and 1.2 respectively, in the above units, the height variations of the lunar perturbations in electron density were calculated. The curves represented by ~~open~~ closed circles (●) and ~~open~~ closed squares (■) in figure 116 represent the cases W_s = 3, W_L = 0.6 and W_s = 3, W_L = 1.2 respectively. It is seen from figure 116 that the theoretical curve corresponding to the case W_s = 3, W_L = 1.2 fits very well with the observed curve. Thus a lunar drift velocity of W_L = 1.2 (i.e an absolute value of 3 m/sec), explains the observed variations reasonably well, and gives an approximate idea of the magnitude of lunar electromagnetic drifts at the equator.

In figure 117, the closed circles (●) represent the observed results at Ahmedabad, while the continuous line gives the computed variations assuming W_s = 3 and W_L = 0.6. It is seen that the theoretical curve for Ahmedabad is very different from that at Huancayo. After a phase reversal at 1.7 scale heights, the amplitude increases with height well beyond the N_{max} level to reach 16 percent at 4.5 scale heights. SHARMA and RASTOGI (1967) also noticed a phase reversal, but at about one scale height below the predicted height. The vertical profile of the lunar tide in electron density can be

calculated at other low latitude stations within the equatorial anomaly zone since the above theory is applicable only for the stations in this zone.

It is suggested that further analysis of lunar variations in N(h) profiles should be made at stations at different latitudes as this would greatly help in understanding the dynamics of the ionosphere.

A P P E N D I X

TABLE-1

L(NU) IN H AT HUANCAYO

NU	C1	ALFA1	C2	ALFA2	C3	ALFA3	C4	ALFA4
				ANNUAL				
00	7.36	327	4.72	206	3.44	77	.79	228
03	4.39	39	3.20	229	2.84	76	2.04	274
06	5.08	3	4.52	204	3.37	64	.59	263
09	4.44	36	4.78	233	2.79	68	.77	278
12	4.15	4	4.81	222	2.71	73	1.18	299
15	5.23	22	4.63	225	2.76	83	1.52	265
18	4.87	50	6.05	235	3.22	94	.85	310
21	1.85	73	2.41	226	2.50	56	1.21	243
MEAN	4.03	17	4.30	223	2.90	74	1.03	271
				D-MONTHS				
00	3.85	39	8.13	260	6.57	105	1.42	276
03	2.46	138	4.13	278	2.74	111	1.80	288
06	3.31	355	4.11	244	4.01	80	.47	332
09	8.80	30	9.32	232	5.52	66	1.47	249
12	5.99	0	4.59	208	2.95	39	1.49	348
15	8.65	16	7.58	224	4.82	72	1.88	226
18	7.73	74	9.03	255	6.59	107	2.40	302
21	4.21	34	3.42	237	3.73	76	1.91	251
				E-MONTHS				
00	12.66	312	7.80	174	5.04	33	1.49	239
03	9.27	33	6.29	218	4.90	74	3.28	267
06	8.14	356	7.87	217	4.93	61	1.75	242
09	3.07	34	5.19	227	2.66	68	.80	311
12	5.75	33	7.74	233	5.35	87	2.37	271
15	7.26	27	5.32	243	3.30	106	1.73	301
18	8.89	36	7.47	229	3.43	83	.85	252
21	3.67	112	4.41	255	3.69	56	1.36	230
				J-MONTHS				
00	8.74	323	3.61	167	1.13	98	1.31	129
03	4.66	23	2.14	159	1.99	34	1.24	264
06	4.09	23	5.09	148	1.49	30	.17	32
09	1.85	71	.70	328	.26	139	.52	294
12	2.87	306	2.30	210	.53	105	.58	310
15	.39	131	1.92	175	.51	61	1.78	269
18	1.47	270	3.34	192	2.72	5	1.07	55
21	.63	228	2.87	137	1.35	333	.50	256

TABLE-2

L(NU) IN H(MAX) AT HUANCAYO

NU	C1	ALFA1	C2	ALFA2	C3	ALFA3	C4	ALFA4
				ANNUAL				
00	3.21	22	6.16	179	1.16	58	2.64	8
03	8.67	120	4.41	155	1.71	212	1.39	221
06	4.85	334	2.90	190	4.87	63	1.58	43
09	5.36	29	1.03	20	5.37	350	1.34	6
12	2.65	20	5.02	197	4.52	31	1.69	355
15	3.88	11	4.43	188	1.71	335	1.42	27
18	6.99	61	5.12	159	6.33	94	1.45	160
21	6.29	145	6.52	198	1.00	355	1.88	145
MEAN	2.96	60	4.03	181	2.11	42	.61	34
				D-MONTHS				
00	11.06	41	12.55	172	3.72	153	3.92	29
03	13.31	122	11.51	163	6.39	169	5.19	136
06	3.18	335	8.26	192	7.40	27	4.10	37
09	13.12	26	1.18	231	12.12	355	7.49	27
12	5.76	331	8.75	205	11.29	3	3.43	324
15	8.27	335	5.09	202	2.94	56	.84	70
18	14.34	62	6.97	143	12.85	95	5.39	130
21	8.44	135	11.65	196	4.82	163	6.78	186
				E-MONTHS				
00	2.52	341	4.48	202	5.49	31	3.15	266
03	13.14	106	2.82	130	6.00	313	7.38	297
06	5.32	338	4.89	244	5.02	75	1.93	70
09	2.45	92	2.98	80	2.48	352	3.37	248
12	4.45	82	4.50	232	4.66	66	2.89	64
15	2.39	104	6.17	186	2.87	303	3.31	13
18	7.29	56	5.19	183	4.74	77	3.95	233
21	10.29	132	6.71	194	4.71	320	2.84	55
				J-MONTHS				
00	3.27	239	1.89	174	1.86	291	2.92	311
03	2.34	209	.71	21	2.23	169	2.92	177
06	6.16	330	4.89	71	5.03	104	1.11	246
09	2.46	347	3.08	345	1.78	314	1.50	176
12	2.21	35	4.61	144	2.64	130	1.26	321
15	4.54	44	2.43	163	2.94	303	.45	44
18	.57	206	3.91	158	1.92	124	1.79	15
21	3.89	225	1.29	207	4.33	20	1.75	74

TABLE-3

L(NU) IN N(MAX) AT HUANCAYO

NU	C1	ALFA1	C2	ALFA2	C3	ALFA3	C4	ALFA4
				ANNUAL				
00	4.25	198	3.09	286	1.33	115	1.05	11
03	4.58	193	3.36	331	1.76	98	1.35	227
06	7.37	149	4.91	262	1.55	186	.69	14
09	.36	191	3.96	300	2.29	158	.91	172
12	6.33	166	5.16	315	.62	103	3.14	327
15	4.03	186	4.75	278	2.21	155	2.08	174
18	5.46	169	5.23	333	1.49	128	1.14	325
21	4.10	175	.79	286	4.55	137	2.15	200
MEAN	4.57	174	3.52	300	1.80	139	.42	259
				D-MONTHS				
00	12.16	199	4.05	347	1.18	86	2.19	354
03	3.93	213	6.95	355	2.68	26	.87	194
06	7.76	157	5.11	285	2.30	62	1.63	27
09	7.13	170	7.83	307	5.22	133	3.51	150
12	9.28	139	7.51	317	4.50	72	5.29	316
15	10.39	182	7.32	268	6.06	163	5.62	171
18	7.61	202	7.19	349	2.00	223	2.76	288
21	11.13	199	1.09	100	6.48	161	3.40	189
				E-MONTHS				
00	2.30	7	7.49	255	2.53	134	1.35	56
03	6.47	214	5.45	297	4.64	131	4.68	236
06	11.36	150	7.36	261	4.94	196	.89	273
09	3.99	341	5.51	278	2.94	214	1.59	221
12	11.02	188	5.43	307	3.76	229	3.73	330
15	3.41	146	5.32	297	.62	87	1.12	140
18	7.35	163	6.36	311	3.62	107	1.38	7
21	5.11	133	4.97	317	5.85	115	3.48	215
				J-MONTHS				
00	3.06	184	1.02	310	.50	76	.41	298
03	5.27	151	.93	129	.74	104	1.13	56
06	3.49	126	3.29	226	1.49	233	.75	55
09	2.35	354	1.43	64	.71	132	1.60	346
12	.61	174	2.65	330	.69	40	.91	22
15	3.14	294	2.02	269	.49	122	1.05	287
18	4.32	117	2.91	342	1.30	99	.84	37
21	1.91	27	2.63	180	2.33	128	.32	64

TABLE-4

L(NU) IN Y(M) AT HUANCAYO

NU	C1	ALFA1	C2	ALFA2	C3	ALFA3	C4	ALFA4
				ANNUAL				
00	3.26	352	3.35	163	.78	297	1.45	317
03	2.54	92	1.01	179	1.91	251	.32	257
06	3.97	330	2.61	146	1.83	26	.52	202
09	2.28	5	1.01	155	1.94	304	.83	200
12	2.61	26	4.66	170	1.31	6	.36	150
15	2.46	340	2.56	163	1.88	320	.22	41
18	2.65	27	3.95	169	1.61	20	.50	90
21	2.30	140	2.13	206	2.88	293	1.84	37
MEAN	1.81	13	2.57	168	1.26	320	.13	8
				D-MONTHS				
00	6.29	6	4.86	173	.56	112	1.65	331
03	4.19	70	2.60	205	3.43	212	.53	30
06	5.14	331	4.12	149	2.96	347	1.04	124
09	6.31	359	4.72	146	2.25	293	.92	263
12	3.63	23	7.91	150	3.54	347	1.32	147
15	4.75	336	2.56	154	.95	357	.82	272
18	6.22	32	6.17	151	3.23	57	1.65	108
21	2.56	138	4.00	273	1.86	236	2.44	24
				E-MONTHS				
00	3.15	334	4.65	165	2.60	300	1.78	304
03	4.96	125	1.52	161	3.70	303	.73	358
06	4.37	350	2.99	187	2.95	24	.77	254
09	.19	151	.52	353	1.92	324	1.92	192
12	2.89	51	4.76	208	1.72	36	.05	0
15	2.02	334	3.69	170	3.28	317	.94	44
18	2.02	54	5.21	194	2.93	343	.77	256
21	3.51	118	5.59	182	6.78	300	4.12	47
				J-MONTHS				
00	1.08	314	1.21	112	.38	239	.94	323
03	1.14	346	1.12	42	1.18	209	1.73	219
06	3.07	299	2.81	91	1.90	111	.93	222
09	.96	39	1.45	294	1.80	294	.76	131
12	1.83	353	2.94	162	.72	167	.25	319
15	.78	290	1.56	162	1.73	311	.81	117
18	1.49	291	1.64	159	.33	291	1.14	42
21	1.79	194	1.42	107	1.25	331	.85	227

TABLE-5

L(NU) IN N(T) AT HUANCAYO

NU	C1	ALFA1	C2	ALFA2	C3	ALFA3	C4	ALFA4
				ANNUAL				
00	3.11	62	4.82	209	1.65	72	3.19	329
03	6.87	134	3.21	280	.36	97	.97	260
06	3.88	109	7.22	233	2.96	58	2.60	279
09	3.86	26	2.76	224	.51	355	.24	210
12	4.94	134	5.90	227	3.71	44	3.47	311
15	1.92	280	3.58	228	.95	37	.31	273
18	5.70	110	4.76	264	4.06	75	2.38	307
21	6.46	152	4.35	244	1.35	84	1.91	161
MEAN	3.24	117	4.30	237	1.82	61	1.32	296
				D-MONTHS				
00	4.79	20	7.01	173	2.05	57	3.18	340
03	8.02	126	1.14	282	3.48	286	1.94	102
06	1.45	358	9.28	204	7.61	16	2.07	241
09	8.68	45	6.10	204	1.45	5	1.99	127
12	6.37	106	12.16	195	10.67	34	6.68	278
15	2.18	284	5.88	228	3.84	109	3.35	202
18	4.69	92	2.74	268	6.12	88	3.44	310
21	13.94	173	6.86	263	3.95	137	3.04	192
				E-MONTHS				
00	7.08	89	8.73	230	2.17	52	4.57	325
03	10.15	136	8.64	280	4.03	99	4.32	262
06	10.42	126	12.98	261	4.86	101	5.50	279
09	2.43	341	3.29	264	.39	41	2.03	241
12	9.53	157	9.49	270	.54	148	4.58	349
15	2.17	235	2.52	241	3.12	326	3.07	10
18	10.10	116	10.54	256	5.19	62	3.17	306
21	9.90	128	5.89	250	2.78	23	3.15	131
				J-MONTHS				
00	.47	243	1.29	265	1.62	130	1.78	325
03	2.78	155	.07	126	.48	152	.84	317
06	2.86	70	2.60	198	1.96	157	1.58	341
09	1.99	353	.04	8	.51	229	1.54	357
12	.71	73	.43	231	1.47	105	1.70	341
15	2.49	320	2.34	218	.95	344	.29	305
18	2.22	117	1.72	314	1.32	56	.46	302
21	2.83	353	3.08	169	.73	23	.52	164

TABLE-6

ANNUAL L VARIATION AT HUANCAYO

PARAMETER	L1	FI1	L2	FI2	L3	FI3	L4	FI4	SOURCE
H	1.01	246	4.23	223	.19	78	.19	0	
N(MAX)	.57	289	3.44	301	.57	61	.34	338	
H(MAX)	2.02	169	3.91	182	.78	156	.72	353	PRESENT ANALYSIS
Y(M)	.66	185	2.51	169	.57	230	.38	319	
N(T)	.44	151	4.22	238	.03	90	.61	25	
H(1951-55)	.77	135	4.09	213	.13	251	.06	284	RASTOGI-1968A
H(1957-59)	1.33	235	5.07	211	.73	103	.37	181	RASTOGI-1968B
H(MAX) (1942-44)	1.46	111	5.20	197	.94	200	.26	276	MARTYN-1947
FOF2(1942-44)	.018	303	.10	330	.013	158	.02	94	MARTYN-1947
FOF2(1951-55)	.006	13	.095	331	.004	286	.002	226	RASTOGI-1968B

TABLE-7
LUNAR M2 VARIATION IN H AT HUANCAYO

MEAN	R2	THETA2	LMT
ANNUAL			
407	(1.76)	.25	00
409	(1.33)	1.41	01
411	(0.77)	1.61	02
413	(0.66)	1.58	03
415	(0.96)	2.95	04
417	(2.52)	5.61	05
422	6.71	6.84	06
439	11.57	7.48	07
470	15.83	7.95	08
505	17.94	8.51	09
530	19.28	8.71	10
543	16.32	8.81	11
522	13.93	8.85	12
497	12.29	8.85	13
470	8.43	8.55	14
449	7.07	8.45	15
433	4.93	8.11	16
421	(1.76)	8.84	17
414	(0.76)	7.78	18
410	(0.48)	8.74	19
408	(0.70)	8.94	20
406	(1.46)	9.64	21
406	(1.21)	9.08	22
407	(1.42)	10.28	23
P.E=1.29			
E-MONTHS			
402	(5.47)	3.38	00
405	(5.03)	4.78	01
408	(4.29)	5.58	02
411	(4.15)	6.41	03
414	(4.83)	7.04	04
415	(6.07)	7.58	05
417	10.17	7.84	06
438	15.62	8.11	07
476	20.20	8.38	08
515	24.24	8.88	09
543	24.88	9.15	10
574	16.83	9.21	11
533	10.88	8.51	12
503	14.11	7.85	13
472	14.44	7.88	14
450	13.92	7.95	15
432	11.55	7.71	16
418	7.87	8.51	17
409	(5.98)	9.51	18
406	(5.86)	10.44	19
403	(6.20)	11.11	20
402	(6.34)	11.84	21
401	(3.95)	.91	22
401	(4.28)	1.91	23
P.E=2.41			

MEAN	R2	THETA2
D-MONTHS		
408	(4.39)	9.91
407	(4.16)	11.05
408	(3.74)	11.65
410	(3.38)	.48
412	(2.83)	1.28
415	(2.55)	4.11
419	(6.71)	6.41
435	12.19	6.95
470	17.20	7.38
508	18.86	7.71
532	22.97	7.81
531	25.15	7.98
512	28.08	8.28
485	22.52	8.71
463	13.02	8.61
446	8.24	8.85
434	(4.51)	8.31
422	(.44)	3.91
416	(3.92)	4.05
411	(4.85)	4.65
409	(5.03)	5.35
408	(3.73)	6.45
407	(3.89)	7.51
407	(4.61)	8.31
P.E=2.34		
J-MONTHS		
412	(4.46)	11=7
414	(3.83)	.88
416	(2.53)	1.18
419	(2.62)	1.18
419	(4.16)	2.01
422	(4.29)	3.88
429	(6.19)	5.61
443	(8.48)	7.15
465	11.54	8.08
492	13.35	8.98
515	14.07	9.35
523	11.90	9.95
521	10.71	11.05
502	8.82	11.35
474	(4.69)	.05
450	(1.83)	11.68
433	(2.21)	11.98
422	(2.62)	1.61
416	(1.17)	5.08
413	(.63)	7.15
411	(1.31)	7.71
409	(3.07)	8.25
410	(2.78)	8.58
412	(3.34)	10.21
P.E=2.27		

TABLE-8

LUNAR M2 VARIATION IN H(MAX) AT HUANCAYO

MEAN	R2	THETA2	LMT	MEAN	R2	THETA2
ANNUAL				D-MONTHS		
328	6.05	10.57	00	364	(10.18)	10.63
317	7.59	.17	01	337	19.40	.43
312	(5.23)	10.13	02	318	(7.28)	10.53
310	(3.94)	11.10	03	306	(5.35)	10.76
308	7.13	10.83	04	299	(7.21)	9.52
315	(4.35)	.27	05	316	(6.13)	8.72
333	6.07	3.97	06	313	(6.37)	6.40
294	(4.32)	1.33	07	296	(7.66)	7.84
317	9.53	7.97	08	319	14.41	7.73
391	14.63	8.43	09	358	20.37	7.93
389	9.48	9.10	10	395	19.30	9.17
402	(3.17)	7.47	11	415	(8.21)	9.23
405	9.38	7.20	12	416	14.08	7.76
408	8.27	7.77	13	418	14.99	8.20
408	7.32	8.27	14	415	14.35	8.30
409	8.75	8.77	15	414	12.79	9.05
409	9.61	8.80	16	418	16.47	8.80
418	12.15	8.90	17	429	21.09	9.05
437	10.12	8.90	18	435	18.21	9.20
465	(5.16)	9.40	19	453	(9.37)	8.75
449	8.91	10.90	20	477	17.95	10.60
403	5.83	1.70	21	452	(9.90)	.80
366	(2.17)	10.33	22	424	(7.00)	11.71
341	(2.34)	11.87	23	387	(9.54)	11.64
P.E=1.91				P.E=4.22		
E-MONTHS				J-MONTHS		
312	(4.07)	10.83	00	309	(4.01)	10.20
308	(5.06)	11.86	01	306	(2.35)	7.96
308	(5.58)	11.00	02	310	(5.45)	8.52
310	(6.66)	.39	03	314	(3.55)	8.90
311	13.12	.20	04	314	(7.15)	9.70
312	13.94	1.63	05	316	(5.43)	11.02
332	(6.98)	5.30	06	355	15.32	2.50
287	(3.92)	8.11	07	299	(2.37)	9.75
316	9.67	8.04	08	315	(4.97)	8.44
365	18.82	8.63	09	351	(6.62)	9.50
395	(6.15)	8.66	10	376	(3.38)	9.60
404	(6.28)	5.46	11	387	(1.83)	6.10
406	10.81	6.70	12	394	(4.58)	6.56
408	11.32	6.95	13	398	(.97)	10.83
407	(7.54)	7.82	14	403	(1.22)	10.76
409	9.42	8.65	15	405	(4.48)	8.20
411	12.56	8.35	16	398	(2.63)	11.62
424	12.65	7.90	17	402	(6.66)	10.42
451	13.81	7.50	18	424	(6.63)	11.25
491	13.49	8.20	19	451	11.69	1.10
443	13.56	10.41	20	421	(7.30)	3.02
387	(6.51)	1.20	21	370	(6.63)	4.00
344	(6.79)	7.90	22	331	(1.93)	1.92
322	(3.20)	7.56	23	315	(3.53)	3.12
P.E=3.11				P.E=2.68		

TABLE-9

LUNAR M2 VARIATION IN N(MAX) AT HUANCAYO

MEAN	R2	THETA2	LMT
ANNUAL			
82	5.67	8.92	00
67	(4.01)	11.00	01
53	(1.91)	2.90	02
43	(3.31)	6.02	03
34	(3.23)	7.92	04
29	(2.10)	7.60	05
43	(1.32)	10.30	06
91	(1.64)	2.26	07
135	(0.53)	4.53	08
148	(3.86)	3.12	09
146	9.60	3.90	10
138	10.86	4.32	11
134	9.56	4.25	12
136	10.66	3.61	13
140	10.53	4.20	14
143	9.88	4.31	15
143	12.19	4.60	16
136	10.46	4.67	17
131	11.86	4.93	18
114	10.81	5.50	19
103	10.08	6.26	20
102	9.86	7.80	21
196	(4.27)	9.38	22
194	(4.52)	8.83	23
P.E=1.54			
E-MONTHS			
99	(9.20)	8.86	00
79	(3.25)	8.52	01
58	(4.14)	6.55	02
44	(4.40)	7.92	03
35	(4.47)	8.52	04
30	(3.02)	6.00	05
46	(3.25)	5.80	06
101	(4.04)	2.93	07
147	(4.23)	5.60	08
167	(5.34)	4.36	09
160	16.28	4.62	10
146	16.56	4.95	11
142	10.53	4.92	12
146	12.35	3.82	13
150	12.48	4.15	14
154	10.88	4.41	15
154	11.99	4.40	16
150	11.92	4.43	17
139	14.12	4.50	18
115	14.33	5.06	19
107	13.68	6.03	20
113	17.31	7.36	21
113	(6.76)	8.40	22
109	9.73	8.90	23
P.E=3.15			

MEAN	R2	THETA2
D-MONTHS		
86	(7.85)	8.93
66	9.86	11.50
53	(7.79)	2.33
43	(9.00)	5.30
37	(6.09)	7.25
30	(2.64)	8.40
59	(4.95)	11.70
110	(1.30)	2.32
146	(2.23)	10.55
166	(4.08)	.65
170	10.20	2.05
163	14.21	3.02
157	15.50	3.42
162	19.44	3.25
168	21.64	4.05
171	19.89	4.10
172	22.87	4.71
167	19.26	4.87
160	19.79	5.16
146	17.03	5.66
124	14.96	6.06
113	12.29	8.27
109	(7.27)	10.61
104	(3.12)	8.53
P.E=3.02		
J-MONTHS		
61	(.61)	11.87
55	(1.75)	11.53
48	(1.55)	11.56
38	(.82)	10.46
29	(.76)	11.50
26	(2.26)	8.70
25	(2.77)	9.62
63	(1.37)	11.10
112	(2.24)	1.75
111	6.27	3.36
109	8.15	4.42
105	6.80	5.30
102	5.57	5.30
101	(2.84)	6.10
102	(2.99)	8.96
104	(1.95)	8.15
104	(1.92)	4.41
101	(.70)	3.33
94	(2.34)	4.93
81	(2.59)	7.20
79	(3.72)	8.21
81	(1.36)	9.44
76	(1.68)	7.93
68	(.86)	9.16
P.E=1.58		

TABLE-10

LUNAR M2 VARIATION IN Y(M) AT HUANCAYO

MEAN	R2	THETA2	LMT	MEAN	R2	THETA2
ANNUAL				D-MONTHS		
50	(2.69)	11.43	00	53	(5.48)	.33
45	(1.39)	2.20	01	43	(5.59)	1.94
43	(1.30)	5.95	02	42	(2.72)	6.30
41	(1.32)	8.32	03	39	(1.85)	7.10
40	(2.86)	9.62	04	38	(5.33)	8.70
43	(.93)	3.53	05	46	(2.27)	5.50
54	4.56	4.30	06	48	(3.54)	5.83
46	(1.64)	9.08	07	44	(3.08)	7.41
52	4.37	8.11	08	49	6.72	7.47
68	8.92	8.97	09	60	10.33	8.20
85	8.86	9.80	10	76	13.45	9.20
89	7.35	10.67	11	87	12.62	10.33
97	(2.90)	9.03	12	93	(3.92)	9.36
97	5.89	8.36	13	92	(6.24)	8.50
91	5.01	8.76	14	82	10.15	8.76
88	5.47	9.90	15	77	8.82	10.06
83	6.43	9.92	16	74	8.35	10.15
83	6.73	9.75	17	77	10.24	10.30
83	8.54	9.60	18	73	11.87	10.30
68	4.22	10.10	19	66	(5.54)	10.90
65	(2.63)	9.17	20	66	7.43	10.30
60	(0.54)	6.00	21	64	(1.66)	1.32
57	(1.73)	9.03	22	64	(2.05)	10.94
57	(0.68)	4.15	23	56	(.62)	6.36
P.E=1.04				P.E=2.09		
E-MONTHS				J-MONTHS		
49	(1.92)	10.06	00	47	(2.14)	10.30
46	(1.36)	9.36	01	45	(1.45)	5.52
44	(1.16)	6.40	02	44	(2.06)	7.95
41	(.88)	8.50	03	43	(1.98)	9.32
40	(2.26)	.23	04	42	(3.52)	9.75
41	(3.48)	2.50	05	42	(1.39)	9.60
55	(3.91)	4.73	06	60	8.23	3.46
42	(2.30)	10.30	07	52	(1.52)	10.45
49	(4.43)	9.03	08	57	(2.98)	8.31
68	12.05	9.37	09	75	5.89	9.54
87	10.86	10.30	10	91	(3.76)	10.50
101	(5.09)	10.53	11	98	5.38	11.64
96	(3.01)	8.40	12	102	(2.04)	9.33
99	12.91	7.86	13	100	(2.85)	.03
92	7.23	8.76	14	100	(2.34)	2.90
89	(6.03)	9.60	15	97	(1.72)	10.16
85	9.91	9.52	16	89	(1.86)	11.30
85	8.68	8.92	17	86	(2.85)	10.52
85	13.20	8.55	18	90	4.17	10.82
71	7.40	8.80	19	67	(3.00)	11.80
67	6.52	7.70	20	61	(2.91)	2.86
60	(4.37)	7.43	21	57	(1.88)	2.72
53	(3.87)	7.56	22	55	(1.67)	10.21
49	(.60)	2.15	23	48	(1.50)	4.10
P.E=2.06				P.E=1.39		

TABLE-11
LUNAR M2 VARIATION IN N(T) AT HUANCAYO

MEAN	R2	THETA2	LMT	MEAN	R2	THETA2
ANNUAL				D-MONTHS		
53	(4.90)	10.00	00	61	(8.74)	10.76
40	(3.58)	0.07	01	41	(10.50)	.37
29	(1.69)	4.01	02	30	(5.51)	2.90
24	(0.74)	6.45	03	26	(4.33)	4.65
18	(1.63)	8.32	04	19	(4.85)	7.25
15	(1.46)	10.85	05	17	(3.13)	9.55
28	(0.72)	3.40	06	37	(.57)	11.50
69	(2.69)	8.55	07	85	(5.32)	7.84
119	7.53	8.10	08	135	15.12	7.93
175	13.14	8.50	09	189	24.13	8.73
211	6.28	8.20	10	237	23.14	9.73
222	9.69	5.10	11	258	(6.62)	.30
220	14.40	5.82	12	255	(8.79)	5.72
224	11.20	5.95	13	261	(8.60)	5.62
220	10.47	6.05	14	253	16.83	5.90
216	6.41	6.52	15	244	(7.07)	5.80
207	(5.14)	6.61	16	239	(11.90)	6.60
194	9.06	7.55	17	230	14.84	7.65
155	8.70	7.65	18	192	15.58	8.10
112	8.95	6.63	19	148	(11.04)	7.30
93	10.73	7.30	20	116	(10.80)	7.97
86	9.08	7.90	21	102	(9.08)	8.70
76	7.69	9.23	22	95	(11.87)	10.20
63	(3.39)	9.53	23	78	(3.37)	10.27
P.E=1.73				P.E=3.98		
E-MONTHS				J-MONTHS		
62	(6.28)	8.73	00	36	(1.85)	10.43
47	(1.77)	9.20	01	31	(.65)	2.10
32	(2.74)	6.62	02	26	(.33)	7.35
24	(2.34)	9.62	03	22	(1.18)	9.60
18	(1.32)	11.76	04	16	(1.71)	9.92
15	(3.05)	1.03	05	13	(1.07)	9.32
29	(2.49)	3.23	06	18	(.71)	6.44
71	(1.30)	8.65	07	52	(2.58)	10.02
128	(5.15)	8.01	08	95	(2.94)	9.14
196	14.49	8.06	09	139	(1.47)	8.90
234	13.67	5.52	10	163	(3.14)	5.32
237	26.30	5.32	11	170	8.40	5.26
233	24.06	5.80	12	172	10.50	6.02
239	23.07	5.95	13	173	(2.48)	6.95
234	15.68	5.85	14	174	(3.48)	9.56
233	10.83	6.40	15	172	(3.84)	8.55
225	(5.23)	6.92	16	157	(1.67)	1.36
211	13.73	6.80	17	142	(4.36)	10.65
166	12.84	6.61	18	108	(2.85)	10.70
113	17.39	6.03	19	75	(1.85)	9.51
98	19.76	7.03	20	66	(2.66)	6.76
95	20.26	7.63	21	62	(1.63)	3.56
79	12.20	8.46	22	53	(1.85)	8.26
71	(7.52)	9.23	23	41	(.36)	5.00
P.E=3.55				P.E=2.09		

TABLE-12

L VARIATIONS AT HUANCAYO

D=MONTHS

PARAMETER	L1	FI1	L2	FI2
H	2.48	170	5.83	242
N(MAX)	2.83	285	4.82	320
H(MAX)	4.04	135	7.54	183
Y(M)	.91	169	3.73	164
N(T)	1.88	243	5.43	214

E=MONTHS

PARAMETER	L1	FI1	L2	FI2
H	1.88	256	5.98	222
N(MAX)	.31	17	5.48	289
H(MAX)	1.21	169	3.64	194
Y(M)	.52	164	3.31	185
N(T)	1.80	100	7.36	259

J=MONTHS

PARAMETER	L1	FI1	L2	FI2
H	2.09	321	2.27	168
N(MAX)	1.23	124	.60	280
H(MAX)	2.54	224	1.39	134
Y(M)	.72	234	.99	131
N(T)	.33	85	.94	213

TABLE-13

L(NU) IN H AT PUERTO RICO

NU	C1	ALFA1	C2	ALFA2	C3	ALFA3	C4	ALFA4
				ANNUAL				
00	1.14	79	.13	185	0.60	175	0.07	232
03	0.96	76	.50	176	0.08	51	0.07	280
06	0.15	27	.50	41	0.26	83	0.34	41
09	0.66	232	.49	51	0.59	257	0.55	335
12	1.14	232	1.62	69	0.52	213	0.09	354
15	0.40	6	1.1	106	0.60	229	0.26	62
18	1.36	227	1.55	66	0.70	225	0.41	29
21	0.81	69	.81	160	0.30	230	0.14	290
				D-MONTHS				
00	1.91	150	1.29	205	1.00	251	.79	204
03	1.99	132	0.30	165	.13	321	.51	104
06	2.03	350	0.66	6	.26	232	.77	45
09	1.45	178	1.51	339	.52	157	.90	318
12	0.56	241	0.92	41	.97	232	.53	304
15	2.77	335	0.88	69	.45	130	.46	141
18	2.50	204	1.28	94	1.45	251	.57	332
21	.95	296	0.58	129	.28	322	.33	265
				E-MONTHS				
00	2.33	50	.66	342	1.20	156	.44	16
03	.62	345	.08	360	.75	299	.67	310
06	.53	21	.60	328	.10	338	.53	127
09	.80	263	.07	177	1.40	266	1.20	355
12	1.52	266	1.77	72	.24	23	.45	99
15	1.13	96	.81	128	.94	215	.58	2
18	1.06	293	1.62	54	.33	193	.86	62
21	2.29	118	.16	227	.62	186	.27	53
				J-MONTHS				
00	1.00	40	.71	81	.74	124	.12	8
03	2.04	47	1.35	178	1.03	110	.35	216
06	2.75	56	1.31	88	1.04	82	.64	334
09	.96	287	1.78	104	.55	290	.32	176
12	1.86	200	2.34	77	.99	190	.09	321
15	1.23	172	1.97	113	1.23	263	.42	65
18	1.35	227	2.00	58	.69	186	.22	34
21	1.89	36	1.92	165	.61	241	.31	272

TABLE - 14

L(H) VARIATION AT SAN JUAN

Season	L_1	β_1	L_2	β_2	L_3	β_3	L_4	β_4	Source of result.
Annual	0.40	3.6	0.62 ± 0.17	0.1	0.24	7.4	0.18	3.8	Present article
			0.98 ± 0.15	0.7					Matsushita (1962b)
D-months	0.30	0.6	0.31 ± 0.30	0.9	0.08	4.0	0.48	3.9	Present article
			0.60 ± 0.40	0.4					Matsushita (1962b)
	0.52	18.6	1.10 ± 0.38	10.0	0.47	3.0	0.12	4.1	Rajarao(1962)
E-months	0.39	16.9	0.44 ± 0.31	1.2	0.35	0.0	0.16	2.2	Present article
			0.91 ± 0.20	0.7					Matsushita (1962b)
	0.61	23.3	0.81 ± 0.29	10.3	0.50	2.9	0.18	4.5	Rajarao (1962)
J-months	0.97	6.0	1.28 ± 0.29	11.5	0.56	0.7	0.13	4.5	Present article
			1.44 ± 0.24	0.7					Matsushita (1962b)
	0.70	2.7	1.39 ± 0.42	10.0	0.64	4.0	0.18	4.3	Rajarao(1962)

TABLE-15

SOLAR AND LUNAR SEMI-DIURNAL TIDE (S2,L2) IN H

SEASON	S2	BETA2	L2	BETA2	L2/S2	S2	BETA2	L2	BETA2	L2/S2
	HUANCAYO					SAN JUAN				
ANNUAL	26.83	332	4.23	223	.16	2.21	272	.62	2	.28
D-MONTHS	25.75	325	5.83	242	.23	4.54	238	.31	27	.07
E-MONTHS	31.79	332	5.98	222	.19	2.06	281	.44	35	.21
J-MONTHS	23.34	339	2.27	168	.10	2.54	346	1.28	346	.51

TABLE-16
LUNAR M2 VARIATION IN H AT PUERTO RICO

MEAN	R2	THETA2	LMT
ANNUAL			
642	2.38	1.90	00
643	2.14	2.67	01
644	1.74	3.67	02
647	1.35	5.14	03
649	1.51	6.50	04
651	1.55	7.97	05
652	1.91	8.57	06
654	1.40	9.87	07
655	1.86	11.47	08
655	2.04	.00	09
655	2.22	.70	10
654	2.33	1.00	11
652	2.37	1.67	12
648	2.41	1.94	13
645	2.06	2.44	14
642	1.71	3.20	15
641	1.17	5.74	16
640	1.96	8.17	17
641	2.34	9.94	18
642	2.97	10.24	19
642	3.26	10.77	20
642	3.02	11.47	21
642	2.50	.00	22
643	1.98	.37	23
P.E=0.29			
E-MONTHS			
638	7.00	2.77	00
639	6.80	3.74	01
641	5.87	4.87	02
643	5.69	6.00	03
648	5.84	6.80	04
649	6.39	7.87	05
650	6.37	8.57	06
651	5.12	9.77	07
652	5.94	11.07	08
652	6.89	.07	09
653	7.36	.84	10
653	7.90	1.57	11
651	8.38	2.54	12
648	8.10	3.50	13
645	7.01	4.40	14
641	5.68	5.14	15
638	5.76	6.47	16
637	7.13	7.80	17
638	8.44	8.97	18
639	8.74	9.90	19
640	8.82	10.80	20
640	8.05	11.80	21
640	7.46	.70	22
640	6.88	1.44	23
P.E=0.28			

MEAN	R2	THETA2
D-MONTHS		
638	(.77)	3.87
640	(.39)	4.90
641	(.23)	9.30
645	(.76)	10.47
648	(.22)	10.54
651	(.80)	11.60
653	(.68)	10.27
658	(.61)	.84
660	1.24	1.80
657	1.06	3.00
654	1.12	2.70
650	(.83)	1.97
645	(.75)	1.57
640	.94	11.94
637	1.01	11.97
637	(.49)	10.97
637	1.60	10.14
637	1.86	10.60
638	2.85	.77
639	1.49	1.77
639	(.44)	10.14
638	(.36)	9.77
638	(.48)	10.44
639	(.70)	9.10
P.E=0.30		
J-MONTHS		
650	3.78	11.17
650	4.05	11.94
651	3.54	1.07
652	2.76	1.94
652	1.55	2.04
653	1.43	2.37
653	1.08	6.47
653	.93	4.77
654	(.60)	5.10
655	1.30	7.87
658	1.86	8.40
660	3.00	9.24
659	3.76	10.10
657	5.21	11.40
654	5.62	.27
650	5.09	1.17
647	3.45	2.34
645	1.68	2.60
646	1.29	1.70
648	(.81)	10.37
648	(.66)	10.66
648	1.46	9.94
648	2.62	9.67
649	2.91	9.57
P.E=0.28		

TABLE-17

WHOLE DAY MEAN M2 VARIATION OF H

SEASON	R2(NU)	THETA2(NU)	R2(TAU)	THETA2(TAU)	R2(NU)/R2(TAU)
		SAN JUAN (1959-61)			
ANNUAL	1.9	9.7	0.8	0.1	2.4
D-MONTHS	2.5	9.0	0.5	0.3	1.0
E-MONTHS	7.0	9.2	0.6	0.6	11.7
J-MONTHS	2.3	1.8	1.4	0.0	1.6
		HUANCAYO (1960-61)			
ANNUAL	1.4	3.2	5.6	8.0	0.3
D-MONTHS	4.2	6.6	9.8	7.2	0.4
E-MONTHS	2.8	8.9	7.2	8.7	0.4
J-MONTHS	8.4	2.4	2.2	9.5	3.8

TABLE - 18

L VARIATIONS AT PUERTO RICO

Parameter studied.	Units.	L_1	ϕ_1	L_2	ϕ_2	L_3	ϕ_3	L_4	ϕ_4
H	Gamma	0.40	36	0.62 ± 0.17	88	0.24	115	0.18	219
h_{max}	Km	0.38	219	(0.62 ± 0.41	301	0.44	335	0.36	304
N_{max}	10^4EL. /CM^3	1.37	199	1.43 ± 0.38	178	0.08	105	0.35	83
N_t	10^{11}EL./CM^2	1.44	188	1.11 ± 0.36	160	0.09	259	0.26	109

TABLE-19

LUNAR M2 VARIAT9ON IN H(MAX) AT PUERTO RICO

MEAN	R2	THETA2	LMT	MEAN	R2	THETA2
ANNUAL				D-MONTHS		
347	(1.12)	4.22	00	330	5.31	3.23
330	4.03	3.41	01	315	9.80	3.25
319	3.22	3.90	02	304	7.93	3.91
322	(.98)	1.43	03	304	3.94	5.12
343	6.29	1.75	04	342	6.35	1.04
350	3.89	2.52	05	345	2.59	3.13
339	5.68	4.40	06	337	6.14	5.25
286	3.31	6.42	07	288	5.45	5.84
281	1.38	5.41	08	265	2.28	6.52
289	(.79)	9.96	09	269	1.21	6.18
302	3.47	8.15	10	273	2.55	7.42
313	3.96	9.46	11	278	1.53	7.70
319	1.71	9.80	12	288	2.68	7.25
321	2.83	10.21	13	296	2.31	7.71
323	1.89	11.54	14	297	2.69	9.13
323	1.42	8.32	15	300	2.19	9.72
320	1.87	.33	16	300	1.54	8.31
315	(1.02)	1.35	17	294	2.79	9.21
317	1.99	2.94	18	296	(.97)	1.72
320	1.47	5.34	19	297	1.48	8.64
343	2.93	5.24	20	315	(.35)	5.81
356	2.99	5.02	21	332	8.22	4.67
363	4.00	6.15	22	336	9.16	5.23
356	4.72	7.08	23	331	4.11	6.64
P.E=0.41				P.E=0.38		
E-MONTHS				J-MONTHS		
351	1.66	9.22	00	369	1.91	6.91
337	1.24	2.51	01	347	2.12	5.24
321	4.31	11.71	02	343	4.02	5.76
319	6.36	.94	03	353	2.24	9.11
344	16.45	2.31	04	353	3.87	9.23
365	12.18	3.17	05	352	5.17	10.60
352	14.13	4.06	06	337	2.32	10.41
282	8.67	5.83	07	297	5.40	10.80
282	8.16	5.66	08	305	6.11	00.05
293	4.56	7.45	09	314	5.73	.33
308	6.79	8.15	10	334	1.37	8.81
319	8.38	9.05	11	350	3.38	10.90
325	7.82	10.77	12	353	2.49	4.46
328	6.09	11.22	13	349	2.58	9.87
330	3.20	.66	14	351	2.31	.24
332	2.71	.14	15	347	4.32	8.00
327	5.76	1.71	16	342	3.32	10.65
322	6.75	3.34	17	340	3.64	10.91
326	6.78	3.95	18	339	4.47	11.97
325	6.61	4.99	19	348	1.75	11.33
353	9.34	5.55	20	372	1.75	1.45
367	4.19	7.11	21	380	1.86	1.14
375	7.57	7.64	22	385	1.58	1.13
365	6.65	7.06	23	384	3.78	7.44
P.E=0.41				P.E=0.44		

TABLE-20

LUNAR M2 VARIATION IN N(MAX) AT PUERTO RICO

MEAN	R2	THETA2	LMT	MEAN	R2	THETA2
ANNUAL				D-MONTHS		
73	(.13)	.65	00	39	2.60	8.17
69	(.36)	6.63	01	38	2.95	8.28
59	1.65	6.44	02	34	2.91	7.96
48	1.38	7.71	03	28	(.99)	8.37
40	1.42	7.95	04	21	1.27	6.92
35	(.77)	8.78	05	20	(.29)	9.31
36	(1.01)	10.48	06	20	(.84)	8.23
63	(.84)	9.13	07	46	1.96	8.24
98	1.57	8.58	08	100	5.21	7.50
123	4.06	8.34	09	139	8.34	7.91
140	3.49	8.42	10	161	11.34	8.25
151	3.47	9.12	11	155	9.04	9.02
157	4.42	9.95	12	145	10.68	9.46
164	4.64	10.49	13	148	7.71	10.00
166	2.08	0.55	14	151	8.45	9.68
162	(.81)	3.32	15	147	3.70	10.31
155	2.46	8.48	16	141	4.81	9.73
148	4.91	9.44	17	138	3.82	8.49
134	3.21	8.10	18	123	3.82	9.12
103	2.48	8.93	19	84	5.57	9.23
188	2.08	9.54	20	56	5.82	9.77
181	1.88	9.81	21	48	4.39	10.87
177	2.20	11.80	22	44	2.74	11.87
175	(.85)	0.11	23	41	(.87)	07.83
P.E=0.40				P.E=0.36		
E-MONTHS				J-MONTHS		
78	1.67	11.04	00	101	3.21	3.06
72	2.52	1.22	01	96	2.29	5.21
63	1.38	4.96	02	79	2.30	5.49
49	2.12	8.10	03	68	1.42	6.58
37	1.69	8.81	04	61	1.65	7.82
32	(.65)	5.55	05	54	2.21	9.28
33	(.33)	3.33	06	56	3.06	10.81
72	1.89	5.25	07	72	3.06	11.08
108	2.63	7.74	08	85	4.16	00.64
136	4.81	7.38	09	94	4.09	11.46
158	3.85	6.63	10	103	5.10	12.69
177	4.76	7.73	11	121	4.23	1.33
187	5.46	9.39	12	140	4.96	1.90
194	7.11	10.49	13	151	2.22	2.01
190	3.63	00.38	14	153	9.03	3.18
189	3.30	7.64	15	150	7.81	3.19
178	7.37	8.61	16	146	5.02	3.96
165	10.80	10.00	17	141	1.67	7.96
151	4.96	9.91	18	130	6.94	6.15
119	3.47	10.75	19	123	3.68	05.91
197	1.34	11.72	20	111	1.90	06.38
188	2.29	08.14	21	107	(.69)	07.88
184	2.80	10.61	22	104	2.28	01.22
182	2.43	10.14	23	102	3.24	01.97
P.E=0.32				P.E=0.44		

TABLE-21

LUNAR M2 VARIATION IN N(T) AT PUERTO RICO

MEAN	R2	THETA2	LMT	MEAN	R2	THETA2
ANNUAL				D-MONTHS		
45	(.55)	.71	00	23	.81	6.62
41	(.70)	3.00	01	20	.87	5.97
36	(.31)	6.67	02	18	.89	7.14
31	(.63)	7.21	03	15	(.56)	6.78
28	(.32)	7.78	04	15	(.34)	7.62
26	(.59)	8.95	05	14	(.33)	8.35
26	(.42)	4.18	06	14	(.52)	7.37
46	(.81)	7.98	07	24	.80	5.75
80	1.53	8.42	08	64	4.85	7.37
108	3.21	9.45	09	95	4.91	7.68
132	4.57	8.71	10	115	6.73	8.25
147	4.43	9.38	11	122	5.14	8.82
164	4.10	10.28	12	128	6.76	9.29
167	4.95	10.49	13	133	6.00	9.50
169	3.28	.71	14	137	6.67	9.71
159	(.46)	7.44	15	122	1.34	9.52
152	1.14	11.64	16	126	2.06	9.20
135	2.44	9.41	17	106	3.69	8.12
106	2.35	4.71	18	78	1.98	8.83
80	1.40	8.47	19	53	4.80	9.33
68	1.52	9.57	20	38	3.79	10.17
59	(.97)	9.22	21	32	1.78	10.93
54	1.65	10.88	22	29	1.60	.30
51	1.19	10.67	23	26	(.34)	3.38
P.E=0.35				P.E=0.26		
E-MONTHS				J-MONTHS		
49	2.56	10.94	00	65	2.18	2.92
44	2.11	.83	01	61	1.56	4.39
39	1.61	.25	02	52	1.73	6.11
33	(.62)	11.86	03	47	1.86	6.88
29	1.06	2.09	04	41	1.70	8.05
26	.96	3.28	05	38	2.41	9.18
24	2.02	3.26	06	41	(.66)	8.63
50	3.50	5.91	07	64	3.77	10.78
89	3.78	6.45	08	89	5.67	.01
120	4.78	7.88	09	108	7.81	11.63
151	5.74	7.95	10	130	4.35	10.91
175	7.28	8.95	11	146	3.52	11.71
197	7.96	10.02	12	169	4.67	1.97
195	7.84	11.09	13	173	2.30	10.92
197	5.99	.84	14	174	7.51	2.71
190	2.09	9.22	15	167	2.98	4.21
176	3.11	11.68	16	155	1.98	2.78
155	3.24	10.70	17	145	2.02	9.71
117	4.79	2.80	18	123	6.11	5.47
190	1.59	11.38	19	99	3.65	5.32
178	(.35)	5.85	20	88	1.37	8.32
167	1.06	9.58	21	80	1.75	7.02
160	3.34	9.77	22	75	(1.14)	11.97
156	3.46	9.94	23	71	(1.27)	0.70
P.E=0.32				P.E=0.43		

TABLE-22

L(NU) IN H(MAX) AT PUERTO RICO

NU	C1	ALFA1	C2	ALFA2	C3	ALFA3	C4	ALFA4
				ANNUAL				
00	.63	277	.94	117	.53	327	.92	105
03	1.31	293	.33	345	2.71	298	1.01	268
06	1.34	324	1.64	287	1.56	202	1.56	104
09	1.21	207	1.21	246	2.01	301	1.49	296
12	1.42	46	.15	328	1.79	8	1.18	18
15	2.35	19	.96	326	2.23	334	2.25	280
18	.89	300	.54	209	.14	358	.58	95
21	.53	40	.65	327	2.42	37	.86	334
				D-MONTHS				
00	2.82	32	.91	82	2.15	47	1.61	63
03	2.75	313	3.93	302	2.93	313	1.44	2
06	2.77	10	1.55	296	2.84	140	3.00	110
09	1.45	205	2.97	273	2.45	295	1.08	281
12	2.13	15	2.37	310	2.16	31	2.25	32
15	3.32	0	2.53	309	4.78	314	3.14	283
18	.64	343	1.04	72	1.59	20	1.61	313
21	3.56	24	4.11	334	4.32	5	1.77	7
				E-MONTHS				
00	1.23	269	1.31	276	1.35	260	2.41	128
03	.81	290	3.32	11	3.58	300	1.52	262
06	2.67	296	3.32	331	2.91	278	1.69	255
09	1.15	111	2.45	344	1.80	315	1.30	254
12	1.05	48	1.74	244	1.15	338	.88	72
15	4.23	64	1.43	59	2.06	51	1.75	333
18	2.04	287	1.88	235	1.37	238	1.34	121
21	3.04	145	.25	325	1.69	87	.71	222
				J-MONTHS				
00	3.01	224	3.20	116	1.13	274	.88	281
03	1.27	243	1.68	31	2.15	262	2.34	223
06	1.20	294	2.48	212	2.82	203	2.31	81
09	2.78	232	4.04	176	3.00	299	1.45	336
12	1.53	83	3.11	94	2.78	359	1.47	328
15	1.65	301	.78	262	2.56	322	3.89	249
18	.15	45	.67	209	.85	136	1.60	112
21	2.24	283	2.44	158	2.91	61	1.31	319

TABLE-23

L(NU) IN N(MAX) AT PUERTO RICO

NU	C1	ALFA1	C2	ALFA2	C3	ALFA3	C4	ALFA4
				ANNUAL				
00	1.10	184	1.93	125	.58	272	1.25	11
03	2.54	312	1.82	158	.85	226	.44	44
06	2.20	287	1.95	169	.41	356	1.02	352
09	1.35	26	1.33	172	.13	3	.57	99
12	2.44	354	2.37	209	.22	303	.75	118
15	3.66	48	2.64	207	.35	340	.47	186
18	.91	72	.84	112	.70	147	.39	296
21	1.38	128	1.31	162	1.90	353	1.07	206
				D-MONTHS				
00	2.91	302	2.69	162	1.84	292	.61	306
03	2.89	18	4.46	182	1.18	215	1.10	294
06	2.03	312	4.66	195	2.45	0	.91	325
09	4.66	357	3.36	160	1.07	192	.57	324
12	3.58	33	4.89	216	1.59	326	1.43	84
15	3.96	28	4.34	192	.74	60	.66	242
18	.76	265	4.52	130	.83	115	1.96	205
21	3.37	55	3.88	179	2.96	304	.95	144
				E-MONTHS				
00	3.87	112	2.78	136	.94	155	3.02	17
03	2.93	329	4.08	155	1.49	249	2.11	120
06	2.86	349	2.92	185	.93	256	1.28	52
09	2.33	114	3.87	248	1.09	51	.64	112
12	2.98	339	3.32	185	2.64	311	.98	182
15	6.51	56	3.48	234	2.02	336	.53	234
18	.95	84	2.96	73	2.89	191	2.33	7
21	1.55	114	1.34	172	2.76	37	1.70	207
				J-MONTHS				
00	3.62	201	2.33	60	.93	338	.55	41
03	5.03	270	3.09	9	.34	138	1.55	4
06	4.81	243	3.05	58	1.29	141	1.74	329
09	.05	240	3.05	79	.97	319	1.56	108
12	2.20	312	1.42	348	2.28	277	.66	115
15	.6	86	.76	179	1.22	190	1.18	135
18	2.60	71	1.68	209	1.70	34	.54	267
21	3.90	193	1.77	34	1.83	4	1.37	243

TABLE-24

L(NU) IN N(T) AT PUERTO RICO

NU	C1	ALFA1	C2	ALFA2	C3	ALFA3	C4	ALFA4
				ANNUAL				
00	.89	206	1.78	124	.35	264	.48	13
03	1.98	293	1.52	109	.96	220	.39	5
06	2.41	280	1.09	128	.16	202	.66	13
09	2.10	331	1.19	154	.31	327	.50	176
12	1.51	10	1.64	198	1.47	323	.96	118
15	3.44	35	2.15	189	.78	337	.87	209
18	.90	35	.89	159	.40	102	.53	249
21	1.27	110	1.19	201	1.33	24	1.04	231
				D-MONTHS				
00	2.03	318	1.50	153	.50	336	.49	320
03	2.60	354	2.00	180	.90	231	.62	354
06	1.56	304	2.83	197	1.71	10	.42	346
09	3.89	356	2.17	173	.53	169	.48	303
12	3.10	51	2.88	228	1.10	352	.41	86
15	4.59	11	3.62	181	1.20	334	.39	236
18	.91	76	.37	221	.67	85	1.51	228
21	3.73	87	2.06	201	2.20	324	1.00	125
				E-MONTHS				
00	2.41	147	2.54	133	.94	189	1.36	8
03	2.74	327	3.58	140	1.39	204	.25	115
06	4.56	289	2.32	105	.60	231	.11	126
09	.77	55	1.59	230	.36	143	.45	181
12	1.56	349	2.33	190	2.16	323	1.48	137
15	6.44	49	1.39	221	.67	12	1.13	222
18	.60	293	2.09	94	1.30	187	.75	3
21	.69	92	.27	196	2.33	63	1.74	222
				J-MONTHS				
00	2.27	211	1.95	88	.88	293	.52	126
03	4.51	236	3.82	32	.72	237	.70	355
06	1.87	236	1.74	44	1.79	179	1.68	16
09	3.40	290	2.52	89	1.78	332	1.43	159
12	1.69	305	1.05	116	2.44	310	1.19	106
15	.42	123	1.68	183	.68	312	1.23	189
18	2.83	35	2.25	201	1.29	32	.56	231
21	1.71	209	1.23	204	2.25	36	2.09	268

TABLE - 25

L VARIATIONS AT PUERTO RICO

Parameter studied.	Units	D-MONTHS				E-MONTHS				J-MONTHS			
		L_1	Φ_1	L_2	Φ_2	L_1	Φ_1	L_2	Φ_2	L_1	Φ_1	L_2	Φ_2
H	Gamma	0.30	80	0.31±0.30	63	0.39	96	0.44±0.31	55	0.97	0	1.28±0.27	104
h_{max}	Km	0.46	92	1.90±0.41	311	1.10	217	1.07±0.41	327	0.35	196	1.32±0.43	148
N_{max}	10^4 EL/CM^3	1.17	216	3.25±0.32	185	1.37	194	1.93±0.34	180	2.24	189	1.21±0.45	51
N_t	10^{11} EL/CM^2	1.30	199	1.96±0.38	191	1.60	192	1.38±0.33	148	1.39	167	0.80±0.43	79

TABLE-26

Amplitude (r_2) and phase (θ_2) of lunar variations of noon value of N_{max}, h_{max} and f_oF_2 at Ahmedabad (1963-65)

Parameter studied.	D-MONTHS				E-MONTHS				J-MONTHS			
	Mean value	r_2	$\frac{100r_2}{\text{Mean value}}$	θ_2 lunar hr.	Mean value	r_2	$\frac{100r_2}{\text{Mean value}}$	θ_2 lunar hr.	Mean value	r_2	$\frac{100r_2}{\text{Mean value}}$	θ_2 lunar hr.
N_{max}	103×10^4 EL/CM^3	7.5×10^4 EL/CM^3	7.3	10.6	159×10^4 EL/CM^3	15.9×10^4 EL/CM^3	10.0	0.8	95×10^4 EL/CM^3	9.8×10^4 EL/CM^3	10.3	0.9
f_oF_2	9.2 MH$_z$	0.43 MH$_z$	4.7	10.8	11.2 MH$_z$	0.68 MH$_z$	6.1	0.9	8.8 MH$_z$	0.58 MH$_z$	6.6	0.7
h_{max}	263 Km.	5.2 Km.	2.0	7.2	300 Km.	5.8 Km.	1.9	11.1	315 Km.	8.00 Km.	2.5	11.3

TABLE-27

Mean noon-time electron density (N), amplitude (r_2) and phase (θ_2) of the lunar semi-monthly oscillation in N, for fixed heights above Ahmedabad (1963-65)

Season	Height (Km)	120	140	160	180	200	220	240	260	280	300
D-months	N(10^4EL/CM^3)	12	17	22	26	36	54	78			
	r_2(10^4EL/CM^3)	0.11	0.19	0.20	0.50	1.53	4.10	6.80			
	r_2/N %	0.9	1.1	0.9	1.9	4.3	7.5	8.7			
	θ_2(lunar hr)	0.1	1.2	0.3	0.6	0.1	0.1	11.8			
E-months	N(10^4EL/CM^3)	14	19	23	27	33	45	64	92	123	151
	r_2(10^4EL/CM^3)	0.30	0.30	0.13	0.23	0.85	2.40	5.30	7.80	8.10	11.70
	r_2/N %	2.1	1.5	0.6	0.9	2.6	5.4	8.2	8.5	6.6	7.8
	θ_2(lunar hr)	11.1	10.4	4.7	3.2	3.5	4.0	3.9	3.1	2.2	1.9
J-months	N(10^4EL/CM^3)	15	21	24	25	27	32	39	49	63	81
	r_2(10^4EL/CM^3)	0.2	0.2	0.12	0.13	0.40	1.10	2.20	3.50	4.60	6.50
	r_2/N %	1.2	0.8	0.5	0.5	1.5	3.5	5.7	7.1	7.3	8.0
	θ_2(lunar hr)	2.2	3.2	4.7	4.1	4.8	4.7	4.3	3.7	3.3	3.5

TABLE-28

LUNAR M2 VARIATIONS AT HUANCAYO

ANNUAL

HEIGHT	R2	P.E	THETA2	N	R2/N	HEIGHT	R2	P.E	THETA2	N	R2/N
**********					S.HR=	) **********					
220	3.04	.27	11.56	14.1	21.5	230	1.82	.36	8.23	22.5	8.1
240	3.80	.41	6.90	31.7	12.0	250	4.95	.45	6.60	41.4	11.9
260	5.48	.47	6.63	49.3	11.1	270	5.70	.48	6.66	55.6	10.2
280	5.08	.52	7.40	59.6	8.5	290	4.16	.59	7.13	61.9	6.7
300	3.50	.67	7.66	65.6	5.3						
**********					S.HR=	1 **********					
230	4.18	.29	7.10	20.1	20.7	240	4.61	.35	6.76	27.8	16.5
250	4.49	.37	6.46	36.2	12.4	260	3.65	.40	6.00	41.5	8.9
270	2.86	.41	5.83	46.6	6.1	280	3.55	.44	6.26	48.7	7.3
290	4.50	.45	5.86	49.8	9.0	300	5.90	.51	2.30	48.1	12.3
**********					S.HR=	2 **********					
220	(.43)	.19	8.33	8.8	(4.9)	230	1.06	.22	7.00	14.1	7.5
240	2.00	.26	6.53	20.5	9.8	250	3.09	.33	5.70	27.6	11.2
260	4.21	.37	5.46	32.8	12.8	270	4.84	.41	5.56	36.9	13.1
280	2.52	.31	5.36	38.4	6.6	290	2.69	.37	4.20	40.0	6.7
300	3.97	.45	3.90	42.4	9.4	310	9.21	.61	4.06	45.4	20.3
**********					S.HR=	3 **********					
230	1.35	.15	9.83	8.2	16.5	240	1.62	.19	7.76	12.3	13.1
250	1.19	.21	7.33	17.5	6.8	260	1.39	.23	8.03	21.4	6.5
270	1.33	.24	8.43	25.0	5.3	280	2.03	.26	7.73	27.4	7.4
290	1.47	.30	7.83	29.8	4.9	300	3.22	.37	8.50	30.2	10.6
**********					S.HR=	4 **********					
230	2.10	.16	3.86	6.3	33.2	240	1.88	.14	4.66	9.9	18.9
250	1.04	.15	5.73	13.4	7.7	260	1.43	.16	6.20	15.3	9.3
270	2.51	.17	6.06	17.6	14.2	280	3.60	.32	5.90	20.2	17.8
290	3.21	.23	6.23	20.6	15.5	300	2.79	.28	7.00	23.5	11.9
310	1.40	.29	9.33	24.2	5.8						

(TABLE-28 contd.)

**********					S.HR=
240	1.69	.13	8.06	6.4	26.1
260	.52	.15	10.26	12.0	4.3
280	1.76	.19	10.56	16.3	10.8
300	2.39	.42	2.50	20.4	11.7
**********					S.HR=
120	.28	.03	5.96	2.3	11.9
140	.15	.02	7.30	3.4	4.3
160	.16	.03	7.00	3.9	4.0
180	.26	.05	7.26	5.5	4.7
200	.42	.10	7.23	9.4	4.4
220	(.56)	.19	4.93	16.8	(3.3)
240	.21	.31	3.53	24.2	.9
260	2.09	.32	.80	24.2	8.6
280	1.73	.29	.40	27.2	6.4
300	3.18	.30	.06	26.6	11.9
320	2.11	.25	.76	23.6	8.9
**********					S.HR=
120	.21	.03	7.26	6.1	3.4
140	(.35)	.02	6.60	7.6	(.7)
160	.11	.03	7.56	9.8	1.1
180	(.13)	.05	8.40	14.4	(.9)
200	(.17)	.08	3.13	22.7	.7
220	1.88	.15	2.33	36.9	5.1
240	3.30	.39	1.00	55.2	6.0
260	4.21	.30	1.96	66.2	6.4
280	3.02	.41	2.33	69.9	4.3
**********					S.HR=
110	.37	.06	5.46	6.0	6.1
130	.06	.02	5.83	11.3	.5
150	.16	.03	7.13	14.4	1.1
170	.19	.04	6.46	19.7	1.0

5 **********					8
250	1.16	.13	9.00	9.7	11.8
270	.84	.16	9.83	14.5	5.8
290	1.78	.20	10.46	17.2	10.3
310	1.44	.35	2.73	20.0	7.2
6 **********					
130	.12	.02	7.73	3.1	3.9
150	.17	.02	7.20	3.6	4.6
170	.19	.03	7.10	4.5	4.2
190	.35	.06	7.36	7.1	4.9
210	(.38)	.14	5.96	12.7	(3.0)
230	(.35)	.25	6.23	21.2	(1.6)
250	1.16	.35	1.20	24.5	4.7
270	2.42	.30	.16	26.2	9.2
290	2.78	.30	11.83	27.0	10.3
310	3.55	.28	.46	25.6	13.9
7 **********					
130	(.02)	.02	5.86	7.1	(.3)
150	.10	.03	7.20	8.4	1.2
170	.16	.04	8.06	11.8	(1.4)
190	(.06)	.06	7.70	17.9	(.3)
210	.80	.11	2.30	29.0	2.8
230	2.93	.21	2.16	45.9	6.4
250	3.70	.47	.73	62.7	5.9
270	3.44	.44	.76	70.5	4.9
290	2.94	.52	2.43	69.6	4.2
8 **********					
120	.36	.03	5.60	10.3	3.5
140	.10	.02	7.33	12.5	.8
160	.18	.03	6.93	16.9	1.1
180	.20	.04	6.23	22.8	.9

(TABLE-28 contd.)

19U	.23	.04	5.60	26.4	.9	200	.28	.05	4.66	30.8	.9
21U	.53	.07	3.60	36.3	1.5	220	1.18	.11	3.03	43.2	2.7
23U	2.29	.15	2.90	51.5	4.4	240	3.64	.20	2.86	60.6	6.0
25U	4.89	.24	2.80	70.0	7.0	260	5.73	.28	2.76	78.9	7.3
27U	5.57	.31	2.73	86.5	6.4	280	4.17	.33	2.70	92.2	4.5
29U	2.66	.37	3.16	96.5	2.8	300	2.19	.41	4.93	98.3	2.2
31U	2.57	.51	5.86	98.1	2.6	320	(1.50)	.65	8.76	98.5	(1.5)
**********					S.HR=	9	**********				
11U	.63	.07	10.10	9.4	6.6	120	.13	.02	11.43	13.6	1.0
13U	.15	.02	11.00	14.8	1.0	140	.19	.02	10.40	16.8	1.1
15U	.21	.03	10.56	19.5	1.1	160	.14	.03	10.66	22.2	.6
17U	.11	.03	11.00	24.6	.4	180	.11	.03	11.86	27.2	.4
19U	.22	.04	1.40	30.1	.7	200	.41	.04	2.16	33.7	1.2
21U	.75	.06	2.46	38.2	2.0	220	1.29	.08	2.63	43.6	3.0
23U	2.15	.10	2.76	49.7	4.3	240	3.38	.14	2.86	56.6	6.0
25U	4.79	.18	2.96	63.9	7.5	260	6.30	.22	3.00	71.3	8.8
27U	7.71	.26	3.03	78.6	9.8	280	8.67	.29	3.06	85.3	10.2
29U	8.81	.33	3.03	91.2	9.7	300	8.99	.36	2.93	96.5	9.3
31U	8.58	.39	2.96	100.6	8.5	320	8.24	.41	2.63	103.5	8.0
33U	6.58	.47	2.73	105.9	6.2	340	6.07	.51	3.06	107.2	5.7
35U	8.98	.53	3.86	109.8	3.2	360	8.16	.57	3.46	112.6	7.2
**********					S.HR=	10	**********				
11U	.51	.07	1.16	11.8	4.3	120	.47	.07	1.20	16.2	2.9
13U	(.04)	.02	1.43	17.5	(.2)	140	.09	.03	1.90	20.2	.4
15U	.11	.03	2.16	23.1	.5	160	.09	.02	2.80	25.4	.4
17U	.10	.03	3.43	27.4	.4	180	.16	.03	4.30	29.5	.5
19U	.27	.04	4.23	32.0	.8	200	.48	.05	3.96	35.0	1.4
21U	.75	.06	3.83	38.7	1.9	220	1.16	.07	3.80	43.0	2.7
23U	1.69	.10	3.70	47.8	3.5	240	2.43	.12	3.76	53.3	4.6
25U	3.34	.16	3.76	59.0	5.7	260	4.44	.20	3.76	64.9	6.8
27U	5.63	.24	3.83	70.9	7.9	280	7.19	.28	3.90	76.2	9.4
29U	7.84	.31	3.83	81.6	9.6	300	8.25	.33	3.73	86.1	9.6

(TABLE-28 contd.)

310	8.83	.36	3.83	90.6	9.7	320	8.96	.39	3.96	94.2	9.5
330	9.53	.42	4.03	97.7	9.8	340	9.02	.44	4.03	100.6	9.0
350	6.09	.47	3.83	101.5	6.0	360	4.61	.50	4.23	104.1	4.4
370	3.51	.54	3.26	106.2	3.3	380	6.14	.55	3.00	108.5	5.7
390	5.60	.60	3.06	111.5	5.0	400	8.75	.67	4.13	115.0	7.6
**********					S.HR= 11	**********					
110	.89	.08	3.30	13.6	6.5	120	.10	.02	4.30	17.8	.6
130	.15	.03	3.66	19.8	.8	140	.14	.03	3.80	22.8	.6
150	.10	.02	5.13	25.5	.4	160	.10	.02	5.66	27.5	.4
170	.10	.03	6.00	29.2	.3	180	.19	.03	5.73	31.0	.6
190	.32	.04	5.30	33.3	1.0	200	.54	.05	4.93	36.1	1.5
210	.83	.06	4.63	39.5	2.1	220	1.23	.07	4.53	43.5	2.8
230	1.77	.09	4.23	48.0	3.7	240	2.43	.11	4.16	53.0	4.6
250	3.14	.14	4.10	58.4	5.4	260	4.03	.17	4.10	64.0	6.3
270	5.02	.21	4.10	69.7	7.2	280	5.73	.27	4.16	75.1	7.6
290	8.82	.38	3.90	81.7	10.8	300	10.41	.48	3.90	87.0	12.0
310	13.95	.56	4.00	92.9	15.0	320	13.21	.51	3.93	95.6	13.8
330	14.88	.65	3.70	99.5	15.0	340	21.41	1.12	3.70	105.7	20.3
350	12.24	.53	4.13	103.1	11.9	360	13.40	.66	4.03	106.4	12.6
370	10.35	.69	3.76	107.0	9.7						
**********					S.HR= 12	**********					
110	.49	.08	2.40	14.5	3.4	120	.10	.02	1.26	18.2	.5
130	.10	.03	9.93	20.3	.5	140	.09	.03	3.50	23.6	.4
150	(.05)	.02	3.73	26.2	(.2)	160	(.03)	.03	9.86	28.0	(.1)
170	(.04)	.03	7.60	29.6	(.1)	180	(.07)	.03	6.40	31.3	(.2)
190	.15	.04	5.30	33.5	.4	200	.29	.05	4.76	36.2	.8
210	.45	.06	5.30	39.4	1.1	220	.64	.08	4.93	43.2	1.5
230	.91	.10	4.66	47.5	1.9	240	1.25	.12	4.46	52.4	2.4
250	2.07	.26	4.40	58.4	3.5	260	2.26	.19	4.30	63.1	3.6
270	2.79	.23	4.20	68.8	4.1	280	3.55	.28	4.10	74.4	4.8
290	4.24	.33	4.06	79.8	5.3	300	4.94	.37	4.06	85.0	5.8
310	5.66	.41	4.06	89.7	6.3	320	6.63	.44	3.90	93.4	7.1

(TABLE-28 contd.)

33∪	6.87	.47	4.00	79.2	7.1	340	8.40	1.29	4.16	105.6	8.0
35∪	9.77	.65	4.36	103.3	9.5	360	7.00	1.72	4.16	109.7	6.4
37∪	3.78	.56	4.40	104.7	3.6						

********** S.HR= 13 **********

11∪	1.15	.08	6.66	13.4	8.5	120	.21	.02	6.50	17.6	1.2
13∪	.35	.03	6.50	19.8	1.8	140	.37	.03	6.50	22.9	1.6
15∪	.31	.03	6.86	25.5	1.2	160	.26	.03	6.83	27.3	.9
17∪	.19	.03	6.46	29.0	.7	180	.14	.03	6.03	30.8	.5
19∪	.14	.04	4.43	33.0	.4	200	.28	.05	3.30	35.8	.8
21∪	.46	.06	3.06	39.0	1.2	220	.74	.08	2.96	42.9	1.7
23∪	1.09	.10	3.00	47.3	2.3	240	1.10	.30	3.20	53.2	2.1
25∪	1.96	.15	3.23	57.6	3.4	260	2.44	.19	3.23	63.4	3.8
27∪	3.04	.23	3.36	69.3	4.4	280	(3.50)	1.55	2.33	81.8	4.3
29∪	4.00	.75	2.66	84.2	4.8	300	4.25	1.01	1.33	92.3	4.6
31∪	(5.20)	2.08	1.90	103.6	5.0	320	5.60	1.62	1.96	106.0	5.3
33∪	6.00	2.00	2.06	112.2	5.3	340	6.40	2.05	2.76	112.9	5.7
35∪	(6.60)	2.25	2.66	115.7	5.7	360	7.17	.59	3.40	107.7	6.6
37∪	5.75	.60	4.00	108.0	5.3	380	6.57	.63	3.33	109.2	6.0
39∪	6.00	2.29	1.36	113.9	5.3						

********** S.HR= 14 **********

11∪	1.13	.08	6.76	12.0	9.4	120	.24	.02	7.80	16.2	1.5
13∪	.34	.03	7.66	18.2	1.9	140	.41	.03	7.63	21.2	1.9
15∪	.35	.03	7.83	23.7	1.5	160	.29	.03	8.06	25.7	1.1
17∪	.23	.03	8.16	27.5	.8	180	.19	.03	8.30	29.5	.6
19∪	.17	.04	7.63	31.9	.5	200	1.00	.05	7.26	34.8	2.9
21∪	2.00	.38	.06	39.5	5.1	220	2.85	.43	.20	43.6	6.5
23∪	3.32	.48	.40	48.4	6.8	240	3.74	.54	.60	53.9	6.9
25∪	4.32	.60	.80	59.9	7.2	260	5.02	.67	1.00	66.4	7.6
27∪	5.80	.75	1.16	73.1	7.9	280	4.26	.33	3.36	77.1	5.5
29∪	5.08	.38	3.43	83.6	6.1	300	5.94	.43	3.46	89.8	6.6
31∪	6.51	.47	3.60	95.5	6.8	320	6.88	.51	3.53	100.4	6.9
33∪	6.90	.53	3.93	104.5	6.6	340	6.71	.54	4.33	108.0	6.2

(TABLE-28 contd.)

350	5.42	.55	4.76	110.1	4.9	360	4.30	.54	4.76	110.9	3.9
370	4.24	.60	4.50	112.9	3.8						

********** S.HR= 15 **********

110	.67	.07	7.86	10.0	6.7	120	.25	.02	8.86	13.7	1.8
130	.19	.02	9.20	15.3	1.2	140	.24	.03	9.50	17.8	1.3
150	.20	.03	9.66	20.2	1.0	160	.13	.03	9.83	22.4	.6
170	.11	.03	10.50	24.5	.4	180	.13	.03	11.40	26.7	.5
190	.14	.16	0.00	29.8	.5	200	.17	.04	.96	32.1	.5
210	.35	.05	2.26	35.4	1.0	220	.50	.07	2.76	39.3	1.3
230	.88	.08	3.00	43.8	2.0	240	1.40	.11	3.03	48.9	2.9
250	3.35	.33	4.63	55.8	6.0	260	4.21	.38	4.36	62.1	6.8
270	5.30	.42	4.16	68.7	7.7	280	5.52	.30	3.13	74.0	7.5
290	6.58	.35	3.20	80.7	8.1	300	7.46	.39	3.30	87.3	8.5
310	8.15	.44	3.40	93.5	8.7	320	7.90	.46	3.66	98.8	8.0
330	7.15	.48	3.76	103.4	6.9	340	6.74	.51	4.26	107.0	6.3
350	7.06	.54	4.56	110.3	6.4	360	5.23	.59	4.33	112.4	4.7
370	5.54	.66	4.80	113.3	4.9	380	5.34	.78	3.93	115.2	4.6
390	5.00	.78	3.86	114.3	4.4						

********** S.HR= 16 **********

110	.15	.07	7.26	7.0	2.1	120	.08	.02	9.96	10.9	.7
130	.06	.02	8.93	11.9	.5	140	.10	.03	8.80	13.5	.7
150	.18	.03	8.76	15.4	1.2	160	.20	.03	8.96	17.6	1.1
170	.19	.03	8.90	20.0	.9	180	(.11)	.04	9.00	22.6	(.5)
190	(.05)	.04	7.73	20.4	(.2)	200	(.09)	.04	4.70	28.6	(.3)
210	(.30)	.41	4.00	33.8	(.9)	220	.61	.06	3.76	36.4	1.7
230	1.09	.08	3.73	41.1	2.6	240	1.76	.11	3.70	46.5	3.8
250	2.71	.14	3.76	52.6	5.2	260	4.09	.19	3.73	59.2	6.9
270	5.69	.24	3.76	67.2	8.6	280	7.45	.29	3.83	73.4	10.1
290	9.07	.34	3.90	80.7	11.2	300	10.51	.39	3.96	87.9	12.0
310	11.28	.43	4.10	94.4	11.9	320	12.27	.47	4.16	100.8	12.2
330	10.92	.51	4.26	105.5	10.4	340	10.90	.55	4.33	110.7	9.8
350	10.88	.58	4.46	114.3	9.5	360	8.42	.62	5.16	115.1	7.3
370	9.01	.70	5.46	120.4	7.5	380	8.93	.77	5.93	120.5	7.4

(Table-28 contd.)

**********					S.HR=	17	**********				
11	(.15)	.06	1.40	4.2	(3.5)	120	.10	.02	8.96	6.9	1.4
13	.07	.02	8.96	7.6	.9	140	.13	.02	9.46	8.3	1.6
15	.18	.03	9.73	9.0	2.0	160	.24	.03	9.60	10.4	2.3
17	.27	.04	9.73	12.2	2.2	180	.31	.04	9.93	14.4	2.1
19	.57	.11	2.53	17.6	3.2	200	.76	.13	2.66	20.9	3.6
21	1.05	.15	2.86	24.8	4.2	220	1.42	.17	3.06	29.4	4.8
23	1.92	.2[illegible]	3.23	34.6	5.5	240	2.63	.24	3.36	40.4	6.5
25	3.50	.28	3.46	46.8	7.5	260	4.50	.32	3.53	53.6	8.4
27	5.74	.36	3.60	60.8	9.4	280	7.83	.47	4.00	68.4	11.4
29	9.55	.55	4.03	75.9	12.6	300	11.41	.64	4.10	83.4	13.7
31	13.33	.72	4.20	90.4	14.7	320	14.55	.81	4.23	97.1	15.0
33	9.97	.43	4.43	100.1	10.0	340	9.14	.47	4.53	104.8	8.7
35	7.78	.52	4.56	108.5	7.2	360	7.39	.57	4.56	112.0	6.6
37	8.49	.64	4.73	116.3	7.3	380	8.92	.74	4.30	120.3	7.4
**********					S.HR=	18	**********				
11	.17	.01	.83	1.8	9.0	120	(.01)	.01	10.63	2.2	(.5)
13	.03	.01	11.50	2.5	1.2	140	.03	.01	2.00	2.7	1.1
15	(.02)	.02	1.13	2.8	(.7)	160	(.05)	.02	11.93	3.1	(1.6)
17	.06	.02	.20	3.4	1.8	180	.09	.03	.43	4.0	2.3
19	(.10)	.04	11.76	4.9	(1.9)	200	(.14)	.05	11.33	6.3	2.3
21	(.16)	.07	10.73	8.3	(1.9)	220	(.14)	.09	10.50	11.3	(1.2)
23	(.25)	.12	7.73	15.5	(1.6)	240	.51	.16	4.96	19.3	2.5
25	.95	.19	4.73	25.1	3.8	260	1.07	.22	6.76	30.8	3.7
27	1.70	.25	5.80	37.6	4.5	280	3.00	.50	4.93	47.1	6.4
29	4.38	.3[illegible]	4.63	53.7	7.2	300	5.46	.54	3.63	63.6	8.3
31	6.55	.49	4.06	71.2	9.4	320	7.71	.51	4.20	78.6	9.4
33	8.31	.43	4.53	84.5	9.3	340	8.98	.42	4.76	90.2	9.5
35	8.28	.56	4.33	96.1	8.6	360	10.28	.49	4.63	99.7	10.3
37	9.06	1.03	6.20	106.5	8.9	380	11.64	.56	5.13	106.7	10.9
39	9.59	.59	5.33	106.7	9.1	400	7.19	.65	5.33	110.7	6.8
41	6.89	.65	5.36	114.6	6.3						
**********					S.HR=	19	**********				
28	6.12	.56	5.23	25.1	24.4	290	5.33	.64	4.40	31.4	17.0

(TABLE-28 contd.)

300	7.63	1.02	6.63	40.4	18.9	310	3.60	.66	7.13	43.6	8.3
320	4.00	.92	6.80	52.2	7.7	330	4.30	.89	6.36	56.6	7.6
340	4.50	.95	6.50	63.8	7.1	350	5.00	1.05	7.06	68.3	7.3
360	4.00	1.08	7.03	72.4	5.5	370	3.29	.72	6.60	73.3	4.8
380	5.37	.77	6.36	76.7	7.0	390	4.83	.60	5.90	79.6	6.1
400	5.16	.60	5.90	81.6	6.3	410	4.94	.63	6.06	82.7	6.0
**********					S.HR= 20	**********					
280	2.25	.49	4.56	26.7	8.3	290	3.17	.52	6.53	32.5	9.6
300	6.90	.53	7.23	35.9	1.8	310	6.93	.54	7.36	42.4	1.5
320	7.17	.54	7.86	47.9	1.5	330	10.75	.55	7.70	53.4	20.1
340	11.93	.55	7.66	57.8	20.6	350	11.67	.58	7.63	60.7	19.2
360	11.62	.56	7.60	63.9	18.2	370	10.06	.58	7.36	66.6	15.1
380	9.32	.62	7.36	71.4	13.1	390	6.87	.66	6.83	73.5	9.3
400	5.76	.65	6.86	77.0	7.5	410	3.77	.73	6.40	78.8	4.8
**********					S.HR= 21	**********					
270	.80	.60	9.06	38.9	2.1	280	1.21	.58	9.96	44.8	2.7
290	2.17	.56	8.96	50.9	4.3	300	4.25	.57	9.03	55.5	7.7
300	4.25	.57	9.03	55.5	7.7	310	4.18	.51	8.83	59.7	7.0
320	5.93	.52	8.26	62.4	9.5	330	6.86	.54	8.40	66.7	10.3
340	5.83	.61	8.36	70.7	7.2	350	5.45	.66	9.46	73.0	7.5
360	8.66	.59	8.13	75.0	11.5						
**********					S.HR= 22	**********					
230	.80	.35	10.86	19.7	4.0	240	.64	.41	1.43	30.5	2.1
250	.80	.46	3.76	38.6	2.0	260	.91	.51	4.13	46.5	2.0
270	1.30	.53	4.20	52.8	2.5	280	1.24	.57	4.33	57.2	2.2
290	.92	.54	3.23	62.6	1.5	300	2.00	.61	3.50	65.1	3.1
310	2.50	.63	2.73	66.9	3.7	320	1.85	.69	1.26	68.7	2.7
330	1.21	.77	3.06	71.5	1.7						
**********					S.HR= 23	**********					
220	2.18	.43	2.73	13.8	15.8	230	2.51	.46	5.76	22.0	11.4
240	4.22	.46	6.46	29.8	14.2	250	4.57	.48	6.66	40.7	11.2
260	5.63	.50	6.63	50.4	11.2	270	7.69	.54	6.66	56.4	13.6
280	8.36	.55	6.76	63.0	13.3	290	6.61	.62	7.00	66.2	10.0
300	7.64	.78	7.66	66.6	11.5	310	7.93	.94	7.90	62.2	12.7

TA2LE-29

LUNAR M2 VARIATIONS AT PUERTO RICO

ANNUAL

HEIGHT	R2	THETA2	N	R2/N
********** S.HR= 0 **********				
220	1.29	1.50	7.5	17.0
250	.67	.93	12.2	5.5
270	1.03	1.53	21.6	4.8
290	2.05	2.56	36.3	5.6
310	1.64	2.90	51.1	3.2
330	1.28	4.10	60.5	2.1
350	2.40	3.13	68.6	3.5
370	2.56	3.40	76.5	3.3
390	3.11	4.56	89.2	3.5
********** S.HR= 1 **********				
220	.95	8.33	6.3	15.0
240	1.84	11.06	13.9	13.2
260	2.52	11.20	26.0	9.7
280	3.29	11.33	39.5	8.3
300	1.97	11.10	51.5	3.8
320	2.70	9.26	61.0	4.4
340	2.74	8.66	68.5	4.0
360	6.95	8.33	74.0	9.4
********** S.HR= 2 **********				
220	1.07	.10	8.4	12.6
240	2.12	.96	17.4	12.2
260	1.18	.63	28.6	4.1
********** S.HR= 21 **********				
220	1.17	.36	5.3	21.9
240	.96	11.86	8.9	10.7
260	.80	.90	16.6	4.8
280	1.61	3.66	29.6	5.4
300	2.43	3.86	44.8	5.4
320	2.75	3.60	55.6	4.9
340	2.58	3.53	65.3	3.9
360	1.75	3.53	72.4	2.4
380	5.90	3.06	89.3	6.6
********** S.HR= 21 **********				
210	.77	3.36	4.2	18.3
230	1.20	10.70	9.9	12.1
250	2.93	10.83	20.0	14.6
270	3.35	11.10	32.7	10.2
290	3.03	11.20	45.7	6.6
310	2.14	10.06	57.2	3.7
330	3.64	8.56	65.8	5.5
350	6.95	9.50	69.5	10.0
370	10.68	7.66	79.7	13.4
********** S.HR= 21 **********				
210	1.18	11.20	5.5	21.3
230	.58	1.30	12.6	4.6
250	1.84	.63	22.9	8.0

(TABLE-29 contd.)

270	.52	.70	34.6	1.5
290	2.22	8.70	44.9	4.9
310	2.17	7.06	51.6	4.2
330	1.43	7.23	57.2	2.5
350	6.42	8.66	63.8	10.1
370	6.64	8.90	67.4	9.8

********** S.HR= 3

200	.14	2.00	2.6	5.2
220	1.32	.80	8.6	15.3
240	.70	4.56	16.3	4.3
260	1.28	6.90	24.3	5.3
280	2.26	8.53	31.8	7.1
300	2.22	6.63	37.9	5.8
320	3.48	6.80	43.8	7.9
340	3.30	7.00	48.4	6.8
360	3.67	8.80	52.2	7.0
380	5.57	4.63	54.3	10.3

********** S.HR= 4

200	.69	9.73	2.2	30.1
220	.94	4.96	6.7	14.0
240	1.08	4.36	11.7	9.2
260	1.18	4.63	16.1	7.3
280	.79	7.03	21.5	3.7
300	4.47	7.93	28.0	16.0
320	4.38	7.56	33.0	13.3
340	3.30	6.80	37.2	8.9
360	4.82	7.36	40.2	12.0
380	4.14	9.03	42.3	9.8
400	5.45	11.46	40.3	13.5

********** S.HR= 5

210	.29	5.50	3.9	7.3
230	.67	7.43	7.0	9.4

280	.45	3.86	39.5	1.1
300	3.50	8.63	49.2	7.1
320	1.93	7.13	54.7	3.5
340	1.75	6.80	60.8	2.9
360	8.07	8.76	66.8	12.1
380	3.49	8.30	66.8	5.2

********** 3

210	.97	1.56	5.9	16.3
230	1.26	4.60	13.0	9.6
250	.35	7.30	19.8	1.8
270	1.77	6.63	28.6	6.2
290	1.70	6.46	34.9	4.9
310	3.76	6.76	40.9	9.2
330	3.96	6.60	46.3	8.5
350	3.41	7.76	50.9	6.7
370	1.31	5.03	54.9	2.4

********** 4

210	.21	6.33	4.9	4.3
230	.42	4.23	9.1	4.6
250	.93	3.80	13.7	6.8
270	.99	5.23	18.6	5.3
290	1.79	7.30	24.5	7.3
310	4.66	7.86	30.7	15.1
330	3.90	7.36	35.2	11.1
350	6.99	7.76	39.4	17.7
370	5.63	7.86	42.0	13.4
390	3.73	.46	41.1	9.1
410	8.00	.43	36.9	21.6

********** 5

220	.82	5.66	5.4	14.9
240	1.10	7.26	8.9	12.2

(TABLE-29 contd.)

25ω	.83	7.63	11.1	7.5	260	.89	7.80	13.6	6.5
27ω	1.51	7.8ω	16.2	9.3	280	1.13	7.53	19.0	5.9
29ω	1.36	7.4ω	21.5	6.3	300	1.72	8.10	23.8	6.8
31ω	1.77	8.3ω	26.1	6.8	320	1.70	7.76	28.3	6.0
33ω	1.71	7.86	30.5	5.6	340	1.62	8.10	32.4	5.0
35ω	1.59	8.10	33.6	4.7	360	1.60	7.76	34.1	4.7
37ω	1.86	9.ω3	34.3	5.4	380	3.01	10.60	35.3	8.5
39ω	2.98	11.23	36.1	8.3	400	4.43	11.06	38.7	11.4
41ω	4.88	10.96	39.8	12.2					

********** S.HR= 6 **********

21ω	.85	9.50	5.2	16.1	220	1.22	10.76	6.9	17.6
23ω	1.01	10.33	8.9	11.3	240	2.31	10.00	11.9	19.3
25ω	.92	10.1ω	13.0	7.0	260	2.36	9.83	15.9	14.8
27ω	2.31	9.5ω	19.0	12.1	280	2.07	9.00	22.1	9.4
29ω	2.03	8.76	24.9	8.1	300	1.73	9.10	27.4	6.3
31ω	1.72	9.5ω	29.9	5.7	320	1.29	9.66	32.1	4.0
33ω	1.57	10.2ω	34.1	4.6	340	3.57	11.30	37.2	9.6
35ω	4.93	11.46	38.4	12.8	360	5.37	11.36	39.7	13.5
37ω	3.11	10.8ω	38.0	8.2	380	1.81	.16	39.3	4.6

********** S.HR= 7 **********

11ω	.04	3.4ω	2.6	1.5	120	.16	9.56	5.0	3.1
13ω	.14	11.1ω	5.9	2.4	140	.18	10.73	6.5	2.8
15ω	.23	10.46	7.2	3.2	160	.26	10.00	8.4	3.1
17ω	.28	10.03	10.2	2.7	180	.22	9.36	12.9	1.7
19ω	.54	8.93	16.6	3.2	200	.54	8.23	19.5	2.8
21ω	.38	.33	23.4	1.6	220	.44	.06	29.4	1.5
23ω	1.89	.2ω	36.2	5.2	240	2.34	11.86	42.7	5.5
25ω	3.00	11.2ω	49.6	6.0	260	4.17	10.76	55.2	7.6
27ω	4.98	1ω.86	60.5	8.2	280	2.73	11.16	63.5	4.3
29ω	3.57	11.56	66.7	5.4	300	3.00	.06	71.2	1.6
31ω	4.89	1.63	74.5	6.6	320	7.83	2.36	78.3	10.0
33ω	9.55	.86	77.0	12.4					

**********			S.HR=	8 **********
110	.13	8.36	4.8	2.7
130	.03	11.93	10.4	.3
150	.11	8.70	13.3	.9
170	.20	9.70	19.1	1.1
190	.51	10.50	29.7	1.6
210	1.11	10.20	47.6	2.2
230	1.35	9.90	69.3	1.9
250	1.83	10.06	87.8	2.1
270	2.26	10.00	104.3	2.2
290	3.99	8.73	118.0	3.4
310	2.42	11.33	125.6	1.9
**********			S.HR=	9 **********
110	.22	7.30	7.3	3.0
130	.15	9.53	14.2	1.1
150	.33	10.26	18.7	1.8
170	.47	10.63	26.0	1.8
190	.82	10.93	36.9	2.2
210	1.43	10.16	55.9	2.6
230	2.54	9.43	81.2	3.1
250	4.31	9.06	104.4	4.1
270	5.23	9.60	126.8	4.1
290	4.62	9.20	143.0	3.2
310	4.47	5.46	145.8	3.1
330	4.40	2.26	144.4	3.0
350	12.65	2.40	133.7	9.5
**********			S.HR=	10 **********
110	.08	9.00	8.7	.9
130	.14	.70	16.9	.8
150	.10	9.50	22.4	.4
170	.23	.36	29.9	.8
190	.83	.20	40.3	2.1

**********			S.HR=	8 **********
120	.03	1.03	9.4	.3
140	.03	7.93	11.5	.1
160	.17	8.90	15.7	1.1
180	.34	10.00	23.5	1.3
200	.77	10.70	37.9	1.9
220	1.49	10.06	58.5	2.5
240	1.77	9.36	79.0	2.2
260	2.70	10.10	96.9	2.8
280	2.64	7.16	112.8	2.3
300	1.50	7.30	122.8	1.2
320	8.12	.26	127.5	6.4
**********			S.HR=	9 **********
120	.04	7.20	13.0	.3
140	.25	9.66	16.3	1.6
160	.39	10.40	22.0	1.8
180	.48	10.43	30.8	1.6
200	.98	10.66	45.2	2.2
220	1.98	9.73	68.4	2.9
240	5.27	9.56	94.1	5.6
260	4.11	9.43	115.6	3.6
280	3.87	9.60	136.8	2.8
300	7.22	7.46	149.0	4.8
320	3.52	4.53	145.7	2.4
340	6.69	3.56	138.9	4.8
**********			S.HR=	10 **********
120	.07	.66	15.4	.5
140	.13	.03	19.3	.7
160	.08	9.33	26.0	.3
180	.40	.13	34.3	1.2
200	1.21	11.96	48.4	2.5

(TABLE-29 contd.)

21	1.55	11.73	58.9	2.6	220	1.79	11.50	71.4	2.5
23	1.75	10.86	84.8	2.1	240	1.95	9.93	98.1	2.0
25	2.84	9.63	110.8	2.6	260	2.61	9.20	122.6	2.1
27	3.48	11.03	133.8	2.6	280	4.58	11.33	143.3	3.2
29	2.59	.16	152.4	1.7	300	1.55	11.43	158.5	1.0
31	5.30	3.50	155.8	3.4	320	8.33	1.20	154.3	5.4
33	7.65	2.33	157.5	4.9	340	16.02	3.96	152.6	10.5
35	8.06	3.56	151.3	5.3	360	9.10	.73	141.3	6.4
**********				S.HR= 11	**********				
11	.30	10.66	9.8	3.1	120	.17	3.60	17.0	1.0
13	.23	.96	18.9	1.2	140	.31	.56	21.6	1.4
15	.32	.63	25.0	1.3	160	.38	.96	28.6	1.3
17	.50	1.30	32.2	1.5	180	.75	1.50	36.5	2.1
19	1.09	1.76	42.1	2.6	200	1.40	1.73	49.4	2.8
21	1.57	1.63	58.8	2.7	220	2.53	1.33	70.5	3.6
23	1.53	1.13	82.5	1.9	240	1.42	.56	95.0	1.5
25	1.50	0.00	107.9	1.4	260	2.32	11.43	120.4	1.9
27	.96	11.33	131.6	.7	280	.70	.13	141.4	.5
29	.47	9.23	150.8	.3	300	1.15	4.96	159.8	.7
31	4.30	5.60	162.3	2.6	320	8.27	6.00	167.5	4.9
33	8.62	5.20	168.0	5.1	340	10.65	5.16	172.2	6.2
35	9.00	3.00	174.6	5.2	360	10.77	1.30	171.4	6.3
**********				S.HR= 12	**********				
11	.71	1.40	9.8	7.2	120	.10	1.33	18.0	.4
13	.13	.93	19.8	.7	140	.12	1.03	22.7	.5
15	.18	1.93	26.1	.7	160	.19	1.93	29.5	.6
17	.22	2.13	33.1	.7	180	.30	1.63	37.1	.8
19	.43	1.03	41.9	1.0	200	.57	.46	48.1	1.2
21	.70	11.83	55.9	1.3	220	1.05	11.30	65.5	1.6
23	1.68	10.93	76.5	2.2	240	2.94	10.56	88.9	3.3
25	3.95	10.20	102.1	3.9	260	4.49	10.16	115.2	3.9
27	5.39	10.16	127.8	4.2	280	4.46	10.06	138.4	3.2

(TABLE-29 contd.)

29∪	5.05	10.53	149.0	3.4	300	5.62	10.90	160.3	3.5
31∪	2.86	10.6∪	166.3	1.7	320	1.68	8.16	176.0	1.0
33∪	4.64	7.6∪	180.6	2.6	340	5.92	7.10	190.4	3.1
35∪	5.44	7.46	194.7	2.8	360	5.31	5.53	194.7	2.7
37∪	7.33	4.5∪	183.4	4.0					
**********				S.HR= 13	**********				
11∪	.35	1.3∪	9.7	3.6	120	.09	8.36	18.0	.5
13∪	.06	7.7∪	19.8	.3	140	.03	9.43	22.6	.1
15∪	.04	1∪.23	25.9	.2	160	.03	10.23	29.2	.1
17∪	.08	5.1∪	32.6	.2	180	.14	4.03	36.2	.4
19∪	.20	3.63	40.6	.5	200	.20	2.83	46.1	.4
21∪	.29	.6∪	53.3	.5	220	.59	11.16	62.3	.9
23∪	1.41	11.16	73.2	1.9	240	2.05	11.03	85.5	2.4
25∪	2.99	10.56	99.1	3.0	260	3.58	10.16	112.6	3.2
27∪	4.05	1∪.0∪	126.0	3.2	280	4.80	10.60	138.6	3.5
29∪	5.03	1∪.43	149.9	3.4	300	5.26	11.36	160.0	3.3
31∪	5.16	1∪.8∪	169.0	3.1	320	3.50	9.76	177.7	2.0
33∪	3.10	9.9∪	187.6	1.7	340	6.25	9.43	194.3	3.2
35∪	1.88	7.03	201.8	.9					
**********				S.HR= 14	**********				
11∪	.25	1∪.46	9.2	2.7	120	.02	5.40	17.2	.1
13∪	.05	4.1∪	18.8	.3	140	.06	2.06	21.3	.3
15∪	.06	.7∪	24.5	.2	160	.12	.43	27.8	.4
17∪	.03	7.7∪	31.0	.1	180	.07	6.93	34.6	.2
19∪	.03	6.53	38.9	.1	200	.10	11.76	44.3	.2
21∪	.41	11.4∪	51.2	.8	220	1.02	11.06	60.1	1.7
23∪	1.57	1∪.56	70.9	2.2	240	1.95	10.30	83.0	2.3
25∪	2.30	9.86	96.5	2.4	260	2.29	10.33	110.6	2.1
27∪	2.73	1∪.4∪	124.2	2.2	280	2.20	10.56	136.3	1.6
29∪	1.32	1∪.33	147.4	.9	300	1.65	10.16	157.6	1.4
31∪	2.38	11.23	166.3	1.4	320	.97	.23	174.5	.6
33∪	2.09	9.63	179.2	1.2	340	2.33	.23	188.0	1.2

(TABLE-29 contd.)

35	1.97	2.30	192.1	1.0	360	3.20	3.50	198.8	1.6
37	6.37	4.26	200.1	3.2	380	8.11	7.60	193.5	4.2
**********				S.HR= 15					**********
11	.48	2.36	8.2	5.8	120	.06	2.36	15.9	.4
13	.09	11.70	17.4	.5	140	.08	1.26	19.6	.4
15	.14	.90	22.4	.6	160	.13	1.66	25.5	.5
17	.10	1.20	28.9	.3	180	.14	2.00	32.6	.4
19	.16	.90	37.0	.4	200	.49	11.96	42.5	1.2
21	.99	11.60	49.7	1.9	220	1.56	11.43	58.7	2.7
23	1.74	11.33	69.5	2.5	240	2.15	11.63	81.8	2.6
25	1.86	.26	94.4	2.0	260	3.28	.10	108.5	3.0
27	2.76	.76	121.0	2.3	280	2.82	.90	133.1	2.1
29	1.82	1.33	144.2	1.3	300	2.84	1.10	155.7	1.8
31	1.40	1.23	164.4	.9	320	1.16	11.46	172.2	.7
33	1.11	9.86	178.1	.6	340	3.10	10.36	185.1	1.7
35	2.44	8.96	191.2	1.3	360	3.75	6.23	192.3	2.0
37	5.35	4.33	194.1	2.8	380	6.01	3.20	19.1	3.1
**********				S.HR= 16					**********
11	.79	3.93	6.8	11.6	120	.11	3.60	13.3	.8
23	.68	11.46	67.7	1.0	130	.07	3.56	14.4	.5
14	.15	3.60	16.1	.9	150	.18	3.46	18.6	1.0
16	.20	2.76	21.4	.9	170	.27	2.40	24.7	1.1
18	.37	2.23	28.4	1.3	190	.47	2.56	33.1	1.4
20	.61	1.90	39.0	1.6	210	.63	1.33	46.8	1.3
22	.68	.50	56.4	1.2	240	.96	10.10	79.9	1.2
25	.79	9.46	92.8	.9	260	.93	7.73	105.8	.9
27	.92	7.16	118.6	.8	280	.51	8.70	129.8	.4
29	2.34	7.56	141.1	1.7	300	.96	7.53	152.0	.6
31	1.43	8.23	160.6	.9	320	2.85	8.56	168.2	1.7
33	3.88	8.66	174.6	2.2	340	6.08	8.83	179.4	3.4
35	8.39	8.70	184.2	4.6	360	6.56	7.86	185.9	3.5
37	7.15	7.23	186.4	3.8	380	7.73	4.06	183.8	4.2

(TABLE-29 contd.)

**********				S.HR= 17	**********				
11∪	.23	3.06	4.5	5.0	120	.10	4.86	9.7	1.0
13∪	.10	5.63	10.5	.9	140	.13	5.63	11.5	1.1
15∪	.03	4.13	13.2	.2	160	.08	1.43	15.4	.5
17∪	.20	1.43	18.1	1.1	180	.43	1.63	21.6	2.0
19∪	.81	1.7∪	26.3	3.1	200	1.05	1.50	32.4	3.2
21∪	1.41	2.36	40.2	3.5	220	1.36	1.56	50.9	2.7
23∪	1.18	.23	63.2	1.9	240	1.55	10.63	76.3	2.0
25∪	2.55	9.86	89.4	2.9	260	2.61	9.73	103.1	2.5
27∪	2.96	9.23	115.9	2.6	280	3.00	9.16	127.8	2.3
29∪	3.04	9.4∪	139.1	2.2	300	2.88	9.76	148.8	1.9
31∪	4.52	9.9∪	157.5	2.9	320	6.43	9.70	165.6	3.9
33∪	8.70	9.16	170.2	5.1	340	11.27	8.93	172.5	6.5
35∪	8.62	9.4∪	172.6	5.0	360	8.22	9.43	173.8	4.7
37∪	4.19	8.86	175.6	2.4					
**********				S.HR= 18	**********				
11∪	.10	1.53	2.6	3.8	120	.38	6.23	5.0	7.4
13∪	.59	5.93	5.6	10.3	140	.71	5.80	6.1	11.5
15∪	.82	5.93	6.9	11.8	160	.92	5.96	8.1	11.3
17∪	1.00	5.83	9.8	10.1	180	.72	5.90	12.1	5.9
19∪	1.45	5.4∪	15.0	9.6	200	1.25	7.40	14.8	8.3
21∪	1.26	5.63	19.4	6.4	220	1.67	4.20	27.3	6.1
23∪	.89	5.43	39.6	2.2	240	.46	5.53	54.3	.8
25∪	1.55	9.16	70.9	2.2	260	3.13	9.70	86.3	3.6
27∪	4.27	9.93	99.9	4.3	280	5.06	10.10	112.4	4.5
29∪	6.28	9.96	122.4	5.1	300	6.76	10.43	132.0	5.1
31∪	6.39	10.6∪	139.9	4.6	320	5.83	11.23	147.8	3.9
33∪	7.11	11.6∪	154.7	4.6	340	5.25	10.33	157.4	3.3
35∪	3.98	10.93	159.4	2.5	360	.90	3.66	163.2	.6
37∪	.53	8.5∪	166.6	.3					
**********				S.HR= 19	**********				
2∪∪	3.62	9.53	6.6	54.1	210	4.17	9.60	13.3	31.4

(TABLE-29 contd.)

22∞	5.01	9.96	21.4	23.4	230	5.61	10.10	29.3	19.1
24∞	5.21	9.63	35.4	14.7	250	4.32	10.30	40.8	10.6
26∞	4.77	10.26	47.6	10.0	270	4.50	9.60	58.5	7.7
28∞	5.98	9.80	69.5	8.6	290	4.85	9.66	80.0	6.1
30∞	5.15	9.93	90.9	5.7	310	6.27	10.03	102.0	6.1
32∞	7.09	10.53	109.4	6.5	330	3.12	10.33	118.4	2.6
34∞	2.03	11.03	122.4	1.7	350	1.03	5.06	130.7	.8
36∞	1.08	4.66	137.1	.8	370	4.04	6.33	143.5	2.8
38∞	1.53	6.93	146.3	1.0	390	3.85	7.30	147.3	2.6
**********				S.HR= 20					
20∞	3.83	3.63	4.5	84.1	210	2.05	2.60	9.3	21.8
22∞	1.96	1.60	14.5	13.5	230	1.70	.06	20.5	8.3
24∞	1.42	11.16	26.2	5.4	250	.82	5.63	31.9	2.6
26∞	.99	1.93	36.2	2.7	270	3.46	10.83	39.1	8.8
28∞	2.67	11.80	44.3	6.0	290	2.68	10.96	49.2	5.4
30∞	2.20	11.40	56.5	3.9	310	2.84	.60	63.3	4.5
32∞	2.19	.16	70.6	3.1	330	3.12	11.46	77.4	4.0
34∞	4.70	11.73	86.2	5.5	350	4.01	11.33	95.8	4.2
36∞	4.23	1.73	104.6	4.0	370	4.06	2.56	113.0	3.6
38∞	4.35	1.30	121.4	3.6	390	3.88	2.86	131.6	2.9
40∞	4.93	4.20	134.2	3.7	410	9.77	5.80	137.8	7.1
42∞	7.60	3.83	139.0	5.5					
**********				S.HR= 21					
21∞	.87	11.96	5.1	16.8	220	1.19	0.00	6.8	17.4
23∞	.83	11.80	8.9	6.8	240	1.22	11.10	12.4	11.2
25∞	1.98	11.20	16.0	10.1	260	1.74	9.90	20.7	7.7
27∞	2.25	9.73	25.9	8.7	280	1.87	9.70	31.4	5.9
29∞	2.03	10.03	37.5	5.4	300	2.01	10.20	44.3	4.8
31∞	2.02	10.80	51.6	4.0	320	2.03	11.30	58.3	3.4
33∞	1.95	10.60	63.9	3.1	340	2.17	11.33	69.9	3.1
35∞	3.68	11.70	74.9	4.9	360	5.66	1.06	80.3	7.0
37∞	8.04	11.90	91.9	8.7	380	6.99	10.40	101.3	6.9

(TABLE-29 contd.)

39∞	6.34	10.76	107.1	5.9	400	6.74	10.36	118.3	5.7
41∞	9.25	10.43	128.3	7.2	420	9.20	.03	131.5	7.0

********** S.HR= 22 **********

21∞	.42	11.46	3.7	11.3	220	.77	11.40	5.5	13.9
23∞	.40	11.13	6.5	5.4	240	.74	9.13	7.7	9.6
25∞	.99	11.5∞	10.1	9.8	260	1.92	.13	13.7	13.9
27∞	3.22	.2∞	17.9	17.9	280	3.22	.13	23.0	14.0
29∞	2.55	.13	28.9	8.8	300	2.40	11.76	35.7	6.7
31∞	2.47	.13	43.7	5.7	320	2.79	.50	51.1	4.5
33∞	2.76	.2∞	58.2	4.3	340	1.96	.73	64.0	3.1
35∞	2.53	1.36	69.0	3.7	360	3.94	.70	75.7	5.2
37∞	2.63	1.56	81.8	3.2	380	8.34	1.16	89.4	9.3
39∞	9.12	1.73	100.3	9.1	400	12.32	.36	105.1	11.7
41∞	15.61	.73	109.5	14.3					

********** S.HR= 23 **********

21∞	6.59	10.13	7.1	92.8	220	3.97	10.66	7.4	53.6
23∞	5.00	10.6∞	8.7	57.3	240	2.35	11.33	9.0	26.1
25∞	1.30	1.36	10.8	12.0	260	1.28	1.30	13.6	9.4
27∞	1.84	1.6∞	17.8	10.3	280	2.32	1.86	22.8	10.1
29∞	2.63	2.03	29.0	9.0	300	2.72	1.86	36.1	7.5
31∞	4.19	2.2∞	44.3	9.5	320	4.39	1.96	51.2	8.6
33∞	3.96	1.9∞	57.2	6.1	340	2.80	2.00	63.5	4.5
35∞	3.57	2.3∞	67.4	5.0	360	3.91	3.20	73.3	5.4
37∞	6.18	2.5∞	80.5	7.7	380	4.00	2.30	86.3	4.9
39∞	6.66	1.3∞	92.6	7.1	400	5.52	11.00	106.6	5.2
41∞	3.28	10.4∞	107.9	8.0	420	10.24	9.30	112.1	9.1

REFERENCES

Appleton, E.V	1946	Nature(Lond.), 157, 691.
Appleton, E.V. and Barnett, M.A.F.	1925	Nature(Lond.), 115, 333.
Appleton, E.V. and Beynon, W.J.G.	1948	Nature(Lond.), 162, 486.
Appleton, E.V. and Beynon, W.J.G.	1949	Nature(Lond.), 164, 308.
Appleton, E.V. and Naismith, R.	1935	Proc.Roy.Soc., A150, 685.
Appleton, E.V. and Lyon, A.J.	1955	Proc.Inter.Conf.Phys.Ionosph.Phys Soc., p20.
Appleton, E.V. and Weekes, K.	1939	Proc.Roy.Soc., A171, 171.
Bailey, D.K.	1948	Terr.Mag.Atmos.Electr., 53, 35.
Baker, W.G. and Martyn, D.F.	1953	Phil.Trans.Roy.Soc., A246, 281.
Bartels, J.	1928	Handbuch der Experimental physik, 25, 624.
Bartels, J.	1936	Terr.Mag.Atmos.Electr., 41, 225.
Bartels, J.	1950	J.Atmos.Terr.Phys., 1, 2.
Bartels, J. and Fanselau, G.	1938	Abh.Geophys.Inst.Postdam Nr-2.
Bartels, J. and Johnston, H.F.	1940	Terr.Mag.Atmos.Electr., 45, 269.
Baxter, R.G.	1967	Planet.Space Sci., 15, 701.
Baxter, R.G. and Kendall, P.C.	1968	Proc.Roy.Soc., A304, 171.
Benkova, N.P.	1940	Terr.Mag.Atmos.Electr., 45, 425.
Berkner, L.V. and Wells, H.W.	1934	Terr.Mag.Atmos.Electr., 39, 215.

Bhargava,B.N.	1963	J.Atmos.Terr.Phys.,25,367.
Bossolasco,M. and Elena,A.	1960	Geofis.Pura.Appl., 46,167.
Brady,A.H. and Crombie,D.D.	1963	J.Geoph. Res., 68,5437.
Bramley,E.N. and Peart,M.	1965	J.Atmos.Terr.Phys.27,1201.
Breit,G. and Tuve,M.M.	1925	Nature (Lond.),116,357.
Brown,R.A.	1956	J.Atmos.Terr.Phys.,9,144.
Brown,R.A.	1965	J.Atmos.Terr.Phys.,27,855.
Brown,R.A.	1967	J.Atmos.Terr.Phys.,29,1087.
Brown,R.A.	1968	J.Atmos.Terr.Phys.,30,1877.
Burkard,O.	1951	J.Atmos.Terr.Phys.,1,349.
Burkard,O.	1965	J.Atmos.Terr.Phys.,27,113.
Burkard,O.	1966	J.Atmos.Terr.Phys.,28,689.
Burrows,K. and Hall,S.H.	1964	Nature(Lond.),204,721.
Butler,S.T. and Small,K.A.	1963	Proc.Roy.Soc.,A271,91.
Cahill,L.J.	1959	J.Geoph.Res.,64,489.
Chakravarty,S.C. and Rastogi,R.G.	1969	Nature(Lond.),223,939.
Chakravarty,S.C. and Rastogi,R.G.	1970	J.Atmos.Terr.Phys.,32,945.
Chapman,S.	1913	Phil.Trans.Roy.Soc.,A213,279:
Chapman,S.	1919	Phil.Trans.Roy.Soc.,A218,1.
Chapman,S.	1931	Proc.Phys.Soc.(Lond.),43,26:
Chapman,S.	1948	Terr.Mag.Atmos.Electr.,53,247:
Chapman,S.	1951a	Proc.Phys.Soc.(Lond.),B64,833.
Chapman,S.	1951b	Compen. Meteorol.Amer.Met. Soc.p.510.

Chapman,S.	1952	Austr.J.Sci.Res.,A5,218.
Chapman,S.	1956	Nuovo Cimento 10(4),1385.
Chapman,S. and Bartels,J.	1940	Geomagnetism, oxford: Clarendon press(chapter 8).
Chapman,S. and Miller,J.C.P.	1940	Month. Not.Roy.Astr.Soc. Geoph.Suppl.,4,649.
Chapman,S. and Rajarao,K.S.	1965	J.Atmos.Terr.Phys.,27,559.
Chapman,S. and Westfold,K.C.	1956	J.Atmos.Terr.Phys.,8,1.
Cowling,T.G.	1932	Month Not.Roy.Astr.Soc.,93,90.
Cowling,T.G.	1945	Proc. Roy.Soc.,A183,453.
Croom,S.A.; Robbins,A.R. and J.O.Thomas.	1959	Nature (Lond.),184,2003.
Davis,T.N.;Burrows,K. and Stolarik,J.D.	1967	J.Geoph.Res.,72,1845.
Davis,T.N.;Stolarik,J.D. and Heppner,J.P.	1965	J.Geoph.Res.,70.5883.
Duncan,R.A.	1956	Austr.J.Phys.,9,112.
Duncan,R.A.	1960	J.Atmos.Terr.Phys.,18,89.
Dunford,E.	1969	Planet.Space Sci.,17,923.
Egadal,J.	1947	Terr.Mag.Atmos.Electr.,52,449.
Egadal,J.	1948	Nature(Lond.),161,443.
Egadal,J.	1956	Publ.Danske.Meteorol.Inst.,No.22.
Fejer,J.A.	1953	J.Atmos.Terr.Phys.,4,184.
Fejer,J.A.	1963	J.Geoph.Res.,68,2147.
Forbush,S.E. and Casaverde,M.	1961	Carnegie Inst. Washington Publ.,620,140.
Gliddon,J.E.C. and Kendall,P.C.	1964	J.Atmos.Terr.Phys.,26,721.

Goldberg,R.A.; Kendall,P.C. and Schmerling,E.R.	1964	J.Geoph.Res.,69,417.
Gupta,J.C.	1970	J.Atmos.Terr.Phys.,32,1159.
Hanson,W.B. and Moffett,R.J.	1966	J.Geoph.Res.,71,5559.
Hasegawa,M. and Ota,M.	1950	I.A.T.M.E. Bull.,13,426.
Hirono,M.	1950a	J.Geomag.Geoelec.,2,1.
Hirono,M.	1950b	J.Geomag.Geoelec.,2,113.
Hirono,M.	1952	J.Geomag.Geoelec.,4,7.
Hirono,M.	1953	J.Geomag.Geoelec.,5,22.
Hirono,M. and Maeda,H.	1954	J.Geomag.Geoelec.,6,122.
Hirono,M. and Maeda,H.	1955	J.Geoph.Res.,60,241.
Harnischmacher,E.	1955	C.R.Acad.Sci.(Paris),240,553.
Jacchia,L.G. and Kopal,F.	1952	J.Meteorol.,9,13.
Kendall,P.C.	1963	J.Atmos.Terr.Phys.,25,87.
King,J.W.; Smith,P.A.; Eccles,D.; Fooks,G.F. and Helm,H.	1964	Proc.Roy.Soc.,A281,464.
Knecht,R.W.	1959	J.Atmos.Terr.Phys.,14,348.
Kotadia,K.M. and Ramanathan,K.R.	1956	Proc.Ind.Acad.Sci.,43,394.
Littlewood,C.A. and Chapman,J.H.	1955	Can.J.Phys.,33,11.
Lyon,A.J.	1963	Proc.Inter.Conf. on .Ionosph., Phys. Soc.(Lond.),88.
Lyon,A.J. and Thomas,L.	1963	J.Atmos.Terr.Phys.,25,373.

Maeda,H.	1953a	J.Geomag.Geoelec.,5,39.
Maeda,H.	1953b	J.Geomag.Geoelec.,5,94.
Maeda,H.	1955	Rep.Ionos.Res.(Japan),9,59.
Maeda,H.	1955a	J.Geomag.Geoelec.,7,75.
Maeda,K.	1952	J.Geomag.Geoelec.4.63.
Maeda,K. and Matsumoto,H.	1962	Rep.Ionos.Space Res.(Japan), 16,1.
Maeda,K.;Uyeda,H. and Shinkawa,H.	1942	Rep.Res.Phys.Inst.Rad.Waves, No.1,2.
Malin,S.R.C. and Chapman,S.	1970	Geophys.J.Roy.Astr.Soc.,19,15.
Martyn,D.F.	1947	Proc.Roy.Soc.,A190,273.
Martyn,D.F.	1948	Proc.Roy.Soc.,A194,429.
Martyn,D.F.	1948a	Nature(Lond.),162,142.
Martyn,D.F.	1949	Nature(Lond.),163,34.
Martyn,D.F.	1950	URSI (Brussels) Special Report No.2.
Martyn,D.F.	1955	Proc.Inter.Conf.Ionosph.Phys., Phys. Soc.(Lond.),254.
Matsushita,S.	1953	Rep.Ionos.Res.(Japan),7,45.
Matsushita,S.	1957	J.Atmos.Terr.Phys.,10,163.
Matsushita,S.	1962a	Ionos.Sporadic E.,Oxford: Pergamon Press, 194.
Matsushita,S.	1962b	Publ.Comemorativa do' 50° Aniversário do observatório Magnético de S. Miguel Açores, 209.
Matsushita,S.	1967	Handbuck der Physik, 49III(2), 547.
Matsushita,S. and Maeda,H.	1965	J.Geoph.Res.70,2535.

Matsushita,S. and Maeda,H.	1965a	J.Geoph.Res.,70,2559.
Maynard,M.C.	1967	J.Geoph.Res.,72,1863.
McNish,A.G.	1937	I.A.T.M.E.Bull.,10,271.
McNish,A.G. and Gautier,T.N.	1949	J.Geoph.Res.,54,303.
Mitra,A.P.	1955	J.Atmos.Terr.Phys.,7,99.
Mitra,S.K.	1946	Nature(Lond.),158,668.
Ogbuehi,P.O. and Onwumechilli,A.	1964	J.Atmos.Terr.Phys.,26,889.
Onwumechilli,C.A. and Alexander,N.S.	1959a	J.Atmos.Terr.Phys.,13,222.
Onwumechilli,C.A. and Alexander,N.S.	1959b	J.Atmos.Terr.Phys.,16,115.
Osborne,B.W.	1952	Nature(Lond.),169,661.
Pedersen,P.O.	1927	Danmarks Naturv.Samfund,A15,244.
Pekeris,C.L.	1937	Proc.Roy.Soc.,A158,650.
Pramanik,S.K. and Hariharan,P.S.	1953	Ind.J.Meteor.Geoph.,4,353.
Pramanik,S.K. and Yegnanarayanan,S.	1952	Ind.J.Meteor.Geoph.,3,212.
Ranzi,I.	1939	Ric.Scient.,10,926.
Rajarao,K.S.	1962	Ind.J.Meteor.Geoph.,13,97.
Rajarao,K.S. and Sivaraman,K.R.	1958	J.Geoph.Res.,63,727.
Rao,K.N.;Rao,D.R.K. and Rajarao,K.S.	1967	Tellus.,19,337.
Rastogi,R.G.	1959a	Can.J.Phys.,37,874.
Rastogi,R.G.	1959b	J.Geoph.Res.,64,727.
Rastogi,R.G.	1961a	Nature(Lond.),189,214.

Rastogi,R.G.	1961b	J.Atmos.Terr.Phys.,22,290.
Rastogi,R.G.	1962a	J.Atmos.Terr.Phys.,24,1031.
Rastogi,R.G.	1962b	J.Res.(N.B.S.),66D,601.
Rastogi,R.G.	1963a	J.Atmos.Terr.Phys.,25,393.
Rastogi,R.G.	1963b	J.Geoph.Res.,68,2445.
Rastogi,R.G.	1963c	Proc.Ind.Acad.Sci.,58,38.
Rastogi,R.G.	1963d	Nature(Lond.),200,1083.
Rastogi,R.G.	1964a	J.Geoph.Res.,69,1020.
Rastogi,R.G.	1964b	J.Inst.Telecom.Engrs.(India), 10,394.
Rastogi,R.G.	1965	Zeit. f. Geoph.,31,27.
Rastogi,R.G.	1966	J.Inst.Telecom.Engrs.(India), 12,245.
Rastogi,R.G.	1968a	J.Atmos.Terr.Phys.,30,497.
Rastogi,R.G.	1968b	Ann. de Geophys.,24,779.
Rastogi,R.G.	1968c	Proc.Ind.Acad.Sci.,68,23.
Rastogi,R.G.	1969a	Ann. de Geophys.,25,73.
Rastogi,R.G.	1969b	Proc.Ind.Acad.Sci,69,250.
Rastogi,R.G.	1969c	J.Atmos.Terr.Phys.,31,759.
Rastogi,R.G. and Alurkar,S.K.	1964	J.Atmos.Terr.Phys.,26,641.
Rastogi,R.G. and Alurkar,S.K.	1966	Proc.Ind.Acad.Sci.,63,75.
Rastogi,R.G. and Trivedi,N.B.	1970	Planet.Space Sci., 18,367.
Risbeth,H; Lyon,A.J. and Peart,M.	1963	J.Geoph.Res.,68,2559.
Rougerie,F.	1961	Ann. de Geophys.,17,145.

Rush,C.M. and Venkateswaran,S.V.	1968	J.Atmos.Terr.Phys.,30,633.
Sastry,T.S.G.	1968	J.Geoph.Res.,73,1789.
Schmeider,O.	1936	Veroffentlichungen Meteor. Inst. Univ.Berlin,1(No.3),1.
Schneider,O.	1963	Nature(Lond.),199,548.
Schuster,A.	1889	Phil.Trans.Roy.Soc.,A180,467.
Schuster,A.	1908	Phil.Trans.Roy.Soc.,A208,163.
Sharma R.P. and Rastogi R.G.	1967	J.Atmos.Terr.Phys.,29,1641.
Sharma R.P. and Rastogi R.G.	1968	J.Atmos.Terr.Phys.,30,453.
Sharma R.P. and Rastogi R.G.	1969	Ann. Geoph., 25,807.
Sharma R.P. and Rastogi R.G.	1970a	Pure.App. Geophys.(formerly Geofis.Pura e Appl.)-~~(in press)~~. 80(III),288
Sharma R.P. and Rastogi R.G.	1970b	Ann. Geoph., 26,337.
Siebert,M.	1961	Advan. Geophys.,7,105.
Singer,S.F; Maple,E. and Bowen,W.A.	1951	J.Geoph. Res., 56,265.
Skinner,N.J. and Wright,R.W.	1964	J.Atmos.Terr.Phys.,26,1221.
Small,K.A. and Butler,S.T.	1961	J.Geoph.Res.,66,3723.
Stewart,B.	1882	Encyclopedia Brittanica,16,159.
Sugiura,M. and Cain,J.C.	1966	J.Geoph. Res.,71,1869.
Sugiura,M. and Fanselau,G.	1966	Godd.Spa. Flight Centre, Rep. (X-612-66-401).
Sugiura,M. and Poros,D.J.	1969	J.Geoph.Res.,74,4025.

Tarpley, J.D.	1970	Planet. Space Sci., 18, 1075.
Thirvengadathan, A.	1954	Ind. J. Meteor. Geophys., 5, 267.
Thomas, L.	1968	J. Atmos. Terr. Phys., 30, 1631.
Thomas, J.A. and Svenson, A.C.	1955	Austr. J. Phys., 8, 554.
Tschu, K.K.	1949	Austr. J. Sci. Res., A2, 1.
Untied, J.	1967	J. Geoph. Res., 72, 5799.
Walker, W.G.	1913	Proc. Roy. Soc., A89, 379.
Weekes, K. and Wilkes, M.V.	1947	Proc. Roy. Soc., A192, 80.
Wright, R.W. and Skinner, N.J.	1959	J. Atmos. Terr. Phys., 13, 217.
Zagulyaeva, V.A. and Fatkullin, M.N.	1966	Geomagn. Aeron., 6, pp726 and 934.
Zagulyaeva, V.A. and Fatkullin, M.N.	1969	J. Atmos. Terr. Phys., 31, 1.
Zagulyaeva, V.A.; Martynova, K.V; Prilezhayeva, N.A. and Fatkullin, M.N.	1967	Geomagn. Aeron., 7, 813.